MODULATORS OF INNATE GUT IMMUNITY TO ENTERIC VIRAL INFECTIONS: MURINE NOROVIRUS (MNV) AS A MODEL

Osama Eltayeb Idris Eisa

St. Edmund's College

Lab of Viral Zoonotic

School of Biological Sciences

University of Cambridge

This dissertation is submitted for the degree of Doctor of Philosophy

January 2018

MODULATORS OF INNATE GUT IMMUNITY TO ENTERIC VIRAL INFECTIONS: MURINE NOROVIRUS (MNV) AS A MODEL

OSAMA EISA

ABSTRACT

Challenged by a huge and diverse antigenic stimulus, the intestinal mucosa has developed a unique immune system that mainly functions to maintain tolerance to innocuous antigens while retaining the ability to respond swiftly to pathogenic threats. Central to this specialised immune system are the Intraepithelial Lymphocytes (IELs). These cells are uniquely located between Intestinal Epithelial Cells (IECs) ready to respond to exogenous antigens in the intestinal lumen. The intestinal immune system is constantly influenced, not only by the commensal microbiota, but also by the nutritional status of the host and the availability of certain essential micronutrients that are derived from a healthy-balanced diet. Additionally, age has a significant impact on the efficiency of gut immunity in responding to infectious pathogens, as reflected by the increased burden of gastrointestinal infections at the extremes of age.

In this thesis, using the Murine Norovirus (MNV) oral infection model, I aimed to characterize intestinal mucosal antiviral-responses with specific focus on the role of IELs, the impact of aging and the influence of certain micronutrients whose effects are mediated through the Aryl Hydrocarbon Receptor (AhR). Employing different knock-out and adoptive transfer experiments, I concluded that, at least in our experimental conditions and in a viral strain-specific manner, the activated IELs are not essential and may play a minor role in the protective response against MNV infection. This work also demonstrated that various MNV virus strains activate IELs differentially and for the first time (to our knowledge) revealed distinct abilities of these different Norovirus variants to infect IECs. Recognising an impaired response in old (2-year) mice, we were also able to identify a specific defect in the IFN-λ response of aged IECs. Furthermore, using the model of MNV infection to investigate the role of AhR signalling, the data I generated suggested a direct link between constitutive AhR signalling and innate interferon-mediated responses. These findings have uncovered a potential preventive/therapeutic targets for enhancing anti-viral responses.

TABLE OF CONTENTS

List of Tables

List of Figures

List of Abbreviations

Adar – Double-stranded RNA-specific adenosine deaminase

AhR – Aryl hydrocarbon receptor

AhRR – Aryl hydrocarbon receptor repressor

AIP – AhR-interacting protein

APRIL – A proliferation Activation ligand of the TNF family

bHLH – basic helix-loop-helix domain

BMMC – Bone marrow derived mononuclear cell

BMP – Bone morphogenic protein

CD – Cluster of differentiation

CpG – Cytidine-guanosine oligodeoxynucleotides

CYP – Cytochrome P450

CXCL – C-X-C motif chemokine ligand

CXCR – C-X-C motif chemokine receptor

DAMP – Danger-associated molecular pattern

DAPI – 4',6-diamidino-2-phenylindole

DC – Dendritic cell

dKO – double knock-out

DNA – Deoxyribonucleic acid

dpi – Days post infection

FACS – Fluorescence-activated cell sorter

Foxp3 – Forkhead box P3

HBGA – Human histo-blood group antigens

hpi – Hours post infection

hrs – Hours

HSP90 – Heat-shock protein 90

HuNV – Human norovirus

IBD – Inflammatory bowel disease

IDO1 – Indole-2,3-dioxygenase

IEC – Intestinal epithelial cell

IEL – Intraepithelial lymphocytes

IFN – Interferon

IKK – Inhibitor of nuclear factor-kappaB (IkappaB)- kinase complex

IL - Interleukin

ILC – Innate lymphoid cell

ILF – Isolated lymphoid follicles

i.p. – Intraperitoneal

IRF – Interferon regulatory factor

ISG – Interferon-stimulated genes

ITC – Isotype control

i.v. – Intravenous

JAK – Janus kinase

LP – Lamina Propria

LPS – Lipopolysaccharide

MAPK – Mitogen activated protein kinase

MDA5 – Melanoma differentiation-associated protein-5

MHC – Major histocompatibility complex

MLNs – Mesenteric lymph nodes

MNV – Murine norovirus

Mx – Myxovirus resistance

NF-kB – Nuclear factor 'kappa-light-chain-enhancer' of activated B-cells

NK cell – Natural killer cell

List of Abbreviations

NOD – Nucleotide-binding oligomerization domain

OAS – 2'-5'-oligoadenylate synthetase

ORF – Open reading frame

PAMP – Pathogen associated molecular pattern

PAS – PER, ARNT, SIM domain

pDC – plasmacytoid DCs

p-IESCs – pluripotent Intestinal Epithelial Stem Cells

PPs – Peyer's Patches

PKR – RNA-activated protein kinase

PRR – Pattern recognition receptor

Poly(I:C) – Polyribocytidylate

Rag – Recombination activating gene

REGIIIγ – Regenerating islet-derived protein 3 gamma

RIG-I – Retinoic acid-inducible gene I

RNA – Ribonucleic acid

RLR – RIG-Like-Receptor

RT-qPCR – Reverse transcription quantitative polymerase chain reaction

sIgA – Secretory IgA

SOCS – Suppressor of cytokine signalling

STAT – Signal transducer and activator of transcription

TBK – TRAF-family-member-associated NF-kappaB activator (TANK)-binding kinase 1

TCDD – 2,3,7,8-tetrachlorodibenzo-p-dioxin

TCR – T cell receptor

TGFβ – Transforming growth factor beta

T_H cell – T helper cell

TLR – Toll-like receptor

TNF – Tumor necrosis factor

Treg cell – Regulatory T cell

TSLP – Thymic stromal lymphopoietin

VF1 – Virulence factor 1

VP – Viral Protein

VPg – 5' terminal genome-linked viral protein

UV – Ultraviolet

1 Introduction

Chapter 1 INTRODUCTION

1.1 The Intestinal Tract: Structure, Regional Specialisation and Ecosystems

As an organ with the main function of digestion and absorption of nutrients, the alimentary tract presents a huge surface area, covering 200-300 m^2 in adult humans[1], to the outside environment. Unlike the tight seal of the skin, the intestinal epithelial layer forms a relatively leaky barrier to allow for the exchange of nutrients and fluids[2]. In addition to the constant exposure to dietary and environmental antigens, the healthy gut harbours a dense and diverse population of several trillion commensal microrganisms[3], 'symbionts', that, at steady state, peacefully cohabit with the host in a mutually beneficial relationship[4]. The intestinal mucosa also represents the main portal of entry for many pathogens, including viruses, bacteria, parasites and fungi, which can cause pathology and disease by local colonization and induction of destructive inflammation and/or by breaching the mucosal barrier and resulting in systemic infection[5,6]. Furthermore, the recent increased awareness about the far reaching influence of the gut's physiology and its microbial contents in promoting the general wellbeing of an individual, and their central role in relieving, mediating and/or aggravating pathological processes throughout the body, has led to the emergence of such terminology as gut-brain[7,8] and gut-endocrine[9,10] axes. This has been associated with a huge escalation on the number, and in-depth quality, of publications analysing and dissecting the intestinal mucosal system. A common caveat, however, in many of the gut-related studies is the assumption that the whole intestinal tract is a single uniform organ, while most macroscopic (endoscopic), histological and functional differences between its various segments suggest otherwise (**Figure 1.1**). Such an assumption will result in an over-generalized, reductionist and incomplete analysis of an otherwise complex, regionally-specialised and interactive biological system.

1.1.1 **Anatomy and Structure**

Stretching as a continuous tube from the gastric outlet to the anus, the intestinal tract is categorised into two major segments; the **small** and **large** intestine, with the ileocecal valve forming the point of division[1]. The small intestine is further subdivided into the **duodenum**, the most proximal part; followed by the **jejunum**; and then the **ileum**. A single layer of columnar epithelium, made of Intestinal Epithelial Cells **(IECs)**, lines the whole intestinal tract and forms the main physical barrier from the external environment. Together with the underlying Lamina Propria (**LP**) and a thin muscular layer, this epithelium constitutes the **gut mucosa** where most of the immunological processes take place. The LP consists of loose connective tissues embedding a dense layer of blood vessels, nerve connections and afferent/efferent lymphatic channels[1,2]. Although they are separated by a thin basement-membrane, the LP and IEC constitute quite distinct immunological compartments (discussed in more detail in **Section 1.2.1**).

Macroscopically, the small and large intestine differ markedly in length, diameter and organisation. Having a narrower diameter, the small intestine in humans forms multiple coils with a length of approximately 6-7 m. Conversely, the colon is much wider, shorter and extends in straight lines into ascending, transverse and descending colon[1,11]. Scanned from the lumen by endoscopy, the different segments of the gut have quite distinct appearances (**Figure 1.1**). The proximal small intestine (duodenum and jejunum) is characterised by long, thin, finger-like projections extending into the lumen, called **the villi**, with the main function of increasing the functional surface area of the absorptive epithelium. This function is further augmented by the presence of extensive **brush borders** (consisting of microvilli) on the luminal surfaces of these epithelial cells. **The crypts**, which are moat-like invaginations of the epithelium around the villi, are also quite distinctive in this part of the gut. As we go down the length of the small intestine, the villi become progressively shorter and broader until we reach the cecum and colon

where they are almost absent and the surface is rather flat[1,11].

These structural and histological differences are reflected in distinct physiological functions of different gut sections. Well-equipped with numerous digestive enzymes and a huge surface area, the upper small intestine is the main site for digestion and absorption of nutrients. Consequently, pathologies that specifically target this site of the gut, such as Coeliac disease, consistently present with malabsorption and malnutrition[2,12]. Having a less impressive brush border and villi, the terminal ileum contributes much less to nutrition, apart from its essential role in absorption of bile salts and vitamin-B12 due to the presence of specific receptors[1,13]. The main functions of the large intestine, on the other hand, are the reabsorption of water and certain electrolytes and disposal of undigested materials. Protected by a thick overlying mucous layer, the large intestine also harbours most of the commensal microbiota[1,11].

Another common misconception is that the lymphatics of the entire gastrointestinal tract are drained into common Mesenteric Lymph Nodes (**MLNs**). Using a Chicago Blue dye injected into a mouse intestine, Carter and colleagues (1974) clearly demonstrated the segmental and quite separate MLN that drain different regions of the gut[14,15]. Additional subtle differences between various gut sections can be revealed by analysis of the cellular constituents and distribution of different gut-associated lymphoid tissues (**GALT**). The size and density of the **Peyer's Patches**, one of the well-characterised members of the GALT, progressively increase from the jejunum to the distal ileum, where they are particularly concentrated[16]. The numbers of Intra-Epithelial Lymphocytes (IEL) (in the epithelial layer) and the $CD11b^+$ dendritic cells (DC), T_H17 and $CD8^+$ T cells (in the LP) gradually decrease as we go down from the proximal small intestine to the colon, while those of macrophages, $CD11b^-$ DC, Foxp3-expressing regulatory T cells (Treg) and IgA-producing plasma cells gradually increase[17–19](**Figure 1.1**). This distinct cellular distribution can be regarded, at least in part, as a direct consequence of the variation in

the major antigenic stimuli at different sites of the gut. The proximal intestine is mainly influenced by dietary antigenic challenge, the intensity of which reduces as we go down the gut and is replaced by a strong commensal microbiota stimulus in the colon (**Figure 1.1**)[11].

1.1.2 **Intestinal Epithelial Cells (IEC)**

The coexistence of the body's largest population of innate and adaptive immune cells, together with trillions of diverse microbial communities in the gut ecosystem, necessitates the presence of a specialised barrier that maintains the physical segregation, while allowing bi-directional crosstalk, between the two. This barrier consists of a monolayer of polarised IECs that exhibit several physical and chemical adaptations to maintain barrier integrity[20]. As discussed earlier, the IEC-layer is organised into crypts and villi. It is continuously renewed by pluripotent Intestinal Epithelial Stem Cells (**p-IESCs**) that reside at the base of the crypts and are capable of both self-renewal and replication to be transformed into terminally-differentiated absorptive and secretory enterocytes[21]. Except for Paneth cells, which move downwards toward the base of the crypt, all other newly-formed enterocytes migrate along an escalator towards the villous tips, from where they are extruded into the lumen after a 4-5 day life span[11,21]. While about 80% of them are uniformly **absorptive**, highly-polarised columnar cells with brush borders at their apical sites containing many digestive enzymes, the functional diversity of IECs depends on the presence of additional specialised enterocyte-subsets. These include the mucin-producing **goblet cells**, the bactericidal-gatekeeper **Paneth cells** and the hormone-secreting **entero-endocrine cells**, in addition to the **Microfold (M) cells** that play a crucial role in sampling luminal antigens[11,21].

The density and proportion of different IEC-subtypes also show a remarkable regional variation. The frequency of goblet cells, for example, progressively increases along the

length of the gut. While they constitute less than 10% of all epithelial cells in the small intestine, they comprise up to 35% of those of the colon, where they maintain a copious layer of mucus that acts as an effective physical barrier to the abundant microbiota at this site[22,23]. In contrast, Paneth cells are only present in the small intestine, particularly concentrated in the terminal ileum. These Paneth cells are long-lived, relatively large epithelial cells that contain abundant secretory granules. They serve crucial functions in maintaining the stem cell niche by providing the IESCs with essential growth signals, in addition to their indispensable antimicrobial functions[24]. The physiological importance of Paneth cells has been highlighted by the central role of their dysregulation, e.g. defective autophagy and unfolded protein responses, in the pathogenesis of inflammatory bowel diseases (IBDs), mainly Crohn's disease[25,26].

The integrity of IEC physical (tight junctions) and chemical (mucus, antimicrobial peptides) barriers is of paramount importance in maintaining and promoting health. This has been illustrated in a number of pathological conditions; such as the association between intestinal barrier dysfunction and progression of IBD[27], and the evolution of chronic HIV and Hepatitis viral infections due to systemic chronic immune activation secondary to increased bacterial translocation[28,29]. Nevertheless, the IEC layer is not, and should not be viewed as, a mere static impermeable barrier. It has become clear now that it actually represents an integral component of a highly regulated, dynamic communication network that actively participates in shaping the constituents of the microbiota, maintaining gut homeostasis and eliciting mucosal immune responses[30] (discussed in more detail in **Section 1.2.1**).

For many years, attempts had been made to grow and characterise IECs *in vitro;* to analyse their differentiation and dissect their intrinsic immune responses independent of other gut-associated immune cells. These attempts included generation of cell-lines, explants and isolated primary epithelial cell cultures. However, none of these methods

provided long-term maintenance of the crypt-villus morphology or reflected the physiological lineage-development of IECs[31]. This was, in part, due to the strict dependence of epithelial cell survival on contact with the extracellular matrix and the requirement of complex growth-factor cocktails for the maintenance, proliferation and differentiation of p-IESCs[31]. Advances in stem cell biology have facilitated the definition of these p-IESCs and have contributed to a better understanding of epithelial self-renewal and differentiation[32–34]. However, it was only in 2009, that Sato *et al*. finally published a protocol for *in vitro* cultivation of **three-dimensional (3-D) intestinal epithelial organoids** in Matrigel. Matrigel is a laminin- and collagen-rich matrix that polymerises at 37°C and forms 3-D structures mimicking the epithelial basal lamina[35]. Based on insights from the *in vivo* growth-factor dependency of p-IESC, Sato *et al.* were able to define the minimally-required growth-factor cocktail to grow and maintain the intestinal organoids *in vitro*[35]. This contains Epidermal Growth Factor (EGF) that is important for p-IESC proliferation, R-spondin-I (an important Wnt agonist) and noggin (a bone-morphogenic protein, BMP, signalling antagonist). Wnt signalling is a key repressor of differentiation. It is very active in the crypt domain and reduces gradually in the villi, allowing for the differentiation of enterocytes as they move along the crypt-villus axis[34]. BMP, on the other hand, is a negative regulator of crypt formation and stem cell proliferation[36]. Its signalling activity is highest in the villous domain.

Under the culture conditions described above, isolated intestinal crypts round-up and grow into 3-D organoid structures, so-called mini-guts, consisting of a central cyst surrounded by crypt-like budding structures[35,37]. This *in vitro* intestinal organoid is a novel, robust culture system that maintains crypt-villus morphology, stem-cell proliferation and differentiation for a potentially infinite time span[38]. It provides a unique tool to specifically analyse IEC immunobiology and, combined with co-culture models, their interaction with other gut-associated immune cells.

1.1.3 **The Microbiota**

The two distinct, but interdependent, mammalian cell-based communities of the gut mucosa, namely the immune and epithelial-mesenchymal cell compartments, are continuously exposed to, and influenced by, a third element of the gastrointestinal ecosystem created by trillions of co-resident microbiota[39]. Colonisation commences immediately upon birth by the largest population of symbiotic bacteria in/on the body, approximately $1x10^{14}$ bacteria, in addition to numerous and diverse viral, fungal and archaeal species[40,41]. Despite the huge diversity, four bacterial phyla have predominantly adapted to the anaerobic intestinal niche; namely the *Bacteroidetes*, *Firmicutes*, *Actinobacteria* and *Proteobacteria*[42,43].

The host-microbiota relationship is the result of millions of years of co-evolution and can be best characterised as either being a (no-cost) commensalism, in which one partner benefits and the other is unharmed; or a mutualistic relationship, in which both partners benefit[44]. The availability of reduced-price, gene-sequencing-based technologies has allowed for a more comprehensive characterisation of bacterial members of each type of the relationship and the identification of 'pathogenic' microbial-community profiles associated with several systemic and local diseases[45]. Moreover, it has facilitated the exploration of other, non-bacterial, constituents of the microbiota, especially the gut Virome[46].

As in any other biological system, there are always 'cheating' players that exploit the norm to obtain benefit without helping to create it. This can occur, for example, by acquiring a mutation that redirects resources toward increased fitness and faster replication of the microorganism itself instead of contributing to pathogen-interference or detoxification[44]. In a healthy gut, the mucosal immune system plays a determining role in developing and promoting anti-exploitation responses to prevent the dominance and systemic spread of the 'cheating' opportunistic and pathogenic organisms[44]. The

adaptations of the epithelial barrier for sampling of luminal contents can accommodate limited and controlled bacterial and antigen translocation to direct appropriate tolerogenic or anti-pathogen responses. By constantly sampling the intestinal contents and initiating local protective immune responses, the gut-associated immune system maintains a state of informed awareness about the composition of the gut microbiota. This state allows the microorganisms to compete for resources in the gut, generating a robust disease-resistant community, while at the same time 'usually' preventing uncontrolled exploitation of the limited resources by potentially harmful organisms[44]. In addition to the local immune system and IECs, the composition of the bacterial microbiota is directly influenced by external environmental factors; especially the diet[47] and the use of broad-spectrum antibiotics that alter the taxonomic, genomic and functional capacities of the human gut microbiota, with effects that are usually rapid and transient but sometimes persistent[48].

The number, composition and diversity of microorganisms varies greatly between different segments of the gut. From being absent to very low (100-1000 organisms/ml) in the harshly acidic environment of the stomach, the number of bacteria progressively increases down the alimentary tract to reach up to 10^{12} per ml in the colon[11]. Some reports suggest a denser bacterial population in the human caecum and terminal ileum than is seen in the colon[49]. Aerobic bacteria are, generally, more prevalent in the upper small intestine while anaerobic species dominate the large intestine[11]. Microbial diversity is most evident in the caecum and least diverse in the distal colon[50]. Both the density and diversity of gut microbiota have been shown to be relevant in many clinical conditions and pathologies. In mice, the higher incidence of tumors in the caecum has been attributed, at least in part, to its greater density of bacteria[51]. Dysbiosis, i.e. alteration in the composition, density and/or distribution of intestinal microbiota, has been linked to the development and progression of many different diseases ranging from psychiatric

illness to metabolic, inflammatory, allergic and autoimmune diseases[52,53].

Among the many substantial benefits of 'healthy' balanced microbiota profiles are the contribution to digestion, provision of essential metabolites such as vitamin-K and biotin, occupation of niches that would otherwise be available to pathogens and promoting immune system development[54]. This is clear in germ-free mice, whose growth is severely compromised in terms of development, immune function and lymphoid organ organisation[55]. Furthermore, it has become increasingly evident that colonization by individual members of the commensal microbiota can influence the regional specialization of the immune system along the length of the intestine. The presence of Segmented Filamentous Bacteria (SFB) in the terminal ileum of mice enhances the production of IgA antibodies and the polarization of T_H17 cells, contributing to the variation in numbers of T_H17 cells observed between mouse-strains from different suppliers[56,57]. Conversely, colonization of the colon by certain anaerobic Clostridia species drives the preferential generation of Treg cells, apparently by promoting a TGFβ-rich environment[58]. Additionally, short-chain fatty acids such as butyrate, acetate and propionate that are produced by colonic bacteria play a central role in influencing the immune functions in this part of the gut. The best characterized example of this is the enhancement of the number and functions of Foxp3-expressing Treg in the colon by the production of butyrate[59].

More recently, some of the beneficial functions of the understudied viral component of the microbiota (Virome) have been elucidated[60], and its role in determining the susceptibility to, and progression of, certain pathologies such as IBDs has been identified[61,62] (discussed in **Section 1.2.2**).

1.2 Intestinal Mucosal Immune System

1.2.1 The Complexity and the Organization

Faced with overwhelming antigenic challenges, and in order to fulfil the delicate task of mounting robust, protective, non-destructive responses to invading pathogens, whilst at the same time maintaining a state of tolerance and non-responsiveness to harmless food antigens and commensal organisms, the intestinal mucosal immune system has evolved as a distinct and sophisticated immunological organ that functions in a flexible, dynamic and multi-layered manner.

At the centre of this complex immune system is the GALT, which consists of a network of highly organized lymphoid structures, including Peyer's Patches (PPs), colonic patches, crypto-patches, isolated lymphoid follicles (ILFs) and mesenteric lymph nodes (MLNs). They are strategically located along the entire length of the gastrointestinal tract and represent the main **Inductive Sites** of the gut immune system[63]. Moreover, they are essentially equipped with all adaptations necessary for luminal antigen sampling, optimizing the chances of naïve lymphocytes encountering their specific antigens, induction of antigen-specific T and B cell responses, and for supporting the activated lymphocytes and their initial differentiation. The PPs, for example, located mainly on the anti-mesenteric side of the small intestine, form a lymphoid microenvironment made up of a large B cell follicle, an inter-follicular T cell region and numerous intervening antigen presenting cells; dendritic cells (DCs) and macrophages[63]. Luminal antigen sampling in the PPs is mediated mainly by the Microfold (M) cells, which represent a unique adaptation of the follicle-associated enterocytes that allows for the uptake and transport of antigens to DCs in the adjacent subepithelial dome region of the PPs[64]. A similar sampling mechanism may occur in ILFs of the colon and in the caecal patches, which were recently suggested to be the main site of induction of IgA-producing plasma cells[65]. Moreover, there is evidence for involvement of goblet cells[66] and trans-epithelial

DCs[67] in active sampling of the gut lumen at sites distant from organized lymphoid tissues. The distinct $CD103^+$ DCs within the sub-epithelial dome are capable of migrating within the PPs, between the basolateral surface of the M-cells and the inter-follicular T cell area to present antigens, and to travel to distant sites such as the MLNs and the LP to orchestrate an adaptive immune response[68]. Moreover, they play an important immunomodulatory role. Depending on the context and under the influence of the overlying epithelial cells, they can induce either tolerance or protective immune responses[69,70]. For instance, in the resting-state; i.e. in the absence of pathogens and the presence of a regulatory cytokine milieu at the enteric surfaces, these DCs release interleukin (IL)-10, TGF-β and vitamin A metabolites that favour the induction of $Foxp3^+$ Treg[71]. Moreover, they can present antigens without up-regulating costimulatory molecules (e.g. CD80/CD86) leading to abortive or Treg responses (reviewed in [69]).

Activated lymphocytes egress from the PPs via the lymphatic system to the MLNs and then to the circulation. Ultimately they take residence in the LP of the intestinal tract, which represents the main **Effector Site** of the gut immune system[72]. The final migration to the LP is dependent on the interaction of site-specific adhesion molecules, such as $\alpha_4\beta_7$, on activated lymphocytes with specific mucosal addressin cell-adhesion molecules on the surface of high-endothelial venules in the LP. Migration is further tuned and refined by the interaction of chemokines, such as CCL25 which is constitutively expressed by IECs, with chemokine receptors, e.g. CCR9, on the surface of activated lymphocytes[73]. The LP is, therefore, occupied by a heterogeneous population of effector-memory and Treg lymphocytes, mononuclear phagocytic cells (macrophages and DCs) and IgA-producing plasma cells (reviewed in [74]). The gut-associated T cells, although frequently displaying an alert-phenotype and hallmarks of recent activation, must remain immunologically hypo-responsive to innocuous antigens while retaining their capacity to respond swiftly to a pathogenic challenge[74,75].

Unlike the migratory $CD103^+$ DCs, $CX_3CR_1^{hi}$ intestinal-resident macrophages lack migratory properties in steady-state condition[76]. In addition to their important functions in phagocytosis and clearance of translocated microbes and apoptotic cells, they maintain a close proximity to and are directly influenced by IECs to maintain steady-state tolerance by producing IL-10 that promotes the survival and local expansion of previously primed Treg cells[77].

NK, NKT, granulocyte and myeloid cell populations are also present in the LP, as well as a recently identified immune cell population of innate lymphoid cells (ILCs). These ILCs are revealing themselves as crucial determinants of lymphoid tissue organogenesis and, again under the influence of IECs, as important modulators of gut homeostasis and immunity[78]. ILCs lack specific markers of conventional innate and adaptive immune cells and are characterised by their differential cytokine expression and developmental requirements. Sharing functional similarities with the three major $CD4^+$ T cells subtypes; i.e. T_H1, T_H2 and T_H17, they are classified into group1, 2 and 3 ILCs, respectively[78–80].

This extensive intestinal immune system is separated from the external environment by a monolayer of polarised **IECs**. By maintaining a continuous cell layer sealed by tight junctions and through secretory adaptations (mucin and antimicrobial peptides), IECs effectively sustain a physical and biochemical barrier integrity[2,20]. This is further augmented by the active transcytosis of secretory IgA complexes across IECs[81,82], providing an adaptive immunity component to the epithelial barrier that regulates commensal bacterial populations and represents the first line of antigen-specific immune defence. Moreover, IECs actively participate in the maintenance of intestinal homeostasis and induction of the appropriate immune response in the gut[30]. Being frontline sensors for microbial encounters, IECs are equipped with a diverse range of pattern recognition receptors (PRRs), reviewed in[83], that enable them to dynamically respond to microbes. Unlike the body's sterile sites, where recognition of foreign microorganism by PRR

initiates a rapid cascade of strong pro-inflammatory responses, the proximity of IECs to an abundance of stimuli from symbiotic commensals necessitates specialised mechanisms to maintain altered or hypo-responsive PRR signalling, and to differentiate between friends (commensal microbes) and foes (pathogens). This ability to express a wide range of negative regulators, in addition to the subcellular segregation and polarised distribution of PRRs in the basolateral and apical surfaces, allows the IECs to act as 'sentinels' for maintaining homeostasis and to differentiate between signals derived from commensal and pathogenic organisms based on their anatomic location[83]. Furthermore, by producing and controlling the levels of such cytokines as thymic stromal lymphopoietin (TSLP) and TGF-β, IECs directly instruct the function of other gut-associated cells[83–85]. As discussed earlier, the IEC-conditioned DCs, macrophages and/or ILCs play a major role in maintaining tolerance and in shaping the innate and adaptive mucosal immune responses in the gut. Moreover, a unique population of intestinal T cells, **IELs**, is located within this epithelial layer above the basement membrane and is thought to play a role in promoting intestinal homeostasis and immunity[86] (discussed in **Section 1.2.3**). Production of IL-7 and IL-15 by IECs is important for the maintenance of these IEL populations[87], while IEC-mediated production of a proliferation-inducing ligand (APRIL) induces T cell-independent class switching of mucosal B cells[87,88].

Thus, under steady-state conditions, and despite the enormous load of microbial and dietary antigens present in the gut lumen, an appropriate immunological tolerance in the gut microenvironment is maintained by a tightly regulated, multi-layered network of different cells. The mechanisms by which this tolerance is broken by oral allergens or pathogenic challenges are, however, much less understood. One intuitive possibility is that the control of inflammation in the intestine may be adapted to rely on the recognition of 'danger' signals associated with pathogenesis, rather than on the presence of microbial signal alone[89].

1.2.2 **Intestinal Mucosal Immune System: Modulation by Viral Infections**

Being one of the main portals of entry for viral pathogens, intestinal mucosal surfaces are commonly involved in the induction, polarization and maintenance of immunity against viral infections[6,90]. Gastrointestinal viral infections constitute a major threat to the population, especially at the extremities of age, and cause significant morbidity and mortality worldwide[91]. However, the majority of the intestinal primary and secondary exposures to viruses are asymptomatic or induce only minor symptoms[92,93], implying efficient mechanisms are employed by the gut mucosa to clear pathogenic viruses or at least to contain them with minimal inflammation and injury.

The first line of defence against invasive viruses is the physical and chemical barrier produced by specialised enterocytes to limit viral spread[94]. At the apical surfaces of the polarized columnar epithelial cells lining the gut, a 500-nm thick glycocalyx layer covers the negatively charged microvilli and limits the uptake of antigens whilst promoting the absorption of nutrients[95]. This is overlaid by a mucin-rich layer containing glycoproteins that competitively bind to cellular surface receptors and act as a barrier to microbes such as rotavirus[96]. Secretory IgA, sIgA, produced by LP plasma cells and transported across the IEC to the lumen, plays an important role in neutralisation and immune-exclusion of infectious viruses[97]. In fact, the induction of rotavirus-specific intestinal IgA correlates with clearance of infection and protective immunity (reviewed in [97]). Furthermore, the IECs, especially the Paneth cells, are significant sources of many soluble-humoral factors and antimicrobial-peptides (including defensins, cathelicidin and lactoferrin) that play a role in innate immunity against enteric viral infections. They are involved in opsonisation and enhancement of phagocyte-mediated killing, potentiation of cellular surveillance, pathogen recognition and direct disruption of viral envelope membranes[98].

During viral infections, virtually all nucleated cells can respond by producing, and being influenced by, type-I Interferons (IFNs) to limit viral replication and spread[99].

However, it is the plasmacytoid DCs (pDCs) that are regarded as the main/major source of type-I IFNs, owing to their ability to respond to a broad range of viral stimuli and rapidly release large amounts of type-I IFNs[100]. Nonetheless, the sheer number of IECs that can sense, and be infected by a replicating virus dictates that they should also be considered as a significant source of type-I IFN in the context of enteric viral infections. Moreover, the influence of IECs on the activation of pDCs can serve to amplify this IFN signalling process[90].

To ensure immediate antiviral defence, IECs and mononuclear phagocytes at enteric surfaces employ multiple PRRs in different cellular compartments to sense the different viral Pathogen-Associated Molecular Patterns (PAMPs)[101,102]. Toll-Like Receptors (TLRs) 3, 7, 8 and 9 are localized within endosomal compartments and recognize viral dsRNA, ssRNA and CpG-containing DNA. The two members of the RIG-Like-Receptor (RLR) family, retinoic acid-inducible gene I (RIG-I) and melanoma differentiation-associated protein-5 (MDA5) are localized in the cytoplasm to recognize 3`-triphosphate bearing RNA and long dsRNA viral structures, respectively[103]. The nucleotide-binding oligomerization domain (NOD)-Like-Receptor, NOD2, can also act as a cytosolic PRR for ssRNA viruses, triggering the activation of interferon-regulatory-factor 3 (IRF-3) and the production of IFNβ[104]. Notably, Danger-Associated-Molecular-Patterns (DAMPs), released subsequent to the death of virally-infected cells, can also trigger the activation of PRRs[101].

As discussed earlier, the PRR-signalling in the gut is tightly regulated to maintain tolerance to the abundant microbial flora (reviewed in [83,85]). Infection with a virulent virus modulates this tolerance toward a more inflammatory-state. Indeed, viruses like rotavirus and coxsackie virus were shown to induce a significant increase in IEC-expression of viral PRRs[105]. Engagement of multiple, diverse viral sensors induces varying signalling pathways that converge on phosphorylation of the TBK/IKKε

complex and activation of downstream IRF3, IRF7 and NFκB pathways to induce the production of type-I and III IFNs in addition to other inflammatory cytokines[106,107] (and reviewed in[99]).

IFNs are potent immunomodulators that are readily produced in response to a variety of viral and bacterial pathogens[6]. Based on differences of biological activities and receptor usage, three distinct types of IFNs are described; type I, II and III. Although all the types are involved in mediating protective responses against pathogenic viruses, only type I and III IFNs are directly produced in response to viral infection[6]. Type-I IFN consists of 13 subtypes of IFNα and a single IFNβ (in humans), and all signal through a common receptor composed of IFNAR-1 and IFNAR-2 subunits[108]. Type-II IFN consists of a single member, IFNγ, which mediates its response by signalling via a receptor consisting of INFGR1 and IFNGR2 subunits[109]. IFNλ1, 2 and 3 constitute the three members of type-III IFN that signal through a heterodimer (IL-28Rα, also known as IFNLR1, and IL10Rβ) receptor and share many of the intracellular signalling pathways and biological activities of type-I IFN[110]. Type-I IFNs and their receptor, as well as the IFNγ receptor, are widely expressed by many cell-types, in contrast to the more restricted expression of IFNγ, type-III IFNs and their receptor IFNLR1. IFNγ is mainly produced by T and NK cells[109] and type-III IFNs by leucocytes, DCs and epithelial cells[110,111]. The type-III IFN receptor is primarily expressed by epithelial cells[110]. In fact, it has been shown that mice lacking a functional type-III IFN receptor have impaired control of oral rotavirus infection. The type-I IFN-system alone was not enough to protect against the infection and systemic administration of IFNλ, but not type-I IFN, to suckling mice was sufficient to suppress rotavirus replication in the gut[112]. This unique ability of the type-III IFNs to induce a protective antiviral response in intestinal epithelial cells that is independent of, and not overlapping with, type-I IFN-induced antiviral responses is quite intriguing.

It has been suggested that this phenomenon could be explained by the IECs-restricted expression of the IFNλ–receptor and the differential expression of type-I IFN receptor in the apical vs the basolateral surfaces of the IECs[112].

Upon binding of type-I and III IFNs to their corresponding receptors, they trigger a JAK-STAT signalling pathway that culminates in phosphorylation, dimerization and nuclear translocation of STAT1-STAT2 molecules. In the cytoplasm, this dimer recruits IRF-9 (to form interferon-stimulated gene factor 3 (ISGF3)), translocates to the nucleus and induces hundreds of IFN-stimulated genes (ISGs)[108,110] including more type-I IFNs. Then, in an autocrine and paracrine positive-autoregulatory manner, these IFNs induce additional ISGs resulting in a non-specific 'antiviral state'. The ISGs, such as RNA-activated protein kinase (PKR), ISG15, RNAseL, 2'-5'-oligoadenylate synthetase (OAS), radical S-adenosyl methionine domain containing 2 (Rsad2), RNA specific adenosine deaminase (Adar) and myxovirus resistance (Mx) proteins, directly impact the early and/or late stages of the virus life cycle with involvement in preventing viral replication, degrading viral RNA, inhibiting viral functions and priming neighbouring cells to enter a refractory antiviral state[113]. In addition, type-I IFN can activate the mitogen activated protein (MAP) kinase and the phosphoinositide 3 (PI3) kinase signalling pathways that also contribute to the antiviral effect[108], regulate inflammasome activation, production of other inflammatory cytokines and mediate apoptosis[114]. Apoptosis provides a mechanism of limiting viral replication without inducing inflammation and can, actually, facilitate the induction of the adaptive immune response[115]. In murine reovirus infection, for example, while enterocytes stained for both structural and non-structural viral proteins, the gut DCs contained only structural components co-localized with apoptotic inclusions and cytokeratin[116], suggesting that DCs can obtain viral antigens from apoptotic enterocytes. Moreover, type-I IFN can also help in bridging the innate and adaptive antiviral immune responses by enhancing the recruitment and maturation of the $CD103^+$

DC, up-regulating MHC class-I molecule expression by IECs, promoting the differentiation and expansion of virus-specific T cell responses, and contributing to generation of antibody responses to mediate neutralisation of virus particles[90,117].

However, it is important to note that IFN signalling is not always pro-inflammatory and, depending on the context, it can indeed contribute to gut homeostasis by both immune-activating and suppressing signals[6]. There is autoregulatory induction of the anti-inflammatory suppressor of cytokine signalling proteins, SOCS-1 and 3[118], the induction of pDC apoptosis in several systemic viral infections as a negative feedback to type-I IFN production[119], and it has also been reported that type-I IFN can drive anti-inflammatory IL-10 and IL-27 production by mononuclear phagocytes and negatively regulate IL-12 expression by DCs during certain viral infections[120,121]. Moreover, a recent report demonstrated that IFNλ acts synergistically with IL-22 to maintain homeostasis, control rotavirus infection and prevent intestinal tissue damage[122].

Furthermore, type-I IFN is constitutively expressed in the intestine[123]. In addition to the expression of IL-10, small intestinal and colonic LP $CD11c^+$ mononuclear cells of conventionally-housed mice were found to constitutively produce IFNβ with high mRNA levels of the downstream molecules, such as ISGs (reviewed in [6]). The driving signal for this basal IFN production in the intestine has long been poorly understood. But recent advances in sequencing technologies and bioinformatics analysis unleashed huge efforts to discover and characterise the viral component of the microbiome and may have provided an answer to why there is constitutive type-I IFN expression. Largely composed of bacteriophages, the human gut Virome was found to show a substantial interpersonal variability regardless of genetic relatedness[124], and a robust intrapersonal stability, in spite of diet modification[125]. Interestingly, in the steady-state and unlike the variable level of expression of the bacterial detection machinery, many mRNAs of viral detection PRRs in mice, especially TLRs, as well as all IFN-receptors and their downstream

mediators, such as JAK1, STAT1, IRF-3 and 9, are stably highly expressed by the IEC throughout the whole length of the small intestine (Dr Marc Veldhoen, personal communication). This has not been confirmed yet by detection at the protein level.

A direct effect of basal type I IFN signalling on IEC function has been described by a recent report, in which mice with an IEC-specific, conditional deletion of the type-I IFN-receptor displayed epithelial cell hyper-proliferation, Paneth cell expansion and increased tumour burden in response to a chemical carcinogen that was dependent on the specific microbiota present in these mice[126]. Furthermore, in an elegant experiment using a model of persistent Murine Norovirus (MNV-CR6), Kernbauer *et al.* (2014) were able to demonstrate that a single virus can functionally replace some of the beneficial effects of the microbiota, and reverse many of the structural and immunological defects that arise in the absence of the microbiota (by antibiotic treatment or using germ-free mice)[60]. The reversal of the abnormalities was partially dependent on type-I IFN signalling in addition to yet unidentified signalling pathways[60]. However, infection with the same persistent virus (MNV-CR6) can also cause pathology: it has been shown to contribute to development of the abnormal Paneth cell phenotype that characterises IBD in mice hypomorphic for the autophagy gene (*Atg16L1*)[62]. MNV also exacerbates intestinal inflammation in *Il10*$^{-/-}$ mice; a commonly used animal model of IBDs[127]. These data suggest a clear, albeit simplistic, example of an environmental factor triggering a disease phenotype in a genetically-susceptible host. They also demonstrate the ability of a single virus to mimic the double-edged effects of the bacterial microbiota in being both beneficial and a contributing factor to disease, and they open the door to redefine the concepts of persistent asymptomatic infection, commensalism and opportunism.

Taken together, these new insights highlight the previously overlooked importance of the Virome and baseline type-I IFN signalling in maintaining intestinal mucosal immunity, homeostasis and function.

1.2.3 **Intestinal Mucosal Immune System: The role of Intraepithelial Lymphocytes**

IELs, which reside within the epithelial layer of the intestine (**Figure 1.2**), compose a large T cell compartment that is highly conserved in all vertebrates[128–130]. Their unique location above the basement membrane in direct contact with IECs and in close proximity to antigens in the lumen is combined with their ability to respond swiftly without the need for clonal expansion or priming. This qualifies them to be a potent frontline immune defence against invading pathogens[128,129]. However, and despite being described for decades, relatively little is known about how exactly they function in this location in the intestinal mucosa especially regarding antiviral responses.

Although almost exclusively T cells, the gut IEL compartment is extremely heterogeneous, consisting of several diverse subsets that differ in the expression of T cell receptors (TCRs), co-receptors and activation markers[129] (**Figure 1.2**). The proportion of these various IEL subsets in the gut is both species and site specific. In humans about 70% of small intestinal IELs are $CD8^+$ T cells, with alpha/beta (αβ) TCR^+ IEL the predominant subtype[131]. Murine small intestine, in contrast, contains a much higher percentage of gamma/delta (γδ) TCR^+ IELs, representing about 70-75% of the total $CD3^+$ T cells in the duodenum and jejunum[132]. This percentage decreases significantly in the ileum[132].

Within this compartment, the diverse population of IELs exhibits a number of common properties that distinguish it from systemic conventional T cells. Firstly, they all display an antigen-experienced phenotype with expression of activation markers, such as CD44 and CD69 (reviewed in [131]). Secondly, they do not recirculate as indicated by studies using parabiotic mice and intestinal grafting[133], and they constitutively express CD103 (also known as the $\alpha_E\beta_7$ integrin) that interacts with E-cadherin on the basolateral surfaces of IEC and is considered to be one of the main adhesion molecules involved in retention of IELs within the epithelial layer[134]. Thirdly, unlike systemic and LP

lymphocytes, $CD4^+$ T cells are under-represented in the IEL compartment[135]. Conversely, $CD4^-CD8^-$ 'double negative' (DN) cells, which are rare in the systemic circulation, can account for more than 10% of murine small intestinal IELs[136]. Moreover, the majority of IELs, especially in the small intestine, express the CD8αα homodimer[137], which is essentially absent from the systemic circulation[138]. CD8αα is a marker of T cell activation[139]. Unlike CD4 and CD8αβ co-receptors, CD8αα expression results in sequestration of the intracellular signalling components outside the immunological synapse[139], hence it is considered to be a TCR repressor that sets a new threshold for activation to prevent (or reduce) the potential for unnecessary or self-destructive immune responses[139,140]. Finally, unlike conventional T cells, the majority of IELs contain abundant cytotoxic cytoplasmic granules and characteristically express both activating and inhibitory NK cell receptors[141,142], which allow them to be rapidly activated by TCR-independent mechanisms. Thus, the IELs can be typified as stress-sensing, highly regulated immune cells that display an alert-phenotype without full activation.

Despite the heterogeneity, two broad subsets of gut IELs can be characterized (**Figure 1.2**) based on similarities of the gene expression profiles[128], the nature of cognate antigens they can recognize and the proposed mechanisms and pathways for their activation[129]. The first subset is referred to as 'natural' IELs (previously termed type-b[143]), and consists mainly of $CD4^-CD8^-$ (DN) cells, cells expressing a TCR composed of the γδ chains and cells that express the CD8αα homodimer together with the αβ TCR. They do not express either CD4 or CD8αβ co-receptors. These 'natural' IELs are progeny of bone-marrow precursors, have a very restricted TCR diversity that tend to include self (auto)-reactive repertoire[142,144], and populate the gut very early in life, *in utero*[145]. It is thought that they acquire their activated-phenotype by going through a thymic self-antigen based positive selection process that results in functional activation, followed by direct migration to the gut[137]. However, neither the identity nor the nature

(proteinaceous or non-proteinaceous) of these putative autoantigen(s) has been identified[128]. Moreover, maturation of these cells in the thymus is a subject of considerable debate with several pieces of evidence from athymic (nude), thymectomized and *Rag*-deficient mice that were reconstituted with bone-marrow from nude mice, suggesting they are a thymic-independent lineage[146,147].

In contrast, the second subset; referred to as 'induced' or type-a[143] IELs, are the progeny of conventional CD8αβ$^+$ or CD4$^+$ TCRαβ$^+$ T cells that are activated post-thymically in response to non-self antigens[129]. Therefore, they comprise mostly tissue-resident memory (T_{RM}) cells that are recruited back to the epithelial compartment after originally being activated in the GALT. In line with being memory cells, global analysis of the TCR-beta chain sequencing revealed that the TCR-repertoire of these 'induced' IELs is oligoclonal, unlike the polyclonal nature of conventional naïve T cells in the periphery[144]. However, compared to memory T cells in other tissues, the co-stimulatory requirements for these 'induced' IELs are distinct[148]. For example, while the co-stimulatory CD40-CD40L interaction is redundant for splenic memory T cell activation, CD40L triggering was shown to be essential for the CD8αβ$^+$ TCRαβ$^+$ induced IEL response[149].

It has been speculated that the early presence of natural IEL in the gut, before birth, allows for a stress-sensing surveillance that recognises conserved antigens and/or responds to inflammatory cytokine cues[129]. A surveillance process that is expected to be tolerant to harmless antigens but protective against invasive stress-inducing pathogens. Indeed, human γδ TCR$^+$ intestinal IELs were shown to interact with (recognise) the stress-induced MHC class I-related (MICA and MICB) molecules[150]. This recognition was independent of antigen processing[150], and most likely involved the stimulatory NKG2D receptors[128]. On the other hand, in response to exogenous antigens exposure, the induced IELs gradually accumulate with age[151]. It has been suggested that this gradual accumulation allows for the development of a focused and 'personalized' mucosal

immune repertoire that is directed against the most likely to be re-encountered environmental antigens[129]. With the passage of time, the induced IELs gradually become the dominant population, while the natural IELs representing a minor population in spite of remaining steady in actual numbers[129,152].

Regardless of the subtype, the maintenance of all IELs is dependent mainly on the constitutive production of IL-7[153] and IL-15[87] by IECs. This is influenced by the intestinal microflora; for example TLR-mediated MyD88-dependent induction of IL-15 by IECs had been shown to be essential for maintenance of CD8αα$^+$ αβ TCR$^+$ and γδ TCR$^+$ IELs[154]. Furthermore, the gut IEL-compartment is also directly affected by the diet. Replacing intact dietary protein, by feeding wild-type mice an equivalent amount of amino-acid based protein(antigen)-free diet from the time of weaning, results in poor development of intestinal immune cells similar to that seen in germ-free mice, with a significant reduction in CD3$^+$ IEL populations[155]. Similarly, interruption of vitamin D signalling, by knocking-out its receptor, results in an intrinsic proliferative defect of the CD8αα$^+$ IELs with a subsequent reduction in their numbers[156].

Collectively, these data, and others, highlight the importance of the aging process and the diet, in addition to the microbiota, as major modulating factors of the intestinal mucosal immune system.

1.2.4 **Intestinal Mucosal Immune System: The Impact of Aging**

A growing body of evidence indicates that the immune system is drastically affected by the inevitable, natural, yet ill-defined aging process[157–159]. Aging, often compounded by malnutrition and dehydration, results in a significant deterioration of both innate and adaptive immune responses with a consequent increase in mortality due to increased incidence of infections and cancer[160]. Moreover, studies in healthy subjects revealed that advanced age is associated with a low-grade chronic hyper-inflammatory state, referred to as 'inflammaging'[161], that has been attributed to elevated circulating pro-inflammatory 'geriatric' cytokines levels, including IL-6, TNF and IL-1β.

Reportedly the age-associated alterations and defects arise in the gut mucosal immune system earlier than in the systemic immune compartments[162]. However, relatively little is known about the precise cellular and molecular mechanisms of gut mucosal immunosenescence[163].

Examples of the reported age-associated changes in gut immunity are: reduced ability to establish oral tolerance to antigens[164], reduced levels of sIgA[165] and alteration of the microbiota community[166]. These are associated with intrinsic regenerative defects in the aging gut-epithelial stem cells[167], significant decline of Paneth cell numbers and secretory function[168], alteration of the amount and chemical composition of the mucus produced by goblet cells[169], and impairment of the functional maturation of M cells[170]. Moreover, in the context of intracellular parasite infection, aged gut-derived DC were found to be suboptimal at priming T cells and were characterized by a significant decline of IL12p70 and IL-15 production accompanied by decreased expression of CD80/CD86 co-stimulatory molecules[171]. Exogenous application of IL-15 was sufficient to restore the co-stimulatory signal and the ability of the aged DCs to prime the T cell response[171]. Interestingly, under steady-state conditions and unlike the young gut-derived DCs, the aged DC fail to induce TGFβ secretion and the differentiation of Treg cells. Instead they

promoted T cells to produce IFNγ[172]. The likelihood of a more pronounced pro-inflammatory activity of the aged gut-derived DCs was not assessed. However, IECs can be a good source of the 'geriatric' cytokines and recent animal studies show that aging can increase IEC production of pro-inflammatory cytokines such as IL-1β and IL-6[173]. Therefore, it has been reasonably suggested that the low-grade chronic 'inflammaging' state typical of old age may originate from the intestinal environment[174]. In addition, or as a consequence of the above, the composition of the intestinal microbial communities is significantly altered in old age[166] with evidence suggesting the growth of more disease-promoting microbial populations[175].

Despite the growing attention and amount of literature concerned with the impact of aging on intestinal mucosal immunity, considerable gaps still exist in our knowledge especially in the cause-effect relationship of the various changes observed with aging in the gut and the response to external influences; i.e. commensals, diet and pathogens[163]. Basic aspects, such as the expression of PRRs by aged IECs and gut associated myeloid cells or the ability of aged IECs to mount an effective anti-pathogen responses were not assessed and are currently unknown.

1.2.5 **Dietary Influences on Intestinal Mucosal Immunity: A Focus on the Role of Aryl Hydrocarbon Receptor (AhR)**

Evidence for the influences of nutritional status and dietary choices in the development, maintenance and shaping of the gut mucosal immune system are continually emerging[176,177]. Protein-energy malnutrition increases the susceptibility of the host to severe and prolonged enteric viral infections[178]. By using a mouse malnutrition-model of Norovirus (MNV) infection, thus minimising host genetic and other environmental variables, Hickman *et al.* (2014) were able to demonstrate a direct (causal) link between malnutrition and the increased severity of MNV infection, as defined by weight loss, reduction of protective immunity and enhanced viral evolution[179]. Furthermore, several epidemiological studies have associated the so-called 'Western diet', deficient in vegetables and micronutrients, with an increased prevalence of several inflammatory disorders, including inflammatory bowel disease[180,181]. Nutrients and pathogens share a number of cellular sensing pathways that can be the mediators for the nutrient-induced chronic inflammatory disorders[182]. Moreover, the impact of the dietary components on the intestinal mucosa can be observed at several levels including the modulation of IEC function and permeability[183], the modification of microbial load and composition[184], in addition to the effects on the development, recruitment and function of the various lymphocyte populations and immune cells in the gut[177]. Many of the ligand-activated transcription factors involved in the development and function of immune cells are directly influenced by or, are themselves nuclear receptors for naturally occurring molecules such as lipids and vitamins[185], thus providing a connection between the cellular transcription machinery of immune cells and dietary components. For example, the nuclear receptors for vitamin A and D metabolites are highly expressed by immune cells occupying the barrier mucosae, i.e. the major sites for acquiring these essential vitamins. By mediating the response to their corresponding ligands, those receptors have

been shown to have very important effects in the differentiation, function and homing properties of T and B lymphocytes and to significantly contribute to gut homeostasis[177,186].

Recently, more attention has been drawn to the Aryl Hydrocarbon Receptor (AhR), an evolutionary highly-conserved basic Helix-Loop-Helix (bHLH) cytosolic transcription factor[187] that is widely expressed in the body, but again significantly high expression has been detected in the immune cells of the barrier sites[188].

The AhR belongs to the family of Per-Arnt-Sim (PAS) domain-containing sensing proteins and has been extensively studied by pharmacologists and toxicologists as a mediator of responsiveness to xenobiotics and to environmental pollutants such as dioxin (and its most potent subtype 2,3,7,8-tetrachlorodibenzo-p-dioxin; TCDD)[189]. Intensive research over three decades has linked AhR signalling to many biological processes such as cell cycle regulation, circadian rhythm and reproduction[190–192]. However, the main physiological function of this evolutionary highly conserved receptor[193] remained elusive and poorly understood. In the absence of a ligand, AhR is found in the cytoplasm bound to chaperon proteins; namely Heat-Shock-Protein-90 (HSP90), co-chaperone (p23) and the AhR-interacting protein (AIP)[188] (**Figure 1.3**). Upon ligand binding, AhR translocates to the nucleus, where it dissociates from the chaperons and hetero-dimerizes with its protein partner AhR-Nuclear Transporter (ARNT). The AhR-ARNT complex binds to genomic DNA regions containing the dioxin-response element (DRE) binding motifs, and induces the transcription of several genes including cytochrome-P450 enzymes; such as CYP1, TCDD-inducible poly(ADP-ribose) polymerase (TIPARP), aldehyde dehydrogenase, and the AhR repressor protein (AhRR)[188,194,195] (**Figure 1.3**).

The physiological functions of AhR might require transient and tightly controlled signalling, as sustained AhR signalling, mediated by dioxin for example, results in pathological consequences[196]. Moreover, a number of regulatory mechanisms are already

in place in the AhR system to ensure this controlled and transient signalling. Examples of these regulatory mechanisms include; the disruption of the AhR/ARNT complex by AhRR, proteasomal degradation of activated AhR and autoregulatory ligand metabolism by the cytochrome-P450 enzymes[188] (**Figure 1.3**). It is important to note that many of the reported AhR functions are mediated through interaction with many other cellular signalling pathways[197]. DRE motifs were found in the promoter region of many genes relevant to immune responses, such as the genes encoding TLRs, IL-6 and TNFα[188]. An interesting interaction between the AhR, STAT1 and NFκB molecules has been detected by Kimura *et al.* (2009)[198]. They observed significantly augmented inflammation in response to LPS in AhR-deficient peritoneal macrophages. Analysis of wild-type macrophages revealed a physical association between activated AhR and STAT1 molecules. This AhR-STAT1 complex blocked the inflammatory cascade initiated by NFκB in response to LPS, a regulatory mechanism that is absent in the *Ahr*$^{-/-}$ macrophages[198] (**Figure 1.3**). The physical interaction between activated AhR and STAT1 molecules had also been shown to down regulate the activity and phosphorylation of STAT1, thus reinforcing the T_H17 transcriptional program by blocking the alternative pathway that leads toward T_H1 effector differentiation[199].

In line with being an environmental sensor, AhR is strongly expressed by different cell types at the barrier sites; i.e. the gut, skin and lung. The hematopoietic immune cells with a high level of AhR expression include T_H17 and, to a lesser extent Treg cells[200,201]. AhR expression in these two cell types has an important role in controlling their reciprocal plasticity and, thus, the development of T_H17-mediated immunopathology[200–202]. Other immune cells expressing high levels of AhR are the gut CD8αα$^+$ IEL[203] and some subsets of innate lymphoid cells (ILCs)[204].

AhR is directly involved in the production of IL-22 by RAR-related orphan receptor gamma t (RORγt)$^+$ ILCs and T_H17 cells[200,204], thus favouring intestinal homeostasis.

Indeed, AhR signalling via IL-22, was shown to inhibit inflammation in mouse-models of colitis and AhR expression was found to be downregulated in intestinal tissues of human patients with IBD[205]. Furthermore, characterization of AhR-deficient (*AhR*$^{-/-}$) mice revealed a pronounced phenotype where there is a reduction in the number of cells normally expressing high levels of AhR; i.e. IELs and ILCs[203,206]. The *Ahr*$^{-/-}$ mice also suffered from a reduced ability to control the microbiota, with a detectable increase in its load and a change in its composition; a heightened-state of immune activation in the gut, with increased levels of IFNγ and/or IL-17; and an increased prevalence of immunopathology[203,207]. Severe phenotypes with development of skin abnormalities, colitis, rectal prolapse and even premature death have also been reported in the literature[208,209]. It is important to note, however, that the development of immunological defects and phenotypic manifestations in *Ahr*$^{-/-}$ mice largely depends on the environmental factors and microbial status of the animal facilities in which the mice are bred[188]. In a clean environment and under strict specific-pathogen free conditions, *Ahr*$^{-/-}$ mice on a C57BL6 background do not exhibit an overt immunopathological phenotype[188,210]. This finding substantiates the notion that AhR signalling might not be essential for the development of a fully functional immune system, but rather functions in fine-tuning of immune responses according to environmental cues[210,211]. It is also worth mentioning that although lacking systemic assessment of differential expression in different organs, microarray data revealed evidence of AhR expression by myeloid cells, including macrophages and DCs, and non-hematopoietic cells such as epithelial cells[212]. The importance of AhR expression in these cells and its contribution to the maintenance of homeostasis and development of protective immune responses are largely unknown. What is known so far is that tissue-specific deletion of AhR in lymphocytes is sufficient to impair the maintenance of IELs and the formation of lymphoid clusters in the intestine, suggesting that the defective maintenance of IELs and ILCs in *Ahr*$^{-/-}$ mice is

cell intrinsic[203,213]. Contrarily, AhR deficiency restricted to skin keratinocytes is sufficient to replicate the hyper-inflammatory phenotype observed in skin lesions of *Ahr*$^{-/-}$ mice[214]. Reportedly AhR is quite promiscuous, i.e. has the ability to bind to, and be activated by, structurally diverse exogenous and endogenous molecules ranging from environmental pollutants, drugs, and dietary components to endogenous essential amino acid by-products such as the tryptophan derivative 6-formylindolo[3,2-b]carbazole (FICZ)[215]. In fact, it has been demonstrated recently that AhR can sense distinct bacterial (*M. tuberculosis* and *P. aeruginosa*) pigments and subsequently induces antibacterial responses, suggesting that the AhR can function as an intracellular PRR[216]. This ligand promiscuity, however, has been challenged by the finding that many of these putative ligands interfere with CYP1 enzyme activity, thereby indirectly activating the AhR by increasing the availability of endogenous ligands[217]. This is further complicated by the fact that, despite many efforts to crystallise the AhR, its 3-dimensional structure has not been resolved yet. As a result, receptor-ligand interactions have so far only be estimated via computer modelling[215]. Hence, the affinity and specificity of many putative AhR ligands remain controversial. The most promising candidates for endogenous ligands are groups of tryptophan photo-oxidized products discovered late in 1987[218], the best and most studied example of which is FICZ. FICZ was found to be a high-affinity AhR ligand that occurs in human and murine skin upon UV-light exposure and activates AhR *in vivo*. Unlike dioxin, it is readily metabolized by the AhR-regulated CYP enzymes and therefore results in transient activation of AhR (reviewed in [219]).

Furthermore, the consequences of AhR activation are quite contextual and depend on many factors including the affinity of AhR for the ligand, the half-life of the ligand and its method of administration[188]. This is best exemplified by contradictory reports regarding the role of different AhR ligands in progression of the mouse model of Multiple Sclerosis (MS). Injection of dioxin (a long-acting AhR-agonist) ameliorates the

autoimmunity and inflammation in this model[201], while local, but not systemic[220], administration of FICZ (a short-acting agonist) aggravates the pathology[200]. These differences can be partially explained by the fact that sustained activation by dioxin will eventually result in down regulation of AhR protein and a loss of function phenotype rather than AhR over-activation[221].

A good indicator of AhR induction is the level of expression of the AhR target gene *Cyp1*, which in the intestine has been directly attributed to dietary AhR ligands[222]. The dietary sources of AhR ligand include cruciferous vegetables, which are rich in glucosinolate glucobrassicin. Enzymatic degradation of this component yields indole-3-carbinol (I3C) which under the influence of stomach acid will be converted to the high affinity AhR ligands; 3,3-di-indolylmethane (DIM) and indolo[3,2-b]carbazole (ICZ)[223]. Interestingly, when compared to control mice that were fed a standard diet, wild-type mice fed a synthetic diet deficient in vegetable materials but supplemented with all essential nutrients had substantially altered intestinal immunity and architecture, similar to that observed in *Ahr*$^{-/-}$ mice, with decline of both IEL numbers and function[203]. Supplementation of the same synthetic deficient diet with only I3C, the AhR ligand precursor, was sufficient to restore the IEL numbers and function to levels comparable to those of mice on a standard diet[203].

Thus, manipulation of the AhR system, either genetically or by diet modification, directly influences the number and function of IELs with subsequent effects on gut homeostasis. Given the potential contribution of activated IELs in the induction of an antiviral state, and the, previously mentioned, possible interactions between AhR- and STAT1-signalling pathways, it is intriguing to investigate the effects of AhR manipulation in the context of enteric viral infection.

1.3 Noroviruses

1.3.1 History, Structure and Classification

Belonging to the Caliciviridae family, noroviruses are icosahedral, non-enveloped, single-stranded, positive-sense RNA viruses, with a genome size of around 7.4 kb[224]. Identified for the first time following a human gastroenteritis outbreak in Norwalk, Ohio in 1968[225,226]; they were originally named Norwalk viruses. They were subsequently discovered in a wide range of species including rodents, cows, sheep and non-human primates[227–230]. The first identification of a norovirus infection of mice in 2003[231], called murine norovirus (MNV), is considered a major landmark in the field as it provided a novel, viable and accessible *in vivo* model to study norovirus biology.

Norovirus genome contains at least three open reading frames (ORFs). ORF1 is translated as a polyprotein that is subsequently cleaved into 6 non-structural proteins including a viral protease, a 5' terminal genome-linked (VPg) protein and an RNA-dependent RNA polymerase. ORF2 and ORF3 encode the major (VP1) and minor (VP2) capsid proteins respectively[232,233]. A fourth reading frame (ORF4) that overlaps ORF2 has been recently identified in the genogroup of noroviruses infecting mice but not in other norovirus genogroups[234]. The protein encoded by ORF4 was termed virulence factor 1 (VF1) and was shown to play a role in delaying both the induction of type-I IFN and apoptosis[234].

Based on the predicted amino acid sequences of the major capsid protein, VP1, which shows the greatest variation due to strong selection pressure by the immune response, noroviruses are classified into five genogroups. To an extent, this classification system correlates with the host-specificity of different viruses. Genogroup I (GI), GII and GIV viruses infect humans, with the GII.4 strain being the most prevalent, while GV viruses infect rodents[235,236]. Human histo-blood group antigens (HBGAs), likely recognised by the protruding domain of the major capsid protein, have been regarded as the main host

receptors for noroviruses, and their differential expression has been considered to be the major determinant of host range and humans susceptibility[237–239]. In fact, the levels of neutralising antibodies blocking this interaction between the virus and HBGAs were shown to correlate with the development of protective immunity against norovirus infection in human[240]. Attempts to harness this for the development of protective human vaccines are currently under extensive research focus[241].

1.3.2 **Human Noroviruses: The burden and the challenges**

Human Noroviruses (HuNoVs) are leading causes of acute, self-limiting gastrointestinal infection. Although asymptomatic (sub-clinical) infections occur frequently[242], a typical illness resolves within 1-4 days, with abdominal cramps, nausea, vomiting and diarrhoea being the common symptoms[243,244]. Viral shedding in the faeces, however, may last for weeks to months in symptomatic/asymptomatic healthy individuals[245], and years in immunocompromised patients[246,247]. A recent report suggested that new emerging variants of HuNoVs result in infections of healthy hosts with a longer average duration of viral shedding compared with that of previously circulating strains[248].

Since the introduction of rotavirus vaccines and control of rotavirus infections, HuNoVs have become the predominant gastrointestinal pathogen within the paediatric population in developed countries[249,250]. They are now considered to be responsible for more than 90% of non-bacterial gastroenteritis cases and the commonest cause of both epidemic and sporadic cases of acute food-born enteric infections worldwide[251–253]. This, in part, is due to the low infectious dose required for infection, the extended viral shedding and the high environmental stability and contagiousness of HuNoVs with rapid person-to-person transmission either directly through the faeco-oral route and/or indirectly from contact with contaminated fomites, food or water[254]. In addition to the increased morbidity and mortality in the most vulnerable population of the very young, the elderly and the

immunocompromised, HuNoV disease causes a substantial economic burden as a consequence of health care costs and loss of productivity; estimated at about US$60 billion in societal costs every year[255].

Due to this huge burden, strong efforts have been employed to bridge the gaps in the understanding of the natural history, pathogenesis, and immunobiology of HuNoVs. For several decades, these efforts had been curbed by the lack of a valid cell culture system and the absence of small animal models for HuNoV[256]. Recent efforts addressing these obstacles have yielded some progress. Firstly, using 'humanised' T and B lymphocyte and cytokine receptor common gamma chain (Rag-γc) double-deficient BALB/c mice, Taube *et al.* (2013) were able to develop the first mouse model of HuNoV[257]. Secondly, by generating human intestinal enteroids (organoids) from stem cells isolated from intestinal crypts, Ettayebi and colleagues (2016) developed a reproducible *in vitro* culture system that allowed the cultivation of multiple HuNoV strains[258]. The extremity of the first model and the high cost of the second, together with the fact that studying factors regulating HuNoV pathogenesis in the natural host, humans, will always be difficult due to ethical considerations, have driven the long-standing usage of surrogate models of related noroviruses in their natural hosts as the most popular and sensible strategy[259]. Among these, MNV provides the most widely used, readily tractable model system to explore viral and host factors regulating norovirus infection[260,261].

1.3.3 **Murine Noroviruses (MNVs): A model of enteric viral infections**

A natural mouse pathogen endemic to wild mice and animal facilities throughout the world[262–264], MNV has been widely used as a model to study the immunobiology of enteric viral infections. However, Owing to distinct features of infection in their respective natural hosts (reviewed in [261]) MNV has always faced criticism as to whether it is a relevant surrogate model for HuNoV infection[261]. Indeed, the MNV model does not

recapitulate all aspects of HuNoV infection. As clinical disease has not been reported after infection of immunocompetent mice[265], MNV is considered an infection-only model. The genetic variation between MNV strains is also much less prominent than that observed between HuNoV strains[266]. Moreover, MNV and HuNoV have distinct differences in their known attachment factors and receptors[261]. Nonetheless, recent data suggest more shared properties between the two viruses in terms of the common carbohydrate nature of their distinct receptors, their potential abilities to establish persistent viral shedding and importantly some aspects of their cellular tropism[261].

The currently prevailing paradigm is that MNV (with the help of the microbiota[267]) first breaches the intestinal epithelial barrier by hijacking the Microfold (M) cell transcytosis pathway[268]. It then infects mononuclear phagocytes of the LP before being trafficked to local lymph nodes, MLN and to distal sites, such as the spleen and liver, by migratory DCs[269–271]. MNV infection of IECs has never been demonstrated *in vitro*, though has been observed *in vivo* after infection of *Stat1*$^{-/-}$ and *Rag1-Stat1*$^{-/-}$ double deficient mice[265,272]. It is important to note, however, that most of the studies supporting the above infection pathway were conducted using the MNV-1 (prototypic strain) as the only pathogen. There was no reference to the possibility that different MNV strains (discussed in more details in subsequent sections) might differ in their initial site of infection and in their broad tissue tropism. Indeed, different MNV strains have quite distinct biological properties despite limited sequence (genetic) variation[266]. Studies that directly compared the tissue tropism of different MNV strains showed that MNV-3 and MNV-O7, both considered to be attenuated strains of MNV, resulted in higher intestinal and lower splenic viral titres compared to those caused by the acute strain MNV-1 ([273] and unpublished work by Dr James Chettle). The picture is even less clear in HuNoV infection, with evidence of initial infection and replication in both IECs[258] and mononuclear phagocytes of the LP[274]. A recent interesting report suggests that both MNV

and HuNoV infect B cells and share a dependence on commensal bacteria for efficient replication[267].

A major determinant of cellular tropism, and overall species specificity is the diversity and differential expression of the attachment receptors. The importance of HBGAs in HuNoV infection was discussed above. The first MNV-1 receptors identified were terminal sialic moieties on gangliosides (Taube *et al*, 2009)[275]. Recently, two members of the mouse-specific type-I transmembrane CD300 protein family, namely CD300LF and CD300LD, have been shown to act as proteinaceous receptors for MNV[276,277]. Experimental (induced) expression of these molecules in multiple, non-susceptible cell lines, including human-derived HeLa cells, supported MNV infection and propagation, while knocking-out the expression of these molecules rendered mice resistant to viral shedding following oral infection with MNV[276,277]. These recent data will pave the way for more investigation of the molecular details of norovirus internalisation.

Generally, the ability to cultivate MNV in multiple *in vitro* cell lines, to genetically manipulate both the virus and the host and the availability of both acute (MNV-1) and persistent (e.g. MNV-CR6, MNV-3, and MNV-O7) strains, add a substantial strength to the MNV model as a tool to study, analyse and dissect not only HuNoV infection but different aspects of enteric viral infections in general.

1.3.4 **Murine Noroviruses (MNVs): Viral determinants of Virulence and Persistence**

Being highly prevalent in research animal facilities[278,279], new isolates and strains of MNV with diverse biological behaviours continue to emerge and be reported. At least 60 new strains of MNV had been defined and uploaded to Genbank during the last decade. Our lab has recently characterised a new strain of MNV, known as MNV-O7, which was originally isolated from a mixed colony of *Stat1*$^{-/-}$ and *Ifngr1*$^{-/-}$ mice. Unlike MNV-1, MNV-O7 was found to cause chronic infection in wild-type mice and attenuated

pathology in *Stat1*$^{-/-}$ mice[280]. In fact, to date, the vast majority of newly identified MNV strains show a phenotype of long-term persistence in wild-type mice and attenuated infection in immunocompromised hosts[273,279,281], in direct contrast to the original MNV-1 (CW1 and CW3) isolate's phenotype of rapid clearance in immunocompetent, and severe and/or persistent disease in immunodeficient hosts[231,265]. This is also in contrast to the perceived acute pathogenesis of HuNoVs. Research has taken place to identify the determinants of these different phenotypes of virulence and persistence with a focus on different aspects of viral factors, tropism and the elicited immune responses.

Several viral proteins have been implicated in **virulence** of different viral strains. Given its function in antagonising the innate immune response and delaying apoptosis, ORF4-encoded VF1 is considered to be an important contributor to MNV virulence *in vivo*[234]. Early studies on MNV revealed an association between the virulent phenotype and the expression of lysine instead of glutamic acid at position 296 of the major capsid protein, VP1[271]. Subsequently, it was shown that this K296E substitution in VP1 is sufficient to attenuate MNV-1 infection in *Stat1*$^{-/-}$ mice[282]. However, there is no evidence, to date, that naturally occurring attenuated strains can be made more virulent by the reverse E296K mutation.

The **persistent** phenotype, on the other hand, has been shown to be associated with superior colonic tropism in the early stages of infection, with the subsequent consideration of the cecum and colon as the major tissue reservoir of persistent MNV strains[283,284]. A single amino-acid substitution (D94E) in the NS1/2 non-structural protein was suggested to be sufficient to determine persistence, with exchange of that region between MNV-1.CW3 (naturally acute) and MNV-CR6 (naturally persistent) conferring a persistent phenotype on CW3 and an acute one on CR6[284]. How this mutation relates to specific cellular tropism (i.e. IECs vs mononuclear phagocytes), and to the subsequent immune responses elicited has not been defined, however.

1.3.5 **Murine Noroviruses (MNVs): The Immunology**

While rather blunt and inevitably complicated by compensatory feedback mechanisms, genetic knockout mouse models have proved to be extremely valuable and tractable for interrogating the MNV-induced immune response[261]. Innate immunity with the production of, and response to, IFNs has been consistently shown to be crucial for the control of MNV infection. It has been reported that the innate viral sensor MDA5 (from the *Ifih1* gene) and, to a lesser extent, TLR-3 are involved in the control of MNV-1 (the acute strain) infection both *in vitro* and *in vivo*[285]. However, neither *Ifih1*$^{-/-}$ nor *Tlr3*$^{-/-}$ mice succumbed to the oral infection with MNV-1 and the virus load in both, although higher, was cleared within the same time frame as wild-type mice, i.e. 5-7 days post-inoculation[285]. This indicates redundancy and involvement of other, not yet identified PRRs in detection of MNV. Downstream of these viral sensors, IRF-3, IRF-5 and IRF-7 have been recognized as the critical mediators of the IFN response to MNV infection[286,287]. Both type-I and II IFNs can inhibit the translation of MNV non-structural proteins[288], and whilst it does not cause serious clinical disease in immunocompetent hosts, oral MNV-1 infection causes fatal disease in IFNαβγ receptor triple-knockout and *Stat1*$^{-/-}$ mice[231]. STAT1-dependent responses rapidly control MNV-1 (the acute strain) infection in the intestine, prevent the development of clinical disease and limit viral dissemination to peripheral tissues[265]. Interestingly, for the persistent strains of MNV, IFNAR1 expression does not control viral shedding nor determine viral titres in the gut but rather regulates the ability of the virus to spread to extra-intestinal sites such as the spleen[289,290]. Two recent complementary studies showed that the faecal shedding of these persistent strains is instead limited by type-III IFN signalling through IFNLR1[289,290]. Thus, intraperitoneal administration of IFNλ was sufficient to cure persistent MNV-CR6 infection[289]. More intriguingly, it has been found that the presence of commensal bacteria suppresses an endogenous type III IFN response that would otherwise prevent and/or

clear this persistent MNV-CR6 infection[290], so a treatment of wild-type mice with broad-spectrum oral antibiotics for 2 weeks prior to inoculation with the persistent MNV-CR6 strain, prevented the establishment of persistent enteric infection by type III IFN-dependent mechanisms[290]. More recently, it has been revealed that the expression of IFNLR1 on intestinal enterocytes (IECs), but not on other cells, is critical to this antiviral effect of IFNλ[291]. While the argument for broad-spectrum antibiotic therapy may be thought of as an impractical due to the anticipated drastic side-effects (although it has already been justified in some severe infections in immunodeficiency cases[292,293]), IFNλ administration is an especially attractive therapeutic approach for HuNoV infection, given its safety profile in treatment of chronic hepatitis C virus[294,295].

Collectively, these data indicate that the IFN-JAK-STAT signalling pathway is particularly relevant in the protective immunity against MNV infection. Redundancy exists at the level of PRRs and also at the level of the downstream ISGs[231], with possible differential roles and importance of different IFN subtypes. However, a functional STAT1 molecule is absolutely necessary for protection from MNV infection.

While it might not be critical for survival, the adaptive immune response appears to play an important role in clearance of MNV infection. Unlike *Stat1*$^{-/-}$ mice, oral infection of *Rag1*$^{-/-}$ or *Rag2*$^{-/-}$ mice with MNV-1 did not induce lethality, however, for up to 90 dpi the mice maintained a high level of virus in faeces, blood and all organs analysed[231]. The long-term infection with the acute strain, MNV-1, in this instance was associated with minor disease and the absence of the overt pathological changes commonly seen after infection of wild-type mice.

Adoptive transfer of splenocytes from MNV-immune, but not from non-immune, wild-type mice was sufficient to clear persistent MNV-1 infection from the intestine of *Rag1*$^{-/-}$ mice by day 6 post-transfer[296,297]. By comparing the effects of transferring immune splenocytes from wild-type mice, μMT mice (genetically deficient in B cells) or from

HELMET mice (lack B cells capable of producing antigen-specific antibodies) into *Rag1*$^{-/-}$ mice, it was demonstrated that B cells and the MNV-1-specific antibodies they produce are essential for the clearance of the virus[297]. Similarly, depletion of either CD4 or CD8 T cells from the transferred splenocytes resulted in a significant increase of the viral titres compared to those of the control depletion[296]. Interestingly, while adoptively transferred immune splenocytes from *Ifng*$^{-/-}$ mice were as effective as those transferred from wild-type mice in clearing the persistent MNV-1 infection from *Rag*1$^{-/-}$ mice, immune splenocytes from *Perforin (Prf1)*-deficient mice were less effective[296], suggesting a superior role of direct cell-to-cell cytotoxicity by T cells compared to their cytokine production in clearing the virus. Moreover, $CD4^+$ and $CD8^+$ T cells seem to play different combinatorial roles in controlling MNV infection. $CD4^+$ T cell deficient mice present with higher tissue titres but normal viral clearance, whilst mice lacking $CD8^+$ T cells exhibit delayed viral clearance[296,298]. Indeed, the persistent phenotype of MNV has been associated with a suboptimal virus-specific $CD8^+$ T cell response[299].

Taken together, the data discussed above suggest that infection with various MNV strains elicits differential innate and adaptive immune responses. While adaptive immunity is critical to control and clear acute strains such as MNV-1; persistent strains, by induction of milder innate immune responses, fail to generate effective antigen-specific T cell responses ([299,300] and Dr James Chettle's, unpublished work). However, it has been shown recently that robust adaptive immunity alone is both **not essential** for cure of persistent MNV-CR6 infection, as in its absence IFNλ treatment was enough[289]; and is **not sufficient** to confer clearance of acute MNV-1, as the virus persists systemically in mice conditionally deficient for type-I IFN signalling in DCs, despite an intact and fully-functional adaptive immunity[301]. Thus, in my opinion, an effective, innate anti-MNV immune response is the key and should be the focus for immuno-protective (–therapeutic) strategy design.

1.4 The overall aim and objectives of this project

The main hypothesis of this thesis was that; owing to their state of activation, abundance and unique location above the basement membrane, **IELs** play an important role in gut mucosal immunity that protects against enteric viral infections. I also hypothesized that this protective anti-viral immunity is directly affected by the **aging process** and by the manipulation of the gut-associated **AhR system**, as both the maintenance and functions of IELs and the efficiency of enteric mucosal immunity in general are directly influenced by aging and by the availability of certain micronutrients that act as ligands to AhR. Using MNV as a mouse-model of enteric viral infections, my overall aim was to address these hypotheses through a combination of *in vivo* and *in vitro* studies.

The main objectives of the project were as follows:

1. Determine the Role of IELs on Early Gut Immunity Against MNV (**Chapter 3**).

2. Investigate the Influence of Aging on Early Gut Immunity Against MNV (**Chapter 4**).

3. Analyse the Effects of AhR manipulation on Early Gut Immunity Against MNV (**Chapter 5**).

2 GENERAL MATERIALS & METHODS

Chapter 2 GENERAL MATERIALS AND METHODS

2.1 Cell Lines

BV-2 cells (a mouse microglial cell line[303]), a kind gift Prof. Ian Goodfellow (Pathology Department, University of Cambridge), were derived from primary microglial cell cultures from C57BL/6 mice immortalised by infection with a v-raf/v-myc oncogene-carrying retrovirus. This cell line was found to share the antigen profile, phagocytic and antimicrobial properties of activated macrophages[304]. The cell line was maintained by growing in Dulbecco's modified Eagle's medium (DMEM) supplemented with 10 % foetal calf serum (FCS), 100 U penicillin/ml and 0.1 mg streptomycin/ml (10%DMEM). The cells were seeded (at 2-5 x 10^4 cells per cm^2) in tissue culture flasks and incubated at 37 º C, 5 % CO_2. Every 3-4 days the cells were split (approximately 1:10) using cell scrapers (Greiner Bio-One).

RAW 264.7 (a mouse monocyte macrophage cell line), was originally established from an ascites of a tumour induced in a male mouse by intraperitoneal injection of Abelson Leukaemia Virus (A-MuLV) (HPA Culture Collections 91062702). This cell line was maintained in an identical manner as that described for BV-2 cells.

2.2 Viruses

MNV-O7, a kind gift from Dr. Amita Shortland (University of Cambridge), was cultured from a faecal sample of a *Stat1*$^{-/-}$ mouse, passaged twice through RAW 264.7 cells then twice through BV-2 cells to generate the MNV-O7P4 virus stock used for the infection assays.

MNV-1.CW3P5 (1 x 10^7 genome copies/ml), a kind gift from Prof. Herbert Virgin (Department of Pathology and Immunology, Washington State University, USA), was passaged twice through RAW 264.7 cells and then twice more through BV-2 cells to generate the MNV-1.CW3P9 stock used for oral infection of mice.

MNV-3 (6.61 x 10^7 $TCID_{50}$/ml), a kind gift from Prof. Ian Goodfellow (Department of Pathology, University of Cambridge), was used immediately as a working stock for the infection assays.

2.3 Generation of high-titre virus (working) stocks and ultra-violet inactivated virus stock

Working virus stocks were grown on BV-2 cells in 10% DMEM by infecting 50% confluent (175 cm^2) tissue-culture flasks with a diluted virus, in 10 ml of media per flask, at a multiplicity of 0.01-0.1 $TCID_{50}$/cell. Infected flasks were incubated for 1 hour at 37 °C with gentle agitation applied every 15 minutes. After this incubation, the media in each flask was topped up to 25 ml and the cells returned to the 37 °C incubator until clear cytopathic effects (CPE) were detected or for 5 to 6 days if CPE were not obvious. The cells were then subjected to 3 cycles of freezing (-80 °C) and thawing and the culture fluid was decanted from the flasks to sterile tubes and centrifuged (2000 x g, 10 min). The resulting clear supernatant, which contained virus, was passed through a 0.22µm filter, aliquoted and stored at -80 °C. Virus titre was determined by measuring $TCID_{50}$ in BV-2 cells and by quantitative RT-PCR.

For some in vitro experiments an UV- inactivated virus stock was used to differentiate the effects of viral attachment and productive viral replication and infection. This inactivated virus stock was generated, tested and stored at -80 °C by Dr. James Chattle (University of Oxford) during his PhD study. Briefly; diluted working stocks of MNV-O7P4 and MNV-1.CW3P9 were mixed at 1:1 ratio. This mixture was subjected to UV-light irradiation (254 nm) for 10 minutes in sterile Pyrex beakers. This was sufficient to achieve a reduction in viral infectivity of at least five orders of magnitude as measured by TCID50 on BV-2 cells.

2.4 *In Vivo* Experiments

2.4.1 Mice

The origin and breeding of specific mice lines will be detailed in subsequent chapters. Unless otherwise stated, the age of the mice used at the beginning of the experiments described ranged between 6 to 14 weeks (mostly 8-12 weeks). In experiments with a mixture of male and female mice, sexes were distributed evenly between different study groups to account for the possibility of sex-specific differences. All mice were housed in individually ventilated cages and fed sterilised water and diet. The experimental procedures were performed at the Departments of Anatomy and Pathology, University of Cambridge. Transport, housing, care and procedures were all carried out in compliance with the University ethical review process and Animals (Scientific Procedures) Act 1986.

2.4.2 Intraperitoneal Injection of Anti-CD3 and Isotype Control (ITC) Antibodies

Anti-CD3 (Biolegend, 2C11, LEAF) and isotype control Armenian Hamster IgG (Biolegend, LEAF) antibodies were prepared to a concentration of 0.125 µg/µl by diluting the stock solution (1 µg/µl) in PBS. Mice were gently restrained (without anaesthesia) and injected intra-peritoneally with 200 µl of the diluted antibody solution administered from a 1 ml syringe attached to a ½ inch, 27-gauge hypodermic needle.

2.4.3 Oral Gavage Infection with MNV

MNV-O7 (O7P4) and/or MNV-1.CW3 (CW3P9) virus stocks were diluted, in PBS, to the required infectious titre. Mice were gently restrained and orally inoculated with 200 µl of the diluted virus inoculum administered from a 1 ml syringe attached to a blunt metal 2 inches 20-gauge curved needle (Vet Tech Solution, UK) with a smoothed 2 mm wide metal sheath. Anaesthesia was not used, except for the antibiotic treatment and aging experiments in which the mice were lightly anaesthetised with isofluorane, held by the skin between the eyes and allowed to swallow the needle, which passed to the stomach.

2.4.4 Sample Collection

Faeces: Faecal samples were collected from individual mice by placing them into separate clean containers for a few minutes and collecting the faecal pellets from that container.

Tissues: mice were euthanized by CO_2 asphyxiation with death confirmed by dislocation of the neck. For viral titration, small segments of the relevant tissues, usually small intestine, mesenteric lymph nodes and spleen were collected into labelled 2 ml Eppendorf tubes.

2.5 Quantification of Infectious Virus Titre by $TCID_{50}$ Assay

A limiting dilution 50 % Tissue Culture Infectious Dose ($TCID_{50}$) assay was used to quantify viruses that do not form plaques. BV-2 cells (at 3 x 10^4 in 100 µl of 10% DMEM) were seeded into 96 flat-bottomed well plates. 10-fold serial dilutions of the virus samples were made in 10%DMEM and 150 µl of the diluted virus were plated into each well with 6 replicates per dilution. The plates were then incubated at 37 º C, 5% CO_2 for 4-5 days. Wells showing cytopathic effects at each dilution were scored by microscopy and the $TCID_{50}$ was calculated using the Reed and Muench formula (Reed, 1938).

2.6 RNA Extraction

Extraction of RNA from different samples (faeces, tissues and cells in culture) was performed using the Mammalian GenElute Total RNA Miniprep kit (Sigma-Aldrich, RTN350), according to the manufacturer's guidelines. Protocols for different samples were identical once the sample was added to the RNA lysis buffer (containing 1% of 2-mercaptoethanol). Briefly, up to a maximum of 400 µl of lysis buffer containing the sample RNA was added to a filtration column and centrifuged

(1min, 16,000 x***g***) to remove the cellular debris and shear genomic DNA. One volume equivalent (i.e. a maximum of 400 µl) of 70% ethanol was added to each sample, and up to a maximum of 700 µl of the resulting mixture was centrifuged (15 sec, 16,000 x***g***) through a GenElute Binding column. Using the washing solution provided in the kit, several column washes were performed and the RNA was then eluted from the column into 50 µl of the kit elution buffer. Processing of different samples to the step of RNA lysis buffer were performed as detailed below.

2.6.1 **RNA Extraction from Faeces**

Weighed faecal samples were suspended into PBS to prepare 10% faecal homogenates. The faecal pellets were homogenised into the PBS by using 5 mm stainless beads in a Mixer Mill MM300 (Qiagen). The homogenates were then centrifuged (2 min, 16,000 x***g***). 50 µl of the resulting supernatant (clear of any pelleted faecal debris) was added to 300 µl of the RNA lysis buffer.

2.6.2 **RNA Extraction from Tissues**

Tissue samples (weighing no more than 40 mg) were homogenised directly into 500 µl RNA lysis buffer (containing 1% 2-mercaptoethanol) using a Mixer Mill MM300 (Qiagen) and 5 mm stainless beads. The samples were then centrifuged (2 min, 16,000 x***g***) and 400 µl of the resulting supernatant was used for RNA extraction.

2.6.3 **RNA Extraction from Cells in *in vitro* Cultures**

RNA was extracted from cell cultures after removal of the supernatant. 96-well cell culture plates were centrifuged (5 min, 2,000 x***g***) and all but 50 µl of the supernatant was removed. 200 µl (i.e. four volume equivalents) of RNA lysis buffer was added to each well and the RNA extraction was performed as described above.

2.7 Quantification of Viral RNA Titre by RT-PCR

The number of vRNA molecules in the extracted RNA samples was estimated by a one-step quantitative RT-PCR analysis using the KAPA One-Step Probe qRT-PCR Universal Kit (Anachem, KK4752) with a 5'-JOE, 3'-BHQ-1 dual-labelled probe (Table 2.1).

Briefly, a master-mix containing 1x KAPA One-Step Probe qRT-PCR master-mix,1x KAPA RT Mix, 0.25 μM of each primer (Q2F and Q2R, Table 1), 0.3 μM probe and the sample RNA was prepared and the PCR performed in a Rotorgene6000 (Qiagen) with the following parameters: reverse transcription (5 min, 42 ° C); RT inactivation and DNA polymerase activation (5 min, 95 °C), followed by 40 cycles of denaturation (5 s, 95 ° C), annealing and extension (30 s, 60 ° C). All the sample, standard and no template control (NTC) reactions were performed in duplicate, and the fluorescence data were collected at the end of each extension phase. Primer and probe sequences and locations are shown in Table 2.1.

Table 2.1 Quantitative RT-PCR prime and probe sequences and locations

Name	Sequence (5' to 3')	Location in MNV-1
Dual-labelled	CCGCAGGAAYGCTCAGCAGTCTT	5028 to 5050
Q2F	GCTTTGGAACAATGGATGCTGAG	5002 to 5024
Q2R	CGCTGCGCCATCACTCATC	5061 to 5079

The number of vRNA copies in each reaction was calculated using a standard curve generated by Dr. Amita Shortland (University of Cambridge) and further validated by Dr James Chettle (University of Cambridge). Briefly, the standard curve was designed using a linearized pT7-MNV-O7-Rz DNA plasmid. The initial concentration of the plasmid DNA was determined using a NanoDrop1000 Spectrophotometer (Thermo Scientific UK), and was then diluted in 10 μg carrier RNA (yeast tRNA, Roche UK 10109223001) per ml in water to obtain 5 x 10^{11} DNA molecules/μl as the highest concentration. A DNA standard curve (R^2= 0.99761, Efficiency 1.01) was obtained by performing a serial 10-fold dilution of plasmid DNA into tRNA/water. The assay was then validated using

10-fold serial dilutions of extracted viral RNA which showed similar efficiency to the DNA standard curve. Data were analysed using the Rotorgene6000 series software 1.7 (Corbett Life Science Research now Qiagen). The sensitivity of the assay was 5 vRNA molecules/reaction with a linear dynamic range of 100 to 10^9 vRNA molecules/reaction. Viral RNA titres from faecal samples were multiplied by the relevant dilution factor to calculate the number of viral genome copies per mg of faeces. Viral RNA titres in tissue samples were expressed relative to the weight (in mg) of the tissue segment analysed, while those of cell culture extract were expressed relative to the concentration of total RNA in the sample.

2.8 Reverse Transcription and Gene Expression Assays

2.8.1 Reverse Transcription

The extracted RNA samples from tissues were reverse transcribed into cDNA, using the QuantiTect Reverse Transcription kit (Qiagen, 205313), according to the manufacturer's protocol except for scaling down the total reaction volume from 200 µl to 12 µl.

2.8.2 Gene Expression Analysis

A Rotorgene SYBR green PCR kit and Quantitect primer assays (Qiagen, Table 2.2.) were used to analyse the gene expression levels in cDNA samples. Using a QIAgility automated pipetting robot (Qiagen), the reactions were set as per the manufacturer's protocol with the exception of scaling down the reaction volume to 15 µl. The PCR was performed in a Rotorgene6000 and the parameters were: DNA polymerase activation (5 min, 95 ° C); 40 cycles of denaturation (5 s, 95 ° C), annealing and extension (10 s, 60 ° C); followed by a melt curve, ramping from 60 ° C to 95 ° C, to check the specificity of the PCR product. For each cDNA sample, PCRs for 2 housekeeping genes (*Rpl38 and Eef2*) were performed. Fluorescence data were collected at the end of each extension phase.

Data analysis was done using the Rotorgene6000 series software (version 1.7) and threshold cycle (Ct) values were assigned from a set threshold value. The "Housekeeping Ct" of a sample is defined as the mean Ct value of the 2 housekeeping genes of that sample. The level of expression of target gene was expressed as $2^{\wedge(-\Delta Ct)}$ multiplied by a factor of 1000. ΔCt was calculated by subtracting Ct value of the gene of interest from "Housekeeping Ct". This is the opposite of the usual subtraction of the housekeeping gene Ct from the gene of interest Ct but allows the graphical presentation to show samples with increased levels of expression higher than those with lower levels of expression.

Table 2.2 Quantitect Primer assays (Qiagen) used for gene expression analysis

Gene symbol	Catalogue numbe	Gene symbol	Catalogue number
Rpl38	QT00145726	*Mx1*	QT01064231
Eef2	QT00167293	*Isg15*	QT00322749
Ifnl3	QT01774353	*Adar*	QT00165592
Ifnb1	QT00249662	*Rsad2*	QT00109431
Ifng	QT01038821	*Prkr*	QT00162715
Tnfa	QT00104006	*Il10Rb*	QT00101367
Tgfb1	QT00145250	*Il28Ra*	QT00494137
Irf3	QT00108759	*MX1 (Human)*	QT00090895
Irf7	QT00245266	*ISG15 (Human)*	QT00072814

2.9 Statistical Analysis

All statistical analyses were performed using Prism Software. As data did not meet the assumption of being normally distributed, they were analysed by the non-parametric Mann-Whitney test. Graphs were produced using Graphpad-Prism 4 (GraphPad Prism Software, CA) and Microsoft Excel (Microsoft, WA).

3 THE ROLE OF INTRAEPITHELIAL LYMPHOCYTES (IELS) IN EARLY GUT IMMUNITY AGAINST MURINE NOROVIRUS (MNV)

Chapter 3 THE ROLE OF INTRAEPITHELIAL LYMPHOCYTES (IELS) IN EARLY GUT IMMUNITY AGAINST MURINE NOROVIRUS (MNV)

3.1 Background

Intestinal IELs constitute a highly-conserved T cell compartment, which is uniquely located above the basement membrane and in close proximity to both IECs and exogenous antigens in the intestinal lumen. They are usually defined as stress-sensing, highly regulated immune cells that, in steady-state conditions, are held in a 'poised' semi-activated state with the display of an alert-phenotype without full activation. Further details about IELs' classification, intestinal distribution and differentiating features that characterise them from systemic lymphocytes, in addition to the factors that influence their maintenance and activation are included in **Section 1.2.3**.

Several studies have focused on the ability of activated IELs to promote reparative epithelial growth[86,305,306], to induce potent cytotoxicity[128] and to produce large amounts of biologically-active soluble mediators, including cytokines and chemokines, that recruit other immune cells[141,307,308]. An interesting report revealed an early protective role of the γδ TCR^+ IELs in the context of *Salmonella enterica ser. Typhimurium* infection[309]. These IELs effectively limit bacterial dissemination by producing the antimicrobial factor RegIIIγ, via a mechanism that depends on bacterial stimulation of IEC-intrinsic MyD88 signalling[309], suggesting a microbiota-dependent crosstalk between IECs and IELs. Older literature reported an immunoregulatory role of murine IELs in response to the *Eimeria* parasite infection[310–312]. A yet to be published report by the Veldhoen group (the Babraham Institute) elegantly demonstrated that at steady-state conditions IELs are kept in a 'poised' state of activation as a direct consequence of alterations in their mitochondrial cardiolipin composition that restrict their metabolic rate, proliferation and effector functions (Konjar *et al*., in revision). Upon inflammation, secondary to *Eimeria*

infection for example, the mitochondrial activity, and hence IEL proliferation and effector functions are released from this repression (Konjar *et al*., in revision).

In contrast, little is really known about the potential contribution of activated IELs to the anti-viral responses of the gut mucosa. In order to address this, and in collaboration with our lab, Swamy *et al.* (2015) employed an *in vitro* IEL-IEC co-culture system, with subsequent *in vivo* validation of the molecular and biological impact, to analyse the effects on IECs upon activation of IELs by agonistic anti-CD3 antibodies[302]. Indeed, one of the most conspicuous impacts of activated-IELs on the IECs was the significant up-regulation of ISGs and other genes of the antiviral response[302]. This induced anti-viral response could be directly attributed to the production of type-I, II and III IFNs by IELs. Agonistic anti-CD3 antibodies result in TCR-mediated activation of IELs[302]. The authors in this report were able to detect inducible phosphorylation of TBK1/IKKε on the activation loop Ser172 following the TCR-triggering of rested IELs. Inhibition of the phosphorylated TBK1/IKKε by a chemical inhibitor significantly reduced the induction of IFNα and IFNλ mRNA upon stimulation of IELs by CD3/TCR complex triggering[302]. As phosphorylated TBK1/IKKε had been shown to be important for the phosphorylation and nuclear translocation of IRF-3 and IRF-7[313], these findings suggest a possible pathway by which the production of type-I and III IFNs can be induced by anti-CD3 stimulation of IELs. Consistent with the 'anti-viral signature' imposed on IECs, activated-IEL supernatant rendered IECs more resistant to encephalomyocarditis virus (EMCV) infection *in vitro*. Moreover, activation of T cells *in vivo*, by intra-peritoneal (i.p.) injection of anti-CD3 antibodies, induced a rapid up-regulation of ISGs in villous epithelial cells and enhanced resistance of mice to a murine norovirus (MNV-O7) infection[302]. Taken together, these data suggest a novel and powerful role of activated IELs in the early innate immune response to enteric viral infections. However, further characterization of this role and of the anti-CD3-MNV experimental model was needed.

For example, assessment of the already documented systemic broad effects of anti-CD3 injections, the influences of microbiota and aging, the differential importance and involvement of different IEL-subsets and the exact *in vivo* contribution of the activated IELs in the observed protective immune response to MNV, are key questions that had not been addressed in previous studies.

Furthermore, the availability of different strains of MNV that can result in either an acute self-limiting infection such as MNV-1.CW3 (hereafter MNV-CW3)[265,271], or a persistent infection, e.g. MNV-O7[314] and MNV-3[283] (discussed in more details in **Section 1.3**), facilitates the analysis of the differential roles of, and influences on, IELs upon infection with acute versus persistent viral strains.

In this chapter I aimed to address questions relevant to the role of IELs in this context.

The chapter is divided into three major sections with the following main objectives:

1) Characterise the anti-CD3-MNV experimental model by:
    a) Assessing the gut-associated and systemic effects of i.p. injections of anti-CD3.
    b) Attempt to improve the model by oral administration of anti-CD3.
    c) Confirm the importance of the IFN-STAT signalling pathway in the observed anti-CD3-mediated protection against MNV.
    d) Assessing the effects of microbiota manipulation, by antibiotic treatment, on the observed anti-CD3-mediated protection against MNV.

2) Apply the anti-CD3-MNV model to determine the *in vivo* role of IELs by:
    a) Using knockout mouse-lines.
    b) Employing an adoptive transfer-model of lymphocytes into *Rag2*$^{-/-}$ mice.
    c) Comparing the role of IEL upon infection with MNV-O7 (persistent strain) vs MNV-CW3 (acute strain).

3) Follow the leads from the results of the above to infer the differential immuno-biological features and cellular tropism of different strains of MNV.

3.2 Materials and Methods

For cell lines, viruses, *in vivo* infection and anti-CD3 administration, sample collection, RNA extraction, viral quantification, reverse transcription, gene expression assays and statistical analysis, please refer to **Chapter 2**. For generation of small intestinal organoids and bone marrow-derived mononuclear cells (BMMCs) cultures please refer to **Section 4.2.3.3** and **Section 5.2.2**, respectively.

3.2.1 Mice

C57BL/6 wild-type, *Il15ra*$^{-/-}$, *Tcra*$^{-/-}$, *Rag2*$^{-/-}$, Tcrd-H2B-eGFP and *Il22*$^{-/-}$ mice were bred at Babraham Institute (The Babraham Institute, Cambridge). 129 wild-type (129S6/SvEvTac) mice were originally purchased from Taconic (Taconic Farms Inc., USA) and a breeding colony is maintained at the Department of Pathology, Cambridge University. *Stat1* knockout (129S6/SvEv - STAT1tmRds, hereafter *Stat1*$^{-/-}$) mice, obtained from Taconic (Taconic Farms Inc., USA), were bred to homozygosity by Dr. Amita Shortland (University of Cambridge) and maintained as a breeding colony at the Gurdon Institute, University of Cambridge.

For mouse transport, maintenance and setting of the experimental mouse groups, please refer to **Section 2.4.1**.

3.2.2 Oral Treatment with Antibiotic Cocktail

C57BL/6 wild-type mice were treated with a 'cocktail' of antibiotics containing streptomycin (5 g/l, Sigma Aldrich), colistin (1 g/l, Melford Laboratories Ltd), ampicillin (1 g/l, Sigma Aldrich) and 5 % (wt/vol) glucose in filter sterilized drinking water for 14 days. Non-treated control mice received only the 5 % (wt/vol) glucose in filter sterilized drinking water. Drinking bottles were changed at least once weekly. Faecal samples from each mouse were collected before and at the end of the treatment.

3.2.3 **Isolation and Adoptive Transfer of Splenic T and B lymphocytes and Intestinal γδ TCR IELs into *Rag2*$^{-/-}$ mice**

Splenic T and B lymphocyte isolation: spleens collected from untreated wild-type or experimental mice were pushed, in PBS, through 70 μm cell filters. The single-cell suspension generated was re-suspended in red blood cell lysis buffer (**Table 3.1**) for 5 min at room temperature. The cells were then washed in PBS and stained for flow cytometry analysis (**Section 3.2.4**) otherwise the $CD3^+$, $CD8^+$ ($CD44^{hi}$) T- or $CD19^+$ B-splenocytes were purified by flow cytometric sorting (BD Influx) for adoptive transfer into *Rag2*$^{-/-}$ mice, *in vitro* MNV-O7 infection (**Figure 3.11**) or gene expression analysis (**Figure 4.3**).

IEL isolation: This part was performed in collaboration with Ulrika Frising under the supervision of Dr Marc Veldhoen. Briefly, the small intestines were collected from GFP^+ γδ T cell knock-in (Gfp-reporter/Donor) mice, the recipient (injected) *Rag2*$^{-/-}$ or wild-type mice after the experimental protocol, flushed with 20 ml cold phosphate buffered saline (PBS) and freed of fat, mesentery and Peyer's patches (PP). The tissue was cut longitudinally and then into small (0.5-1 cm) pieces and incubated at 37 º C, with vigorous shaking (200 rpm) for 10 min, and then moderate shaking (100 rpm) for 20 min in 15 ml of IEL buffer (**Table 3.2**). Cells released into the supernatant were filtered through a 70 μm filter and collected by centrifugation at 500 x***g*** for 8 min. The cells (extracted from up to two small intestinal samples) were then re-suspended in 20 ml 37.5 % isotonic Percoll (Sigma, P1644) and centrifuged (700 x***g***; 10 min) at room temperature to separate the IELs from the upper layer of epithelial cells. The supernatant was discarded and the pellet (containing IELs) was washed once with PBS, re-suspended in IEL buffer (**Table 3.2**), filtered through a 70 μm sieve and stored at 4 º C. Cells were then either stained for flow cytometric analysis (**Section 3.2.4**) or enriched for GFP^+ γδ TCR IELs by flow cytometric sorting (BD Influx) for adoptive transfer into *Rag2*$^{-/-}$ mice.

For certain experiments (**Figure 3.9**) this protocol of isolation was modified to include the lymphocytes of PPs by not removing them at the dissection of the gut, increasing the duration and vigorousness of the shaking step (220 rpm for 30 min) and mashing the gut tissue through filter after the shaking. Lymphocytes of the LP were isolated by incubation of the undigested tissue after the shaking step into a digestion mixture containing 1 mg Collagenase D/ml (Roche, 11088882001) and 0.1 mg DNase/ml (Sigma, DN25) for 40 min at 37 ° C.

In order to inject the *Rag2*$^{-/-}$ mice with the GFP^{+} FACS-sorted γδ TCR IELs, CD3^{+} or CD19^{+} FACS-sorted splenocytes, the mice were briefly acclimatised in a warming cabinet at 37-40 º C for 10-15 min and then restrained. Each mouse was injected with about 2 x 10^5 γδ TCR IELs or about 1 x 10^6 splenic T, B cells or both into the tail vein using insulin syringes. Mice were kept for 3-4 weeks to allow for lymphocytes proliferation and reconstitution of the intestinal compartments. After the experimental protocol (of anti-CD3/isotype control antibody injection and/or MNV infection) and the sacrifice of the mice, and as a quality control procedure, splenic and small intestinal specimens from the recipient *Rag2*$^{-/-}$ mice were collected in cold PBS and put through the same protocols above to isolate the GFP^{+} γδ TCR IELs and splenocytes, to confirm the efficiency of the adoptive transfer reconstitution of the splenic and intestinal compartments.

Table 3.1 Constituents of Red Blood Cell Lysis Buffer

Amount	Reagent	Supplier (Catalogue Number)
0.15 M	NH_4Cl	*BDH-AnalaR (100173D)*
10 mM	Na_2HCO_3	*Sigma (S8875)*
0.5 M	EDTA	*Boehringer Mannheim (808270)*
pH 7.4		

Table 3.2 Constituents of IEL Buffer

Amount	Reagent	Supplier (Catalogue Number)
500ml	MgCl- and CaCl-free PBS	*Sigma (D8537)*
50ml	Fetal Bovine Serum (Heat inactivated)	*Sigma (F9665)*
5ml	Sodium Pyruvate, 100 mM	*Sigma (S8636)*
10ml	HEPES, 1 M	*Sigma (H0887)*
10ml	EDTA, 0.5 M	*Fluka (O3690)*
5ml	Pen/Strep (100x)	*Gibco (15140-12)*
100µl	Polymyxin B, 50 mg/ml	*Sigma (81334)*

3.2.4 **Flow Cytometric Analysis**

Single cell suspensions of splenocytes, IELs and LP lymphocytes were generated as described in **Section 3.2.2**. BMMC were extracted from long bones (femur and tibia) of mice and differentiated as detailed in **Section 5.2.2**. Cells were washed in PBS, and re-suspended in Iscove's modified Dulbecco's medium (IMDM) supplemented with 10 % foetal calf serum (FCS), 100 U penicillin/ml and 0.1 mg streptomycin/ml (10% IMDM).

3.2.4.1 **Staining of Surface Molecules**

Cells were re-suspended in FACS buffer (2.5 % FCS, 0.05 % sodium azide in PBS) containing 20 µg 2.4G2/ml to block Fc receptors (BD Biosciences). Antibody cocktails prepared in FACS buffer were added to the cells and incubated at 4 ° C, 30 min. Cells were washed twice with FACS buffer and fixed with 1 % paraformaldehyde in PBS.

3.2.4.2 **Staining of Intracellular Cytokines and Molecules**

Cells were re-suspended in 10% IMDM supplemented with 0.5 µg ionomycin, 0.5 µg phorbol-12,13-dibutyrate and 1 µg Brefeldin A per ml (Sigma-Aldrich: I3909, P1269, B7651) and incubated at 37 ° C, 5 % CO_2. After 4 hrs incubation, the cells were re-suspended in FACS buffer and stained for surface molecules as described previously prior to fixation in 1 % paraformaldehyde in PBS at 4 ° C overnight. Cells were washed,

re-suspended in permeabilisation buffer (FACS buffer containing 0.5 % saponin, Sigma-Aldrich, 47036), and incubated for 10 min at room temperature. Antibody cocktails, prepared in permeabilisation buffer, were added to cells and incubated at room temperature for 20 min to stain the intracellular cytokines and viral double stranded RNA (dsRNA). The cells were then washed twice with permeabilisation buffer, once with FACS buffer and maintained in FACS buffer until time of analysis.

For viral dsRNA (**Figure 3.11**), primary mouse monoclonal (J2) antibody (Scicons, 10010500) was used with subsequent detection by anti-mouse PE-conjugated secondary antibodies (Dako, R0439).

For mitochondria staining by Mito-Tracker Green (Invitrogen, M7514) (**Figure 3.13**), the IELs were stained for surface markers as previously described but were not incubated in paraformaldehyde prior to permeabilisation as fixation inhibits the staining.

3.2.4.3 **Antibodies**

Table 3.3 lists the antibodies used for the extracellular and intracellular staining and their sources. Cells were stained with cocktails containing up to four antibodies with FITC/Alexa Fluor 488, PE, PerCP-Cy5.5 or APC/Alexa Fluor 647 conjugates.

Table 3.3 List of antibodies used for flow cytometry

Marker	Fluorophore	Clone	Isotype	Catalogue no.
CD19	PE	1D3	Rat $IgG_{2a\kappa}$	553786
CD3	FITC	145-2C11	Armenian Hamster $IgG_{1\kappa}$	553061
CD4	Alexa Fluor 647	RM4-5	Rat $IgG_{2a\kappa}$	557681
CD4	FITC	RM4-5	Rat $IgG_{2a\kappa}$	553046
CD8a	PerCp-Cy5.5	53-6.7	Rat $IgG_{2a\kappa}$	100733 *
CD8a	PE	53-6.7	Rat $IgG_{2a\kappa}$	553032
CD11c	FITC	HL3	Armenian Hamster $IgG_{1\lambda2}$	553801 *
CD108	PerCp-Cy5.5	2e7	Hamster IgG isotype control	121415
IA/IE	Alexa Fluor 647	114.15.2	Rat $IgG_{2a\kappa}$	107617

Table 3.3 continued overleaf

Continue Table 3.3 List of antibodies used for flow cytometry

Marker	Fluorophore	Clone	Isotype	Catalogue no.
CD80	PE	16-10A1	Armenian Hamster $IgG_{2\kappa}$	553769
CD86	PE	GL1	Armenian Hamster $IgG_{2\kappa}$	553692
IFN-γ	AlexaFluor647	XMG 1.2	Rat $IgG_{1\kappa}$	557735
IL-10	PE	JES5-16E3	Rat $IgG_{1\kappa}$	505005*

** Indicates antibodies obtained from Biolegend, otherwise from BD Biosciences*

3.2.4.4 **Detection of Cell Markers by Flow Cytometry**

Cells were acquired using an Accuri C6 flow cytometer (BD Biosciences, CA) and expression of cell markers was analysed using the Accuri C6 software. Relevant isotype control antibodies were used to exclude non-specific binding and cells stained with them did not display additional staining compared with the unstained controls. Spectral overlap between fluorescence channels was compensated electronically using double negative and single positive stained cells to set compensation values.

3.2.5 **Immunofluorescent staining of organoids**

This part was performed by our collaborators in The Babraham Institute, with the help of Ms. Ulrika Frising. Briefly, small intestinal organoids were generated as detailed in **Section 4.2.3.3**, seeded into ibidi µ-slides and incubated for 2-4 days at 37 ° C, 7 % CO_2. The intestinal organoids were then fixed in 4 % formaldehyde for 20 min, permeabilised with 1 % TritonX-100, blocked in 2 % BSA/1 % TritonX-100/PBS and stained for proliferation markers at 4 ° C overnight using anti-Edu, anti-Ki67 and anti-EpCam primary antibodies. The following day, the samples were stained with AF555, AF488, APC-coupled secondary antibodies, respectively. The samples were washed once with PBS and then mounted with Vecta-shield Hard Mounting medium containing DAPI (Vector, H-1500). Images were acquired on a Zeiss 780 confocal microscope and exported using Imaris software.

3.3 Results

3.3.1 Characterization of the Anti-CD3-MNV Experimental Model

3.3.1.1 Effects of Intraperitoneal (i.p.) Injection of Anti-CD3

To assess the effects of stimulation with agonistic anti-CD3 antibodies, I injected C57BL/6 wild-type mice i.p. with 25 μg of the stimulatory antibodies. The unstimulated-control mice received isotype-control (ITC) antibodies. After 3 hrs, the mice were sacrificed and gut sections, mesenteric lymph nodes (MLN) and spleen were collected. IELs were extracted from gut sections as outlined in **Section 3.2.3**, and analysed together with the MLN samples for mRNA expression of the cytokines; TNFα, IFNγ, IFNλ3 and IFNβ1 (**Figure 3.1A & B**). Small gut sections from the duodenum and ileum were further examined for the expression of the ISGs; *Mx1* and *Isg15* and the cytokine TNFα (**Figure 3.1D**). There was a clear upregulation of almost all the genes analysed after i.p. administration of anti-CD3; *Tnfa*, *Ifng*, *Ifnl3* and *Ifnb1* in the IEL and MLN compartments, and *Mx1* and *Isg15* in the gut tissues. In the IEL compartment the expression of TNFα and IFNγ in the anti-CD3-stimulated mice was almost 10-fold that of the isotype controls. This was associated with a strong induction of the anti-viral cytokines (IFNλ3 and IFNβ1); the expression of which was almost undetectable in the isotype controls (**Figure 3.1A**). The spleen samples were analysed by flow cytometry (**Figure 3.1C**) with the gating detailed in **Supplementary Figure 3.1** used as the strategy for the analysis. In order to account for the expected late induction of the cytokine proteins, an additional post-stimulation time-point was included with mice being sacrificed 8 hrs after i.p. injection of anti-CD3. Comparison of the proportions of IFNγ-expressing CD8 T cells revealed a marked increase after 8 hrs of anti-CD3 stimulation, with the percentages doubled those of the controls (**Figure 3.1C**).

The results of this experiment are in agreement with the findings of Swamy *et al.*[302], that i.p. injection of anti-CD3 antibody results in marked systemic and local (gut) activation of $CD3^+$ T cells with the production of many cytokines (both inflammatory and anti-viral) that culminate in induction of a strong anti-viral state in the gut[302].

To assess the biological impact of such activation, I infected C57BL/6 wild-type mice with a standardized (5×10^6 $TCID_{50}$) dose of MNV-O7, 8 hrs after (**Figure 3.1E**) or before (**Figure 3.1F**) i.p. injection with 25 μg of anti-CD3 or ITC antibodies. Forty hours after the infection, the mice were sacrificed and gut sections (duodenum, jejunum, ileum) and MLN were collected and analysed for viral titres. Except for minor changes in virus-kinetics, anti-CD3 stimulation both after and before MNV-O7 infection resulted in robust inhibition of viral replication and significant reduction of the viral titres in all tissues examined (**Figure 3.1E** & **F**). It was noted that the efficacy of this anti-CD3-induced inhibition of viral replication decreased distally down the GI tract and in the MLNs. The lowest viral titres of the anti-CD3-injected mice were measured in the duodenum and the highest were observed in the ileum and MLN (**Figure 3.1E** & **F**). This gradation of the anti-viral effect induced by anti-CD3 broadly correlated with the density of IELs that is found along the length of the small intestine[132], supporting the hypothesis that activated IELs functionally enhance innate resistance to enteric viral infections[302]. The observed reduction of MNV-O7 viral titres in the MLNs of wild-type mice after anti-CD3 stimulation could either be due to an anti-CD3-triggered inhibition of the migration of the MNV-infected mononuclear cells from the gut to the MLN, direct killing of the virus/virus infected cells in the MLNs or a combination of both.

Taken together, the data presented in this section suggested a potential role of importance for IEL and confirmed that anti-CD3-mediated stimulation, with the associated 'cytokine storm', resulted in an effective gut-mucosal anti-viral state that is sufficient to both

prevent the establishment of, and clear, MNV-O7 infection especially in the proximal parts of the gut.

3.3.1.2 **Oral Administration of Anti-CD3 Antibody Does Not Activate IELs**

In an attempt to minimize the systemic effects of i.p. anti-CD3 injections, I administered three different doses (5 μg, 25 μg and 50 μg) of the agonistic anti-CD3 antibody orally into wild-type mice and assessed the resultant local and systemic immune activation as described in the previous section (**Section 3.3.1.1**). Indeed, oral administration of anti-CD3 did not induce systemic responses as the cytokine levels in the MLN and the percentages of IFNγ-expressing CD8 T-splenocytes remained low and comparable to those of the isotype controls (**Figure 3.1B** & **C**). However, there was no activation of IELs, even with the highest dose of oral anti-CD3 and the cytokine levels in this compartment remained also low and comparable to the controls (**Figure 3.1A**). Evidence exists in the literature that orally-administered anti-CD3 antibodies overcome the gastric digestion and, especially at low doses, become biologically active through stimulation of regulatory T cells and induction of oral tolerance[315,316]. Unlike with the i.p. injected anti-CD3, we did observe an increasing level of TNFα expression with the higher doses of oral anti-CD3 administration especially in the ileal samples (**Figure 3.1D**). This was associated with a minor increase in ISG expression, which was of less amplitude than that seen by i.p. injected anti-CD3.

Thus, we concluded from this experiment that, unlike systemic (i.p.) injection, oral administration of agonistic anti-CD3 antibodies did not trigger the activation of IELs, though at higher doses it may result in a non-specific inflammatory response that induces a minor anti-viral-state in the gut.

3.3.1.3 **The Role of STAT-1 in the Anti-CD3-MNV Experimental Model**

Given the well documented importance of the STAT-1 pathway in the early control and prevention of lethal MNV infection[231,265], we investigated the effects of anti-CD3 stimulation in STAT-1 deficient (*Stat1*$^{-/-}$) mice. As demonstrated in **Figure 3.2A**, *Stat1*$^{-/-}$ mice maintained very high viral titres in all gut sections examined, regardless of anti-CD3 or isotype antibody treatment. This was associated with absence of induction of ISG (*Mx1*) expression in gut sections (duodenum and ileum) after anti-CD3 stimulation (**Figure 3.2B**), despite good upregulation of IFNγ cytokine expression (**Figure 3.2C**). Interestingly, unlike the wild-type controls, there was no detectable levels of IFNλ cytokine expression in the gut sections of *Stat1*$^{-/-}$ mice even after anti-CD3 stimulation. This might be due to the absence of the positive feedback loop mediated through the JAK-STAT pathway[110], however this result should be taken with caution as the IFNλ levels were extremely low in the crude intestinal samples of wild-type mice (**Figure 3.2C**). The picture was different in the MLN. Although very high levels of MNV-O7 viral titres were seen in *Stat1*$^{-/-}$ mice compared to wild-type controls, there was a statistically significant reduction of the MLN viral titres after anti-CD3 stimulation of *Stat1*$^{-/-}$ mice (**Figure 3.2A**). This finding suggested the presence of STAT1-independent mechanisms of viral control in the MLNs, which could be, at least in part, mediated by the marked induction of pro-inflammatory cytokines (TNFα and IFNγ) by anti-CD3 stimulation in the MLN of *Stat1*-deficient mice compared to the wild-type counterparts (**Figure 3.2D**).

Thus, in spite of the wide array of different cytokines triggered by anti-CD3 stimulation, absence of the STAT-1 pathway in the gut prevented the anti-CD3-induced MNV protection. A finding that supported the importance of this pathway in early gut mucosal immunity against MNV. It is important to note that in this experiment we used 129 mice as wild type controls because the *Stat1*$^{-/-}$ mice available were from 129-mouse

background (**Section 3.2.1**). The MNV-O7 infection kinetics in the small intestine of 129 wild-type mice differ from that in C57BL/6 mice, with approximately one to two orders of magnitude lower viral titres in the duodenum (Compare **Figure 3.1E** and **Figure 3.2A**). Nonetheless, stimulation with anti-CD3 antibody had a comparable protective effect against MNV-O7 infection in both wild-type mouse strains.

3.3.1.4 Effects of Antibiotic Treatment in the AntiCD3-MNV Experimental Model

We next aimed to determine the role of microbiota in our experimental model of anti-CD3 stimulation and MNV-O7 infection. For that, we treated C57BL/6 wild-type mice with an antibiotic cocktail in drinking water for 14 days and then compared their response to that of non-treated, age matched control mice. The efficacy of this antibiotic cocktail treatment in the eradication of the non-specific microbiota has previously been confirmed by 16S analysis of the faecal samples in previous reports (Konjar *et al*., in revision). Notably, all antibiotic-treated mice developed diarrhoea and caecal swelling, which was detected at the time of sacrifice and indicated the effectiveness of the broad-spectrum antibiotics used.

Administration of anti-CD3 antibody was protective in both antibiotic-treated and untreated age-matched mice (**Figure 3.3**). The only difference that could be observed was a slightly (less than a log) higher MNV-O7 viral titres in the antibiotic-treated ITC-injected mice compared to their untreated counterparts. This difference was statistically significant in all gut tissue examined. However it is not in agreement with recent reports in the literature, where antibiotic treatment resulted in reduction in MNV viral titres and clearance of persistent MNV infections[267,290]. Possible explanations for this discrepancy may be the differences in the antibiotic mixtures, tissue examined (gut segments vs faeces) and/or in MNV strains used. Perhaps, more importantly is the different time points at which viral titres were analysed. Indeed, Baldridge and colleagues (2015)

observed differential MNV-CR6 levels at 4 and 24 hrs post-infection, with significantly higher titres of faecal viral shedding in antibiotic treated mice at 24 hrs compared to untreated mice, suggesting a delayed intestinal transit time of the viral inoculum with antibiotic treatment, which was then confirmed by Evan blue dye oral administration[290]. Moreover, we observed a significant reduction of the ileal viral titres of antibiotic treated wild-type mice 7 days post-inoculation of MNV-CW3 (**Figure 3.13**, discussed in more details in subsequent sections).

Thus, the data presented in this section indicated that the efficacy of anti-CD3-triggered protection from MNV-O7 infection is not influenced by the presence or antibiotic modulation of the microbiota.

3.3.2 **The Contribution of Gamma/Delta (γδ) TCR$^+$ IEL to the Anti-CD3-Mediated Inhibition of MNV Viral Replication**

Given the broad and systemic effects of anti-CD3 stimulation, we aimed to investigate the exact *in vivo* role of 'innate' γδ TCR$^+$ IEL in the protection observed following anti-CD3 administration. To that end, we employed knockout mouse-lines and adoptive transfer models described in the following sections.

3.3.2.1 **The Knockout Mouse lines**

Firstly, I compared the anti-viral responses of wild-type, *Il15ra*$^{-/-}$ and TCRalpha (*Tcra)*$^{-/-}$ mice using the exact same experimental protocol of anti-CD3 administration followed by MNV-O7 viral infection (**Figure 3.4**).

Knocking out the alpha subunit of the IL-15 receptor results in severe deficiency of the CD8αα$^+$ IELs (both the αβ TCR$^+$ and γδ TCR$^+$) as well as variable reduction of other cell types (including the NK, NKT and memory CD8αβ$^+$ T cells)[317,318]. As observed in

Figure 3.4A, there were no differences in the anti-CD3 response between wild-type and *Il15ra*$^{-/-}$ mice. Both established a similar level of MNV-O7 infection when injected with non-specific ITC antibody, whilst upon anti-CD3 stimulation, anti-viral protection was induced that decreased in the distal small intestine similarly in both mouse lines. This observation strongly suggested, at least in the context of our experimental conditions, that CD8$\alpha\alpha^+$ IELs are not essential for the protection against MNV-O7 infection stimulated by anti-CD3 antibodies. However, it does not rule out the possibility that activated IEL might have a role which is masked by the broad array of cytokines induced by anti-CD3 stimulation in *Il15ra*$^{-/-}$ mice.

In order to investigate this possibility, we used *Tcra*$^{-/-}$ mice in which only $\gamma\delta$ TCR$^+$ T cells are available to respond to anti-CD3 injection[319]. A complicating factor of this mouse model is the development of a microbiota-dependent, spontaneous and chronic form of inflammatory bowel disease with age due to an exacerbated number and function of the $\gamma\delta$ TCR$^+$ T cells, which accumulate in older mice[320–322]. For this reason, we used (relatively) young *Tcra*$^{-/-}$ mice (8-10 weeks) and included non-infected controls, which did not show overt features of inflammation in gut sections when examined by histopathology (**Supplementary Figure 3.2**). As observed in **Figure 3.4B**, the *Tcra*$^{-/-}$ mice (with or without anti-CD3 antibody treatment) had significantly lower MNV-O7 viral titres (two log reduction in the duodenum) compared to wild-type mice. This might be due to a high basal inflammatory state, even without overt features of inflammation in histology slides, in these *Tcra*$^{-/-}$ mice (with a high steady-state level of pro-inflammatory cytokines and/or abnormally hyperactive $\gamma\delta$, $\gamma\beta$ and $\delta\beta$ T cells) preventing the establishment of the infection. Anti-CD3 stimulation of the TCR$^+$ T cells in these mice only slightly enhanced this protection, mainly in the proximal part of the gut.

3.3.2.2 **Adoptive Transfer of γδ IELs Into *Rag2*$^{-/-}$ Mice**

Due to the limitations of the *Tcra*$^{-/-}$ mouse model and to further analyse the role of γδ TCR^{+} IELs, we performed an adoptive transfer experiment of IELs into *Rag2*$^{-/-}$ mice. It has already been documented that IELs, isolated from small intestinal epithelia of wild-type mice and injected into lymphopenic mice (such as *Rag2*$^{-/-}$), will circulate and home back to the small intestine, expand in an IL-15-dependent manner and express the $\alpha_4\beta_7$ integrin, CCR9 and CD103 ($\alpha_E\beta_7$ integrin); important for retention within the epithelial compartment ([323] and Konjar *et al*., in revision). Interestingly, the injected (γδ TCR^{+}) IELs re-establish intra-epithelial populations that reflect the normal distribution in wild-type mice; with the highest number of γδ TCR^{+} IELs in the duodenum and the lowest in the ileum (Dr Marc Veldhoen, personal communication). Having TCRd-eGFP knock-in mice, we were able to FACS-sort the intestinal γδ TCR^{+} IELs (without triggering the TCR receptor and stimulating the cells) using the protocol outlined in **Section 3.2.3**. Purified IELs were then injected intravenously (i.v.) into *Rag2*$^{-/-}$ mice (approximately 2 x 10^5 cells per mouse) which were maintained for 3-4 weeks to allow for the proliferation and the reconstitution of the gut IEL compartment. Then matched groups of wild-type, IEL-conditioned *Rag2*$^{-/-}$ mice and *Rag2*$^{-/-}$ mice not receiving IELs were compared using the same experimental protocol of anti-CD3/ITC stimulation and MNV infection.

We injected only purified GFP^{+} γδ TCR^{+} IELs and after the (3-4 week) incubation period I performed a quality control flow cytometric analysis of the spleens and small intestinal segments of the injected *Rag2*$^{-/-}$ mice to assess the efficacy of the reconstitution (**Figure 3.5**). Indeed, 4 weeks after the adoptive transfer, GFP^{+} IELs were not detected in the spleens of the IEL-conditioned *Rag2*$^{-/-}$ mice (**Figure 3.5A**). In the IEL compartment, GFP^{+} IELs could be detected in the injected *Rag2*$^{-/-}$ mice and most of them had reconstituted cells to approximately 35-40% of the normal levels of γδ TCR^{+} IEL

(**Figure 3.5B & C**). As expected the majority of the injected GFP^+ IEL were either $CD8^+$ or double negative with complete absence of a GFP^+CD4^+ subtype. It is important to note that our collaborators at the Babraham Institute used to be able to get better yields (of 60-75%) of GFP^+ IEL in the gut of injected *Rag2*$^{-/-}$ mice after 4 weeks of transferring the same number of cells per mouse. The discrepancy is most likely due to a technical problem in my experiment with the longer transit time of sample collection in the Dept. of Pathology then sample processing in the Dept. of Veterinary Medicine.

Comparing the responses to MNV-O7 infection (**figure 3.6**), the most striking finding was the significantly low MNV-O7 viral titers in all *Rag2*$^{-/-}$ mice analysed, both in the tissues and faecal samples. A similar resistance to MNV infection in *Rag1*$^{-/-}$ mice has been reported in the literature using other persistent strains of MNV; MNV-3[298] and MNV-CR6[290]. These findings support the emerging theory of lymphocytes, particularly B cells being important for the establishment of and cellular targets for certain MNV strains infection[267]. Another possibility is that *Rag-1* or *-2* knockout mice, like the *Tcra*$^{-/-}$ mice, may also have a high basal innate inflammatory state, especially from innate lymphoid cells, that may function in generating an inhibitory environment influencing the establishment of the infection. Frustratingly, the low viral titres in *Rag-2* deficient mice make it difficult to assess the role of injected IELs, which in general resulted in a minor trend of viral titre reduction in the gut sections, MLNs (**figure 3.6A**) and faecal samples (**figure 3.6B**) analysed. The difference between (*Rag2*$^{-/-}$ + IEL) and *Rag2*$^{-/-}$ was statistically significant only in the jejunum samples. Stimulation of these injected IELs with anti-CD3 antibodies, resulted into more reduction of the MNV-O7 viral titres in all tissue examined (**figure 3.6A**). However, the anti-CD3-mediated inhibitory effect in these IEL-injected *Rag2*$^{-/-}$ mice (ranging between 0.5 to 1 log difference, by comparing the mean viral titres of the anti-CD3- vs ITC-injected mice) was much less than that observed in the wild-type controls (ranging between 1.5 to 3 log difference).

In a small follow-up experiment, we compared the responses of wild-type, IEL-conditioned *Rag2*$^{-/-}$ mice and *Rag2*$^{-/-}$ mice not receiving IELs using the acute strain of MNV; MNV-CW3. Interestingly, although lower than those of MNV-O7, the viral titres of MNV-CW3 were quite similar and comparable in both wild-type and *Rag2*$^{-/-}$ mice (**figure 3.7**). The differences between MNV-CW3/MNV-O7 infection profiles of wild-type/*Rag2*-deficient mice is discussed in more details in the subsequent **Section 3.3.3**. The number of IELs injected into *Rag2*$^{-/-}$ mice in this (MNV-CW3) experiment were the same as those used for the (MNV-O7) experiment (**figure 3.6A**). The same batch of mice was used. However, by comparing **figure 3.6** and **figure 3.7** there was a clear difference between the anti-CD3-mediated inhibitory effect on MNV-O7 vs MNV-CW3 viral titres. Unlike MNV-O7, stimulation of the injected IELs by anti-CD3 antibodies resulted in inhibition (2 log reduction) of MNV-CW3 titres in *Rag2*$^{-/-}$ mice similar to, and in the distal parts of the gut (jejunum and ileum) even better than, that observed in wild-type controls (**figure 3.7**). This observation suggested that the effects of the anti-CD3-activated IEL might be more prominent in the context of MNV-CW3 infection. I was unable to do statistical tests in this experiment due to the small sample size.

Taken together, our knockout and adoptive transfer experiments suggest that, in the context of our experimental conditions, the activated (γδ TCR) IELs are not essential and may play a minor role in the anti-CD3-mediated early innate protection against the persistent strain (MNV-O7) infection. Their role may be more prominent in the context of the acute strain (MNV-CW3) infection. It is important to note, however, that these experiments do not exclude a role for the more conventional 'induced' subtypes of IELs, i.e. αβ TCR^{+} CD8αβ^{+} and CD4^{+} IELs. These would include resident-memory T cell subsets that have been shown to be able to induce a rapid, strong and non-specific innate antiviral state upon reactivation by their specific antigen by producing IFNγ, TNFα and IL-2Rβ-dependent cytokines[324].

3.3.3 **Insights into MNV Immunobiology Drawn from the Wild-type/*Rag2*-Deficient Experimental Model**

During the course of investigating the *in vivo* role of IELs we observed interesting and characteristic differences between the MNV-O7 (persistent strain) and MNV-CW3 (acute strain) short-term infection of wild-type and *Rag2*$^{-/-}$ mice. I decided to follow that lead with the aim of further elucidating the differential cellular tropism and immuno-biological features of different MNV strains.

3.3.3.1 **MNV-O7 (but Not CW3) Showed Differential Infection Profiles of Wild-Type vs *Rag2*$^{-/-}$ Mice**

The first observation was the preferentially enhanced viral replication of MNV-O7 in intestinal tissues of C57BL/6 wild-type mice when compared to that of *Rag2*$^{-/-}$ mice. A feature that was not observed in infections with the acute strain; MNV-CW3. Thus, when we orally infected aged-matched wild-type and *Rag2*$^{-/-}$ mice with equal doses of the two virus-strains and sacrificed the mice 40 hrs P.I. (**Figure 3.8**); the MNV-O7 viral titres of the wild-type mice were significantly (almost two log) higher than those of the *Rag2*$^{-/-}$ mice in all tissues examined (**Figure 3.8A**). Confirming its superior intestinal tropism (Dr James Chettle's, unpublished data), the viral titres of the MNV-O7-infected wild-type mice were higher than those of the MNV-CW3-infected counterparts. However, no major differences in viral titre were observed when comparing MNV-CW3 infection of wild-type vs *Rag2*$^{-/-}$ mice (**Figure 3.8B**) except for a minor (non-statistically significant) trend of viral titre reduction in the distal gut (ileum) of *Rag2*$^{-/-}$ mice.

The efficient establishment of MNV-O7, but not CW3, infection preferentially in the wild-type mice as compared to *Rag2*$^{-/-}$ mice strongly suggested a differential specific cellular tropism of the two different MNV strains; a possibility that will be addressed in subsequent sections. One can also hypothesize from the data presented in this section that

the presence of RAG-dependent T and B lymphocytes (in wild-type as opposed to *Rag2*$^{-/-}$ mice) is detrimental (or counterproductive) to the host in the context of MNV-O7 infection.

3.3.3.2 **Adoptive Transfer of Splenic B and αβ T lymphocytes Into *Rag2*$^{-/-}$ Mice**

In order to examine the above hypothesis, we employed the adoptive transfer strategy, however, this time we injected B and/or T lymphocytes FACS-sorted from the spleen of C57BL/6 wild-type control mice into the lymphopenic (*Rag2*$^{-/-}$) hosts. Further details about the procedure are outlined in **Section 3.2.3**.

After the (3-4 week) incubation period, flow cytometric analysis revealed a clear establishment (reconstitution) of the T and/or B splenic compartments of the injected *Rag2*$^{-/-}$ mice (**Figure 3.9A**) with percentages of lymphocytes comparable to those of wild-type controls (**Figure 3.9D**). However, only transferred CD3^{+} T cells (not CD19^{+} B cells) were detectable in the LP and IEL compartments of the splenocyte-conditioned *Rag2*$^{-/-}$ mice (**Figure 3.9B, C & D**). It is important to note that a modified protocol for lymphocyte isolation was used in this experiment (**Section 3.2.3**) to include the PP lymphocytes, which explain the high percentages of CD19^{+} B cells in the IEL compartment of wild-type controls (**Figure 3.9C**). The inability of the injected CD19^{+} B lymphocytes to reach and populate the lymphopenic gut tissues of *Rag2*$^{-/-}$ mice was interesting and supports the findings of previous reports where *Rag*-deficient hosts reconstituted with either unfractionated or CD25^{-} splenocytes (both of which contain nearly 60% B cells) displayed very low frequencies of circulating B cells two weeks after the transfer[325], and most of the i.p. or i.v. injected B lymphocytes were found to localise mainly into the spleen and peripheral (popliteal and inguinal) lymph nodes of *Rag2*$^{-/-}$ or B lymphocyte-deficient mice[326,327].

Analysis of the 40 hrs P.I. MNV-O7 viral titre revealed a significant (stepwise) increase in the intestinal viral titres of the (T and/or B) splenocyte-injected *Rag2*$^{-/-}$ mice when compared to those of non-injected *Rag2*$^{-/-}$ controls (**Figure 3.10**) with about one log rise upon transfer of either B or T lymphocytes and about one and a half log increase upon transfer of both types of lymphocytes. The increase in MNV-O7 viral titres in the splenocyte-conditioned *Rag2*$^{-/-}$ mice was consistent throughout the length of the small intestine, however, the level of infection never reached that of wild-type controls, which remained at least one log higher than that of all *Rag2*$^{-/-}$ mice (**Figure 3.10**).

Thus, although there was variation in their ability to reconstitute the lymphopenic intestinal compartments upon injection into *Rag2*$^{-/-}$ mice, adoptively transferred T and/or B splenocytes promoted the establishment of MNV-O7 infection. A possible explanation, at least in part, for this observation is that these transferred systemic lymphocytes provided additional targets for MNV-O7 infection, i.e. the virus infected the T cell, though there are no previously-reported evidence for that, and/or infected the B cells, which has indeed been reported before for some strains of MNV[267,328,329]. However, I could not detect the transferred B-splenocytes in the gut tissues of the recipient *Rag2*$^{-/-}$ mice (**Figure 3.9**). Alternatively, the presence of these systemic lymphocytes may create or reflect a more favourable host environment for MNV-O7 infection of other cell targets (i.e. mononuclear phagocytes and/or IECs).

3.3.3.3 **MNV-O7 Does Not Infect B- and T-Splenocytes *in vitro***

To assess the possibility of MNV-O7 infecting B- and T-splenocytes, I FACS-sorted the lymphocytes from the spleen of C57BL/6 wild-type mice as in the previous section, co-cultured them *in vitro* with MNV-O7 at MOI of 0.05 and compared the viral growth to that of bone marrow-derived mononuclear cells (BMMCs) extracted from the long bones of the same wild-type mice (**Figure 3.11A**). Unlike the exponential viral replication

observed in the infected BMMCs during the 48 hrs infection period, there was no growth of the MNV-O7 virus in the FACS-sorted T and B lymphocytes. This was further confirmed by the absence of the viral dsRNA signal inside the splenocytes compared to the clear signal observed, using flow cytometry, in the BMMCs 12 hrs post-MNV-O7 infection (**Figure 3.11B**). It is important to note that I did not include the supplementation of Human histo-blood group antigens (HBGA), which was shown to enhance the *in vitro* infection of B cells by MNV[267], in my *in vitro* co-culture model.

Collectively, the data presented in this section indicated a counterproductive role of T and B lymphocytes in the context of MNV-O7 infection that resulted in increased viral titres in gut segments. The finding that MNV-O7 does not replicate in T- and B-splenocytes, at least in the context of our *in vitro* culture conditions, suggested the presence of other cytokine- and/or contact-dependent mechanisms by which these lymphocytes promote the establishment of MNV-O7 infection and its replication in other cellular targets. A major gut-homeostatic factor that is produced mainly by lymphocytes[330,331] is IL-22, and this was a possible candidate for such a role. However, comparing the MNV-O7 infection of *Il22*$^{-/-}$ mice to that of wild-type controls (**Supplementary Figure 3.3**) did not reveal any significant differences of the intestinal viral titres during the acute (40 hrs) infection setting and if anything, a trend of higher viral titres in the proximal gut of *Il22*$^{-/-}$ mice was observed after 14 days of MNV-O7 infection when compared to the wild-type counterparts (**Supplementary Figure 3.3**). This finding clearly did not exclude the possibility of other yet to be identified factors, or even IL-22 cytokine effects that had been compensated in the *Il22*$^{-/-}$ mice, promoted by the adoptively transferred lymphocytes that facilitate the MNV-O7 infection.

3.3.3.4. MNV-CW3 (but Not O7) Infection of Wild-type Mice Resulted in Significant Changes in The IEL Compartment

Returning to the differences between MNV-CW3 (acute strain) and MNV-O7 (persistent strain), we recognised interesting differential effects on the cellularity of the IEL compartment upon infection of wild-type mice with equivalent doses of either of the two viral strains (**Figure 3.12**). Forty hours after the oral inoculation of virus, there was no difference between the MNV-O7-infected and non-infected wild-type mice in terms of cellular compositions of the IEL compartment with respect to B and T lymphocytes proportions. Both had small populations of $CD19^+$ B cells, and almost 3 times higher percentages of $CD8^+$ T cells compared to that of $CD4^+$ T cells (**Figure 3.12A & B**). Upon MNV-CW3 infection, on the other hand, a sharp rise in the proportions of $CD19^+$ B cells and a significant increase of the $CD4^+$ T cell percentages were observed (**Figure 3.12A & B**). There was no significant change in the $CD8^+$ T cell population. As $CD19^+$ and $CD4^+$ cells are not normally present in such high proportion in the IEL compartment at steady-state conditions[129,135], their accumulation post-MNV-CW3 infection suggested recruitment from the LP and/or systemic circulation.

The observations presented above were further supported by utilising a recently proposed staining protocol for the IELs' activation status with Mito-tracker Green (Konjar *et al*., in revision). Mito-tracker Green is a carbocyanine-based probe reported to localize to mitochondria independent of membrane potential[332–334]. In the yet to be published report, Konjar *et al.* (2017) showed that at steady-state conditions Mito-tracker Green-based mitochondrial detection was markedly reduced in resting IEL compared with splenic naïve and memory CD8 T cells. Upon oral infection of the mice with the unicellular intestinal parasite *Eimeria vermiformis* or injecting anti-CD3 antibodies i.p., the mitochondrial detection of the IELs increased in a time-dependent manner and correlated

with increased proliferation and induction of effector functions, such as IFNγ and TNFα production, by the IELs (Konjar *et al*., in revision).

To apply this staining protocol in the context of MNV infection, we orally infected C57BL/6 wild-type mice with equivalent doses of either MNV-O7 or MNV-CW3. The mice were sacrificed at 2, 4 and 7 days P.I. and ileal samples were used to quantify the viral titres (**Figure 3.13A**). As expected the MNV-O7 viral titres were about 2 log higher than those of MNV-CW3 at all time-points examined. The rest of the collected small intestinal samples were used to extract the IELs to be stained with the Mito-tracker Green probe (refer to **Section 3.2.3** and **3.2.4** for more details). Analysis of the median fluorescent intensities (MFI) of the $CD8^+$ IELs revealed no significant changes after MNV-O7 infection (**Figure 3.13B**). MFI values, and hence the mitochondrial staining, remained significantly lower than those of naïve ($CD8^+CD44^{lo}$) and memory ($CD8^+CD44^{hi}$) splenocytes and comparable to those of uninfected (steady-state) controls. Infection with MNV-CW3 resulted in a significant peak of $CD8^+$ IELs' MFI within the first 48 hrs P.I. (**Figure 3.13B**). MFI values gradually tapered off subsequently, but remained significantly higher than those of the uninfected baseline.

These MNV-CW3 infection-associated changes in the $CD8^+$ IEL were microbiota-dependent. Treatment of the mice with a mixture of broad-spectrum antibiotics for 2 weeks prior to MNV-CW3 infection resulted firstly in significant drop of the day-7 P.I. ileal viral titres (**Figure 3.13A**) and secondly in complete disappearance of the $CD8^+$ IEL mitochondrial staining changes at different time points post-MNV-CW3 infection (**Figure 3.13B**), including day-2 and day-4 P.I. where the MNV-CW3 viral titres were comparable to those of the antibiotic-untreated controls. This suggested that the absence of the mitochondrial staining associated with antibiotic treatment was not due to a reduced viral titre.

Taken together, the differences between MNV-O7 and MNV-CW3 in establishment of intestinal infection in wild-type vs *Rag2*$^{-/-}$ mice and their differential effects on the IEL compartments of wild-type mice pointed toward differences in the initial cellular targets of the two viral strains. The ability to infect enterocytes (IECs) is a strong possibility for such differential consequences. Thus, a hypothesis could be that MNV-CW3 does not infect the IECs, and in order to get access to the LP and systemic compartments (where mononuclear phagocytes, i.e. its major cellular targets, are abundant) it causes an epithelial barrier dysfunction associated with intestinal microbiota translocation. This results in microbiota-dependent IEL activation, recruitment of B and CD4^{+} lymphocytes from the LP and/or circulation to the IEL compartment and the development of robust inflammatory (protective) immune reactions. The final outcome is an acute self-limiting infection. In contrast, I hypothesised that MNV-O7 does infect IECs but non-lytically. This may in part explain the increased intestinal MNV-O7 titres upon adoptive transfer of splenocytes into *Rag2*$^{-/-}$ mice, which have been reported to improve IECs homeostasis, replication and differentiation[335–338]. Moreover, it certainly provides an attractive explanation for the persistent, insidious nature of the MNV-O7 infection as infection of the IECs may preclude the development of barrier dysfunction, microbial translocation and/or the subsequent overt inflammatory responses.

3.3.3.5 **Small Intestinal Organoids Support MNV-O7 and MNV-3 (Persistent Strains) Replication but Not MNV-CW3 (Acute Strain) Infection**

To test the above hypothesis, we examined the ability of different MNV strains to infect IECs. Several attempts had been made in the past to address this ability using *in vivo* experimental models and traditional *in vitro* epithelial cell cultures, however with inconsistent and contradictory results[265,270–272]. In collaboration with Ulrika Frising of the Veldhoen Lab, we decided to tackle this question by using small intestinal organoid

system, which has the advantages of preserving the 3-D structure of the IECs and reflecting their physiological lineage-development (more details in **Section 1.1.2**). Indeed, by infecting intestinal organoids generated from small intestinal samples of wild-type mice with different strains of MNV (MNV-O7, -3 and –CW3) at an MOI of 5, we could demonstrate clear differential replication patterns in IEC-based cultures (**Figure 3.14A**). As an additional control in this experiment, we included UV-irradiated virus stock (comprising a mixture of MNV-O7 and –CW3) to differentiate between viral binding (internalisation) and viral replication. MNV-CW3 (acute strain) was unable to replicate as viral genome copy analysis showed a flat growth curve similar to that of the UV-irradiated control infection. The two persistent MNV strains (MNV-O7 and -3), on the other hand, displayed a fluctuating but progressive increase in the viral titres (**Figure 3.14A**). The high viral titres of MNV-O7 and -3 at 1 hr P.I. indicated their increased ability to attach to the IECs compared to MNV-CW3. However, the viral growth of MNV-O7 within the 45 hrs infection period (from about 1 x 10^6 to 2 x 10^6 vRNA/μg total RNA) was much less impressive than that observed for MNV-O7-infected BMMCs (**Figure 3.11A**). This suggested a decreased ability of IEC to support MNV-O7 infection as compared to that of BMMCs, which may have resulted from increased sensitivity to viral infection and/or induction of strong antiviral responses. Indeed, staining of 24 hrs MNV-O7-infected intestinal organoids revealed a marked shutdown of most replication-marker signals that are normally observed in non-infected growing organoids (**Figure 3.14B**).

Thus, unlike the acute (MNV-CW3) strain, persistent strains of MNV infect IECs, a finding that may explain their insidious course and their ability to cause persistent viral infection.

3.4 Discussion

Intestinal IELs compose a large, heterogeneous T cell compartment that is highly conserved in all vertebrates[128,129]. Their unique location above the basement membrane allows for extensive crosstalk with the IECs and qualifies them to be important modulators of immune responses to invading pathogens. Indeed, their ability to promote reparative epithelial growth[86,305,306], and to induce protective (and/or immunoregulatory) responses in the context of bacterial and parasitic infections[309–312], have been well reported in the literature. However, their contribution (role) to gut mucosal anti-viral responses to enteric viral infections remained largely unknown.

In this chapter, I was able to show that *in vivo* activation of $CD3^+$ T cells in wild-type mice, by intraperitoneal injection of agonistic anti-CD3 antibody, resulted in induction of a strong antiviral state in the gut mucosa that prevented the establishment of MNV-O7 infection. This protective effect was STAT1-dependent. However, the protective effect of anti-CD3 cannot be attributed to the activation of the gut-associated T cells only. The anti-CD3 antibody has a marked systemic, 'cytokine storm'-like effect as indicated by the activation of lymphocytes in the spleen and MLNs. Moreover, although the gradation of this protective effect, being strongest in the duodenum and weakest in the ileum, correlates well with the distribution of the $CD3^+$ IELs in the small intestine, the observation of the same gradation in the *Il15ra*-deficient mice strongly excludes an essential role of (at least $CD8\alpha\alpha^+$) IELs in this gradation effect. A possible alternative explanation for the high viral titres detected in the ileum is an acceleration of gut motility, and thus the viral inoculum, induced by anti-CD3 stimulation.

We could not detect any difference in the response of antibiotic-treated mice to anti-CD3 stimulation and the subsequent MNV-O7 titre suppression compared to that of antibiotic untreated controls. This indicated that our experimental system was not sensitive enough (rather blunt) to detect the fine disturbances and changes in the architecture and immune

function of the gut induced by the antibiotic modulation of commensal bacteria. Alternatively, different treatments or reconstituted gnotobiotic mice need to be studied.

The lack of a known specific IEL stimulatory ligand and the inability to specifically target and activate the IELs by oral administration of anti-CD3 antibodies necessitated the use of more complex knockout and adoptive transfer experimental models to track down the contribution of IELs in the protective biological readout induced by i.p. injection of anti-CD3 antibodies. The possibility of a heightened basal inflammatory state and development of several compensatory feedback mechanisms in immunodeficient (*Il15ra*$^{-/-}$, *Tcra*$^{-/-}$ and *Rag2*$^{-/-}$) mice, added further complexities in studying immunity against MNV-O7 infection and defining the role of IELs in the anti-viral immunity. Taken that into account, the *Il15ra*$^{-/-}$, *Tcra*$^{-/-}$ and *Rag2*$^{-/-}$ adoptive transfer experiments all suggested that activated (γδ TCR^{+}) IELs are not essential and may only play a minor role in the protection against MNV-O7 infection induced by anti-CD3 stimulation, at least in the context of this experimental model. The similarity of the anti-CD3 stimulation response of MNV-CW3-infected IEL-injected *Rag2*$^{-/-}$ to that of wild-type controls suggested a more prominent role of these (γδ TCR^{+}) IELs in the protection against this acute strain of MNV, and pointed towards differential immuno-biological characteristics and cellular targets of different MNV strains.

Indeed, by further dissection of these differences we were able to demonstrate the differential viral replication profiles of MNV-O7 (but not CW3) upon infection of wild-type vs *Rag2*$^{-/-}$ mice. Further analysis revealed a counterproductive role of systemic T and B lymphocytes in the context of MNV-O7 infection that resulted in increased viral titres in gut segments of *Rag2*$^{-/-}$ mice. Under our *in vitro* infection conditions, MNV-O7 did not infect the splenic-derived T and B lymphocytes. This observation suggested that the enhanced establishment of MNV-O7 infection upon adoptive transfer of T- and/or B-splenocytes into *Rag2*$^{-/-}$ mice was most likely due to production of soluble and/or contact

dependent factor(s) that create a more favourable host environment for MNV-O7 replication in other cellular targets (i.e. IECs and/or mononuclear phagocytes).

Further analysis of the differential immuno-biological characteristics of different MNV strains revealed the ability of MNV-CW3, but not MNV-O7, to cause the recruitment of LP and/or systemic lymphocytes to the IEL compartment and to activate IELs in a microbiota-dependent manner. This observation raises several questions. The first is whether it is IEL activation itself that mediates recruitment of the LP/systemic $CD4^+$ T and B cells? Secondly; is there an interaction (inter-dependence) between the two cell types? Thirdly; what is the importance of such a response in production of protective anti-MNV antibodies[297]. We were also able to show the ability of MNV-O7 (and MNV-3), but not MNV-CW3, to infect IEC-based organoid cultures.

In a recent report, Zhu *et al.* (2016) observed similar differential effects of MNV-CW3 versus MNV-3 infection in activation of, and induction of granzyme B production by, $CD8^+$ (both αβ and γδ TCR) T cells in the PP and IEL compartments[300]. The model proposed in this report was that MNV-CW3 infects B cells (in PPs) and induces their expression of MHC class I molecules. These infected B cells act as antigen presenting cells to activate cytotoxic $CD8^+$ T cells and their granzyme B production, and play an important role in control of the acute (MNV-CW3) infection[300]. MNV-3, on the other hand, although it similarly infects PP B cells, does not stimulate the upregulation of antigen presentation molecules and subsequently displays an impaired control of the acute stage of infection. The MNV-3-mediated inhibition of B cell antigen presentation was shown to be partially dependent on the expression of strain-specific viral structural (VP2) protein[300]. A caveat of this model, in my opinion, is the discrepancy of viral titre comparisons between the B cell deficient (μMT) and C57BL/6 wild-type mice. In an earlier report by the same group, (**1-day P.I.**) viral titres of MNV-CW3 in the terminal ileum and MLNs were significantly higher in the wild-type mice compared to μMT

mice[267], supporting the hypothesis that MNV-CW3 targets the PP's B cells. However, in the more recent report, infection with the same virus (MNV-CW3) resulted in markedly higher (40-fold and 11-fold) viral titres in the distal ileum and MLN of μMT mice compared to their wild-type counterparts when measured **3 days P.I.**[300], supporting the proposed importance of B cells in control of acute MNV-CW3 viral infection. The discrepancy is apparently due to a significant and rapid drop of the wild-type mouse viral titres between 1 and 3 days post-MNV-CW3 infection. I did not observe a similar drop (fluctuation) of viral titres when infecting C57BL/6 wild-type mice with MNV-CW3 (**Figure 3.13A**). Furthermore, I could not demonstrate the infection of splenic B cells by MNV-O7 (**Figure 3.11**) nor MNV-CW3 (data not shown) at least in the conditions of our *in vitro* infection model. A possible explanation for these contradictory observations might be the different methods of measuring MNV viral titres (I used qPCR vRNA titres in my experiments, Zhu *et al.* used $TCID_{50}$ infectious virus titres) and the different B cells examined for *in vitro* MNV infection (splenic B cells vs PP B cells).

To our knowledge, the data presented in this chapter are the first to report distinctive abilities of different MNV strains to infect IECs. The finding that MNV-CW3 (the acute strain) did not infect IECs, together with the associated microbiota-dependent activation of IELs, suggested the development of epithelial barrier dysfunction and microbiota translocation. Further analysis to confirm and determine the extent of this barrier dysfunction, and to identify the specific component(s) of the microbiota that involved in IEL activation, will be of interest. Similarly, the ability of the persistent strains (MNV-O7 and -3) to infect and replicate in IECs while, at least for MNV-O7, not activating the IELs, open the door to further analyse the IEC-IEL crosstalk and to investigate the possibility of inhibitory (IL10- and/or TGFβ-mediated, for example) signal interactions in addition to the well documented stimulatory MyD88-dependent IL-15/IL-7 interaction model[153,154,309].

4 THE INFLUENCE OF AGING ON EARLY GUT IMMUNITY AGAINST MURINE NOROVIRUS (MNV)

Chapter 4 THE INFLUENCE OF AGING ON EARLY GUT IMMUNITY AGAINST MURINE NOROVIRUS (MNV)

4.1 Background

Population aging was manifest as a universal phenomenon by the beginning of the current millennium[339,340]. Being a triumph of development, medical advancement, economic wellbeing, improved education, nutrition and sanitation, this worldwide trend of aging is definitely a cause for celebration[340]. However, the social, economic and health implications of this phenomenon are profound, global and need to be addressed by multiple disciplines. Although the percentage of old people is currently higher in industrialised countries, the pace of population aging is much more rapid in developing countries with exhausted economic resources and, thus, less time to adjust to the transition from a young to an old age structure[341]. The prevalence of chronic diseases and severity of most acute illnesses increase sharply in the aging population adding further strain and cost to already overburdened health-care systems. A major challenge lies in sustaining healthy aging and maintaining good quality of life over the full lifespan by decreasing the risk, and improving the outcome, of age-associated illness[342].

The bulk of age-related literature highlights the drastic effects of the aging process in both innate[158] and adaptive[159] immune defences. Often compounded by dehydration, malnutrition, chronic antibiotic use and other comorbidities, the age-associated immune deterioration is thought to arise in the gut mucosa earlier than in the systemic immune compartments[162]. Several age-associated gut mucosal changes have been reported, and the 'aged' intestinal environment has been suggested to be the main driver of the low-grade 'inflamm-aging' typical of old age[174] (Refer to **Section 1.2.4** for more details). The increased basal production of pro-inflammatory cytokines, such as TNFα, IL-6, IL-1 and IFNγ[161,343], does not translate into more effective immune responses. Paradoxically, it

correlates with decreased ability to respond to foreign antigens, to maintain tolerance to self-antigens, increased susceptibility to infection/cancer and reduced responses to vaccination[344–347]. The incidence and burden of HuNoV infections, for example, are much higher in the elderly with an associated mortality rate estimated to be nearly 200 % higher among individuals 65 years and older compared to those < 5 years of age[348,349]. Yet, little is really known about the exact cellular and molecular mechanisms of gut mucosal immune-aging, and how those age-associated changes relate (in a cause/effect fashion) to the increased susceptibility to, and severity of, enteric infectious diseases.

The importance of IFN production and signalling in immunity against enteric viral infections, especially Noroviruses, was discussed and highlighted in previous sections (**Section 1.2.2 and 1.3.5**). Consistent with the heightened pro-inflammatory yet unproductive immune state of the elderly, Pillai *et al.* (2016) recently reported that influenza virus-infected peripheral blood monocytes from old (> 65-year-old) human donors have impaired anti-viral interferon (IFN-β) production, but retain intact and normal inflammasome responses, compared to those from younger donors[350].

Although type-I and -III IFNs share similar signal transduction pathways and regulate the same modulators of IFN responses with a strong possibility of extensive *in vivo* crosstalk and interdependence[111,351,352], the preferential expression of IFNλ-receptor (IL-28Rα/IL10Rβ) at the epithelial barriers results in differential, distinct and tissue-specific roles of these IFNs in mediating antiviral responses[112,353]. Both type-I and –III IFNs are produced in response to influenza A virus infection, however it is the IFNλ that predominates in the lung secondary to intranasal inoculation of the virus[354], and intranasal administration of IFNλ induced strong anti-influenza responses without the inflammatory side-effects of IFNα treatment[355]. Similarly, in the gut, the IFN-anti-viral responses are spatially well-orchestrated to tackle different enteric viral infections. Using

young-adult (6-8 weeks of age) mice, Mahlakoiv *et al.* (2015) clearly demonstrated that IFNα/β has a minimal effect on intestinal epithelial cells whereas IFNλ has a minimal effect on cells of the lamina propria[356]. They attributed this differential response to the respective high and low expression levels of IFNλ-receptor and IFNα/β-receptor on the surfaces of IECs[356], however as discussed earlier it can also be explained, at least in part, by the IEC's apical-surface trafficking of IFNα/β-receptor[112] (**Section 1.2.2**). Consequently, rotaviruses with their specific tropism for mature enterocytes of the small intestine[357] are controlled exclusively by IFN-λ with no defined role for type-I IFNs[112,357]. Replicating in both epithelial and non-epithelial cells of the gut[358], reoviruses are controlled cooperatively by IFNα/β and IFNλ, with IFNλ limiting replication in epithelial cells and IFNα/β restricting infection in non-epithelial cells[356]. In norovirus infection, type-I IFNs prevent extra-intestinal spread, while IFNλ inhibits the persistent shedding of the virus in faeces (discussed in **Section 1.3.5**). Interestingly, this effect of IFNλ has been demonstrated only for the persistent strains of MNV (MNV-CR6 and MNV3[290,291]) that, as shown earlier, have the ability to replicate in IECs (**Chapter 3**).

A recent report showed even more intriguing differential roles of type-I and –III IFNs. By comparing the responses of neonatal and young-adult (6-8 weeks of age) mice, Lin and colleagues (2016) could demonstrate that IECs were sensitive to both IFN types in neonatal mice. However, their responsiveness to type-I, but not type-III IFNs, diminished in adult mice[359]. This revealed an unexpected age-dependent change in specific contribution of type-I versus type-III IFNs to anti-viral defences in the gut. What happens upon transition from adult to old age is unknown, nor how this will reflect on the outcome of enteric viral infections.

In this chapter I aimed to address these questions. Using MNV-O7 as a model of enteric viral infections, and in collaboration with the Veldhoen group (The Babraham Institute, Cambridge) we set the following specific objectives:

1) Demonstration of increased burden of enteric viral infections with aging in an *in vivo* experimental MNV-mouse model.
2) Determining the immunological defect underlying the phenotype in elderly mice and defining it as (a) specific signalling defect(s).
3) Examining the reversibility of the defect and the possibility of therapeutic options.
4) Setting up an experimental model to compare and translate our findings from above to human samples.

4.2 Materials and Methods

For cell lines, viruses, *in vivo* infection and anti-CD3 stimulation, sample collection, RNA extraction, viral quantification, gene expression assays and statistical analysis, please refer to **Chapter 2**. For splenic CD8 T cells and IEL extraction please refer to **Section 3.2.3**.

4.2.1 Mice

Male C57BL/6 wild-type mice; **young-adult** (8-12 weeks old) and **old** (15 months or 24 months), were bred and housed to age at the Babraham Institute under Specific Pathogen Free (SPF) conditions. They were supplied to us, at the specific ages above, by our collaborator Dr Marc Veldhoen (The Babraham Institute, Cambridge). For mouse transport, maintenance and setting of the experimental mouse groups, please refer to **Section 2.4.1**.

4.2.2 *In vivo* Treatment with IFNλ

Recombinant Murine IFNλ-2 (PeproTech, 250-33) was prepared to a concentration of 0.125 μg/μl by reconstituting the stock (250 μg) in PBS (containing 0.1% BSA). Mice were gently restrained (without anaesthesia) and injected intra-peritoneally with 200 μl of the diluted cytokine solution administered from a 1 ml syringe attached to a ½ inch, 27-gauge hypodermic needle.

4.2.3 ***Ex Vivo*** **Intestinal Epithelial Cell (IEC) Culture and Generation of Intestinal Organoids**

This part of the animal experiments was done by our collaborator in the Babraham Institute, Cambridge, with the great help of Dr Marc Veldhoen, Marisa Stebegg and Ulrika Frising. The human organoids were generated, from endoscopic samples taken from healthy young-adult volunteers, and treated for 6 hrs with recombinant human IFNλ–2 (PeproTech, 300-02K) by our collaborator in Addenbrooke's Hospital, Cambridge, with the help of Dr Matthias Zilbauer and Ms Komal Nayak.

4.2.3.1 **Isolation of Highly-Enriched 'crypt' IECs**

Epithelial cells from the small intestine (of mice after sacrifice or from endoscopic human samples) were isolated using a procedure adapted from Sato and Clever's method[37]. Briefly, murine small intestines were collected from wild-type C57BL/6 mice, divided into two equal halves (proximal; duodenum and distal; ileum), opened longitudinally and cut into small (0.5 – 1 cm long) pieces. The small intestinal pieces were then washed (5-7 times) with $MgCl_2$- and $CaCl_2$-free PBS until the supernatant became clear, and incubated in 2 mM EDTA-PBS solution for 20 min on a shaker (50 rpm) at 4º C to loosen the Ca^{2+}-dependent epithelial cell-to-cell contacts. The small intestinal pieces were subsequently washed into PBS and subjected to several (6-7) rounds of manual mechanical disruption by shaking the tissues; i.e. manually moving the tube up and down at a rate of about 3 times per second, in 20 ml PBS for 10-15 seconds. Following each round of manual shaking; the small intestinal fragments were left to settle down by gravity and the resultant clear cell suspension, which is enriched for intestinal crypts, was collected into a separate tube and labelled as fraction 1. This procedure was repeated until a total of 6-7 fractions were generated. The contents of each fraction were inspected by microscopy, and the 'dirtiest' fractions; i.e. containing many

loose villi and cell debris (usually the first ones), were discarded. The remaining fractions were passed through a 70 μm cell strainer and pooled into BSA-coated 50 ml Falcon tubes.

Isolation of colonic IECs (For **Supplementary Figure 4.3**) followed the same protocol as above, except for longer incubation in the thermal shaker (for 1 hrs instead of 20 min) with a higher concentration of EDTA (30 mM instead of 2 mM EDTA-PBS) and longer manual disruption rounds (for 5 min instead of 15 seconds) to increase the yield of the more strongly-attached colonic IECs.

4.2.3.2 **Further Processing of Isolated IECs for Gene Expression and Short-Term Culture**

IECs, isolated by the procedure above, were pelleted at 4º C with 500 x***g*** for 5 min and washed once into cold PBS (400 x***g***; 4 min). When the gene expression of freshly isolated IECs was investigated (**Figure 4.3**), the cells were transferred to Eppendorf tubes into 1.5 ml of PBS, centrifuged (600 x***g***; 5 min) and the pellets were stored at -80º C for future RNA isolation (**Section 2.6.3**), reverse transcription and gene expression analysis (**Section 2.8**). Alternatively, when short-term *ex vivo* IEC culture was wanted (**Supplementary Figure 4.2. 4.3**), IEC survival was improved by seeding into Matrigel droplets (Corning, 356231) and cultivation in growth factor-rich medium optimised for organoid growth by Sato and Clever[37]. Firstly, the IECs were washed once into cold basal culture medium (**Table 4.1**) at a reduced centrifugation force of 300 x***g*** for 3 min to reduce the number of single cells in the pellet. The resultant supernatant was discarded and the pellet was re-suspended in Matrigel diluted to 40 % in cold basal culture medium. The cells were subsequently seeded at 50 μl droplets/well of a pre-warmed 24-well culture plate, which was then incubated for 15-30 min at 37º C to allow Matrigel polymerisation. Once the Matrigel droplets had gelled, 400 μl of growth factor-rich

medium (**Table 4.2**) was added to each well and the plate was incubated at 37º C with 7 % CO_2. IECs were cultured ex vivo for a maximum of 24 hrs and treated with either; 30 ng recombinant murine IFNλ-2/ml (PeproTech, 250-33) or 2.5 ng recombinant murine IFNγ/ml (PeproTech, 315-05), both of which were pre-diluted in basal medium and added to the wells in a total volume of 10 µl. After the indicated time points, the IECs were transferred to Eppendorf tubes into 1.5 ml of PBS, centrifuged (600 x***g***; 5 min) and the pellets stored at -80º C for future RNA isolation (**Section 2.6.3**), reverse transcription and gene expression analysis (**Section 2.8**).

4.2.3.3 **Generation of Intestinal (Duodenal) Organoid cultures**

IECs (crypts) obtained from one duodenum by the procedure outlined in **Section 4.2.3.1** were washed once into cold PBS (400 x***g***; 4 min), re-suspended in 400 µl 100 % Matrigel (Corning, 356231) and seeded as 50 µl droplets into 6-8 wells of a pre-warmed 24-well culture plate. The plate was placed at 37º C to allow Matrigel solidification and then 500 µl of growth factor-rich medium (**Table 4.2**) was added to each well. The crypts developed into full intestinal organoids within 2-3 days of incubation at 37º C with 7 % CO_2. The culture medium was changed every 3-4 days and the organoids were maintained by passaging (at a split ratio of 1:2) every 7 days. The duodenal organoids were treated by the addition of 10 µl of basal medium (**Table 4.1**) containing one of the following:

- For murine organoids, **Supplementary Figure 4.1**: 25 ng recombinant murine IFNλ/ml or 25 ng recombinant murine IFNα (2b subtype)/ml.
- For human organoids, **Figure 4.5**: 25 ng recombinant human IFNλ/ml (PeproTech, 300-02).

- For the organoid-MNV time points experiment (**Figure 3.14**): the stocks of the various viruses used (MNV-O7, MNV-1.CW3, MNV-3 and UV-irradiated stocks) were diluted to the correct concentration to infect organoids at an MOI of 5 in basal medium and added to the well containing the duodenal organoids in total volume of 10 µl.

After the indicated time points, the organoid's IECs were transferred to Eppendorf tubes into 1.5 ml of PBS, centrifuged (600 x***g***; 5 min) and the pellets were stored at -80º C for future RNA isolation (**Section 2.6.3**), reverse transcription and gene expression analysis (**Section 2.8**) or quantification of viral RNA titre by RT-qPCR (**Section 2.7**).

Table 4.1 Constituents of Basal Culture Medium

Amount (ml)	**Reagent**	**Supplier (Catalogue Number)**
500	Advanced DMEM/F12	*Gibco (12634-010)*
5	HEPES buffer solution	*Gibco (15630-056)*
5	GlutaMax-I (100x)	*Gibco (35050-038)*
5	Pen/Strep (100x)	*Gibco (15140-12)*

Table 4.2 Constituents of Growth factor-rich medium

Amount	**Reagent**	**Supplier (Catalogue Number)**
1 ml	basal culture medium	*Table 4.1.*
10 µl	10x N2 supplement	*Invitrogen (17502-048)*
20 µl	5x B27 supplement	*Invitrogen (12587-010)*
2 µl	500 mM N-acetylcysteine	*Sigma (A9165-25G)*
1 µl	500µg rmEGF/ml	*Life Technologies (PMG8043)*
1 µl	100µg rmNoggin/ml	*eBioscience (34-8004-82)*
10 µl	100µg rhR-spondin-I/ml	*PeproTech (120-38)*

rm; recombinant murine. rh; recombinant human.

4.3 Results

4.3.1 Demonstration of Increased Burden of MNV Infection in Old Mice

To assess the effect of aging on the susceptibility to, and early protection against, enteric viral infections, we compared faecal and intestinal tissue viral burdens of young (8-week old) and old (24-month old) C57BL6 wild-type mice within 7 days of infection with a standardised dose of the persistent strain of MNV (MNV-O7). An infectious viral dose of 5×10^6 $TCID_{50}$ was administered orally and the kinetics of virus shedding in faeces from infected mice were followed for a week with daily faecal sampling for viral titration (**Figure 4.1A**). On day 7 P.I. the mice were sacrificed and viral titres were measured in gut sections and MLNs (**Figure 4.1B**). As expected, MNV-O7 infection of young wild-type mice resulted in persistent viral shedding in faeces that tended to drop within the first 3 days of infection (about two-log reduction) and then was maintained at a fairly steady level of about 10^4 viral genome copies per mg of faeces. Seven days P.I. the tissue viral titres were higher (almost a log difference) in the MLN compared to intestinal segments.

Whilst they had comparable viral loads on day 1 P.I., the 24-month old wild-type mice maintained a significantly higher MNV-O7 viral titre in excreted faeces and in all tissues examined, with approximately a 3-fold rise in the distal small intestine and MLNs, compared to those of younger counterparts. There was a minor reduction in faecal virus shedding during the first few days of infection, however it was less impressive than that of young mice and the faecal viral titres were maintained at around 10^5 viral genome copies per mg of faeces.

Thus, although the wild-type mouse-MNV-O7 experimental model is sub-clinical (asymptomatic) and so does not allow for assessment of the clinical impact, it clearly demonstrated the increased viral burden and impaired control of a persistent enteric virus in the elderly.

4.3.2 **Immunological Basis of the Old Mouse Phenotype**

To investigate the immunological defect underlying the increased burden of MNV-O7 infection observed in old mice we used the *in vivo* anti-CD3/MNV-O7 model, which allowed us to probe the anti-viral defence capacity of the gut mucosa under different conditions (**Chapter 3**). The characteristics, effects, limitations and procedure of this experimental model has been detailed previously (**Section 3.3.1**). Briefly mice were orally infected with MNV-O7 8 hrs after i.p. injection of either agonistic anti-CD3 or non-specific isotype control (ITC) antibodies. Mice were sacrificed 40 hrs after virus challenge to determine the degree of protection observed at different sites of the small intestine and draining MLNs. In young (8-12 weeks old) wild-type mice stimulation with anti-CD3 resulted in a broad, systemic cytokine response with release of all three types of IFN, up-regulation of immune-protective ISGs and induction of an effective antiviral-state in the gut (**Chapter 3**). In **Figure 4.2** we compared the control of virus replication in young (8-week old) and old (24-month old) C57BL6 mice using this model. As shown in the figure, young mice were able to significantly control and prevent the establishment of overt MNV-O7 infection following stimulation with agonistic anti-CD3 antibodies. After ITC antibody injection, both old and young mice had comparable levels of virus in intestinal tissues, however the old (wild-type) mice had a strikingly reduced capacity to suppress the viral load upon anti-CD3 stimulation and maintained significantly higher viral titres in all tissues examined compared to anti-CD3-injected young controls. There was a trend for reduction of the virus titre with anti-CD3 stimulation of old mice in the middle small intestine (jejunum) and MLNs, however it was statistically insignificant when compared to that of ITC-injected controls and much (about two orders of magnitude) less than that observed in the young mice.

These findings were of particular interest and encouraged the investigation of whether the observed old mouse phenotype was due to reduced production of protective antiviral

cytokines by intestinal lymphocytes, mononuclear phagocytes and/or IECs. Another possibility is that the defect could be due to the impaired ability of IECs and/or mononuclear phagocytes to respond to these protective cytokines and mount effective anti-viral immune responses.

4.3.3 **Is there a Cytokine Production vs Response Defect Or Both?**

To track the anti-viral protective responses mediated by anti-CD3 stimulation, we compared the anti-viral gene expression of 8-week old (young) and 24-month (old) wild-type mice 3 hrs post-stimulation by i.p. administration of anti-CD3 antibody. Due to the reduction in naïve/memory T cell ratio in the elderly with the proportional accumulation of fully differentiated memory T cells with aging[360,361], we decided to isolate the splenic $CD8^+$ memory ($CD44^{hi}$) T cells from the young and old mice to compare memory T cell cytokine mRNA expression directly. We also isolated and compared the responses of IELs and IECs from the small intestine of all mice (**Figure 4.3**). Consistent with the 'infamm-aging' theory, RT-qPCR analyses revealed elevated expression levels of the pro-inflammatory cytokines (TNFα and IFNγ), both in the splenic CD8 memory T cells and IEL fractions of the 2-years old wild-type mice, almost double that of the young counterparts (**Figure 4.3A** & **B**). In fact, the old C57BL6 mice reacted poorly to anti-CD3 injections, with the clinically-observed development of pili-erection, tremors and decreased mobility, suggesting the development of a severe 'cytokine-storm' compared to the young controls. The young-old differences in other IFNs were less impressive with comparable expression levels of IFNβ and IFNλ mRNA by both CD8 memory T cells and IELs. As discussed earlier, the systemic cytokine expression stimulated by anti-CD3 antibodies culminated in an effective anti-viral state in the gut with induction of several ISGs. This was evident in the duodenal and ileal IECs extracted from young mice that showed clear up-regulation of all ISGs examined; *Mx1*, *Adar*, *Rsad2* and *Prkr*

(**Figure 4.3C**). The mRNA levels of these ISGs were, however, markedly reduced in the duodenum and ileum of the 2 years old, aged, anti-CD3-treated mice. The difference was clearer for certain ISGs, namely *Mx1* and *Rsad2*, with almost 10 orders of magnitude reduction in the expression in the old mice compared to that of young controls.

Taken together, the data presented in **figure 4.3** strongly suggested that the aging process negatively affected the IFN responsiveness of IECs and their ability to mount an effective anti-viral state. Although the expression level of type-II IFN seemed to be elevated, rather than reduced, with relatively stable expression levels of type-I and –III IFNs by old lymphocytes, it is important to note that these data do not conclusively exclude the possibility of a production defect. The aging process might have post-translational effects that modify cytokine production at the protein level. Moreover, given their sheer numbers, location, and ability to sense and respond to replicating viral particles, IECs and mononuclear phagocytes (DCs and macrophages) are important sources of type-I and –III IFNs that have not been addressed and examined in this experiment.

4.3.4 A Specific, Age-Dependent Small Intestinal Defect in IECs' Response to IFNλ

This section was done in collaboration with Ms. Marisa Stebegg at the Babraham Institute, Cambridge. Following the hypothesis drawn from the previous sections that aging affects IFN responsiveness of IECs, we aimed to analyse and dissect the mechanism by *in vitro* and *ex vivo* experimental models. To that end, we firstly confirmed the previously reported observation of superior responses of IECs to type-III IFNλ rather than to type-I IFNs[112,356]. In **Supplementary Figure 4.1** small intestinal organoids were established from the gut of young (8-12 weeks old) C57BL6 wild-type mice, and were treated with equivalent doses (25 ng/ml) of either recombinant murine IFNα (2b subtype) or IFNλ-2 for the indicated time points. Indeed, the expression levels

of the ISGs *Mx1* and *Isg15* increased exponentially with time after IFNλ treatment, with *Isg15* expression reaching a 1000-fold increase after 24 hrs. This was associated with induction of IFNλ expression by IECs at late time-points. In marked contrast, *Ifnl* mRNA levels and ISG expression remained constantly low upon IFNα treatment compared with IFNλ. Thus, the *in vivo* anti-CD3 mediated induction of protective ISGs, and hence the anti-viral state, in small intestinal IECs is most likely mediated through production of, and in response to, type-III IFNs.

Following this conclusion, we directly compared the IFN-responsiveness of small intestinal IECs isolated from young (8-week old) and old (24-month old) wild-type mice (**Figure 4.4**). For short-term *ex vivo* cultures, IECs were maintained under the same cultivation conditions as intestinal organoids, preserving cell-cell contact, to achieve optimal IEC survival (**Section 4.2.3.2**). After *ex vivo* treatment with recombinant murine IFNγ for 6 hrs, IECs from small intestines of old mice showed a comparable response to those sourced from young mice when assessed for IFNγ-induced *Ido1* mRNA expression (**Figure 4.4**). The expression of another IFNγ-responsive gene, *Cxcl9*, was different with old IECs displaying a significantly stronger expression compared to the young counterparts, a finding in line with the 'inflamm-aging' theory, as CXCL9 recruits the pro-inflammatory $CXCR3^{+}$-cells that produce the prototypical inflammaging cytokine IFNγ[362,363]. Furthermore, this IFNγ response confirmed that the aged IECs were not in an overall state of hypo-responsiveness. We did, however, observe a significant reduction in expression levels of the IFNλ-induced genes *Mx1* and *Isg15*, in aged small intestinal epithelium compared to those of the young controls (**Figure 4.4**). *Isg15* mRNA levels of old mice were decreased by almost three-fold, while a two-fold reduction was detected for *Mx1* levels.

This was associated with a less prominent, but statistically significant, drop in the expression levels of the *Il28ra* subunit of the IFNλ-receptor in the IECs sourced from old mice, while those of the *Il10rb* subunit remained unchanged (**Supplementary Figure 4.2A**). Unfortunately, we could not link these data with the protein levels of the IL-28Rα subunit because anti-mouse IFNλR antibodies are currently unavailable and the anti-human IL-28Rα antibody, that was tested, failed to produce specific staining in mouse samples.

We further confirmed that the IFNλ-defective response was specific for IECs isolated from the small intestine of old mice, as those extracted from the colon had, if anything, a similar or even slightly higher expression levels of ISGs in response to IFNλ treatment compared to those of the young counterparts (**Supplementary Figure 4.2A**). Importantly, this specific, small-intestinal, IFNλ-response phenotype appeared to be age-dependent. The defect became more apparent with advancement of age. Fifteen-month old mice had a very similar, but less pronounced phenotype compared to that of 24-month old mice (**Supplementary Figure 4.2B**). Compared to the young controls, expression levels of *Isg15* were significantly reduced in IFNλ-treated duodenal IECs sourced from 15-month old wild type mice, while the decrease in *Mx1* expression was not statistically significant. This was also associated with a reduction (at the transcription level) of the *Il28ra* subunit of IFNλ-receptor, and as expected, a stable unchanged IFNλ-responsiveness of colonic IECs (**Supplementary Figure 4.2B**).

4.3.5 **The IFNλ–Defect of The Elderly Is Treatable**

To investigate whether the specific IFNλ-hyporesponsive phenotype of the aged small intestinal IECs was due to an irreversible, inherent defect or if it could be overcome by exogenous IFNλ administration, we persistently infected young and old mice with MNV-O7, as described in **Section 4.3.1**. On day-1 and -3 P.I. the mice were treated i.p. with

25 μg IFNλ (per mouse per injection) or with PBS as a control (**Figure 4.5**). Young mice responded swiftly to IFNλ injections with significant reductions in viral titres in faeces and gut tissues, confirming previously reported data[289]. Interestingly, the 24-month old mice responded to IFNλ treatment in a similar and indistinguishable manner compared with the young mice. MNV-O7 was rapidly cleared from older mouse faeces, within 1 day of the second IFNλ dose (**Figure 4.5A**), and significantly reduced in the gut sections and MLNs to very low levels (**Figure 4.5B**) following IFNλ treatment. It is important to note that I did not titrate the dose of IFNλ to determine the minimal dose required for an effect. This means that the high dose that I used in this experiment (two injections of 25 μg per mouse) might saturate the system. Saturation of the IFN-lambda receptors may have caused the lack of difference between young and old mice that was observed.

These data strongly suggested that the reduction observed in IFNλ-responsiveness of old mice is not an inherent cell defect that is persistent and cannot be reversed. I propose that it is rather an accumulation of adverse effects, most likely linked to the age-associated gut mucosal inflamm-aging environment and/or the age-related microbiota changes, that render the old mice hypo-responsive to endogenous IFNλ and, thus, more susceptible to severe enteric viral infections. The data also suggested that the defect might be broader than just IEC-hyporesponsiveness to IFNλ. There may also be a combined, yet unidentified, reduction in the production of protective IFNs (IFNλ) by other immune cells and/or IECs themselves, that contributes to the development of the characteristic phenotype in the old mice.

4.3.6 **The Organoid/ IFNλ Experimental Model is Viable in Human Samples**

In collaboration with Dr Matthias Zilbauer's lab at Department of Paediatrics, University of Cambridge, we evaluated human organoids to test the feasibility of comparing our results in mice with human samples. Small intestinal organoids were generated from

endoscopic samples taken from two young-adults (age 23-26 years old) healthy volunteers in Addenbrooke's Hospital. The human organoids were subsequently treated with recombinant human IFNλ for 6 hrs and the expression levels of the ISGs: *MX1* and *ISG15* mRNA were measured by RT-qPCR (**Figure 4.6**). Compared to the untreated controls, IFNλ treatment resulted in a strong induction, almost 3-fold, of both ISGs, confirming the sensitivity of the young-adult human IECs to IFNλ. We are planning to extend this experimental protocol, in collaboration with Prof Tim Spector group, King's College, London, in order to analyse and compare the responses of small intestinal organoids generated from elderly (>65 years old) volunteers.

4.4 Discussion

The aging process significantly impacts the gut mucosal homeostasis and alters the outcome of enteric (noro)virus infections. The data presented in this chapter demonstrate a clearly increased viral burden phenotype in aged wild-type mice infected with MNV-O7. We analysed the immunological basis of the phenotype, identified a specific age-dependent defect that could be reversed by exogenous IFNλ treatment, and proposed an *in vitro* experimental model to compare and translate the results to humans.

There remain questions to be answered. The exact cause(s) of the phenotype observed in old mice and the specific molecular mechanism(s) of IEC IFNλ-hyporesponsiveness remain to be elucidated. The transcriptional defect of the IL-28Rα subunit of IFNλ-receptor is of interest, but needs to be confirmed at the protein level. Earlier reports linked the age-associated reduced IFN responses of innate immune cells to impaired STAT1 signalling. Yoon *et al.* (2004) observed impaired JAK/STAT signalling in aged macrophages from old BALB/c wild-type mice; these macrophages were found to be hyporesponsive to IFNγ[364]. Quian and colleagues (2011) reported a reduced level of

STAT1 protein and phosphorylation in DCs isolated from aged (73.6 ± 6.0 years old) human donors and infected *in vitro* with West Nile virus[365]. Interestingly, in this study the authors observed no significant age-related changes in expression or nuclear translocation of signalling molecules in initial anti-viral responses, however, DCs isolated from older volunteers had diminished induction of late-phase responses (e.g., STAT1, IRF7, and IRF1), suggesting a defective regulation of type-I IFN[365]. To our knowledge, the data presented in this chapter are the first to report age (beyond the adult-life)-related changes of the IECs responses to IFNs. Moreover, the fact that IFNγ uses certain signalling mediators, such as STAT-1, that are shared with the IFNλ transduction-pathway will allow their exclusion as sites of the defect, as IECs sourced from old mice are functionally responsive to the former but not the later.

The regional variation in the IFN-responses of IECs along the full length of the intestinal tract further highlights the naivety of the assumption that the gut is a single uniform organ and adds to a growing body of evidence for intestinal immune compartmentalization (**Section 1.1**). The difference between duodenal and ileal IEC expression of ISGs roughly correlates with the regional difference in viral loads. Generally, colonic IECs had much reduced levels of ISG expression in response to IFNλ treatment, almost half that of IECs isolated from small intestine (**Supplementary Figure 4.2**). This might be a contributory factor for the preferred colonic tropism (higher viral titres) observed in MNV infection and the colonic persistence of many viruses including MNV[283,284].

The differential effects of the aging process, with age-associated IFNλ-hyporesponsiveness being apparent in the small intestine and absent in the colon, suggests that the defect might be more linked to the inflamm-aging environment in the gut mucosa rather than to the age-related changes in the microbiota. Further experiments with germ-free mice, antibiotic treatment and/or faecal transplantation will be necessary

to address and substantiate/support this hypothesis. Furthermore, employing the adoptive-transfer experimental model used in the previous chapter (**Chapter 3**) with transfer of young/old lymphocytes and/or mononuclear phagocytes into young/old *Rag2*$^{-/-}$ or *Ccr2*$^{-/-}$ mice will be important in interrogating these different immune cells and identifying their role in the development of this age-specific immune defect.

5 MANIPULATION OF THE ARYL HYDROCARBON RECEPTOR (AhR) INFLUENCES EARLY GUT IMMUNITY AGAINST MURINE NOROVIRUS (MNV)

Chapter 5 MANIPULATION OF THE ARYL HYDROCARBON RECEPTOR (AhR) INFLUENCES EARLY GUT IMMUNITY AGAINST MURINE NOROVIRUS (MNV)

5.1 Background

AhR is a highly conserved, ligand-activated transcription factor that is abundantly expressed at barrier sites, including the gut. For details about AhR signalling, ligands, expression, regulation, interactions and immunological relevance please refer to **Section 1.2.5**. Highly expressed by specific barrier-associated immune cells, the role of AhR signalling in immunity against infectious diseases continues to draw increasing attention. The ability of AhR to recognise distinct bacterial (*M. tuberculosis* and *P. aeruginosa*) virulence factors, and to subsequently induce protective anti-bacterial responses, has led to the suggestion that AhR can be regarded as an intracellular PRR[216]. The influence of AhR on immunity against viral infection, however, has so far only been investigated in the context of 'stimulation' by exogenous AhR-ligands, such as dioxin. Firstly, dioxin (also known as TCDD) administration enhances the replication of human cytomegalovirus in a fibroblast cell line through an AhR-dependent mechanism[366]. Secondly, 3-Methylcholanthrene (3-MC), a chemical homologue of dioxin, induces the replication of HIV-1 replication in a latently-infected promyelocytic cell line[367]. Thirdly, dioxin-induced AhR activation reduces the survival rate of mice infected with influenza-A virus (IAV)[368,369], and indirectly diminishes the induction of IAV-specific CD8 T cell responses through its immunoregulatory effects on DCs[370] (discussed in more detail below). Lastly and interestingly, by using a mouse-model of IAV infection and directly (side-by-side) comparing the immunomodulatory properties of the two most commonly used high-affinity AhR-ligands, i.e. dioxin and FICZ, Wheeler *et al.* (2014) were able to demonstrate clear differential consequences of stimulation by the two distinct AhR-ligands on innate and adaptive anti-viral responses[371]. Both dioxin and FICZ suppressed

the virus-specific CD8 T cell response, whereas dioxin, but not FICZ, enhanced neutrophil recruitment and pulmonary inducible nitric oxide synthase (iNOS) production in response to IAV infection[371]. Moreover, stimulation by a different AhR ligand (DIM) results in a completely different clinical outcome of viral infection[372]. One report suggested a protective anti-viral effect of the AhR ligand (DIM) by demonstrating a significant suppression of reovirus infection and faecal shedding in mice orally gavaged with DIM compared to controls[372]. However, caution should be taken in the interpretation of this finding as DIM has a number of AhR-independent signalling effects[373], a fact that had not been accounted for in the above report by, for example, including *Ahr*$^{-/-}$ mice as an additional control[372].

In my opinion, additional emphasis and efforts should be applied to investigating the physiological significance of constitutive AhR-signalling, and the effects of induction by endogenous and natural AhR ligands, in the context of protection against viral infections. A landmark in the field is the demonstration of a direct link between the gut-associated AhR system and the biology of IELs[203]. Manipulation of the AhR system, either genetically (*Ahr*$^{-/-}$) or through diet modification, was sufficient to alter the number and functions of IELs[203]. A primary aim of this chapter was to extend this previous research by applying an *in vivo* experimental model and analysing the consequences of such AhR-manipulations on the outcome of enteric (Noro)virus infections. However, AhR has some indispensable roles in reproduction[192,374], and *Ahr*$^{-/-}$ females show reduced fertility and reduced litter size. Therefore, in order to maintain a colony for the *in vivo* experiments we relied on breeding *Ahr*$^{-/-}$ males with AhR heterozygous females. This resulted in significant delays and a difficulty in generating consistent age- and sex-matched experimental groups. Moreover, most likely due to microbiota- and age-differences, there was a significant variation in the number of IELs in *Ahr*$^{-/-}$ offspring obtained by this breeding strategy (Dr Marc Veldhoen, personal communication). For these reasons (and

others), it proved to be quite difficult to meet the aim above within the time frame of my PhD.

Another interesting finding, which is directly relevant to anti-viral immune responses, is the possible interactions and cross-talk between the AhR- and IFN-STAT1-signalling pathways. The consequences of the physical association between activated AhR and STAT-1 molecules[198,199], have been discussed previously (**Section 1.2.5**). A recent report identified AhR-interacting protein (AIP), one of the cytoplasmic chaperones of inactive AhR, as a novel inhibitor of interferon-regulatory factor-7 (Irf-7)[375]. Irf-7 phosphorylation and nuclear translocation are crucial steps in IFN-signalling and the induction of a subsequent anti-viral state (further details in **Section 1.2.2**). Upon viral infection of murine embryonic fibroblasts, AIP potently antagonises the nuclear localisation of Irf-7 and significantly reduces subsequent type-I IFN production and signalling[375]. Thus, the release of AIP from the cytoplasmic-AhR complex upon ligand activation might represent another mechanism through which the AhR activity modulates innate antiviral immune responses. I aimed to further address these findings by developing and characterising an *in vitro* bone marrow-derived mononuclear cell (BMMC) experimental model, with the specific objective of analysing the influences of such interactions and cross-talk on the viral replication of MNV-O7.

The AhR is constitutively expressed by mononuclear phagocytes: macrophages and DCs[212]. This expression is further augmented by exposure to LPS and CpG[198,376]. Functional AhR signalling in DCs is required for normal induction of indoleamine 2,3-dioxygenase (IDO) expression[376,377]. IDO is an immunosuppressive enzyme that catabolises tryptophan into Kynurenine (Kyn) and other metabolites in DCs[378]. Kyn was reported to promote Foxp3-expression and regulatory T cell differentiation[376], and is (itself) considered to be a putative AhR agonist[215], providing a possible positive feedback loop for AhR-induced immune tolerance. FICZ-mediated activation of AhR in bone

marrow-derived DCs (BMDCs) of wild-type mice decreased the expression of CD11c and increased that of MHC-class II (MHC-II), CD86 and CD25[379]. Comparing BMDCs from bone marrow of wild-type and *Ahr*$^{-/-}$ mice differentiated in the presence of granulocyte-monocyte colony-stimulating factor (GM-CSF), Vogel and colleagues (2013) demonstrated characteristic phenotypic differences of the *Ahr*$^{-/-}$ BMDCs with a significant increase in the proportion of immature cells[380]. In this report, the authors used CD11c expression to identify DC populations and MHC-II expression to determine the DC-maturation status[380].

Using MNV-O7 as a model of enteric viral infections, the objective of this chapter was to investigate the role of AhR in enteric virus infection. Specifically, to:

1) Compare MNV-O7 viral titres in wild-type and *Ahr*$^{-/-}$ mice in the context of acute and chronic (persistent) infection.
2) Explore different BMMCs differentiation protocols and select the most appropriate protocol for further studies.
3) Characterise the phenotypic features (surface marker expression) of BMMCs derived from wild-type and specific (AhR-related) knock-out mouse lines; *Ahr*$^{-/-}$, *Ahrr*$^{-/-}$ (*Ahr repressor*$^{-/-}$) and *Cyp*$^{-/-}$ (*cytochrome p450*$^{-/-}$).
4) Assess MNV-O7 replication in these different BMMCs.
5) Analyse the early IFN-mediated anti-viral immune responses induced in different BMMCs in response to poly(I:C) stimulation by gene expression analysis and ELISA.
6) Evaluate the influences of ligand-mediated manipulation of AhR signalling on wild-type BMMC differentiation/maturation and MNV-O7 viral replication kinetics.

5.2 Materials and Methods

For cell lines, viruses, *in vivo* infection, sample collection, RNA extraction, viral quantification, reverse transcription, gene expression assays and statistical analysis, please refer to **Chapter 2**. For flow cytometric analysis of the BMMC surface marker expression please refer to **Section 3.2.4**.

5.2.1 Mice:

C57BL/6 wild-type, *Ahr*$^{-/-}$, *Ahrr*$^{-/-}$ and *Cyp*$^{-/-}$ mice were bred at the Babraham Institute under Specific Pathogen Free (SPF) conditions. The mice, or their long bones for BMMC extraction, were supplied by our collaborator Dr Marc Veldhoen (The Babraham Institute, Cambridge). For mouse transport, maintenance and setting up of the experimental mouse groups please refer to **Section 2.4.1**.

5.2.2 Generation of Bone Marrow-Derived Mononuclear Cells (BMMCs) and Their Treatment with AhR-Agonist (FICZ) or AhR-Antagonist (CH223191)

Bone marrow was extracted from the long bones (femurs and tibias) of mice by flushing with Iscove's modified Dulbecco's medium (IMDM) supplemented with 10 % foetal calf serum (FCS), 100 U penicillin/ml and 0.1 mg streptomycin/ml (10% IMDM), using 5 ml syringes and 25G needles. The bone marrow was filtered through a 70 μm cell strainer and centrifuged (5 min, 1280 x***g***) at 4 ° C. Cells were subsequently resuspended at a density of 1 x 10^6 cells per ml in 10% IMDM supplemented with either GM-CSF (20 ng/ml) alone or GM-CSF (20 ng/ml) with IL-4 (10 ng/ml). For certain experiments, BM cells extracted from wild-type mice were differentiated in 10% IMDM supplemented with GM-CSF (20 ng/ml) and either 500 nM FICZ (Tocris, 5304) or 3 μM CH223191 (Tocris, 3858).

The cells were immediately transferred into six-well tissue culture plates, at 2 ml per well, and incubated for 8 days at 37 º C, 5 % CO_2. For specific experiments (**Supplementary Figure 5.2**), microscopic images were taken of the differentiating cells on Day 0, 3, 6 and 8. During this 8 day incubation period, the specific medium of each differentiation protocol was renewed once (usually in day 5 of the incubation) by aspiration of the old medium in the wells, with the removal of floating cells in the process, and replacing it with a fresh medium (consisting of exact same components) for the final 3 days of differentiation.

To harvest the cells in day 8 of differentiation, the 6-well plates containing the cells were placed on ice for at least 30 min. The cells were then mechanically scraped from the wells and centrifuged (5 min, 400 x***g***) in 50 ml tubes. Cells were washed once in ice-cold 10% IMDM, centrifuged again (5 min, 400 x***g***) and finally re-suspended into 10% IMDM at the required cell density for subsequent assays.

5.2.3 **MNV-O7 Infection of BMMCs**

BMMCs generated by the protocols described above were seeded into individual wells of 96-well tissue culture plates (flat-bottomed), at a density of 2 x 10^5 cells per well. Cells were allowed to adhere to the plates for at least 16 hrs at 37 º C, 5 % CO_2. After this incubation period, the medium was removed from the wells and replaced with the MNV-O7 virus inoculum diluted to the stated multiplicity of infection (MOI) in warm 10% IMDM, or replaced with 10% IMDM alone (mock infection). Cells were incubated with the virus for 1 hrs, 37 º C, 5 % CO_2 with gentle agitation every 15 min. After this 1 hrs infection period, the viral inoculum was removed and cells overlaid with warm PBS as a part of a washing step. Plates were centrifuged (5 min, 400 x***g***) after which the PBS was removed and replaced with warm 10% IMDM. Cells corresponding to the 1 hrs post infection (P.I.) time-point were processed at this stage, by removal of the supernatant,

lysis of the cells for RNA extraction (**Section 2.6.3**) and quantification of the viral RNA titres by RT-qPCR (**Section 2.7**). Otherwise, cells were returned to the incubator (37 º C, 5 % CO_2) until the required time points (9, 12, 24 and 48 hrs P.I.) for similar processing.

5.2.4 **Treatment of BMMCs with Poly(I:C) and Gene Expression Analysis**

BMMCs generated by the method detailed in **Section 5.2.2** were seeded into individual wells of 96-well tissue culture plates (flat-bottomed), at a density of 2 x 10^5 cells per well. Cells were allowed to adhere to the plates for at least 16 hrs at 37 º C, 5% CO_2. After this incubation period, the medium was removed from the wells and replaced with 10% IMDM supplemented with 100 μg Poly(I:C)/ml (Sigma-Aldrich, P1530). Cells corresponding to the baseline time point were processed at this stage, by removal of the supernatant for ELISA analysis (**Section 5.2.5**), and lysis of the cells for RNA extraction (**Section 2.6.3**), reverse transcription and gene expression analysis (**Section 2.8**). Otherwise, cells were returned to the incubator (37 º C, 5 % CO_2) until the required time points (1, 3, 6, 9, 12 and 24 hrs P.I.) for similar processing.

5.2.5 **IFN-β Enzyme-Linked Immunosorbent Assay (ELISA)**

The concentration of IFN-β in supernatants collected from individual wells of the poly(I:C)-treated cell cultures (**Section 5.2.4**) was quantified by ELISA. The mouse IFN-β ELISA Kit (Biolegend, 439407) was used according to the manufacturer's protocol.

5.3 Results

5.3.1 Comparison of MNV-O7 Viral Load in Wild-type and AhR-Deficient Mice

In order to assess the role of constitutive AhR signalling in immunity against enteric viral infection, we compared the viral load in tissues following infection with a standardised dose of MNV-O7. An infectious viral dose of 5 x 10^6 $TCID_{50}$ was administered orally to C57BL6 wild-type and *Ahr*$^{-/-}$ mice. To assess the effects of AhR signalling during acute infection, a group of mice was sacrificed 40 hrs after viral challenge to determine the viral burden at different sites of the small intestine and draining lymph nodes (MLN) (**Figure 5.1A**). The remaining infected mice were maintained to establish chronic (persistent) infection and were followed by RT-qPCR measurement of viral shedding in faeces. On day 21 P.I. all mice were sacrificed and viral titres were measured at various sites of the small intestine (**Figure 5.1B**).

As shown in **Figure 5.1A**, MNV-O7 virus replicated in the wild-type mice and established homogeneous levels of infection throughout the length of the small intestine (duodenum, jejunum and ileum) and in the MLN. In contrast, virus replication in *Ahr*$^{-/-}$ mice was more variable. The mouse to mouse variation and the range of the viral titres detected in the *Ahr*$^{-/-}$ mice were much greater than that seen in the wild-type counterparts. Initially, I thought this variation could be explained, at least in part, by the fact that *Ahr*$^{-/-}$ mice have a variable deficiency of the CD8αα^{+} (natural) IELs[203] (and Dr M Veldhoen, personal communication). However, the data presented in **Chapter 3**, especially the comparable levels of MNV-O7 infection in the *Il15ra*$^{-/-}$ and wild-type mice, suggested that these natural IELs are not essential and, if anything, play a minor role in resisting the establishment of MNV-O7 infection. Another possible explanation for this variation observed is the wider range of age (between 8 – 16 weeks) of *Ahr*$^{-/-}$ mice used to set up the experimental groups. This, as explained earlier, was unavoidable due to the difficulty in breeding *Ahr*$^{-/-}$ mice colony. It is important to note, however, that I could not detect a

specific correlation between the MNV-O7 viral titres and the increase/decrease of mouse age at the time of infection (data not shown).

Another important observation that can be drawn from the acute infection setting was the '**partial**' **resistance** to MNV-O7 infection displayed by the *Ahr*$^{-/-}$ mice (**Figure 5.1A**). The median viral titres of the *Ahr*$^{-/-}$ mice were significantly lower than those of the wild-type controls in all tissues examined. The difference was more apparent in the proximal parts of the gut (duodenum, jejunum) and in the MLNs. This resistance of *Ahr*$^{-/-}$ mice to MNV-O7 replication was also evident at chronic infection time points (**Figure 5.1B**). Though fluctuating, the overall faecal shedding of MNV-O7 was significantly lower in the AhR-deficient mice compared to that of wild-type controls. The tissue viral load on day 21 P.I. was also clearly reduced in all segments of *Ahr*$^{-/-}$ gut examined (**Figure 5.1B**). It is worth noting that, in another small preliminary study, I was able to detect a similar sort of resistance in the same gut tissues of *Ahr*$^{-/-}$ mice using the acute strain MNV-1.CW3 (data not shown). These findings suggest that the resistance to viral infection exhibited by the *Ahr*$^{-/-}$ mice is not specific to the MNV-O7 strain and might not even be specific for the MNV virus.

Thus, compared to the wild-type controls, *Ahr*$^{-/-}$ mice established variable levels of MNV-O7 infection with a partial resistance to viral replication that was more apparent in the proximal gut and MLNs. This resistance did not prevent the progression to chronic persistent infection, however, it was associated with a significant reduction of viral shedding in faeces, and of gut tissue viral titres.

5.3.2 **MNV-O7 vRNA Titres vs Infectious Virus Titres**

To confirm the correlation between the vRNA (RT-qPCR) titres and the infectious virus titres of MNV-O7, I used a $TCID_{50}$ virus titration assay optimised for MNV-O7 infection by Dr James Chettle (**Section 2.5**). Indeed, measurement of MNV-O7 infectious virus

titres by this assay, on samples obtained from the same mice used in the experiment above (**Figure 5.1A**), showed the exact same differences between wild-type and *Ahr*$^{-/-}$ mice with maintenance of the same layout of the figures (**Supplementary Figure 5.1A**). Furthermore, a strong correlation between viral genome copy number and $TCID_{50}$ infectious titre was detected with an R-squared value of 0.844 (**Supplementary Figure 5.1B**). However, the $TCID_{50}$ assay was consistently less sensitive, with about three orders of magnitude lower viral titres compared to those obtained by RT-qPCR. This discrepancy between vRNA copies and infectious titres has been detected in previous reports[266,314], and has been attributed to an inherent problem of the $TCID_{50}$ assay in which the induction of primary anti-viral responses by the BV-2 cells used in the assay prevents the spread of the cytopathic changes across the entire well and thus leads to its scoring as negative, as well as to the presence of non-pathogenic virus, non-packaged viral RNA and defective-interfering particles (Dr James Chettle's, unpublished data).

5.3.3 Selection of a Differentiation Protocol to Generate Bone Marrow-derived Mononuclear Cells (BMMCs)

I aimed to address and further analyse the resistance to MNV-O7 infection observed in the *Ahr*$^{-/-}$ mice by developing and characterising an *in vitro* BMMC-based experimental model. The successful replication of MNV in phagocytic cells (macrophages and DCs) has been described in several reports[271,285–287,381,382]. However, the exact protocol used to generate these phagocytes from the bone marrow and, consequently, their expression of surface markers varies significantly from one study to another. In an unpublished work, Dr James Chettle (PhD thesis, University of Cambridge, 2015) observed higher levels of both initial binding and replication of MNV-O7 in mononuclear phagocytes differentiated by a protocol that include the use of a combination of GM-CSF and IL-4 compared to those of cells generated by other differentiation protocols. In the field of AhR research, the most commonly used differentiation protocol for the generation of

bone marrow cells is the one using GM-CSF alone[376,377,379,380]. Another problem is the confusion in the terminology used to describe the derived cells. It seems that the terms bone marrow-derived DCs and macrophages are used interchangeably between different reports using various differentiation protocols[271,383,384]. Helft and colleagues (2015) clearly demonstrated the heterogeneity of cells generated in GM-CSF bone marrow cultures[385]. The bone marrow cells generated by different differentiation protocols are termed bone marrow-derived mononuclear cells (BMMCs) in this chapter to avoid this confusion.

To select a single differentiation protocol that may allow a meaningful comparison of the replication patterns of MNV-O7 and the early cellular responses to poly(I:C) stimulation, I cultivated and differentiated bone marrow precursors derived from wild-type and *Ahr*$^{-/-}$ mice according to one of two different protocols: either in the presence of GM-CSF alone or in the presence of a combination of GM-CSF and IL-4. At different time points during the 8 day maturation period, I compared the microscopic features of the growing cells (**Supplementary Figure 5.2A**) and at the end of that incubation period, I stained the cells with fluorescent antibodies to common macrophage/DC surface-markers for flow cytometric analysis (**Supplementary Figure 5.2B**).

On early days of maturation, cells from wild-type and *Ahr*$^{-/-}$ mice looked similar by phase contrast microscopy using both types of differentiation protocols. However, with time the *Ahr*$^{-/-}$ cells started to become bigger and had more vacuoles than their wild-type counterparts in the presence of IL-4, while the GM-CSF-only protocol resulted in more fibroblast (DC)-like cells, with dendrites in both wild-type and *Ahr*$^{-/-}$-derived cells (**Supplementary Figure 5.2A**).

Distinct patterns of surface-markers expression were also observed by flow cytometry. The differences between wild-type and *Ahr*$^{-/-}$ BMMCs are addressed in more detail in subsequent sections. The main objective of this experiment was to compare the two

commonly used protocols for differentiation, and the most distinguishable difference was the expression of CD8α by wild-type but not *Ahr*$^{-/-}$ BMMCs in the presence of IL-4 (**Supplementary Figure 5.2B**). CD8α^{+} DCs are responsible for cross-priming cytotoxic T cells *in vivo*[386], and the induction of CD8α expression on wild-type BMMC in the presence of IL-4 has been reported before[387–389]. However, the absence of such induction in the AhR-deficient cells has not previously been reported. There was also a difference in CD86 expression between wild-type and *Ahr*$^{-/-}$ BMMCs in both differentiation protocols.

All in all, given the differences observed when using the GM-CSF + IL-4 protocol and to be able to compare baseline cells as similar as possible, I chose the GM-CSF-only differentiation protocol to generate BMMCs from different mouse lines for subsequent experiments.

5.3.4 **Phenotypic Analysis of BMMCs by Flow Cytometry**

BMMCs from C57BL6 wild-type, *Ahr*$^{-/-}$, AhR repressor-deficient (*Ahrr*$^{-/-}$) and Cyp1 triple-knockout (*Cyp*$^{-/-}$) mice were differentiated with GM-CSF for 8 days. Elimination of the AhR autoregulatory mechanisms, by knocking out the AhRR or Cyp1-enzymes, results in augmentation and prolongation of the endogenous ligand-mediated constitutive AhR signalling[390,391].

Confirming previous reports[380,392], *Ahr*$^{-/-}$ BMMCs were less mature than the wild-type controls with a clear reduction in MHC class II and CD86 expression (**Figure 5.2A**). No clear differences were observed between the two sets of cells in the expression of CD11c and CD80. Augmentation of endogenous AhR signalling in *Ahrr*$^{-/-}$ and *Cyp*$^{-/-}$ resulted in more subtle changes with a minor increase in MHC class II expression and a reduction in CD11c expression (**Figure 5.2A**). Dividing the CD11c^{+} BMMCs according to their MHC class II expression (as in [380]) into immature (MHC-II^{lo}), and moderately (MHC-II^{int}) and

highly (MHC-II^{hi}) mature cells revealed a characteristic reduction of the highly and moderately mature cells in BMMCs extracted from *Ahr*$^{-/-}$ mice compared to those derived from wild-type controls, with the frequencies dropping from 7.5 % and 41.7 % to 2.0 % and 15.2 %, respectively (**Figure 5.2B**). Contrarily, the proportions of these mature cells increased markedly in the *Ahrr*$^{-/-}$ and *Cyp*$^{-/-}$ BMMCs compared to the wild-type counterparts, with a clear shift of cells towards higher MHC class II expression (**Figure 5.2B**). This increase in the percentages was actually an under representation, as the associated reduction in CD11c expression (in the *Ahrr*$^{-/-}$ and *Cyp*$^{-/-}$ BMMCs) affected my ability to gate the cells using a clear cut off with CD11c expression.

5.3.5 **Replication Profiles of MNV-O in Wild-type and AhR-Manipulated BMMCs**

To determine the effects of genetic manipulation of constitutive AhR signalling on the ability of different BMMCs to support MNV-O7 replication, BMMCs generated as in **Section 5.3.4** were infected with MNV-O7 at an MOI of 0.03 or 0.05. Infection of BMMCs extracted from the 4 different mouse lines (wild-type, *Ahr*$^{-/-}$, *Ahrr*$^{-/-}$ and *Cyp*$^{-/-}$) showed similar viral growth kinetics within the first 12 hrs P.I., as MNV-O7 displayed only low levels of vRNA replication (**Figure 5.3A & B**). Beyond this point, however, viral replication in the wild-type BMMCs was substantially greater than that observed in the *Ahr*$^{-/-}$ BMMCs, with the peak at 48 hrs P.I. being almost 3-fold higher in the wild-type cells. MNV-O7 replication showed a slight, albeit statistically significant, rise in the *Ahrr*$^{-/-}$ BMMCs (**Figure 5.3A**), while the replication in the *Cyp*$^{-/-}$ cells was similar to that detected in wild-type controls (**Figure 5.3B**). The appearance of the differential replication patterns at later time points post-infection suggests that the differences are not related to the initial binding and internalisation of the virus, but rather most likely attributed to variation in later viral replication processes.

Taken together, these data indicate the major impact of genetically modifying the

endogenous ligand-mediated constitutive signalling of the AhR pathway on the phenotypic characteristics and maturation of BMMCs with the associated influences on the ability of these cells to support MNV-O7 replication. The resistance to MNV-O7 replication in *Ahr*$^{-/-}$ BMMCs mirrored that observed in *Ahr*$^{-/-}$ mice when infected *in vivo* (**Figure 5.1**). Moreover, when we orally infected *Cyp*$^{-/-}$ mice with MNV-O7, the viral titres in different gut sections and MLNs were comparable to those of MNV-O7-infected wild-type mice (**Supplementary Figure 5.3**), simulating the identical viral growth curves in BMMCs extracted from these mice. These findings strengthen the validity of the *in vitro* BMMC model and its relevance to study the influences of AhR signalling on immunity against MNV.

5.3.6 **Gene Expression Patterns of Poly(I:C) Stimulated BMMCs**

In an attempt to correlate the different MNV-O7 viral replication profiles observed in the BMMC populations with possible variations in the early IFN-mediated anti-viral responses, I treated BMMCs, generated as in **Section 5.3.4**, with a standardised dose of poly(I:C) and analysed the anti-viral genes expression patterns induced at different time points within the first 24 hrs of stimulation (**Figure 5.4**). Poly(I:C) is an agonist of TLR-3 that induces a potent type I IFN response[393,394]. Indeed, poly(I:C)-treated **wild-type** BMMCs displayed a robust induction of *Ifnb1* expression that peaked within the first hour of stimulation (**Figure 5.4**). The expression fluctuated and reduced subsequently, however, remained higher than that of the unstimulated cells even at 24 hrs post-stimulation. This IFN-β induction was followed by increased expression of the intermediate regulators, *Irf3* and *Irf7*, and the ISGs, *Mx1* and *Isg15* (**Figure 5.4**). With some variation, the induction of these genes in general started after 3 hrs, and peaked within 6-9 hrs, of poly(I:C) stimulation. Of note, unlike other mRNA, there was a detectable baseline expression of the *Irf3* before stimulation with poly(I:C) (**Figure 5.4**).

This finding was consistent with the previously documented constitutive expression of this regulatory mediator (Irf3) in most cells[395].

Compared to wild-type controls, *Ahr*$^{-/-}$ BMMCs showed a significantly enhanced poly(I:C)-stimulated anti-viral response (**Figure 5.4**). Except for similar *Irf3* expression, the induction of all other genes was both stronger and more prolonged in the *Ahr*$^{-/-}$ BMMCs. At 6 hrs post-poly(I:C) stimulation, the expression levels of *Irf7*, *Mx1* and *Isg15* in the *Ahr*$^{-/-}$ BMMCs were almost double that observed in the wild-type cells. This enhanced expression was maintained until 12 hrs post-stimulation for *Mx1* and *Isg15* and for the full 24 hrs for *Irf7*. The expression patterns of the *Ahrr*$^{-/-}$ and *Cyp*$^{-/-}$ BMMCs, on the other hand, were more complicated (**Figure 5.4**). Although associated with considerable variation in the maximum (peak) expression time point, the magnitudes of poly(I:C)-mediated induction of *Irf3*, *Irf7* and *Mx1* genes were comparable in both types of BMMCs and the wild-type controls. The expression of *Ifnb1*, however, was clearly reduced with mRNA levels measured at different time points lower than those of wild-type counterparts. The *Isg15* gene expression was unusual, as while that of *Ahrr*$^{-/-}$ BMMCs was nearly equivalent to the wild-type' expression, the *Cyp*$^{-/-}$ BMMCs displayed an augmented induction of *Isg15* expression especially between 6-12 hrs of poly(I:C) stimulation (**Figure 5.4**).

Collectively, the data presented in this section demonstrate differential poly(I:C)-stimulated, IFN-mediated anti-viral gene expression patterns of BMMCs generated from wild-type and AhR-(genetically) modified mouse lines. The augmented response observed in the *Ahr*$^{-/-}$ BMMCs with stronger and extended type I IFN and ISG expression, is consistent with the resistance displayed by these cells to MNV-O7 replication and logically correlates with the ability of *Ahr*$^{-/-}$ mice to suppress *in vivo* viral infection.

5.3.7 **Production of IFN-β by different BMMCs**

To exclude the possibility of a discrepancy between the mRNA and protein levels, due to a post-translational modification, I performed an ELISA assay to measure the levels of IFN-β in the supernatant of poly(I:C)-stimulated BMMCs at baseline and 24 hrs post-stimulation. The amount of INF-β produced by *Ahr*$^{-/-}$ BMMCs was significantly higher than that of the wild-type control cells (**Figure 5.5**). A finding which reflected the same gene expression differences discussed in the previous section. The same was true for the *Ahrr*$^{-/-}$ and *Cyp*$^{-/-}$ BMMCs, which showed reduced (barely detectable) levels of INF-β production 24 hrs post-poly(I:C) stimulation compared to wild-type counterparts (**Figure 5.5**).

5.3.8 **Ligand-Mediated Modulation of AhR Signalling**

To provide additional evidence for the involvement of AhR signalling in the early induction and regulation of anti-viral immune responses, I treated BMMCs generated from C57BL/6 wild-type mice with either the AhR-endogenous ligand, **FICZ**, or the AhR-specific antagonist, **CH223191**, while having cells derived from *Ahr*$^{-/-}$ mice as a control. FICZ is a tryptophan-derivative with a strong affinity for the AhR comparable to that of dioxin (**Section 1.2.5** for more details). CH223191 is a potent AhR antagonist (IC_{50}: 30 nM), which has been reported in several studies to significantly inhibit endogenous AhR signalling[396–398].

Treatment of *Ahr*$^{-/-}$ BMMCs with either FICZ or CH223191 had no effects on their phenotypic differentiation and surface marker expression (**Figure 5.6**), indicating that the changes observed in the wild-type cells are AhR-dependent. Consistent with previous reports[379,392], administration of CH223191 decreased the expression of MHC class II, CD11c, CD80, CD86 (**Figure 5.6A**) and reduced the proportion of moderately (MHC-II^{int}) and highly (MHC-II^{hi}) mature wild-type BMMCs (**Figure 5.6B**). Although less

apparent, treatment with FICZ had the opposite effect on the wild-type cells.

Infection of these CH223191 and FICZ-treated wild-type BMMCs with MNV-O7 revealed characteristic viral replication patterns quite similar to those observed in the AhR-deficient (*Ahr*$^{-/-}$) and AhR-hyperactive (*Ahrr*$^{-/-}$ and *Cyp*$^{-/-}$) BMMCs, respectively. Thus, MNV-O7 replication in wild-type BMMCs treated with CH223191, albeit not reaching that of *Ahr*$^{-/-}$ cells, was clearly reduced compared to the untreated controls (**Figure 5.7**). Treatment of wild-type BMMCs with the AhR-agonist FICZ only slightly increased viral replication compared to the untreated cells (this was not significant). Again, the different patterns of replication became apparent beyond the 12 hrs P.I. time point, suggesting a modulation in the viral replication cycle rather than in initial cellular binding and internalisation.

Although not confirmed experimentally, the different patterns of MNV-O7 replication in these AhR agonist/antagonist-treated BMMCs are most likely consequences of alteration in the early IFN-mediated anti-viral responses similar to those observed in the knockout BMMCs (**Figure 5.4**). Generally, the findings observed in these two last figures indicate that ligand-mediated modulation of the AhR signalling affects the phenotypic maturation of wild-type BMMCs and their ability to support MNV-O7 replication. They further support the relevance of the AhR pathway in the innate anti-viral immune response and the viability of modulating AhR signalling to influence the outcome of a viral infection.

5.4 Discussion:

AhR is a highly conserved, ubiquitously expressed cytosolic transcription factor, which has been the centre of extensive immunological research owing to its demonstrated roles in maintenance and functions of specific immune cells at barrier sites, its potential contribution to the development and progression of inflammatory disorders at these sites (including the gut and lung) and its proposed ability to link environmental (dietary/inhaled) cues to intracellular immunological signalling and responses. A pressing challenge, however, is the need for a major paradigm shift from, or at least a reconciliation of, a detoxifying system that responds to man-made exogenous toxins and a physiologically relevant biological system that is influenced by endogenous and naturally occurring ligands.

In this chapter, my main findings were that in the absence of constitutive AhR signalling (as in an *Ahr*$^{-/-}$ background) there was an associated increased resistance to MNV-O7 infection and replication both *in vivo* and in an *in vitro* BMMC experimental model. The same resistance to viral replication was observed when the AhR-endogenous signalling was inhibited in wild-type BMMCs by adding the AhR-specific antagonist CH223191. Augmentation of constitutive AhR signalling either resulted in higher replication of MNV-O7 virus, as in *Ahrr*$^{-/-}$ and FICZ-treated BMMCs, or did not affect the rate of viral growth, as in *Cyp*$^{-/-}$ mice and BMMCs. The lack of change in viral titre in *Cyp*$^{-/-}$ BMMCs (where the absence of the feedback endogenous ligands metabolism augments the whole signalling pathway, **Figure 1.3**) compared to the observed increase in virus replication in the *Ahrr*$^{-/-}$ BMMCs (where the augmentation is restricted mainly to the nuclear part of the pathway) suggested more intricate and complex interactions between the AhR and IFN-STAT1 signalling pathways than anticipated and warrant further investigation. These different abilities to support MNV-O7 infection were associated with distinct phenotypic characteristics and maturation status of the specific BMMCs and are reflected

in different (both in terms of magnitude and duration) IFN-mediated anti-viral responses following poly(I:C) stimulation. Although displaying the phenotypic features of immaturity at baseline, *Ahr*$^{-/-}$ BMMCs demonstrated a stronger and more prolonged poly(I:C)-stimulated anti-viral response that was associated with a significant ability to inhibit MNV-O7 replication. It is important to note, however, that as we examined bone marrow derived cells, this might not be a full reflection to the characteristics of mononuclear phagocytes at the site of infection, i.e. the gut, where macrophages and DCs are known to have higher thresholds for activation[68,69] and different functional capabilities[71,76].

Nonetheless, the findings presented in this chapter are in concordance with other published data. The characteristic enhanced anti-viral response of *Ahr*$^{-/-}$ BMMCs following poly(I:C) stimulation, with higher expression of type I IFN and anti-viral ISGs, supports the hypothesis of possible cross-talk between the functional AhR system and the IFN-STAT1 anti-viral pathway through interaction at the level of active AhR binding to the STAT1 molecule[198,199] and/or at the level of AIP chaperone protein modulating the activation of the signalling intermediate Irf7[375]. The latter was further supported by the persistently augmented expression of *Irf7* in the poly(I:C)-stimulated *Ahr*$^{-/-}$ BMMCs (at least for the first 24 hrs following stimulation) (**Figure 5.4**). Moreover, a recently published report confirmed the negative regulatory effect of constitutive AhR signalling on type I IFN responses during infection with various (both DNA and RNA) viruses[399]. In this comprehensive report, Yamada *et al.* (2016) elegantly demonstrated that AhR endogenous signalling up-regulates the expression of ADP-ribosylase TIPARP, one of the target genes of AhR-signalling (**Figure 1.3**), which in turn interacts with the kinase TBK-1, suppresses its activity by ADP-ribosylation and hence regulates type I IFN production[399].

Taken together, either through AhR-STAT1, AIP-Irf7, TIPARP-TBK1, another not yet identified interaction or a combination and contribution of all, these data indicate a direct link between constitutive AhR signalling and innate interferon-mediated anti-viral responses that can be exploited as a potential preventive/therapeutic target for enhancing anti-viral responses. Ligand-dependent activity of AhR was shown to reduce inflammation in skin samples of psoriasis patients[214], and protected mice from severe intestinal inflammation[400]. Being natural and mostly dietary-derived, AhR ligands are proposed as highly attractive options for site-directed therapeutics for many inflammatory conditions, including IBDs. However, the data presented in this chapter, together with the recent insights discussed above, indicate that the ramifications of AhR activation are wide and, as the case in steroid treatment, might be associated with increased risk of (viral) infections. Further illumination of the exact and specific contribution of different mechanisms by which the cross-talk occurs between AhR and various other signalling pathways, including the IFN-STAT1 pathway, would have several potential applications to better understand the nature and the impact of AhR modulation and might facilitate the development of novel, more precisely-targeted modes of intervention applicable to both inflammation and infection.

6 GENERAL DISCUSSION & CONCLUDING REMARKS

Chapter 6 GENERAL DISCUSSION & CONCLUDING REMARKS

6.1 Limitations and Areas of Improvements

The data presented in my thesis has covered a range of topics that may, at first sight, appear unconnected. Nonetheless, I kept MNV as my sole pathogen, and the gut mucosal immune system as the main theme of all my work. The diversity of the topics covered was unintentional. It was a direct consequence of the unfortunate combination of some unavoidable obstacles (such as a difficulty in breeding some mouse lines, the inability to set-up and maintain homogeneous experimental groups in term of age and sex, the variability in the responses obtained in some experiments and the necessary prolonged mouse incubation period for the aging and adoptive transfer experiments) and some unexpected results (such as the finding that natural IEL might not be essential for MNV protection and reduced viral titres in the *AhR*$^{-/-}$ mice) in addition to other causes. Although these factors may be regarded as drawbacks, the tackling of different aspects and the attempts to answer different questions has allowed me to explore many different experimental techniques and to improve my understanding of the gut mucosal immunity.

A major caveat to our experimental model of investigating the anti-viral role of IEL is the broad activity of the agonistic anti-CD3 antibody, which when injected intraperitoneally results in bystander T cell activation systemically. The resulting biological readouts that I detect in wild-type mice cannot be attributed only to the activity of the gut associated immune system. My attempts to activate the IELs by oral administration of anti-CD3 were unsuccessful, likely due to the thick mucus layer that protects the epithelial surfaces. I, therefore, employed more complex knockout and adoptive transfer experimental models to assess the potential contribution of IELs in the protection induced by anti-CD3 antibodies. The results obtained from these experiments may not necessarily reflect the physiological responses occurring in homeostatic gut conditions,

especially with the possibility of a heightened basal inflammatory state and development of several compensatory feedback mechanisms in the immunodeficient (*Il15ra*$^{-/-}$, *Tcra*$^{-/-}$ and *Rag2*$^{-/-}$) mice. One possible way to overcome this, in my opinion, is the use of *in vitro* intestinal organoid-IEL co-culture system. In the light of our findings that the persistent strains of MNV (MNV-O7 and -3) can infect intestinal organoids, this model may be relevant to investigate the role of IEL in the context of MNV infection. However, it may not reflect all aspects of the gut mucosal immune response as certain factors (such as the microbiota) are not represented.

6.1 Summary, Interpretation and Future Work

The gut is the largest surface area in the body directly exposed to the external environment, the food we eat and the microbes that help us digest it. The gut mucosa has developed a complex and unique immune system that allows for an intense scrutiny of the epithelial surfaces to prevent the establishment and invasion of harmful microorganisms, while at the same time operating robust mechanisms to differentiate between 'friend' and 'foe' and allow commensal microorganism survival. Using a mouse-model of MNV infection, the main aim of this PhD thesis was to investigate the role of three major modulators; namely the IEL, the AhR signalling and the effect of aging on the specialised gut mucosal immunity. The data obtained during this study lays the groundwork for better understanding not only of Norovirus pathogenesis and immunobiology, but also in the broader sense the mucosal immune response against enteric viral infections, with possible translational applications for development of better immuno-protective (vaccine) and immuno-therapeutic (anti-viral) strategies.

Building on previous work in our lab by Dr. James Chettle to define the anti-viral role of IELs, and to identify features of viral pathogenesis and immune response associated with both persistence and virulence of different MNV strains, in this thesis I used the

experimental anti-CD3-MNV model to investigate the role of IELs and to employ the model in the context of different knockout and adoptive transfer experiments. I concluded that, at least in our experimental conditions and in a viral strain-specific manner, the activated ($\gamma\delta$ TCR^+) IELs are not essential and may play a minor role in the protective response against MNV-O7 infection. Their role might be more prominent in the context of acute (MNV-CW3) infection. These data do not exclude a role of the more conventional 'induced' subtypes of IELs, i.e. $\alpha\beta$ TCR^+ $CD8\alpha\beta^+$ and $CD4^+$ IELs. Future work concerning this aspect may include the application of the newly developed intestinal organoid-IEL co-culture system as a reductionist approach to assess/study the fine IEC-IEL interactions in the context of MNV infection.

In this section of the thesis we were able to demonstrate the differential abilities of different MNV strains to activate IELs in a microbiota-dependent manner, and for the first time (to our knowledge) to identify the distinctive abilities of these various viral strains to infect IECs. Considering the close genetic similarity between different MNV strains[278], it was quite remarkable to observe such striking differences in cellular tropism and immunological sequelae. It is important to recognise that HuNoV strains display much more substantial genetic diversity, and I would predict that they may display an even broader range of interactions with the host immune system. Further analysis of the expected barrier dysfunction associated with the acute strain (MNV-1.CW3) infection and the specific microbiota component(s) that are involved in IEL activation may prove advantageous for developing better clinical management protocol and vaccine strategies. Moreover, investigating this phenomenon in the context of reovirus (replicating in both epithelial and non-epithelial cells of the gut[358]) and rotavirus (with their specific tropism for mature enterocytes[357]) infections may reveal a common feature for all enteric viral infections.

Recognising a different response in old (2-year) mice, we followed that lead and were able to identify a specific defect in the IFN-λ response of aged IECs. The demonstration of the reversibility of the defect (by administration of a high dose of exogenous IFN-λ) and the setting up of a viable experimental model to compare and translate our findings to human samples will pave the way for development of better therapeutic modalities for the severely affected elderly population. Furthermore, the *in vivo* experimental MNV-mouse model and/or the intestinal organoids will facilitate the identification of the exact cause(s) of the phenotype observed in old mice and the specific molecular defect(s) of the IEC's IFN-λ-hypo-responsiveness. It is my intention to age a colony of *Rag2*$^{-/-}$ and *Ccr2*$^{-/-}$ mice, compare their response to MNV infection to that of old wild-type controls and to employ the adoptive-transfer experimental model with transfer of young-vs-old lymphocytes and/or mononuclear phagocytes into young-vs-old *Rag2*$^{-/-}$ or *Ccr2*$^{-/-}$ mice in order to identify the role of the aged phenotype of different immune cells in the development of the age-specific immune defects.

Extending our model of MNV infection to investigate the role of AhR signalling, the data I generated suggested a direct link between constitutive AhR signalling and innate interferon-mediated anti-viral responses that can be exploited as a potential preventive/therapeutic target for enhancing anti-viral responses. My results were in agreement with recently published reports identifying AhR-STAT1, AIP-Irf7 and/or TIPARP-TBK1 interactions as potential crosstalk points between the two signalling pathways. Further analysis of the precise contribution of these (and possibly other) different mechanisms will help in better understanding of the role of AhR signalling and in the development of targeted modes of intervention applicable to both inflammation and infection.

Figures

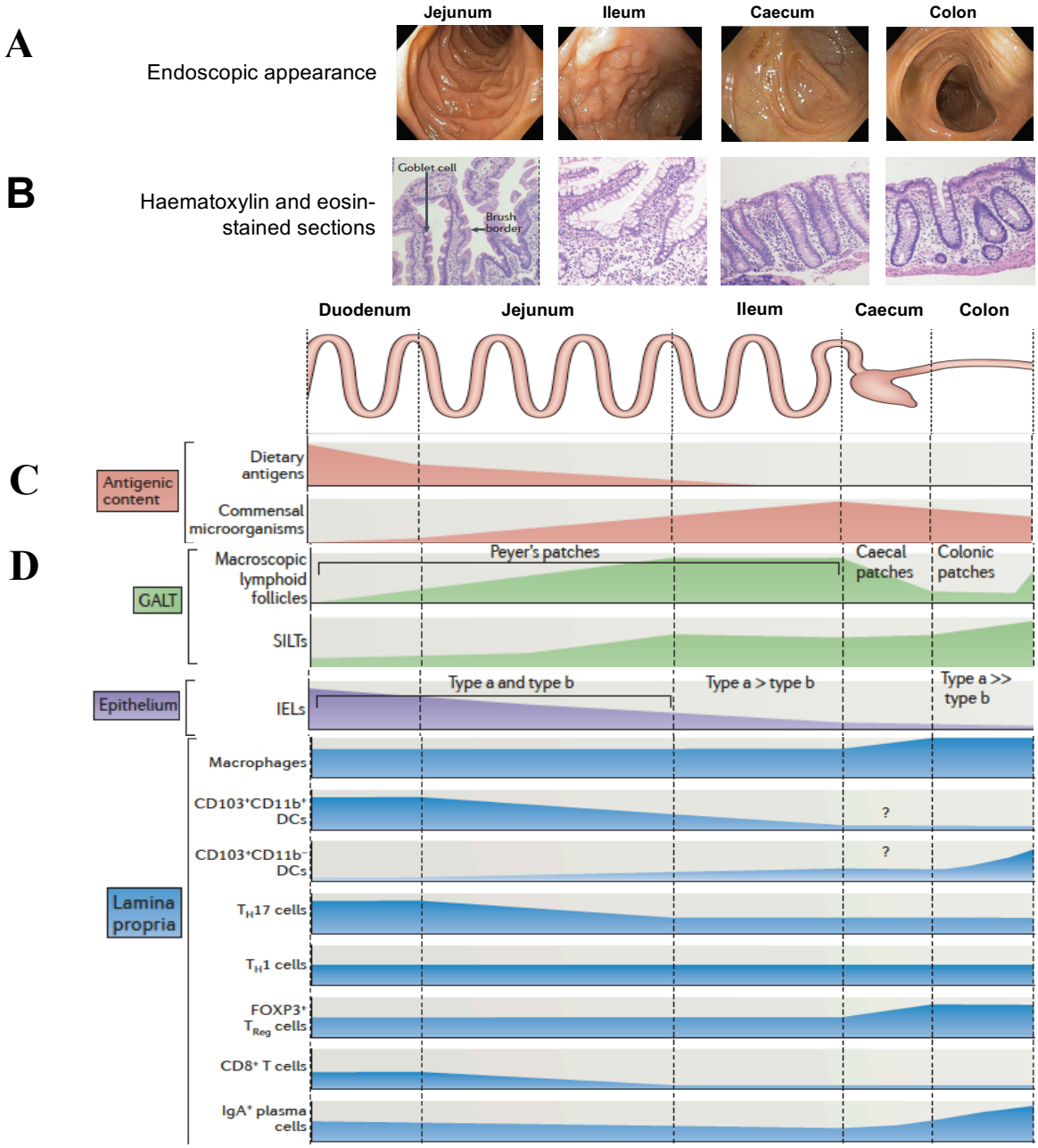

Figure 1.1 Regional specialisation of the intestinal tract and gut mucosa in terms of differences in macroscopic (**A**) and histological (**B**) features, antigenic stimuli (**C**) and cellular constituents/distribution of the lymphoid tissues and immune apparatus (**D**). Data mostly drawn from studying the gut mucosa in mice. Although less clear, due to lack of specific segmented studies, similar specialisation and immune cell distribution are expected in human intestines[1]. The figure was adopted from Mowat *et al* (2014)[11]. ***GALT****:* Gut Associated Lymphoid Tissues. ***SILTs****:* Solitary Isolated Lymphoid Tissues. ***IEL****:* Intra-Epithelial Lymphocytes. ***DCs****:* Dendritic Cells. T_H*:* T Helper. ***FOXP3****:* Forkhead Box P3. T_{Reg}**:** regulatory T cells.

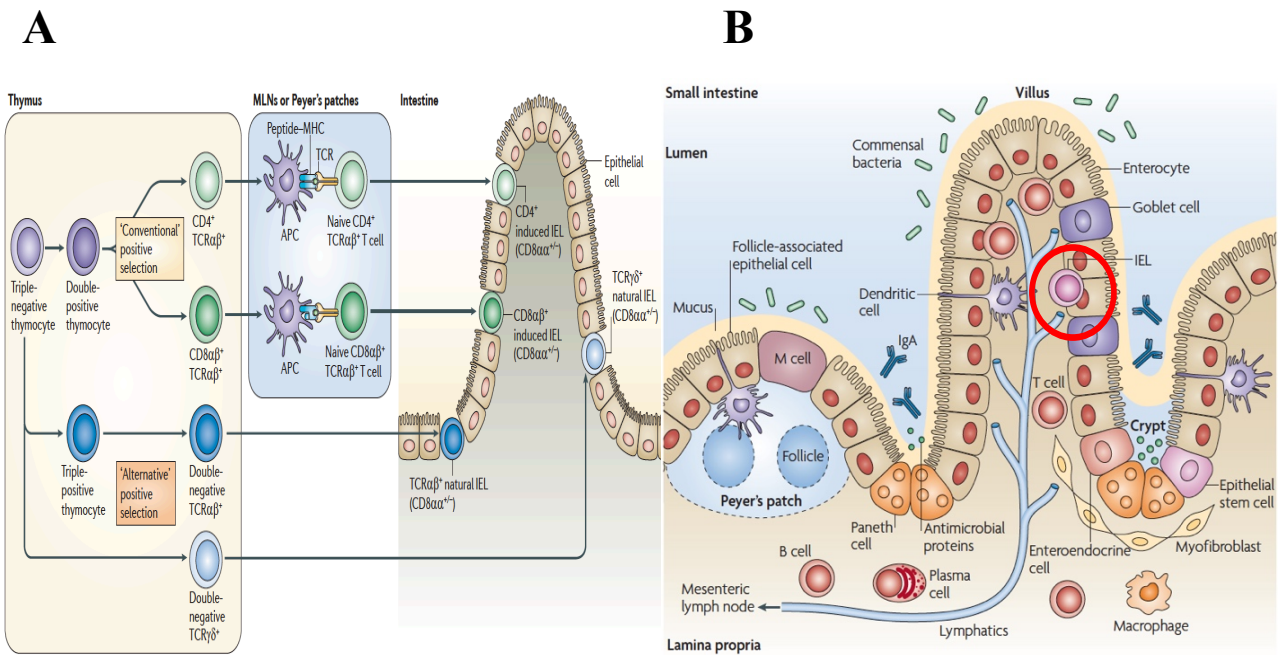

Figure 1.2 Intraepithelial Lymphocytes (IEL). Thymic development and differentiation into **Natural** IELs (blue coloured) by alternative positive selection, and **Induced** IELs (green coloured) by conventional positive selection (**A**). The Natural IELs migrate directly to the gut, while the Induced IELs undergo priming at the secondary lymphoid organs (MLNs and Peyer's Patches) before travelling to the gut. The figure also shows the unique location of IEL within the epithelial compartment (**A**) and (**B**) red circle. The figure was modified from Cheroutre *et al.* (2011)[129] and Abreu (2010)[130].

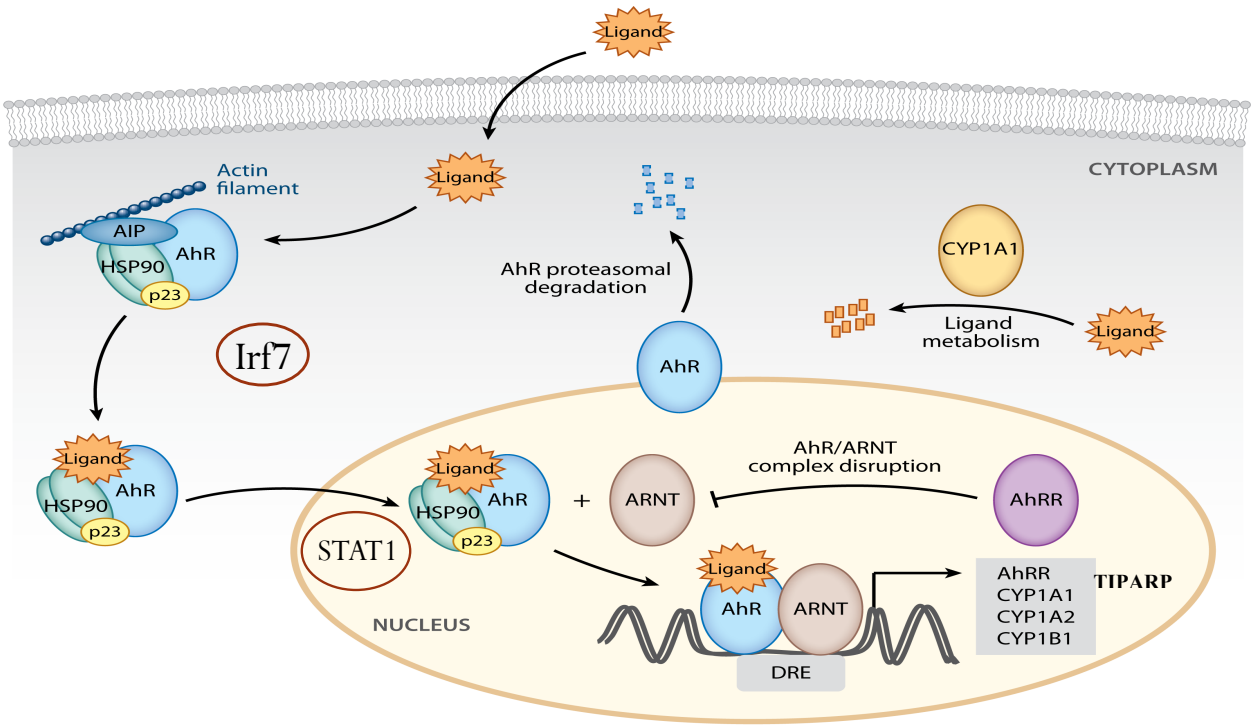

Figure 1.3 Aryl Hydrocarbon Receptor (AhR) Signalling. Inactive AhR in the cytoplasm forms a complex with HSP90, p23 and AhR-interacting protein (AIP). Upon ligand binding, AhR translocates into the nucleus, where it dissociates from the chaperones and forms a complex with AhR-nuclear transporter (ARNT). This complex binds to dioxin-response elements (DRE) and induces the expression of many genes including cytochrome P (CYP1) enzymes, TCDD-inducible poly(ADP-ribose) polymerase (TIPARP) and AhR repressor (AhRR). Possible crosstalk with the STAT1 pathway includes: AhR-STAT[198] and AIP-Interferon regulatory factor 7 (Irf7)[375] interactions. The figure was adopted from Stockinger *et al.* (2014)[188].

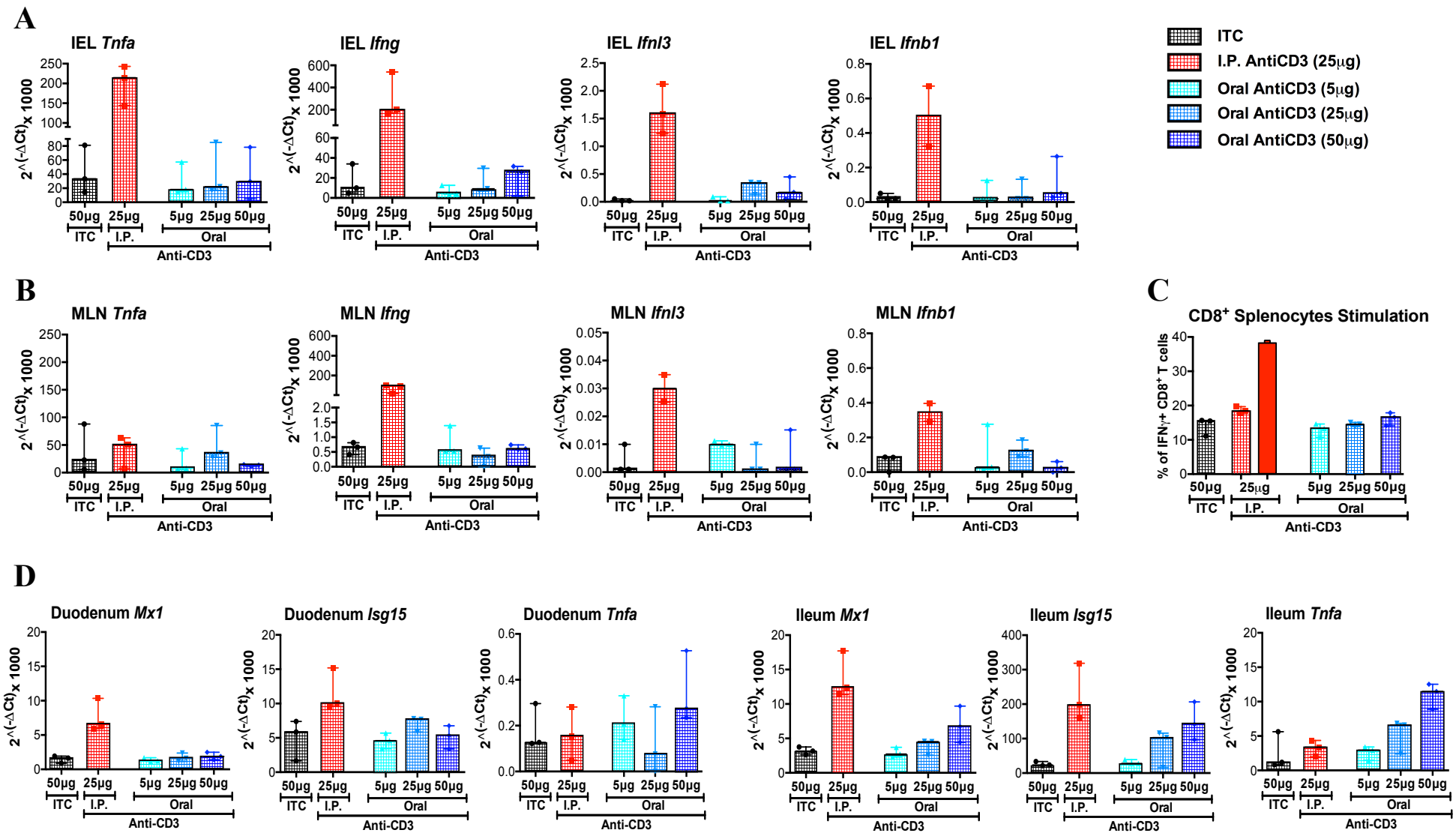

Figure 3.1 continued overleaf

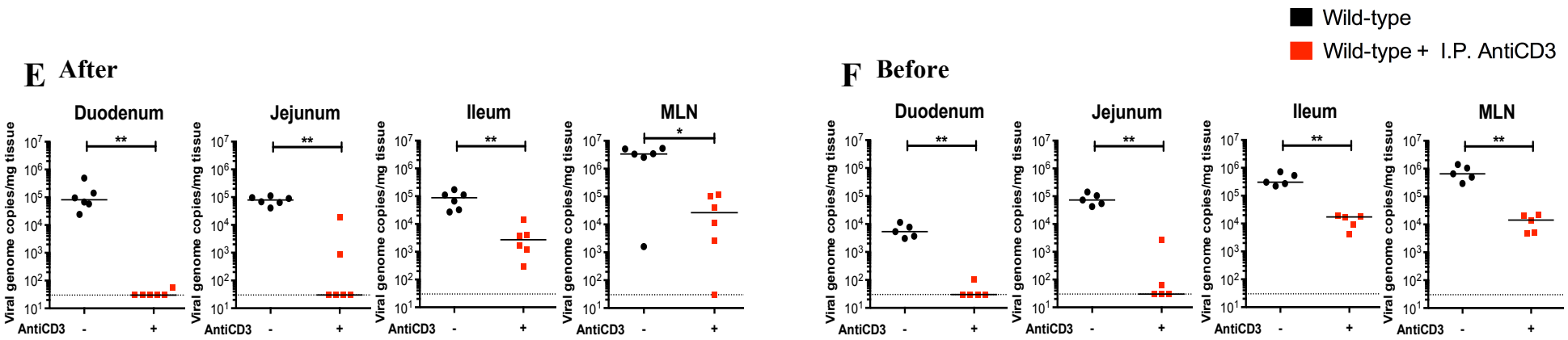

Figure 3.1 The effects of intraperitoneal (I.P.) vs (Oral) administration of anti-CD3 antibodies in wild-type mice.

C57BL/6 wild-type mice administered anti-CD3 antibodies either orally (with one of three different doses; 5 µg, 25 µg, 50 µg) or I.P. (dose of 25 µg). The controls (black bars) received 50 µg of isotype control (ITC) antibodies. Three hours later, mice were sacrificed and gut sections, MLNs and spleens were collected. Intraepithelial lymphocytes (IEL) were extracted from gut sections as outlined in **Section 3.2.3**. RNA was extracted from IELs (**A**), MLN (**B**) and gut sections (Duodenum and Ileum) (**D**), reverse transcribed and analysed for the gene expression of the cytokines; TNFα, IFNγ, IFNλ3 and IFNβ1 (**A** and **B**), TNFα and the ISGs; *Mx1* and *Isg15* (**D**). The spleen samples (**C**) were analysed by flow cytometry as detailed in **Section 3.2.5**, with analysis of an additional time-point at 8 hrs post-stimulation with I.P. anti-CD3 (solid red bar) and plotting the percentages of IFNγ-expressing $CD8^+$ T-cells.

(**E** and **F**) C57BL/6 wild-type mice were infected orally with 5 x 10^6 $TCID_{50}$ (MNV-O7) 8 hrs after (**E**) or before (**F**) being injected I.P. with 25 µg of either anti-CD3 (+) or ITC (-) antibodies. 40 hrs after the infection, mice were sacrificed and gut sections (Duodenum, Jejunum, and Ileum) and MLNs were collected. RNA was extracted from the tissues and viral titres (RNA copy numbers) determined by RT-qPCR. Titres were normalised to the weight of the tissue sections. The dotted line indicates the limit of detection (30 viral genome copies per mg tissues). Each point represents an individual mouse. The line in each dataset represents the median viral titre. Statistical significance was determined by Mann-Whitney test (*; $P<0.05$, **; $P<0.01$).

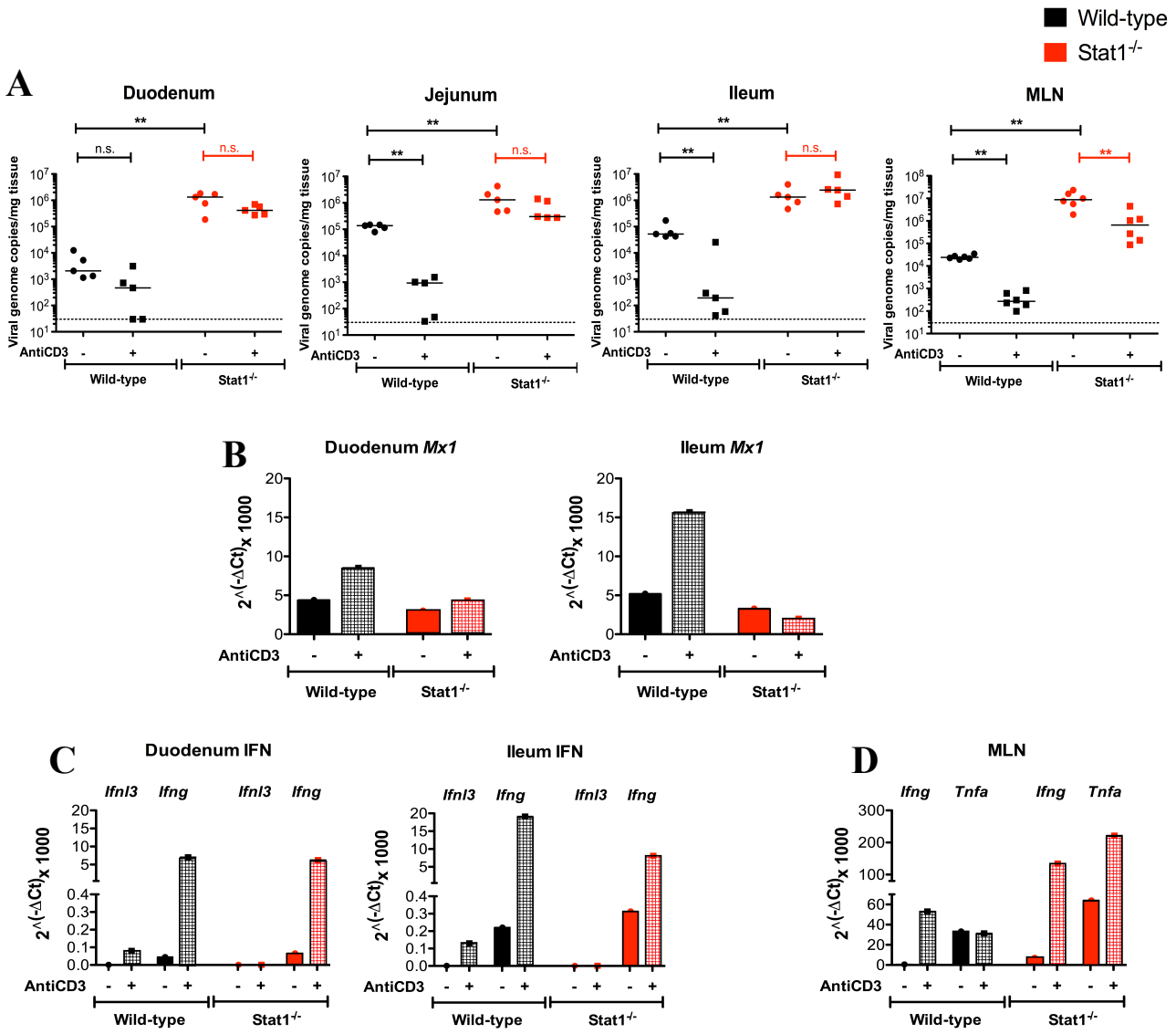

Figure 3.2 STAT-1 is absolutely essential for the protection against MNV-O7 in the gut.

(**A**) 129 wild-type and *Stat1*$^{-/-}$ mice infected orally with MNV-O7 (5 x 10^6 $TCID_{50}$) 8 hrs after intraperitoneal injection with 25 µg of either anti-CD3 (+) or isotype control (-) antibodies. 40 hrs after the infection, mice were sacrificed and gut sections (Duodenum, Jejunum, and Ileum) were collected. RNA was extracted from the tissues and viral titres (RNA copy numbers) measured by RT-qPCR. The titres were normalised to the weight of the tissue sections. Dotted line indicates the limit of detection (30 copies/mg). Statistical significance was calculated by Mann-Whitney test (n.s.; not significant, **; P<0.01). (**B**, **C** & **D**) Anti-CD3 treated (+) and untreated (-) 129 wild-type and *Stat1*$^{-/-}$ mice were sacrificed 3 hrs after treatment with anti-CD3. Gut sections (Duodenum, Ileum) and MLNs were collected, RNA was extracted, reverse transcribed and analysed for the gene expression of the ISG: *Mx1* (**B**) and the cytokines IFNλ3 and IFNγ (**C**), IFNγ and TNFα (**D**).

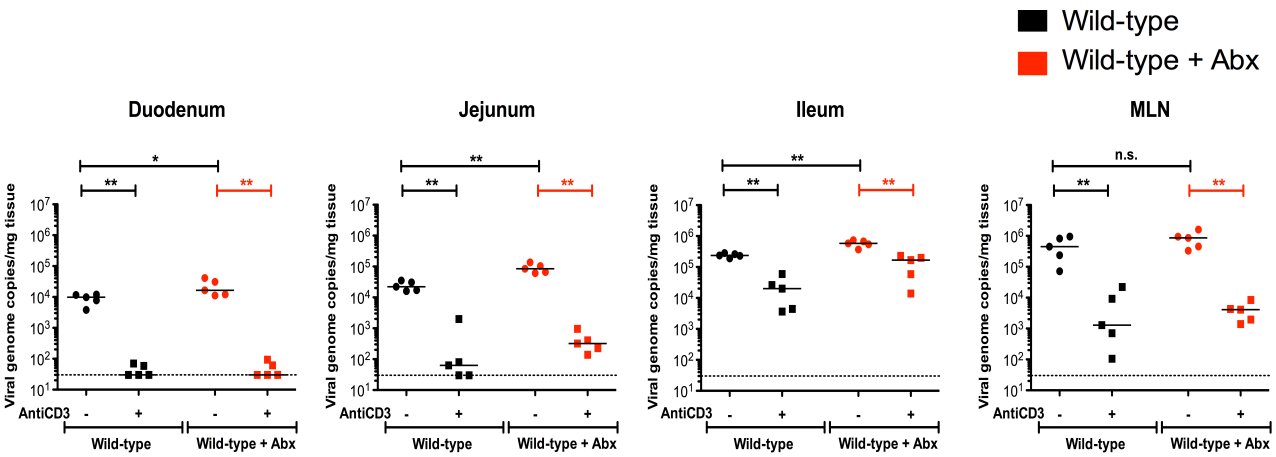

Figure 3.3 Effect of Antibiotic treatment in the Anti-CD3/MNV-O7 experimental model.

C57BL/6 wild-type mice were treated orally with antibiotic cocktail (Abx) for 2 weeks and compared to untreated age-matched wild-type mice. C57BL/6 mice without antibiotic (black dots) and with antibiotic (red dots) were infected orally with MNV-O7 (5 x 10^6 $TCID_{50}$) 8 hrs after being injected (I.P.) with either anti-CD3 (+) or isotype control (-) antibodies. 40 hrs after infection, mice were sacrificed and gut sections (Duodenum, Jejunum, Ileum) and MLN collected and analysed for viral RNA titres determined by RT-qPCR. The titres were normalised to the weight of the tissue sections. Each point represents an individual mouse. The line in each dataset represents the median viral titre. Statistical significance was determined by Mann-Whitney test (n.s.; not significant, *; $P<0.05$, **; $P<0.01$).

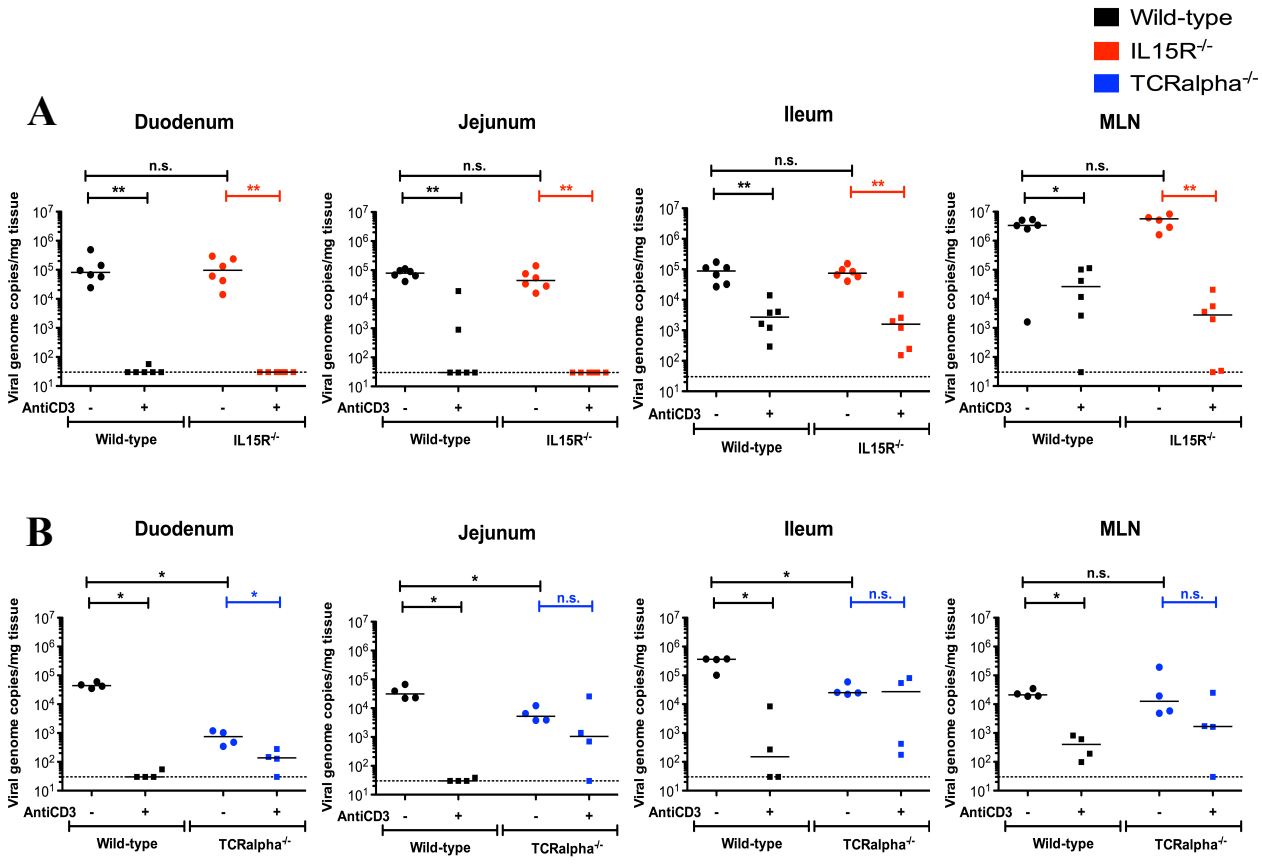

Figure 3.4 Gamma/Delta TCR$^+$ IELs are not essential for, and play a minor role in, the inhibition of MNV-O7 viral titres mediated by anti-CD3 injection.

C57BL/6 wild-type, *Il15ra*$^{-/-}$ (**A**) and *Tcra*$^{-/-}$ (**B**) mice infected orally with MNV-O7 (5 x 10^6 $TCID_{50}$) 8 hrs after being injected intraperitoneally with 25 µg of either anti-CD3 (+) or isotype control (-) antibodies. 40 hrs after infection, mice were sacrificed and gut sections (Duodenum, Jejunum, and Ileum) and Mesenteric lymph nodes (MLNs) were collected. RNA was extracted from the tissues and viral titres (RNA copy numbers) were determined by RT-qPCR based on a standard curve. The titres were normalised to the weight of the tissue sections. The dotted line indicates the limit of detection (30 copies per mg tissue). Each point represents an individual mouse. The line in each dataset represents the median viral titre. Statistical significance was determined by Mann-Whitney test (n.s.; not significant, *; P<0.05, **; P<0.01).

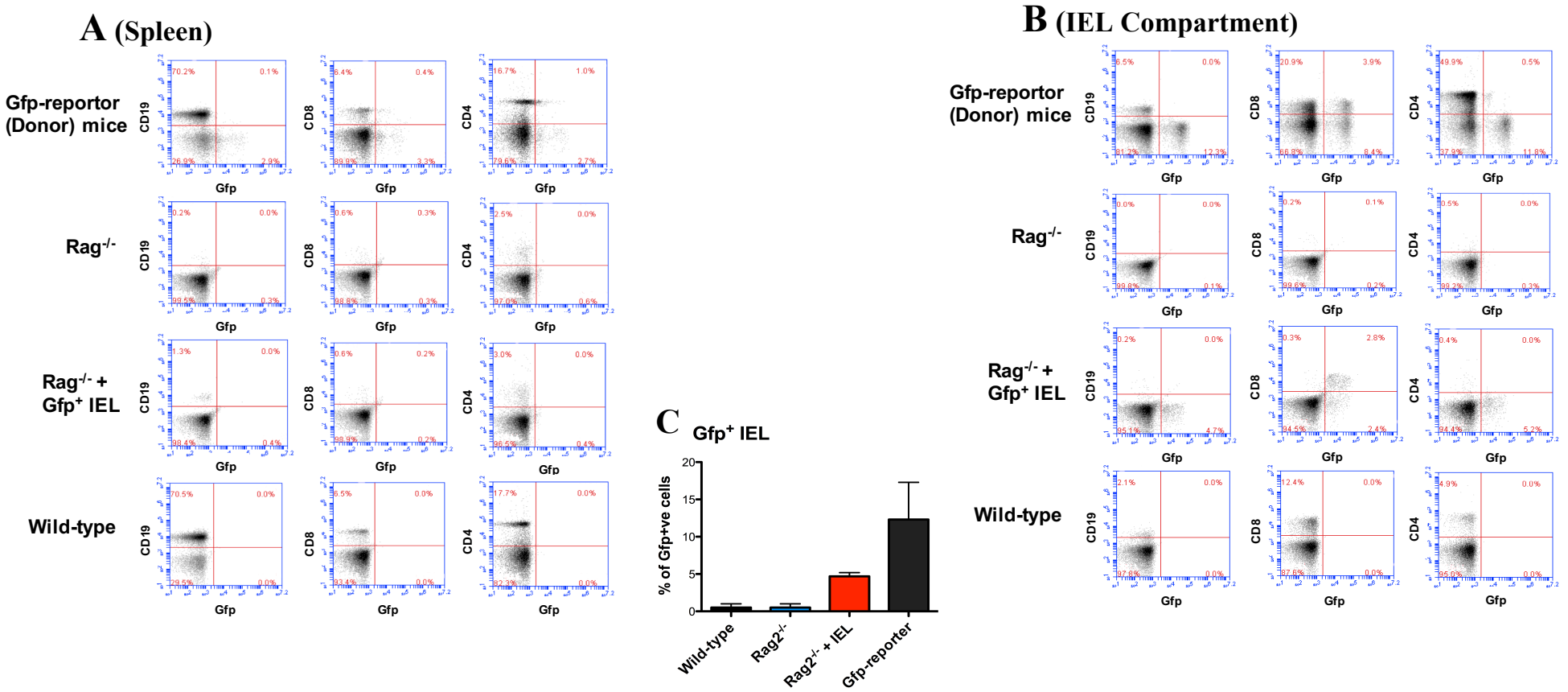

Figure 3.5 Flow cytometric analysis of Spleens and IEL-compartments post-adoptive transfer of Gfp$^+$ IEL.

Rag2$^{-/-}$ (*Rag*$^{-/-}$) mice injected intravenously with Gfp$^+$ IELs (at ~ 2 x 10^5 cells/mouse) extracted from Gfp-reporter (donor) wild-type mice. Four weeks post-adoptive transfer mice were sacrificed and spleens and gut sections were collected. IEL were extracted from gut sections as outlined in **Section 3.2.3**. The splenocytes (**A**) and IELs (**B**) were analysed by flow cytometry as detailed in **Section 3.2.4**, with detection of the surface markers CD19, CD8 and CD4 on y-axes and Gfp expression in x-axes. The percentages of Gfp$^+$ IELs were plotted in (**C**). Tissues extracted from Gfp-reporter (donor), non-injected *Rag2*$^{-/-}$ and C57BL6 wild-type mice were included for comparison.

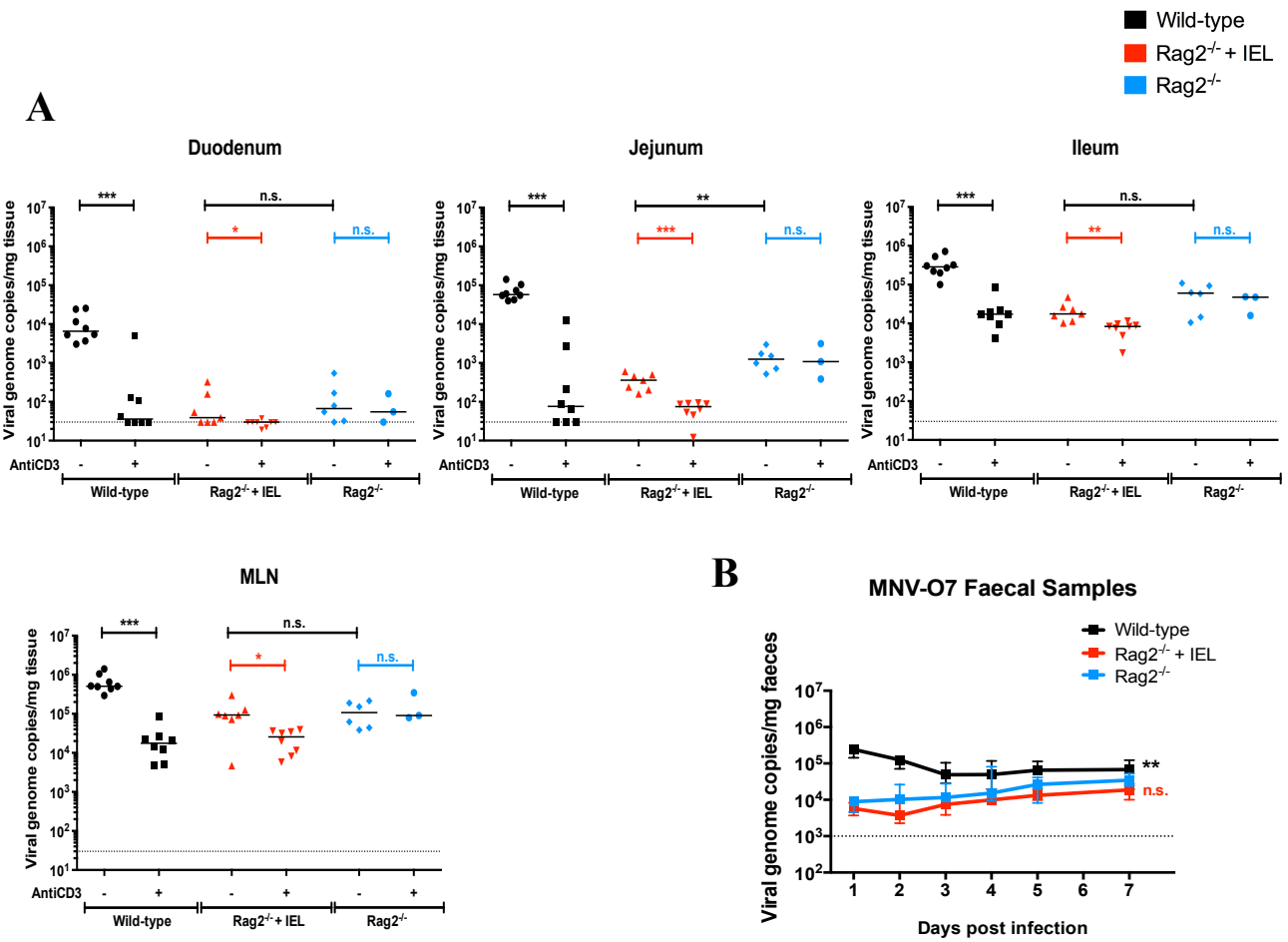

Figure 3.6 MNV-O7 infection of Wild-type, *Rag2*$^{-/-}$ injected with Gfp^{+} IELs and *Rag2*$^{-/-}$ mice.

(**A**) *Rag2*$^{-/-}$ mice injected intravenously with Gfp^{+} IELs (at ~ 2 x 10^5 cells/mouse) purified from Gfp-reporter (donor) wild-type mice. 4 weeks post-adoptive transfer the (*Rag2*$^{-/-}$ + IEL) mice were compared to wild-type C57BL/6 and non-injected *Rag2*$^{-/-}$ controls by oral infection of MNV-O7 (5 x 10^6 $TCID_{50}$) 8 hrs before being injected I.P. with 25µg of either anti-CD3 (+) or isotype control (-) antibodies. 40 hrs after the infection, mice were sacrificed, gut sections (Duodenum, Jejunum, and Ileum) and MLNs were collected and analysed for the level of viral RNA titres measured by RT-qPCR. The titres were normalised to the weight of the tissue sections. The dotted line indicates the limit of detection (30 copies/mg). (**B**) The same MNV-O7-infected mice (as in **A**) were not treated with anti-CD3 antibodies and were maintained for 7 days with faecal samples collection at the indicated days post-infection. RNA was extracted from faecal samples and viral titres (RNA copy numbers) were determined by RT-qPCR. Shown are the numbers of genome copies of MNV per mg of faeces. Statistical significance was determined by Mann-Whitney test (**A**) and 2way ANOVA (**B**). (n.s.; not significant, *; P<0.05, **; P<0.01, ***; P<0.0001).

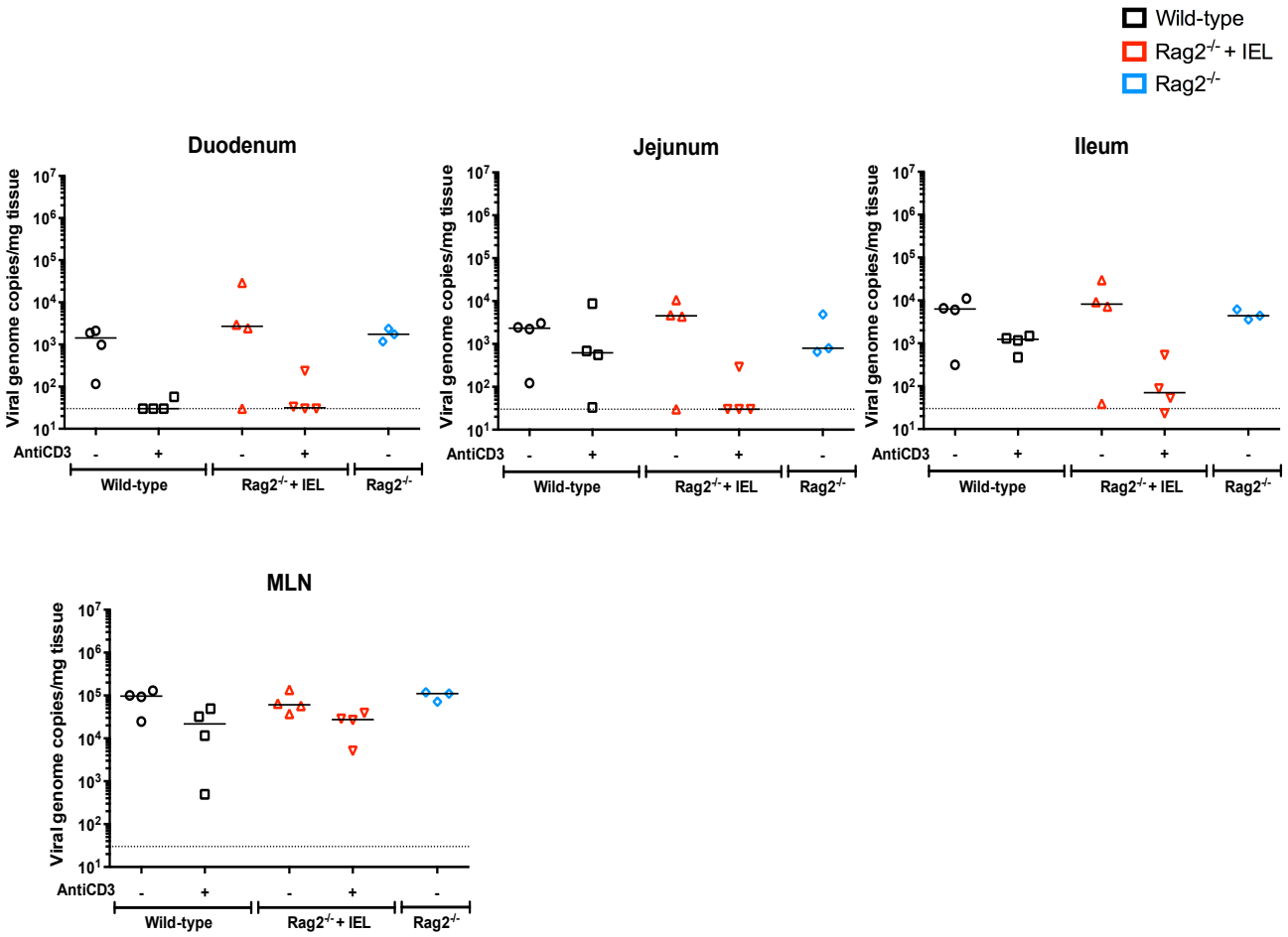

Figure 3.7 MNV-CW3 infection of Wild-type, *Rag2*$^{-/-}$ injected with Gfp^{+} IELs and *Rag2*$^{-/-}$ mice.

Rag2$^{-/-}$ mice injected intravenously with Gfp^{+} IELs (at ~ 2 x 10^5 cells/mouse) purified from Gfp-reporter (donor) wild-type mice. 3 weeks post-adoptive transfer the (*Rag2*$^{-/-}$ + IEL) mice were compared to wild-type C57BL/6 and non-injected *Rag2*$^{-/-}$ controls by oral infection of MNV-CW3 (5 x 10^6 $TCID_{50}$) 8 hrs before being injected intraperitoneally with 25 µg of either anti-CD3 (+) or isotype control (-) antibodies. 40 hrs after infection, mice were sacrificed, gut sections (Duodenum, Jejunum, and Ileum) and MLNs were collected and analysed for the level of viral RNA titres measured by RT-qPCR. The titres were normalised to the weight of the tissue sections. The dotted line indicates the limit of detection (30 copies/mg). Each point represents an individual mouse. The line in each dataset represents the median viral titre.

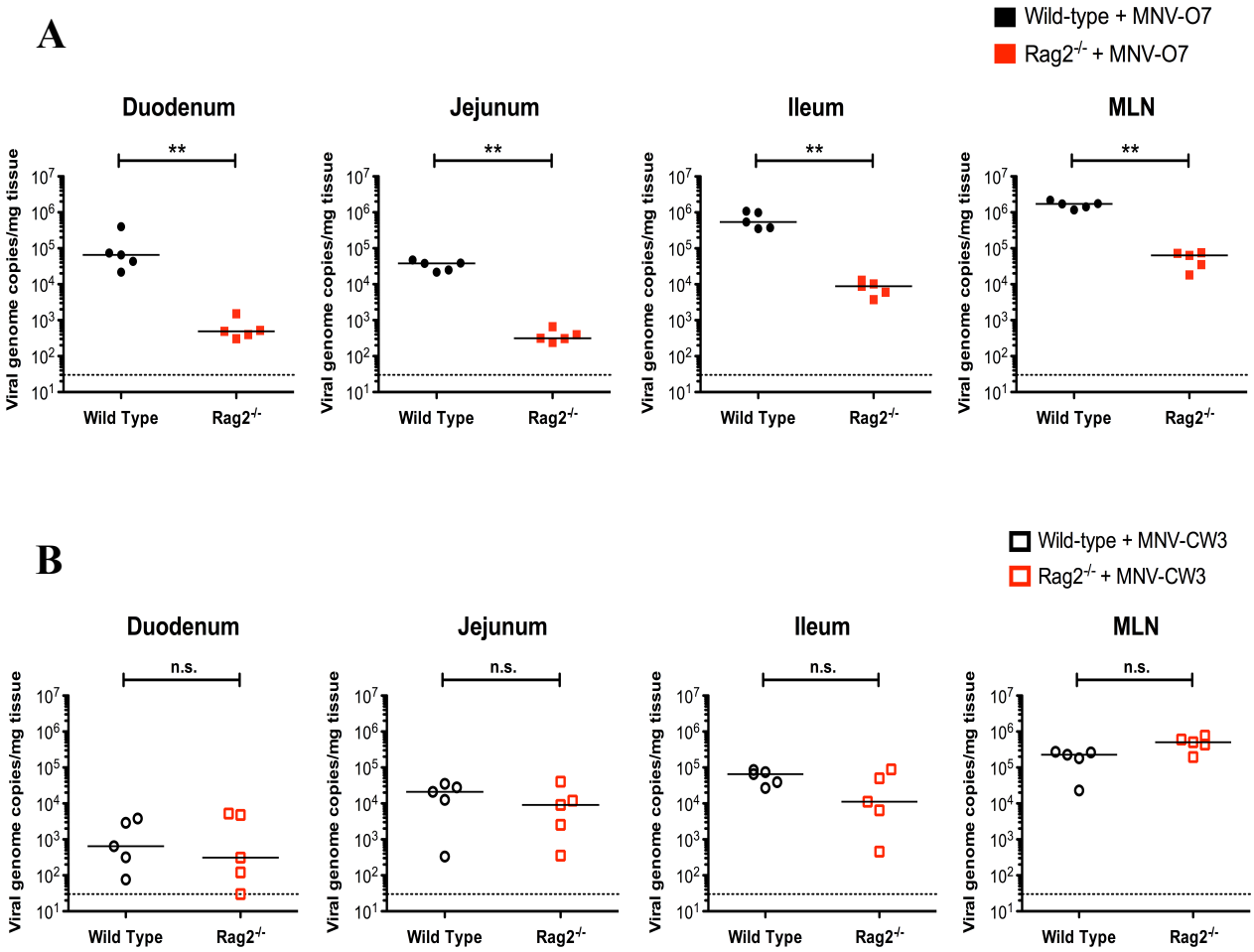

Figure 3.8 Comparison of MNV-O7 vs MNV-CW3 infection of wild-type and *Rag2*$^{-/-}$ mice.

Wild type (C57Bl/6) and *Rag2*$^{-/-}$ mice infected orally with 5 x 10^6 $TCID_{50}$ MNV-O7 (**A**) or MNV-CW3 (**B**). 40 hrs after infection, mice were sacrificed and gut sections (Duodenum, Jejunum, Ileum) and MLN were collected. RNA was extracted from the tissues and viral titres (viral RNA copy numbers) were determined by RT-qPCR. The titres were normalised to the weight of the tissue sections. Dotted line indicates the limit of detection (30 viral genome copies per mg tissues). Each point represents an individual mouse. The line in each dataset represents the median viral titre. Statistical significance was determined by Mann-Whitney test. (n.s.; non-significant, **; P<0.01).

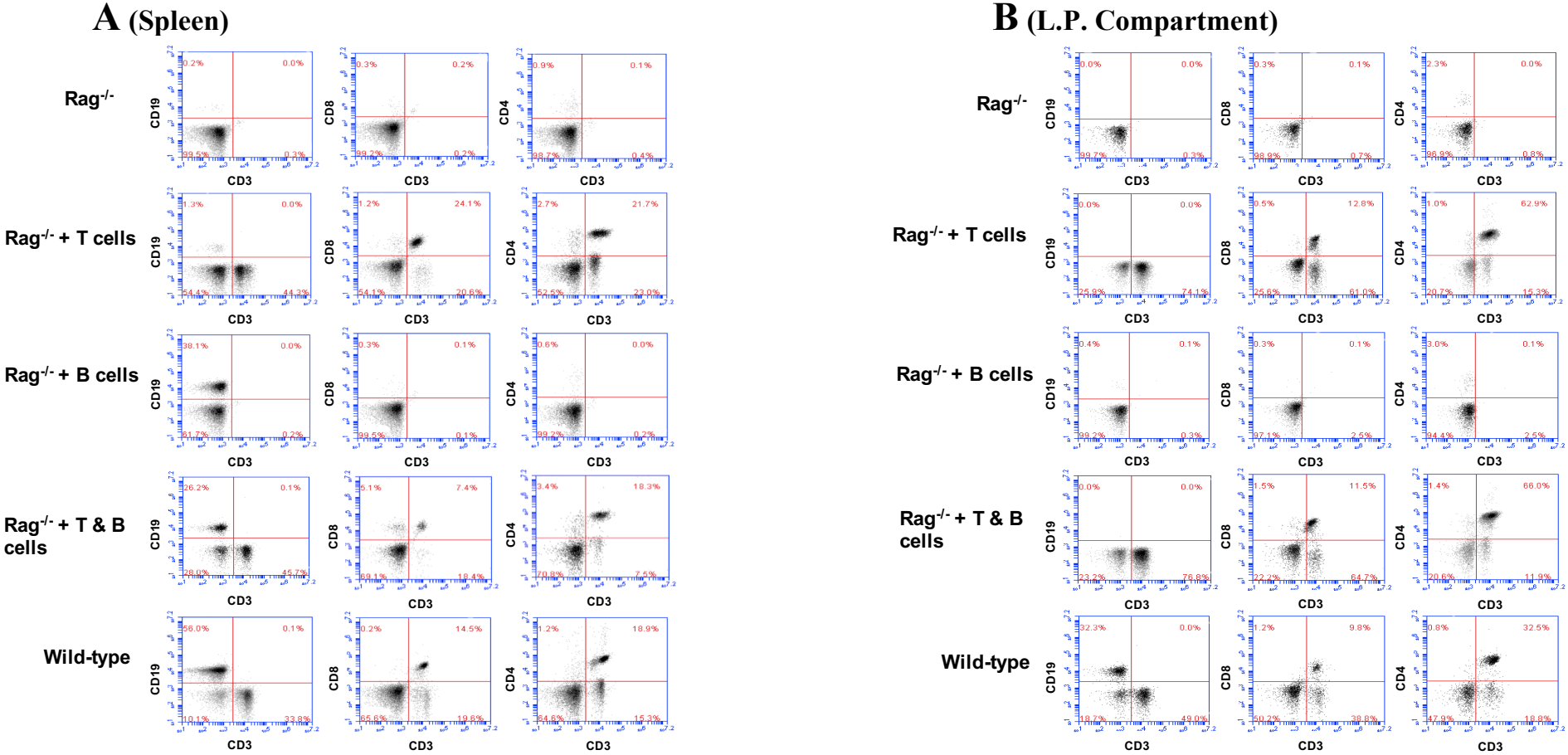

Figure 3.9 continued overleaf

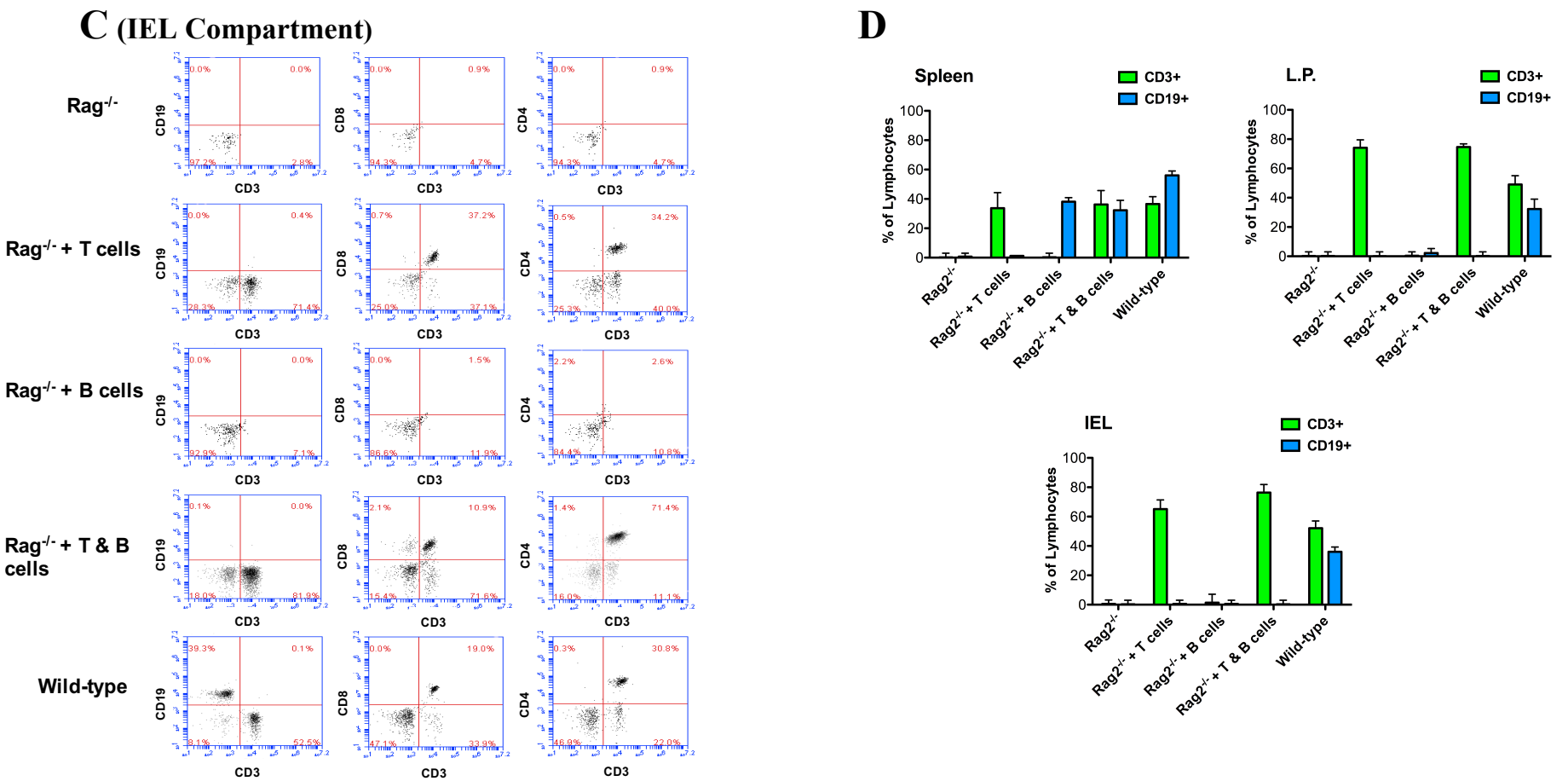

Figure 3.9 Flow cytometric analysis of Spleens, L.P. and IEL-compartments post-adoptive transfer of T and B Splenocytes.

Rag2$^{-/-}$ (*Rag*$^{-/-}$) mice injected intravenously with either CD3^{+} T lymphocytes (at ~ 1x10^{6} cells/mouse), CD19^{+} B lymphocytes (at ~ 1x10^{6} cells/mouse), or both, purified from spleens of wild-type mice. 3 weeks post-adoptive transfer mice were sacrificed and spleens and gut sections were collected. L.P. lymphocytes and IEL were extracted from gut sections as outlined in **Section 3.2.3**. The splenocytes (**A**), L.P. Lymphocytes (**B**) and IEL (**C**) were analysed by flow cytometry as detailed in **Section 3.2.4**, with detection of the surface markers; CD19, CD8 and CD4 in y-axes and CD3 expression in x-axes. The percentages of CD3^{+} and CD19^{+} lymphocytes in each compartment were plotted in (**C**). Tissues extracted from non-injected *Rag2*$^{-/-}$ and C57BL6 wild-type mice were included for comparison.

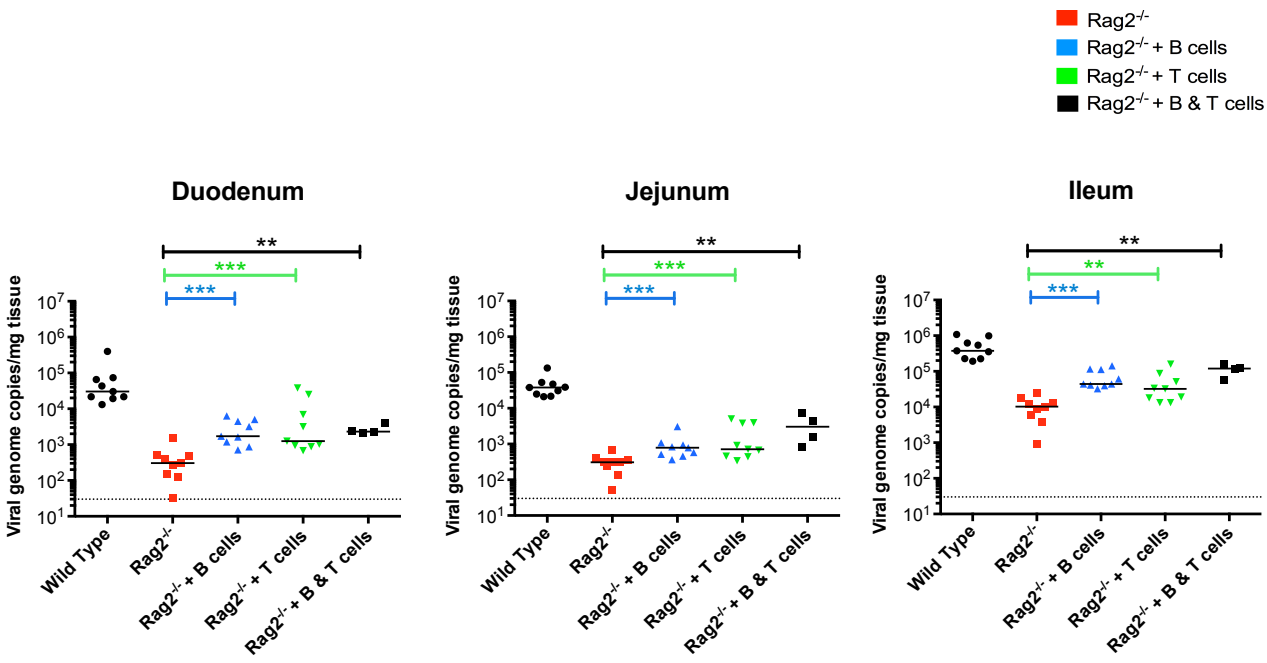

Figure 3.10 MNV-O7 infection of Wild-type, *Rag2*$^{-/-}$ injected with T- and B-Splenocytes and *Rag2*$^{-/-}$ mice.

Rag2$^{-/-}$ mice injected intravenously with either T lymphocytes (at ~ 1x10^6 cells/mouse), B lymphocytes (at ~ 1x10^6 cells/mouse), or both, purified from spleens of wild-type mice. 3 weeks post-adoptive transfer the (*Rag2*$^{-/-}$ + B), (*Rag2*$^{-/-}$ + T) and (*Rag2*$^{-/-}$ + B & T cells) mice were compared to wild-type C57BL/6 and non-injected *Rag2*$^{-/-}$ controls by oral infection of MNV-O7 (5 x 10^6 $TCID_{50}$). 40 hrs after the infection, the mice were sacrificed, gut sections (Duodenum, Jejunum, and Ileum) were collected and analysed for the level of viral RNA titres measured by RT-qPCR. The titres were normalised to the weight of the tissue sections. The dotted line indicates the limit of detection (30 copies/mg). Each point represents an individual mouse. The line in each dataset represents the median viral titre. Statistical significance was determined by Mann-Whitney test (**; P<0.01, ***; P<0.0001).

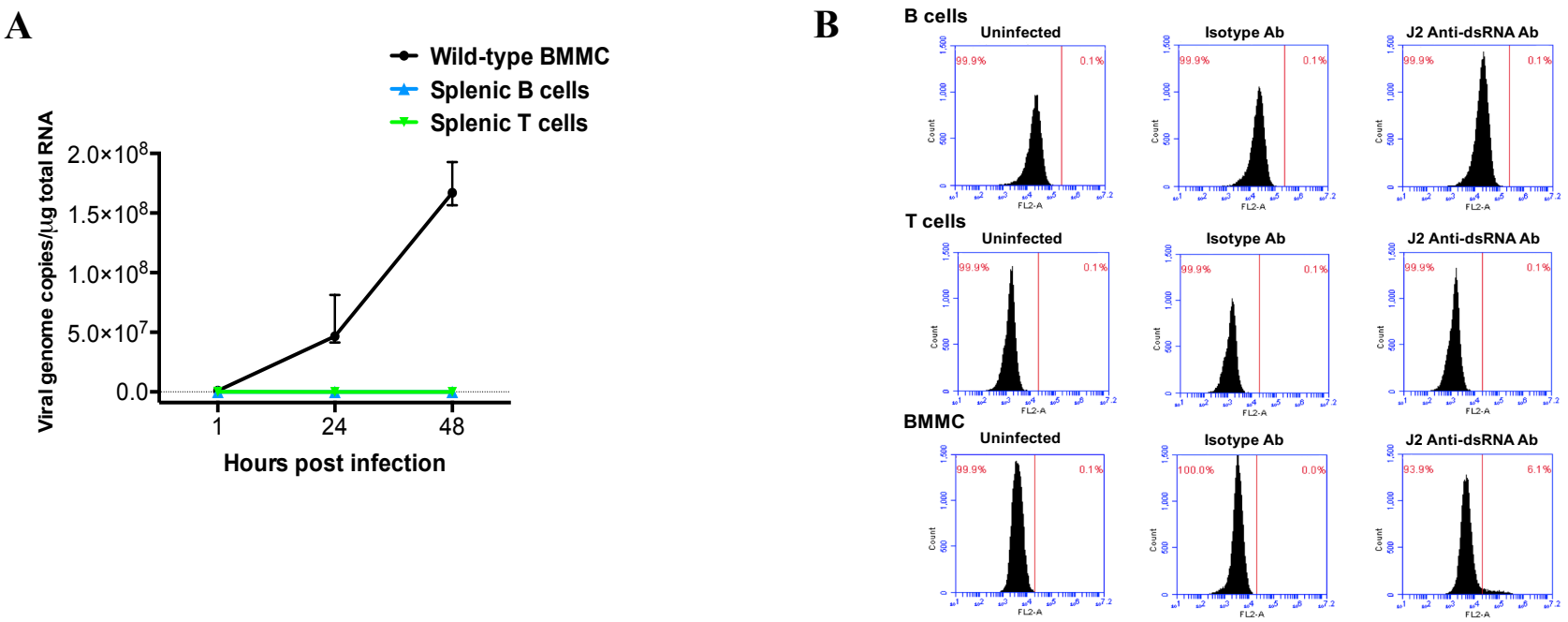

Figure 3.11 MNV-O7 does not infect B- and T-splenocytes *in vitro*.

B and T lymphocytes were sorted from the spleens of C57BL/6 wild-type mice (total number of 3 mice) and the long bones of the same wild-type mice were used to extract bone marrow-derived mononuclear cells (BMMC) that were differentiated with 20 ng GM-CSF/ml for 8 days. The cells were subsequently infected with MNV-O7 virus at MOI of 0.05. After 1 hrs incubation with the virus, the cells were washed with PBS and incubated at 37°C. (**A**) At specific post-infection times (1, 24 and 48 hrs), RNA was extracted from the cultured cells and viral titres (vRNA) were measured by RT-qPCR. vRNA was expressed as the number of molecules per μg of total RNA in the sample well. Data points represent the mean vRNA level from triplicate wells, with error bars showing the range for each triplicate.

(**B**) 12 hrs MNV-O7 infected cells (splenic B & T cells and BMMCs) were fixed, permeabilised, stained with the J2 mouse anti-double stranded RNA (dsRNA) monoclonal and anti-mouse PE-conjugated secondary antibodies and analysed by flow cytometry as detailed in **Section 3.2.4**. The B cells were shifted to the right because they were pre-stained with anti-CD19 (PE) antibodies for the sorting from the splenocyte pool.

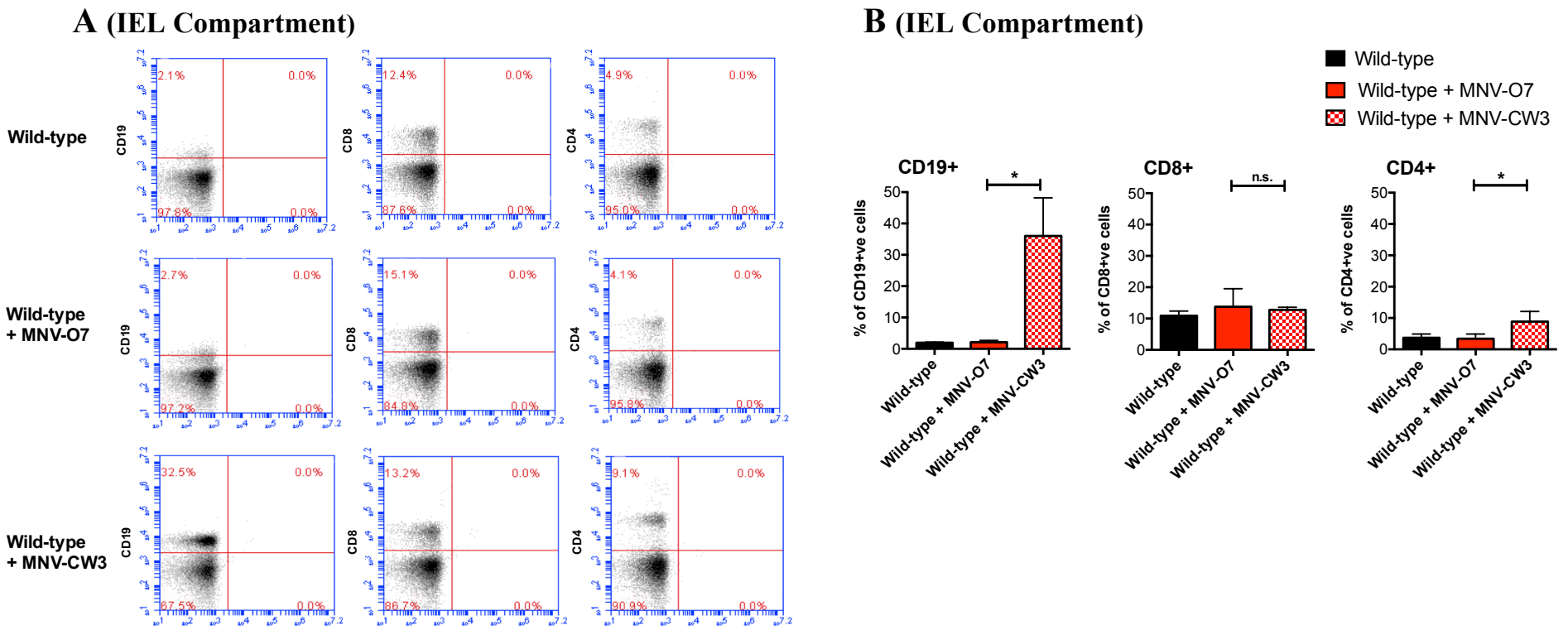

Figure 3.12 MNV-CW3 (but not -O7) infection of wild-type mice results in significant changes in the IEL compartment.

C57BL/6 wild-type mice were either uninfected or orally infected with 5 x 10^6 $TCID_{50}$ of MNV-O7 or MNV-CW3. 40 hrs after infection, the mice were sacrificed and gut sections were collected. IEL were extracted from gut sections as outlined in **Section 3.2.4** and analysed by flow cytometry (**A**) as detailed in **Section 3.2.5** with detection of the surface markers CD19, CD8 and CD4 on the y-axes. The percentages of each lymphocyte subset are plotted in (**B**). Statistical significance was determined by Mann-Whitney test (n.s.; not significant, *; $P<0.05$).

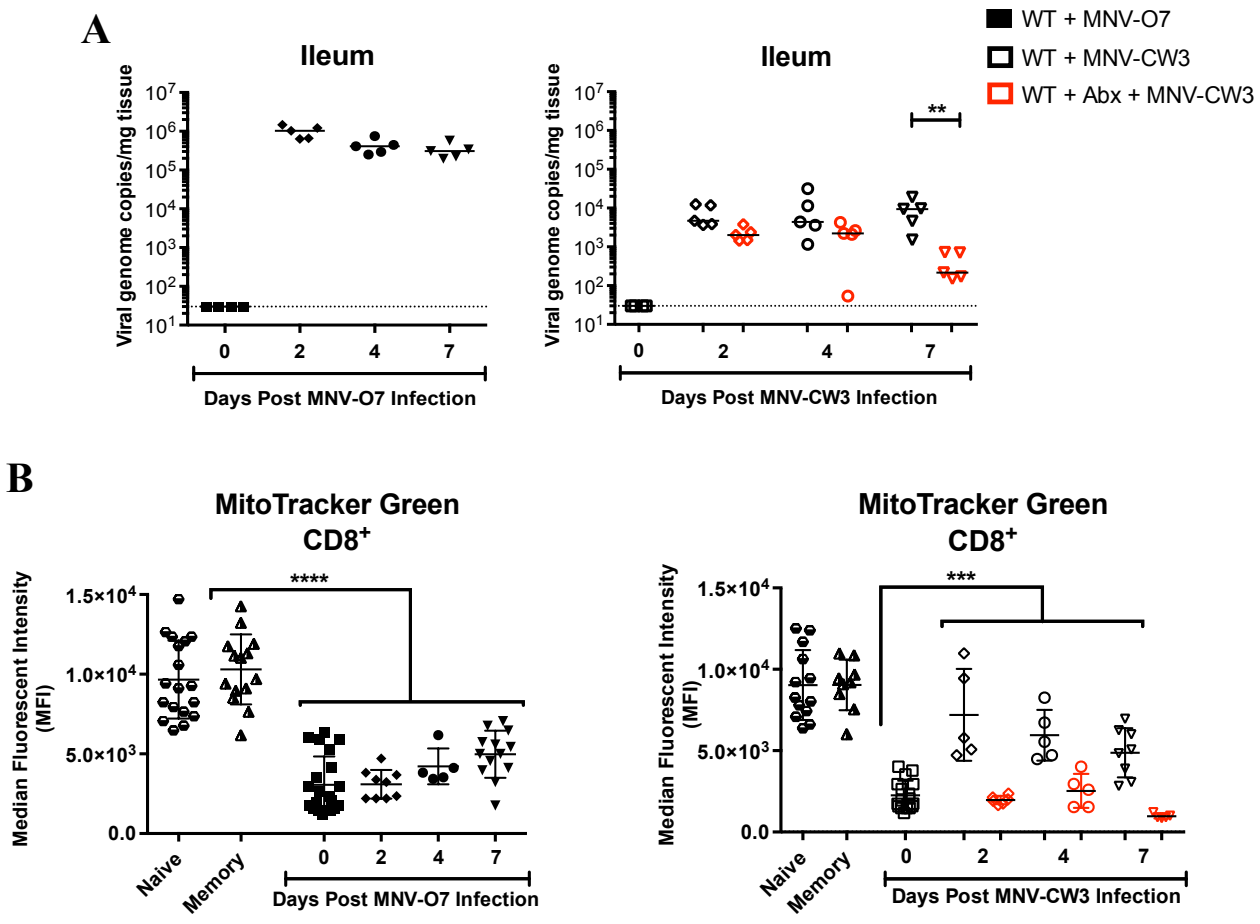

Figure 3.13 MNV-CW3 (but not O7) infection of wild-type mice results in significant changes in the IEL compartment that are Microbiota-dependent.

C57BL/6 wild-type (WT) mice were either uninfected or orally infected with 5 x 10^6 $TCID_{50}$ of MNV-O7 or MNV-CW3. Half of the MNV(CW3)-infected mice were treated orally with antibiotic cocktail (Abx) for 2 weeks prior to infection and compared to untreated age-matched MNV(CW3)-infected wild-type mice. At the indicated times post-infection, mice were sacrificed and intestinal tissues collected. Small segments of the ileum were analysed for the level of viral RNA titres measured by RT-qPCR (**A**). The titres were normalised to the weight of the ileum section. The dotted line indicates the limit of detection (30 copies/mg). Each point represents an individual mouse.

The remaining of the small intestinal tissues were used to extract IEL as outlined in **Section 3.2.3**, and the IEL were permeabilised and stained by MitoTracker Green for flow cytometry analysis (**B**) as detailed in **Section 3.2.4**. Plotted are the Median Fluorescent Intensity (MFI) of splenic $CD8^+CD44^{lo}$ (naïve), $CD8^+CD44^{hi}$ (memory) T-cells and small intestinal $CD8^+$ IELs harvested at indicated time points post infection. Statistical significance was determined by Mann-Whitney test (**; $P<0.01$, ****; $P<0.00001$). The IEL MitoTracker Green staining was performed, and data kindly provided, by Ulrika Frising (The Babraham Institute, Cambridge).

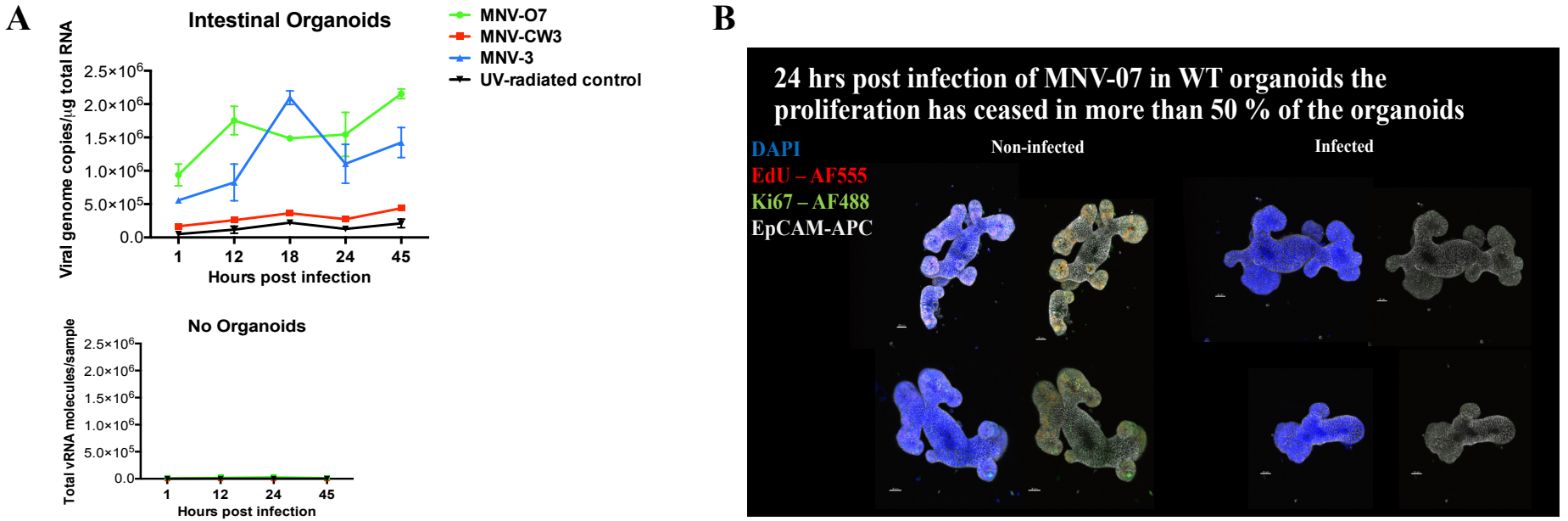

Figure 3.14 Persistent strains of MNV (MNV-O7 and MNV-3), but not acute strain (MNV-CW3), infect Intestinal Epithelial Cells.

Wild type C57BL/6 mice, 8-12 weeks of age, were sacrificed and small intestinal organoids were established as per the protocol outlined in **Section (4.2.3.2)**. Intestinal organoids were infected with either MNV-O7, MNV-CW3 or MNV-3 at an MOI of 5. After 1 hrs incubation with the virus, the cells were washed with PBS and incubated at 37 ° C. Data from organoids infected with a UV inactivated cocktail of O7 and CW3 are also included. (**A**) At indicated time-points (1, 12, 18, 24 and 45 hrs) post-infection RNA was extracted from the cultured cells and viral titres (vRNA copy numbers) were measured by RT-qPCR. vRNA copy number was expressed as the number of molecules per μg of total RNA in the sample well. Data points represent the mean vRNA level from triplicate wells, with error bars showing the range for each triplicate. The bottom graph display the viral titres in the absence of the intestinal organoids. (**B**) Non-infected and 24 hrs MNV-O7-infected organoids were fixed in 4 % formaldehyde, permeabilised, blocked and stained for proliferation markers at 4 ° C overnight using anti-Edu, anti-Ki67 and anti-EpCam primary antibodies. The following day, the samples were stained with AF555, AF488, APC-coupled secondary antibodies, respectively. DAPI served as counterstain for nuclei. Images were acquired on a Zeiss 780 confocal microscope in two independent experiments. Shown are representative pictures. Scale bar = 50μm. The organoids were generated, stained, and picture kindly provided, by Ulrika Frising (The Babraham Institute, Cambridge).

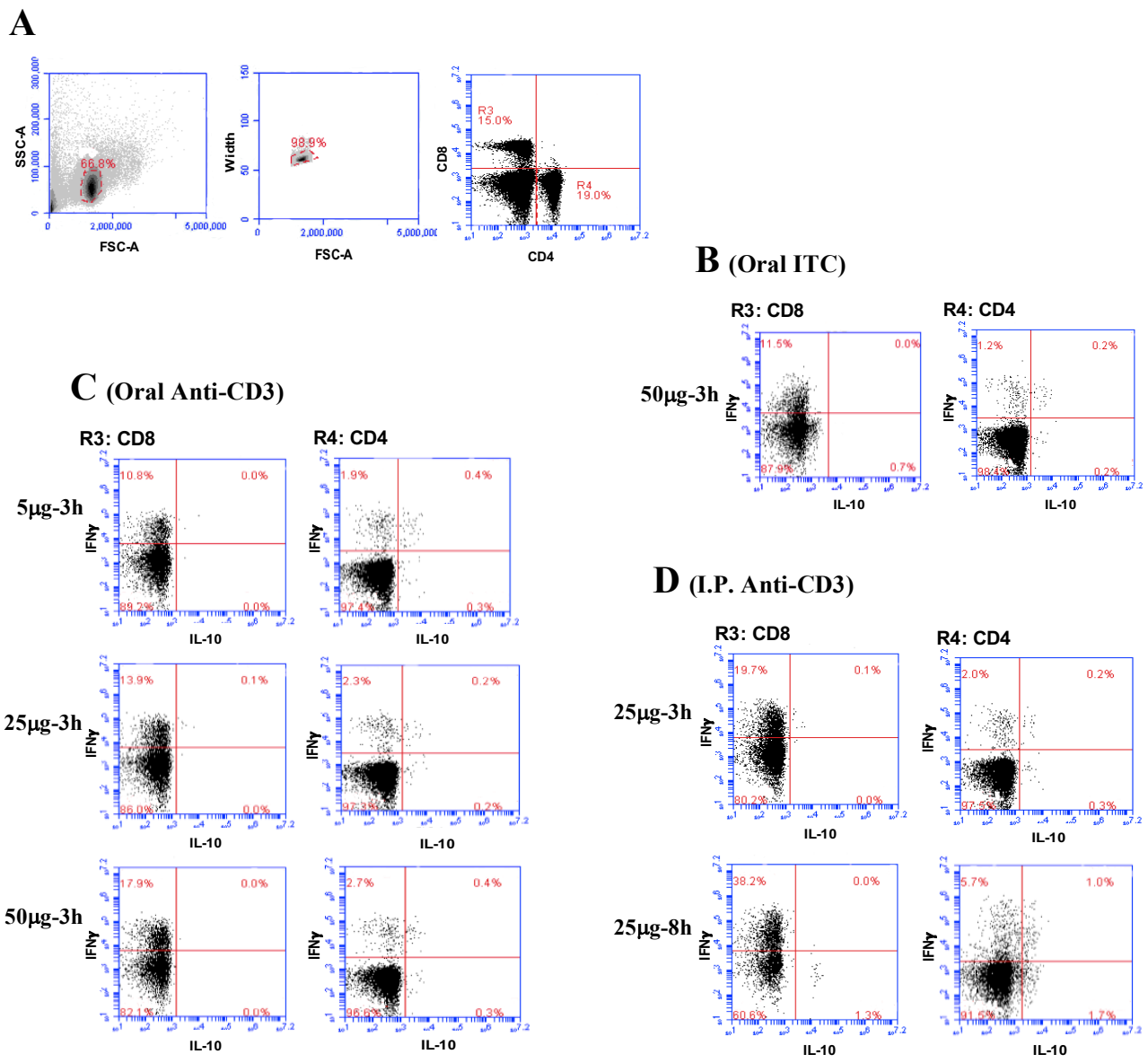

Supplementary Figure 3.1 Strategy for flow cytometric analysis of spleens.

Splenocyte activation following administration of anti-CD3 or isotype control (ITC) antibodies to C57BL/6 wild-type mice was analysed according to the gating strategy above. Samples were stained with various cocktails of fluorophore conjugated antibodies targeting surface markers or cytokines (following fixation and permeabilisation) are shown (refer to **Section 3.2.4** for details).

(**A**) Prior to plotting the data, all samples were gated to exclude dead cells, based on forward scatter (FSC-A) versus side scatter (SSC-A) and to remove doublets (FSC-A versus pulse width). No background staining was observed on cells stained with matched isotype control antibodies and these cells were used to help set the quadrant gates. The cells were then gated into $CD8^+$ (R3) and $CD4^+$ (R4) and subsequently analysed for the expression of IFNγ and IL-10. For oral ITC-administered mice (**B**) oral anti-CD3-adminstered mice (**C**) and I.P anti-CD3-injected mice (**D**). The data are representative of 3 replicates of each condition.

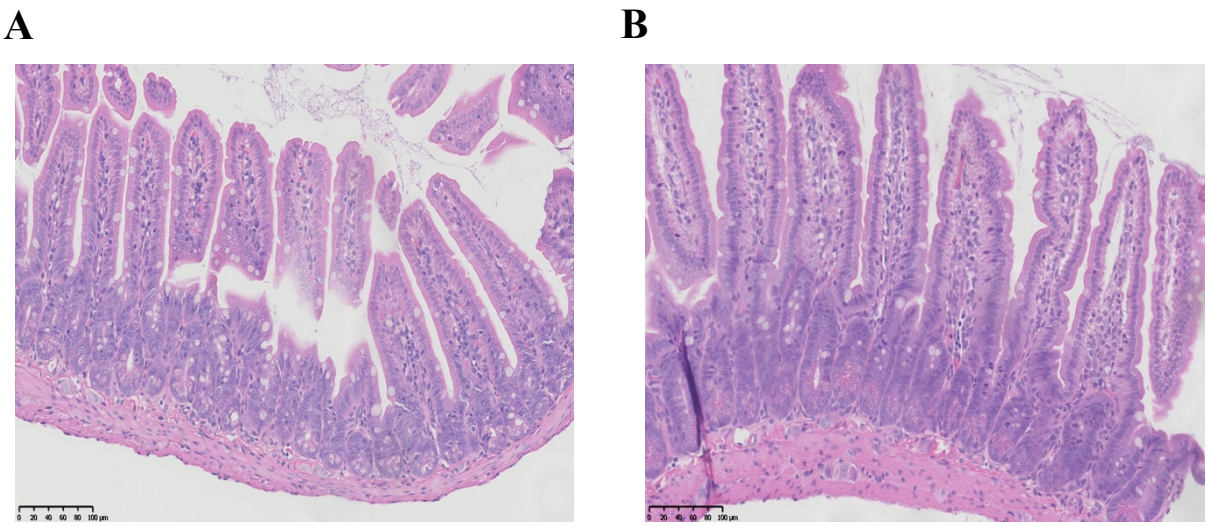

Supplementary Figure 3.2 Representative gut histopathology of Wild-type and *Tcra*$^{-/-}$ mice.

Small ileal samples were taken from non-infected wild-type (**A**) and *Tcra*$^{-/-}$ (**B**) mice during necropsy, flushed with PBS and placed in 10 % buffered formalin saline. After 24 hrs fixation period, samples were embedded in paraffin, cut into 3 mm sections on glass slides and stained with haematoxylin and eosin. Preparation of slides and staining was performed in the Diagnostic Histopathology Section, Department of Veterinary Medicine, University of Cambridge. The slides were viewed using a Nano-zoomer Digital Slide Scanner (Hamamatsu). Images were processed from the scans using the NDP.view2 software (Hamamatsu). Images shown were taken at 20x magnification.

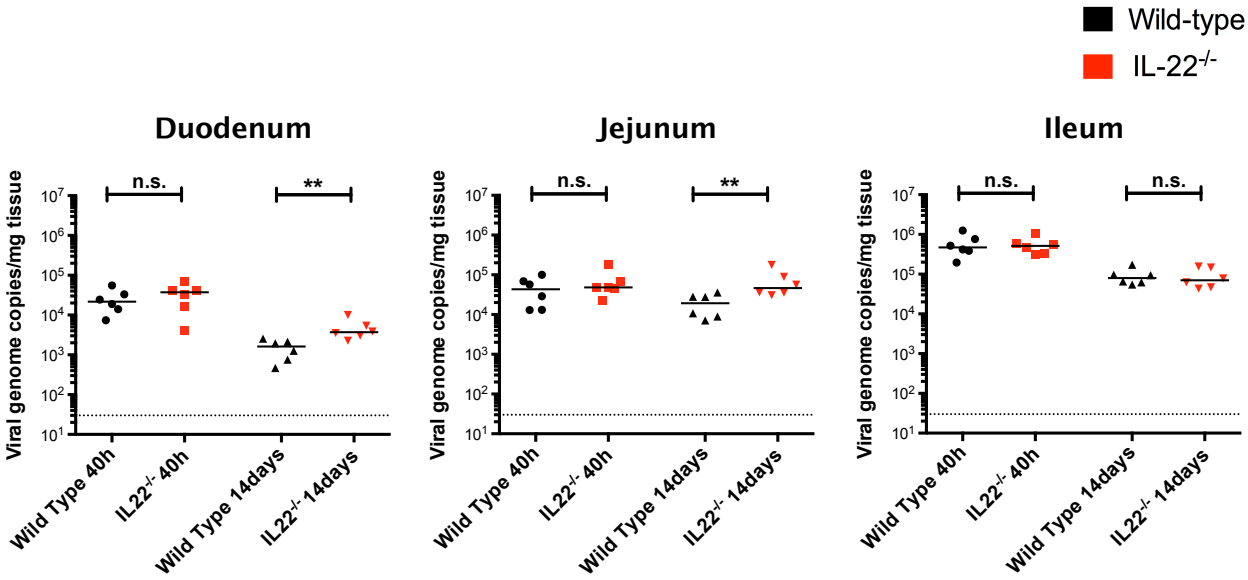

Supplementary Figure 3.3 MNV-O7 infection of Wild-type and *Il22*$^{-/-}$ mice.

5 Wild type (C57Bl/6) and *Il22*$^{-/-}$ mice were infected orally with MNV-O7 (5 x 10^6 $TCID_{50}$). Forty hours (square-shaped dots) and 14 days (triange-shaped dots) after the infection, mice were sacrificed and gut sections (Duodenum, Jejunum, and Ileum) were collected. RNA was extracted from the tissues and viral titres (viral RNA copy numbers) were measured by RT-qPCR. The titres were normalised to the weight of the tissue sections. Dotted line indicates the limit of detection (30 viral genome copies per mg tissues). Each point represents an individual mouse. The line in each dataset represents the median viral titre. Statistical significance was detremined by Mann-Whitney test. (n.s.; non-significant).

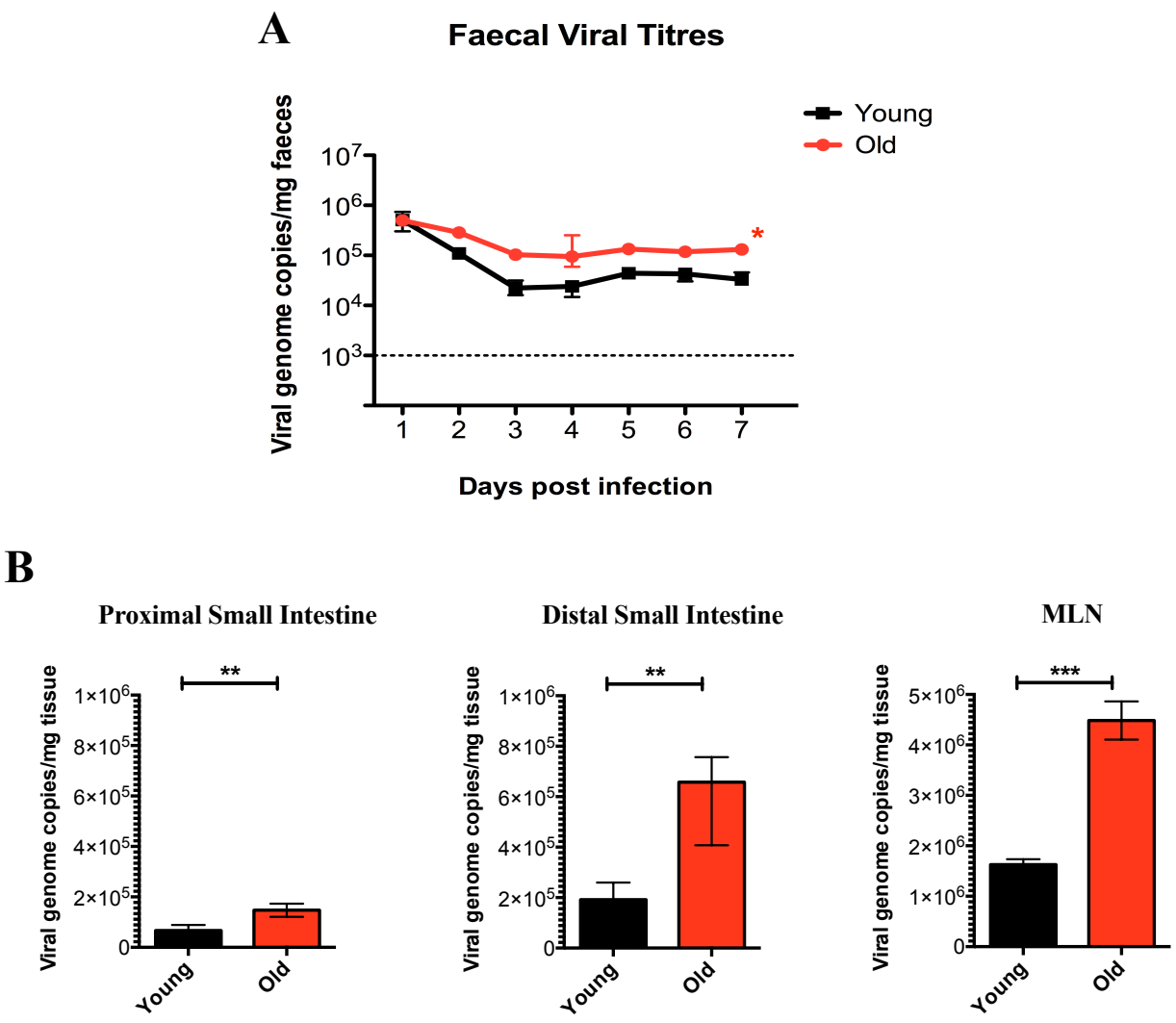

Figure 4.1 Old mice exhibit impaired control of a persistent MNV-O7 infection.

Wild type (C57Bl/6) mice, 8-week (Young) or 24-month (Old) of age, were challenged orally with MNV-O7 (5 x 10^6 $TCID_{50}$). Faecal samples were collected at the indicated days (1-7) post-infection (P.I.). The mice were sacrificed and intestinal tissues and mesenteric lymph nodes (MLN) collected in day-7 P.I.. RNA was extracted from the faeces/tissues and viral titres (RNA copy numbers) were measured by RT-qPCR. Shown are the numbers of genome copies of MNV per mg of faeces (**A**) and tissue (**B**). Statistical significance was calculated by 2-way ANOVA (**A**) and an unpaired t test (**B**). (*; P<0.05, **; P<0.01, ***; P<0.0001).

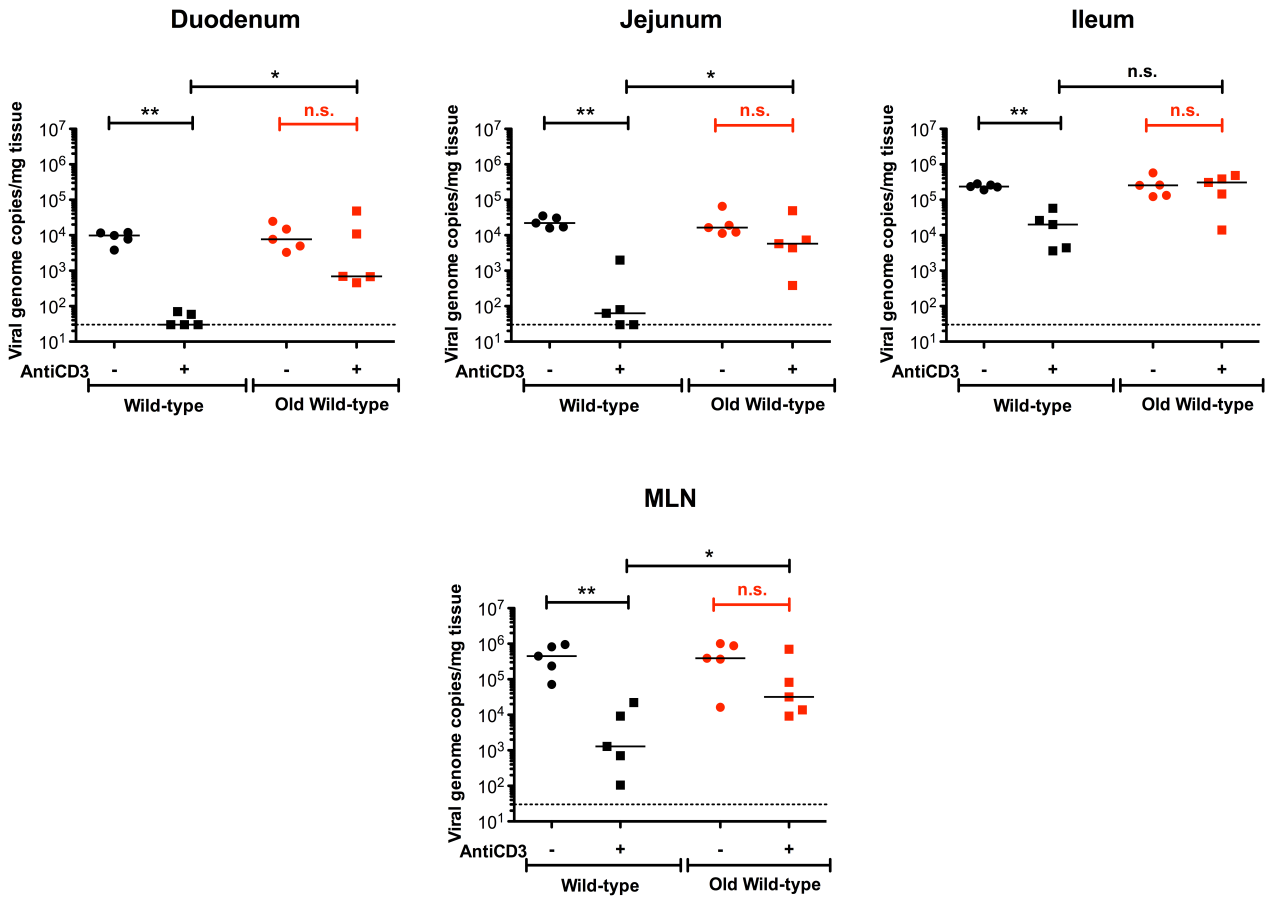

Figure 4.2 Old mice exhibit impaired control of small intestinal MNV viral infection after *in vivo* anti-CD3 stimulation.

Wild type (C57Bl/6) mice, 8-week or 24-month (Old) of age, were infected orally with MNV-O7 (5 x 10^6 $TCID_{50}$) 8 hours after being injected intraperitoneally with 25µg of either anti-CD3 (+) or isotype control (-) antibodies. 40 hrs after the infection, the mice were sacrificed and gut sections (duodenum, jejunum, and ileum) and mesenteric lymph nodes (MLN) were collected. RNA was extracted from the tissues and viral titres (RNA copy numbers) measured by RT-qPCR. The titres were normalised to the weight of the tissue sections. Dotted line indicates the limit of detection (30 viral genome copies per mg tissues). Each point represents an individual mouse. The line in each dataset represents the median viral titre. Statistical significance was calculated by Mann-Whitney test (n.s; non-significant, *; P<0.05, **; P<0.01).

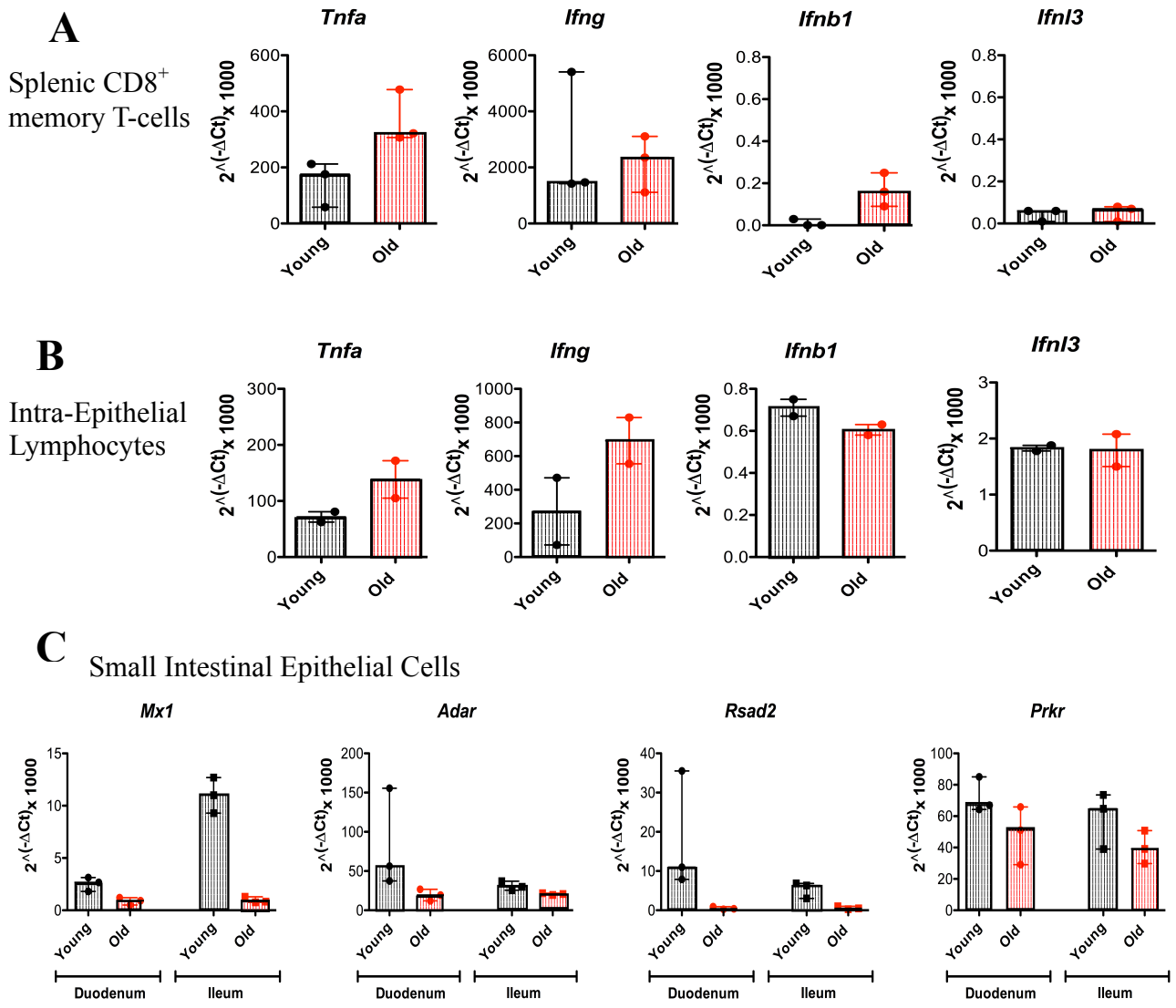

Figure 4.3 *In vivo* anti-CD3 stimulation of old mice resulted in systemic and gut-associated inflamm-aging with impaired small intestinal antiviral response.

C57Bl/6 mice, 8 weeks (Young) or 24 months (Old) of age, were injected intraperitoneally with 25µg of anti-CD3 antibodies. Mice were sacrificed 3 hrs post-stimulation. Splenic $CD8^+$ memory ($CD44^{hi}$) T cells (**A**), intra-epithelial lymphocytes (**B**) and small intestinal (proximal and distal) epithelial cells (**C**) were sorted and isolated. RNA was extracted from each cell population, reverse transcribed and analysed for the gene expression of TNF and IFNs (**A** and **B**) and ISGs; *Mx1*, *Adar, Rsad2* and *Prkr* (**C**). Expression levels are shown as $2^{\wedge(-\Delta Ct)}$, normalised to the mean of two housekeeping genes (*Rpl38*, *Eef2*) and multiplied by a factor of 1000. Error bars indicate the range of values obtained.

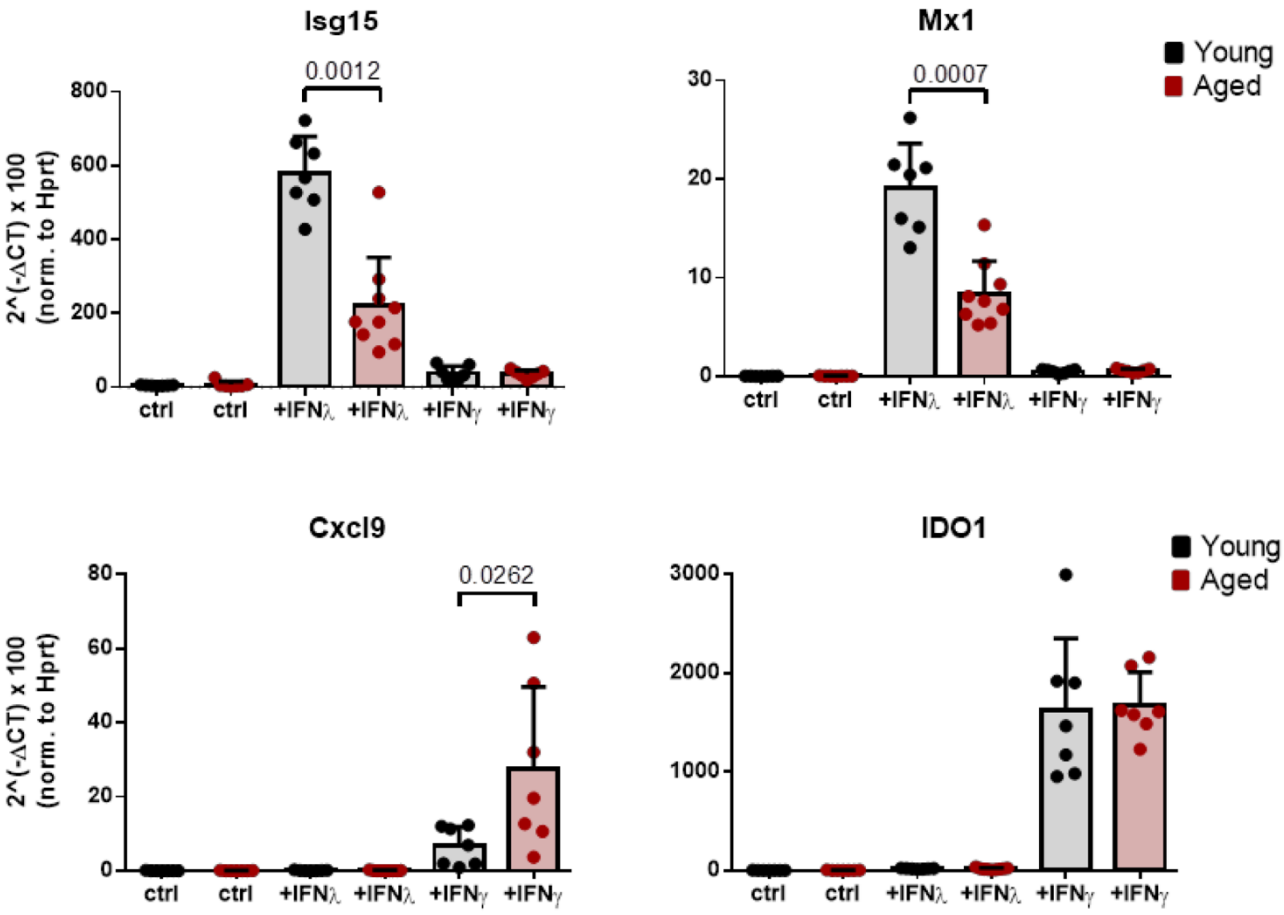

Figure 4.4 IFN response of old versus young small Intestinal Epithelial Cells.

Wild type (C57Bl/6) mice, 8-week (Young) or 24-month (Old) of age, were sacrificed and small intestinal epithelial cells (IECs) were purified, seeded into Matrigel droplets and cultured into growth factor-rich medium alone (**Ctrl**) or medium plus either 30 ng IFNλ/ml (**+IFNλ**) or 2.5 ng IFNγ/ml (**+IFNγ**) for 6 hrs. The IECs were then harvested, lysed, RNA extracted and analysed for the gene expression by RT-qPCR. IFN-specific responses were analysed by the expression levels of the IFNλ–responsive genes: *Mx1* and *Isg15,* or the IFNγ-responsive genes: *Cxcl9* and *Ido1*. Expression levels are shown as $2^{\wedge(-\Delta Ct)}$, normalised to the expression of *Hprt* housekeeping gene and multiplied by a factor of 100. The data shown were pooled from two independent biological repeats (n=7), each dot represents a single data point with error bars indicating standard deviations. These *ex vivo* experiments and the figures displayed above were performed in collaboration with, and data kindly provided by, M. Stebegg (The Babraham Institute).

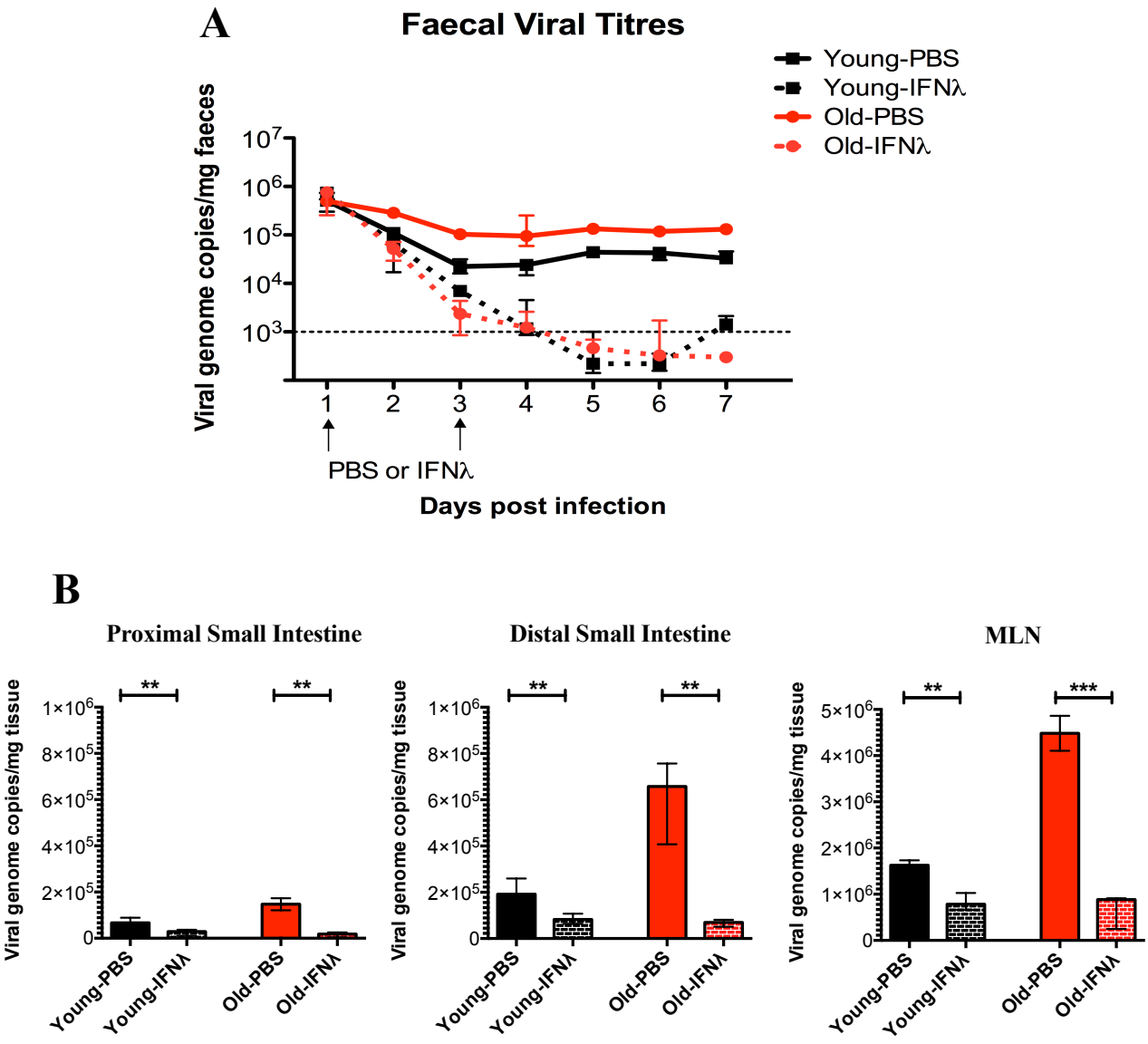

Figure 4.5 *In vivo* therapy with a high dose of IFN-λ reversed the anti-viral defect in old mice. Wild type (C57Bl/6) mice, 8-week (Young) or 24-month (Old) of age, were challenged orally with MNV-O7 (5 x 10^6 $TCID_{50}$). Mice were injected with 25 µg of IFN-λ or phosphate-buffered saline (PBS) intraperitoneally 1- and 3-days post-infection (P.I.). Faecal samples were collected at the indicated days (1-7) P.I. The mice were sacrificed and intestinal tissues and mesenteric lymph nodes (MLN) collected on day-7 P.I. RNA was extracted from the faeces/tissues and viral titres (RNA copy numbers) were measured by RT-qPCR. Shown are the numbers of genome copies of MNV per mg of faeces (**A**) and tissue (**B**). Statistical significance was calculated by an unpaired t test (**B**). (**; P<0.01, ***; P<0.0001).

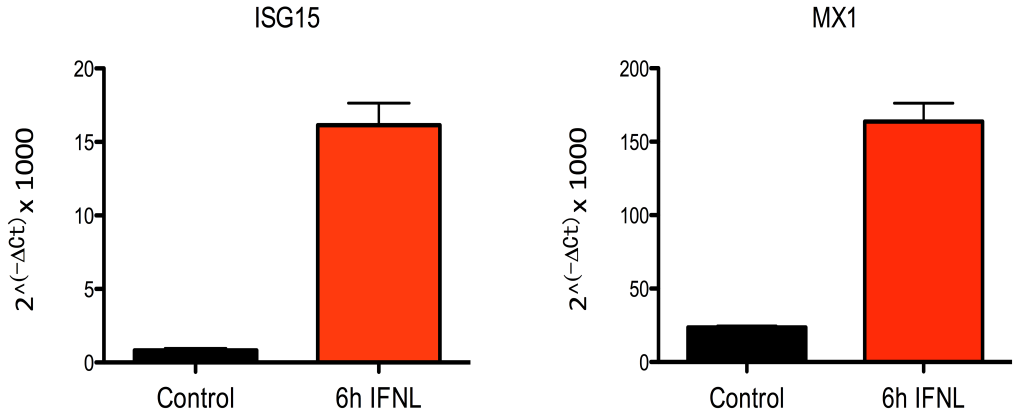

Figure 4.6 Human Intestinal Organoids were responsive to IFN-lambda.

Small intestinal organoids were generated from endoscopic samples taken from two young-adult (in their 20s), healthy human volunteers in Addenbrooke's hospital. The organoids were treated with 25 µg of recombinant human Interferon lambda (L) for 6 hrs and intestinal epithelial cells were then lysed, RNA extracted, reverse transcribed and analysed for the expression of the human ISGs: *MX1* and *ISG15*. Expression levels were depicted as mean $2^{\wedge(-\Delta Ct)}$, normalised to the mean of two house-keeping genes (Rpl38, Eef2) and multiplied by a factor of 1000. Error bars indicate the range of results. The organoids were generated and treated with IFN-λ (IFNL) by our collaborators (Dr. Matthias Zilbauer's lab) at Department of Paediatrics, University of Cambridge. I performed the RNA extractions and RT-qPCR analysis.

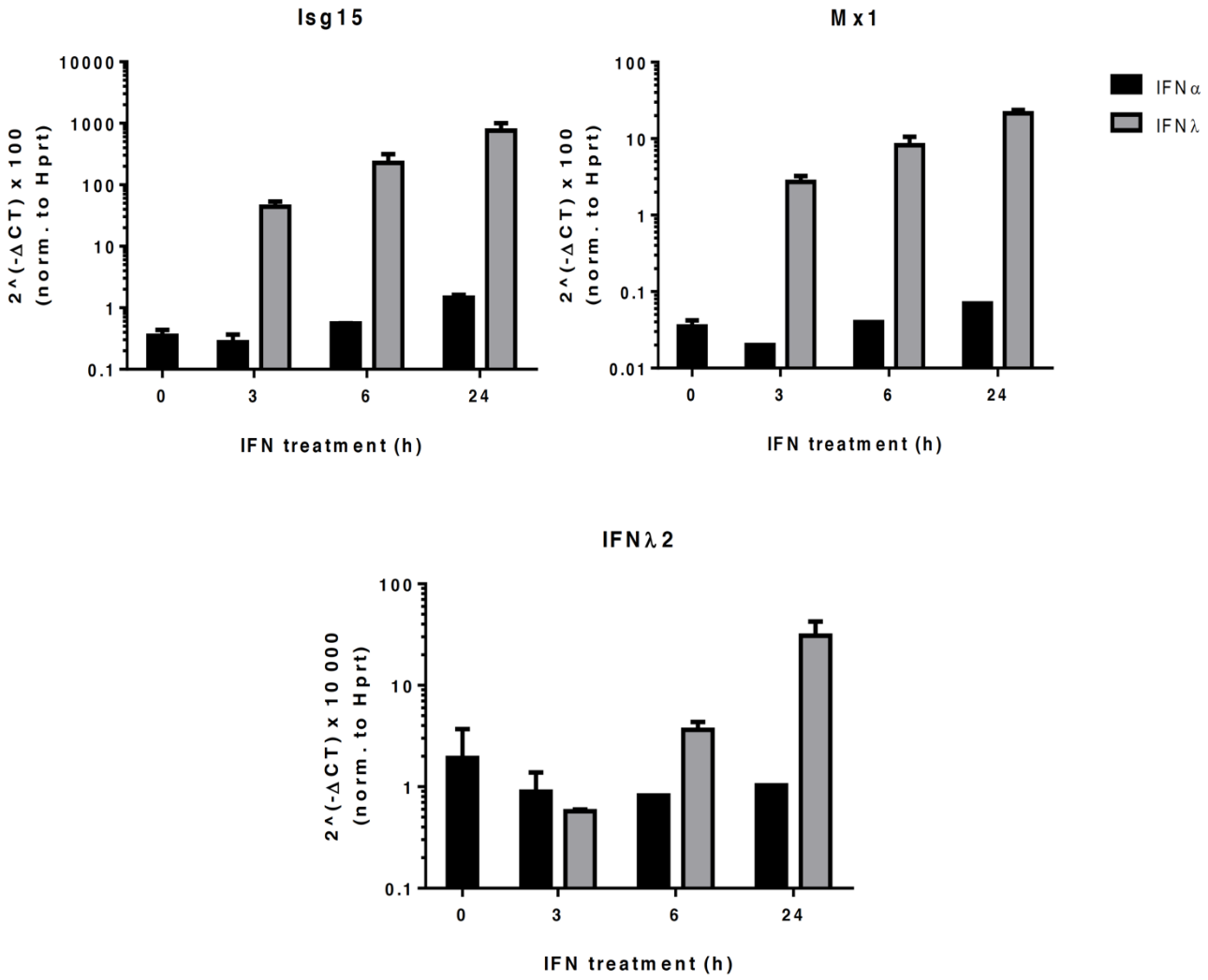

Supplementary Figure 4.1 Small Intestinal Epithelial Cells (IECs) are more responsive *ex vivo* to type-III IFN compared to type-I IFN

Wild type (C57Bl/6) mice, 8-week of age, were sacrificed and small intestinal organoids were established as per protocol outlined in **Section 4.2.3.2**. Intestinal organoids were treated with 25 ng/ml of either IFNα–2b (black bars) or IFNλ–2 (grey bars) for the indicated time points. Intestinal organoids were then harvested, IECs lysed, RNA extracted and analysed for the gene expression of IFNλ2 and ISGs: *Mx1* and *Isg15* by RT-qPCR. Expression levels are shown as $2^{\wedge(-\Delta Ct)}$, normalised to the expression of *Hprt* house-keeping gene and multiplied by a factor of 100 or 1000. Error bars indicate standard deviations. These *ex vivo* experiments and the figures displayed above were performed, and data kindly provided, by M. Stebegg (The Babraham Institute).

A. 24 months old mice

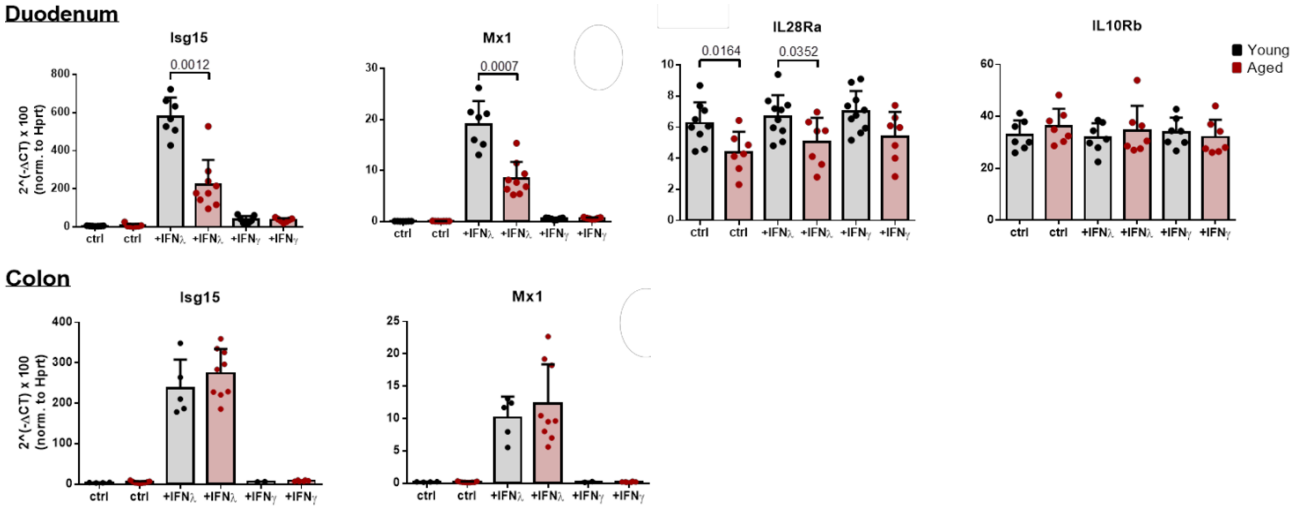

B. 15 months old mice

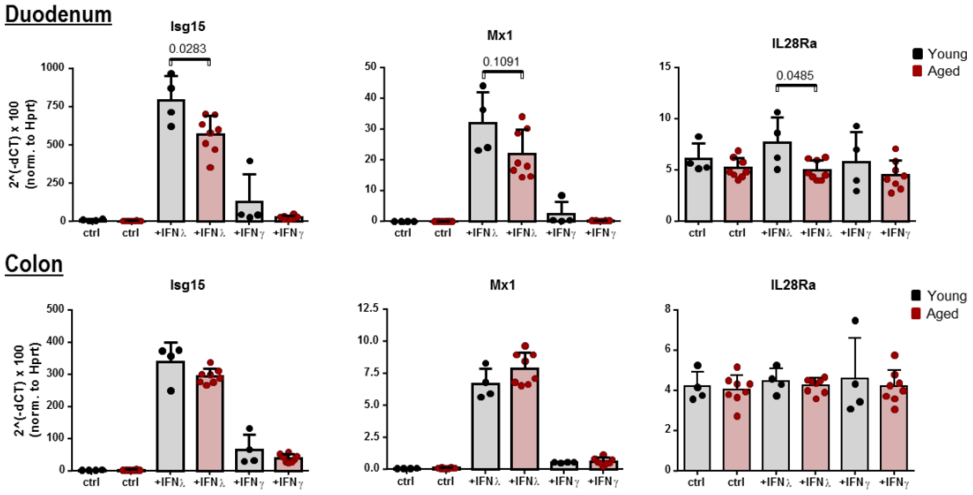

Supplementary Figure 4.2 The defective IFNλ response in old mice is confined to the small intestine and is more apparent at certain age groups.

Intestinal epithelial cells (IECs) were isolated from the small intestine and colon of 8-week old (young) mice and either 24-month old mice (**A**) or 15-month old mice (**B**). Purified IECs were cultured as described in **Section 4.2.3.2**. and analysed for the expression of IFNλ–responsive genes: *Mx1* and *Isg15,* and the IFNλ–receptor subunits: *Il28ra* and *Il10rb*. The data shown were pooled from at least two independent biological repeats, each dot representing a single data point and error bars indicates standard deviations. These experiments and the figures displayed above were performed in collaboration with, and data kindly provided by, M. Stebegg (The Babraham Institute).

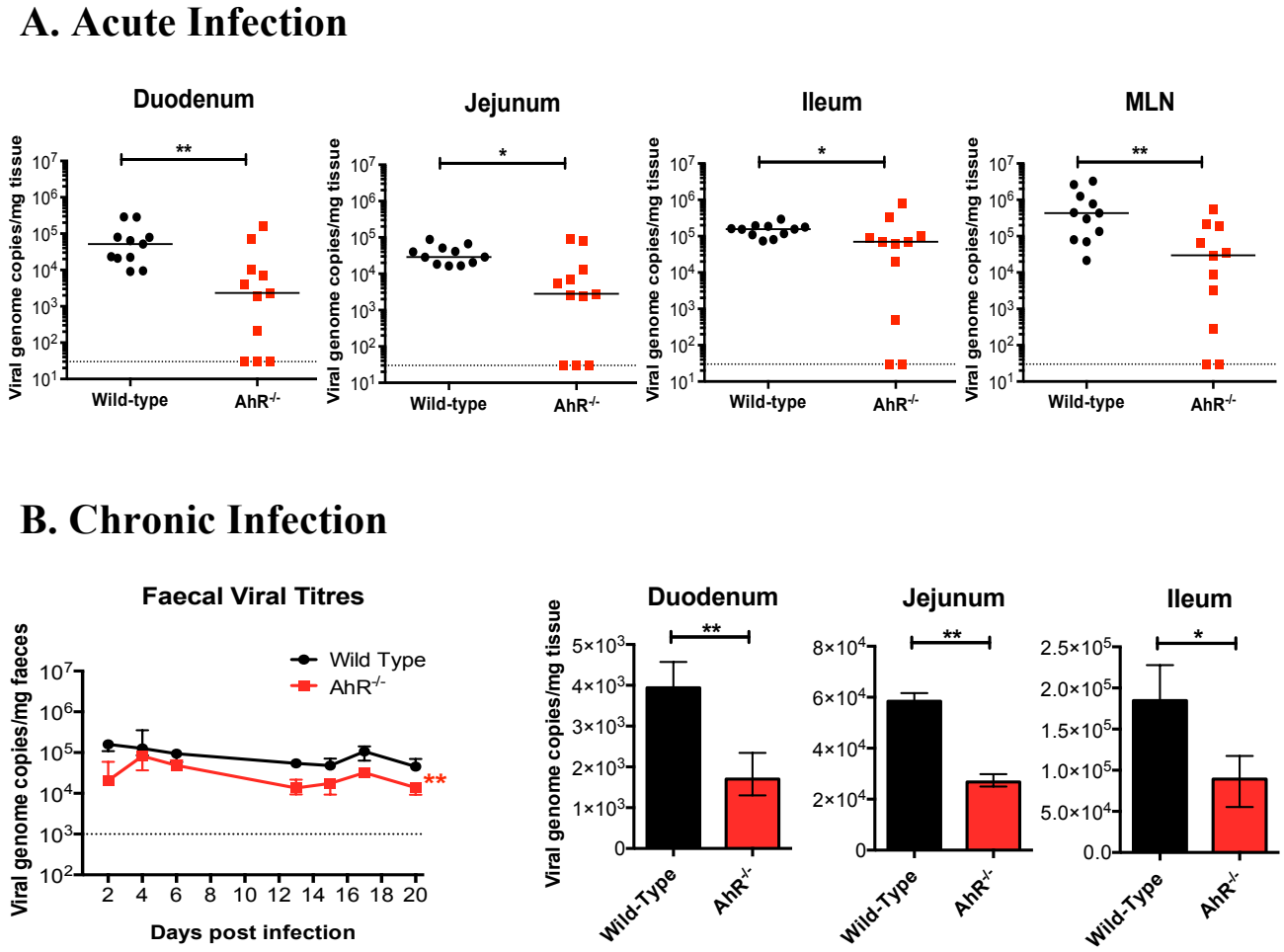

Figure 5.1 MNV-O7 Infection of Wild-Type and *AhR*$^{-/-}$ Mice.

Wild-type (C57BL/6) and *Ahr*$^{-/-}$ mice were infected orally with MNV-O7 (5 x 10^6 $TCID_{50}$). (**A**) 40 hrs after the infection, the mice were sacrificed and gut sections (duodenum, jejunum, and ileum) and mesenteric lymph nodes (MLN) were collected. The dotted line indicates the limit of detection (30 viral genome copies per mg tissue). Each point represents an individual mouse. The line in each dataset represents the median viral titre. (**B**) Faecal samples were collected at the indicated days P.I.. The mice were sacrificed and intestinal tissues collected in day 21 P.I.. RNA was extracted from the faeces/tissues and viral titres were measured by RT-qPCR and normalised by the weight of faeces/tissue. The data shown were pooled from two independent biological repeats. Statistical significance was calculated by Mann-Whitney test (**A**) and 2-way ANOVA (**B**) (*; P<0.05, **; P<0.01).

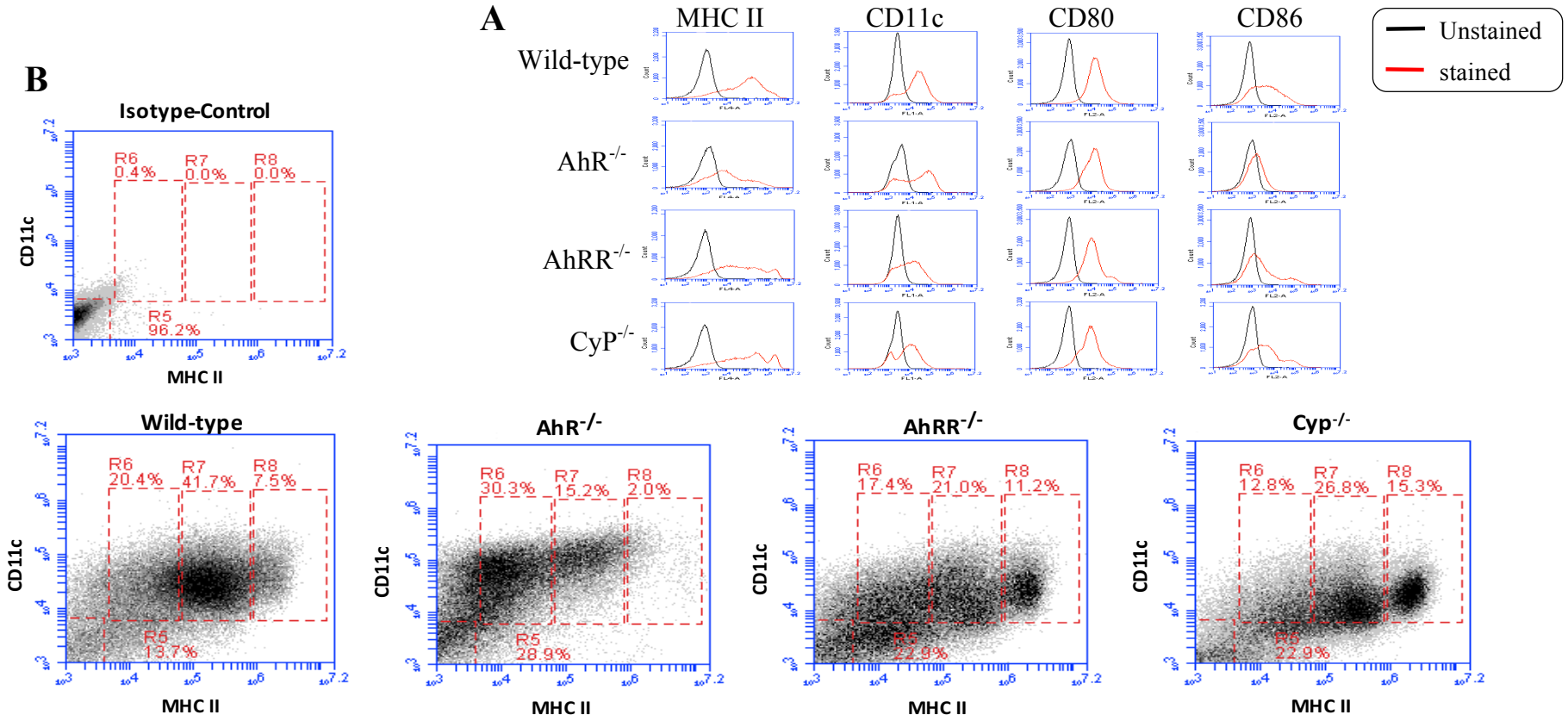

Figure 5.2 Flow Cytometry of Bone Marrow-Derived Mononuclear Cells (BMMC) derived from Wild-Type, *Ahr*$^{-/-}$, *Ahrr*$^{-/-}$ and *Cyp*$^{-/-}$ mice. BMMC from wild-type, *Ahr*$^{-/-}$, *Ahrr*$^{-/-}$ and *Cyp*$^{-/-}$ mice differentiated with GM-CSF were analysed by flow cytometry for the expression of the surface markers MHC class II, CD11c, CD80 and CD86 (**A**). The different BMMC were gated on CD11c and MHC class II expression for differentiation into immature (R6), moderate (R7) and high (R8) maturation states (**B**). The data are representative of two independent experiments.

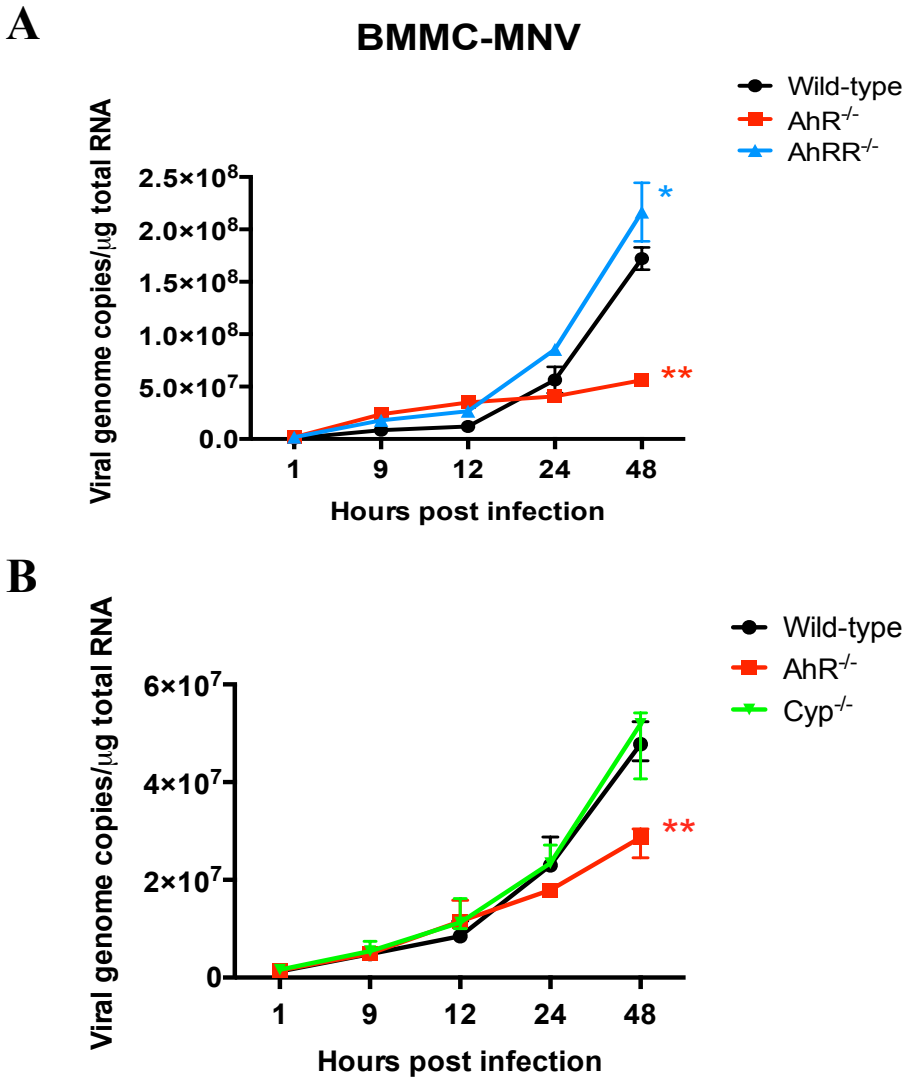

Figure 5.3 MNV-O7 replication in Wild-Type, *Ahr*$^{-/-}$, *Ahrr*$^{-/-}$ and *Cyp*$^{-/-}$ BMMCs.

BMMC generated from wild-type, *Ahr*$^{-/-}$, *Ahrr*$^{-/-}$ (**A**) and *Cyp*$^{-/-}$ (**B**) mice were differentiated as in **Figure 5.2**. The BMMC were infected with MNV-O7 virus at an MOI of 0.05 (**A**) and 0.03 (**B**). After 1 hrs incubation with the virus, the cells were washed then incubated at 37 ° C. At specific times post-infection (1, 9, 12, 24 and 48 hrs), RNA was extracted from the cells and viral titres (vRNA copy numbers) were measured by RT-qPCR. vRNA copy number was expressed as the number of molecules per µg of total RNA in the sample well. Data points represent the mean vRNA level from triplicate wells, with error bars showing the range for each triplicate. Statistical significance was calculated by 2-way ANOVA (*; $P<0.05$, **; $P<0.01$).

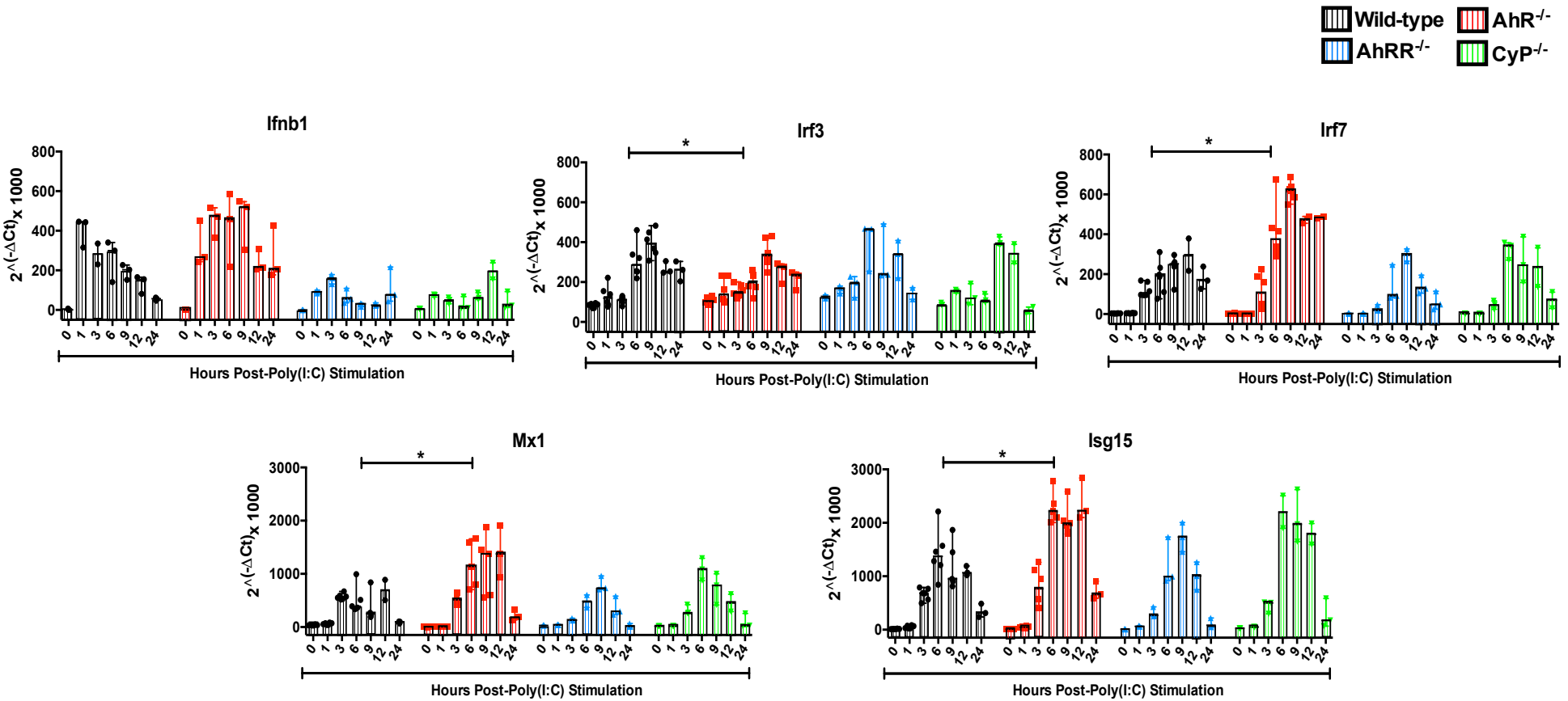

Figure 5.4 RT-qPCR-based Gene Expression Analysis of BMMCs Following Poly(I:C) Stimulation.

BMMC generated from wild-type, *Ahr*$^{-/-}$, *Ahrr*$^{-/-}$ and *Cyp*$^{-/-}$ mice were differentiated as in **Figure 5.2** and seeded into individual wells. The BMMC were subsequently treated with 100 µg Poly(I:C)/ml and at specific time points RNA was extracted from each well, reverse transcribed and analysed for the expression of genes *Ifnb1*, *Irf3*, *Irf7*, *Mx1* and *Isg15*. Data points represent the expression levels, which are shown as $2^{\wedge(-\Delta Ct)}$, normalised to the mean of two housekeeping genes (*Rpl38*, *Eef2*) and multiplied by a factor of 1000. Error bars indicate ranges. The data shown were pooled from two independent repeats (except for *Ifnb1*). Statistical significance was calculated (at 6 hrs post-stimulation) by Mann-Whitney test (*; P<0.05).

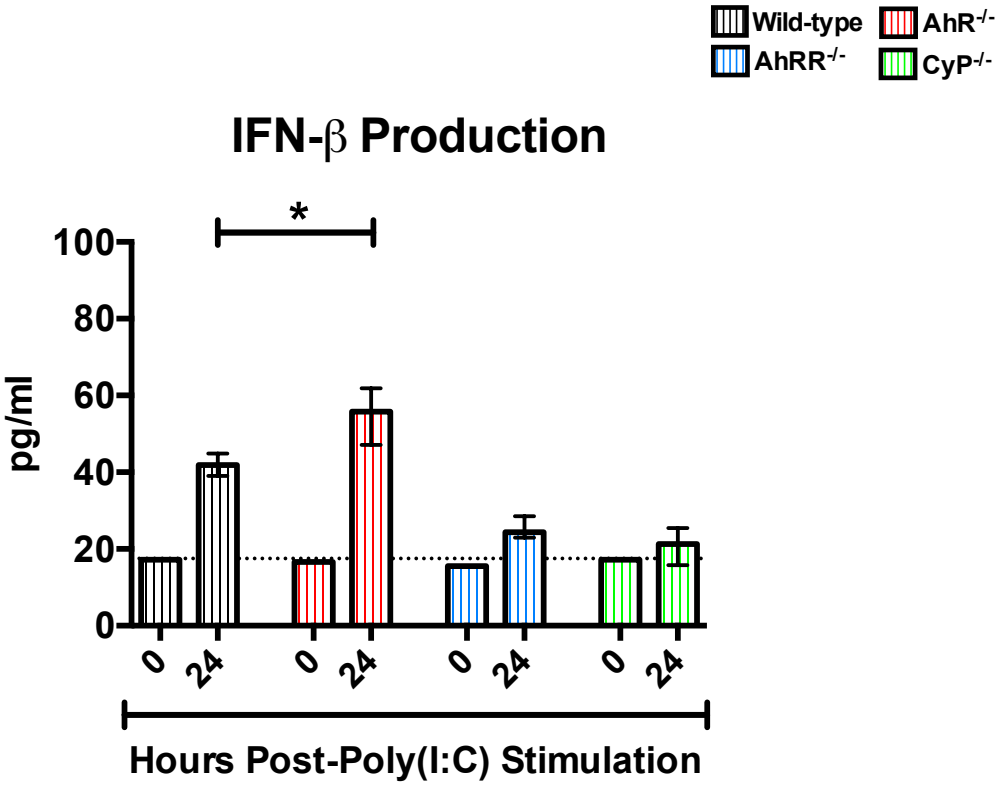

Figure 5.5 Production of IFN-β by BMMC following Poly(I:C) Stimulation.

BMMC generated from wild-type, *Ahr*$^{-/-}$, *Ahrr*$^{-/-}$ and *Cyp*$^{-/-}$ mice were differentiated as in **Figure 5.2** and stimulated with 100 μg poly(I:C)/ml as in **Figure 5.4.**. At 0 and 24 hrs post-poly(I:C) stimulation, the supernatant from individual wells was collected for an ELISA assay to quantify the amount of IFN-β produced by the cells. The dotted line indicates the limit of detection (17.5 pg/ml). Bars represent the median of three technical replicates of a single sample, with error bars showing the range of these replicates. Statistical significance was calculated by an unpaired t test. (*; $P<0.05$).

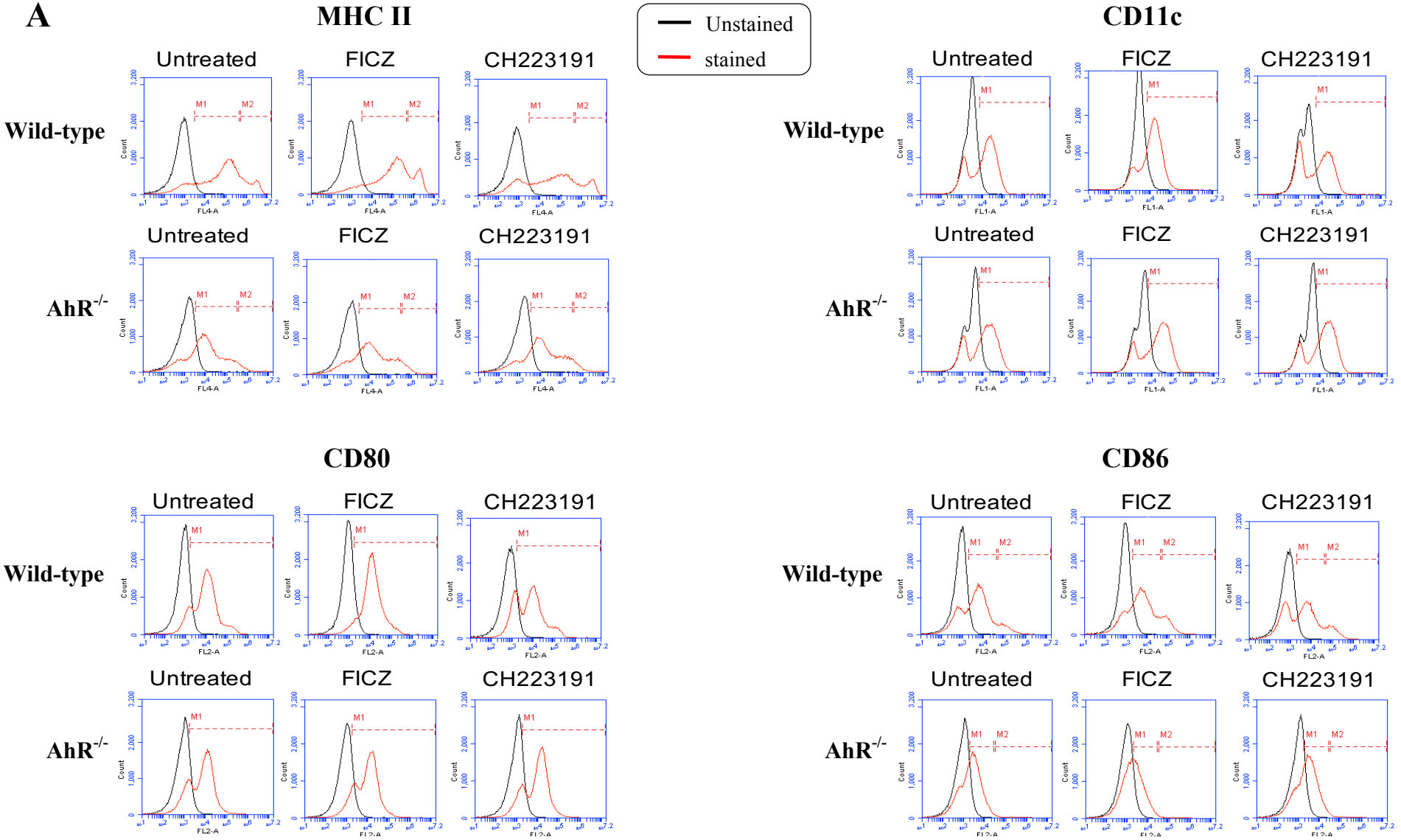

Figure 5.6 continued overleaf

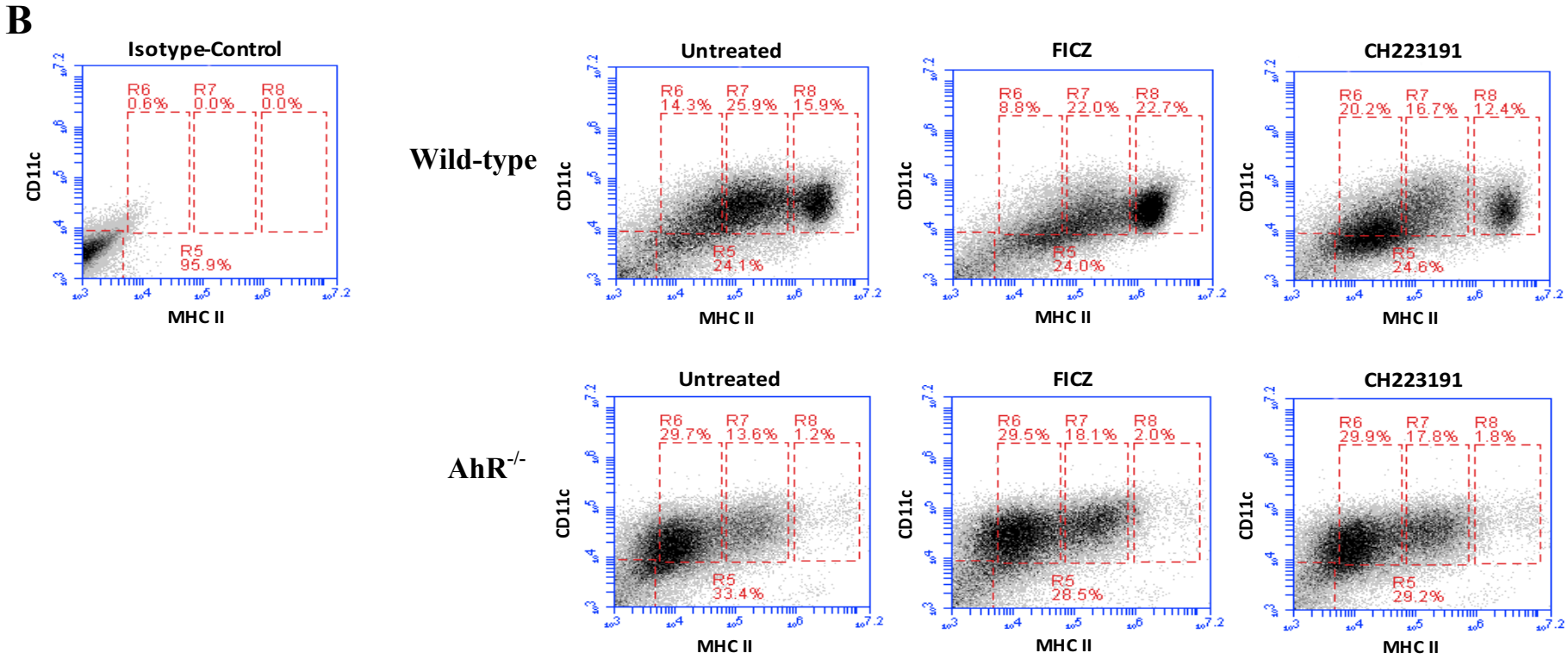

Figure 5.6 Flow Cytometry of Wild-Type and *AhR*$^{-/-}$ BMMC treated with an AhR agonist (FICZ) and AhR antagonist (CH223191).

BMMC from wild-type and *Ahr*$^{-/-}$ mice were differentiated with GM-CSF (untreated) or in combination with either 500 nM FICZ or 3 µM CH223191 (CH). The BMMC were analysed by flow cytometry for the expression of the surface markers MHC class II, CD11c, CD80 and CD86 (**A**). M1 and M2 gates show the proportions of positive cells. The different BMMC were gated on CD11c and MHC class II expression for differentiation into cells of immature (R6), moderate (R7) and high (R8) maturation status (**B**). The data are representative of two independent experiments.

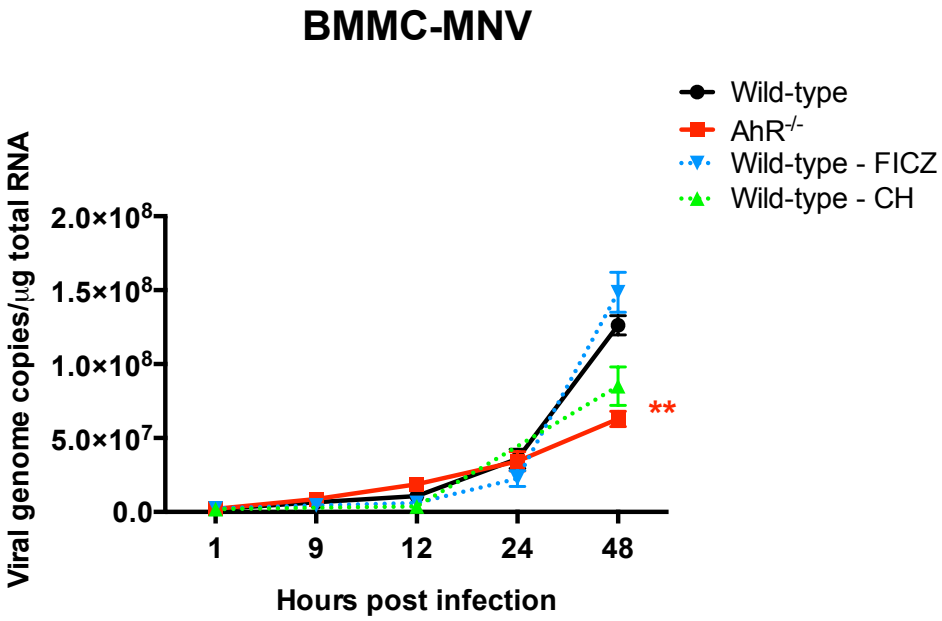

Figure 5.7 MNV-O7 replication in BMMC Derived from Wild-Type and *Ahr*$^{-/-}$ mice and treated with an AhR-agonist (FICZ) and AhR-antagonist (CH223191).

BMMC generated from wild-type and *Ahr*$^{-/-}$ mice were differentiated as in **Figure 5.6**. The BMMC were infected with MNV-O7 at a MOI of 0.05. After 1 hrs incubation with the virus, the cells were washed then incubated at 37 ° C. At specific post-infection times (1, 9, 12, 24 and 48 hrs), RNA was extracted from the cultured cells and viral titres (vRNA copy numbers) were measured by RT-qPCR. vRNA copy number was expressed as the number of molecules per µg of total RNA in the sample well. Data points represent the mean vRNA level from triplicate wells, with error bars showing the range for each triplicate. Statistical significance was calculated by 2-way ANOVA. (**; $P<0.01$).

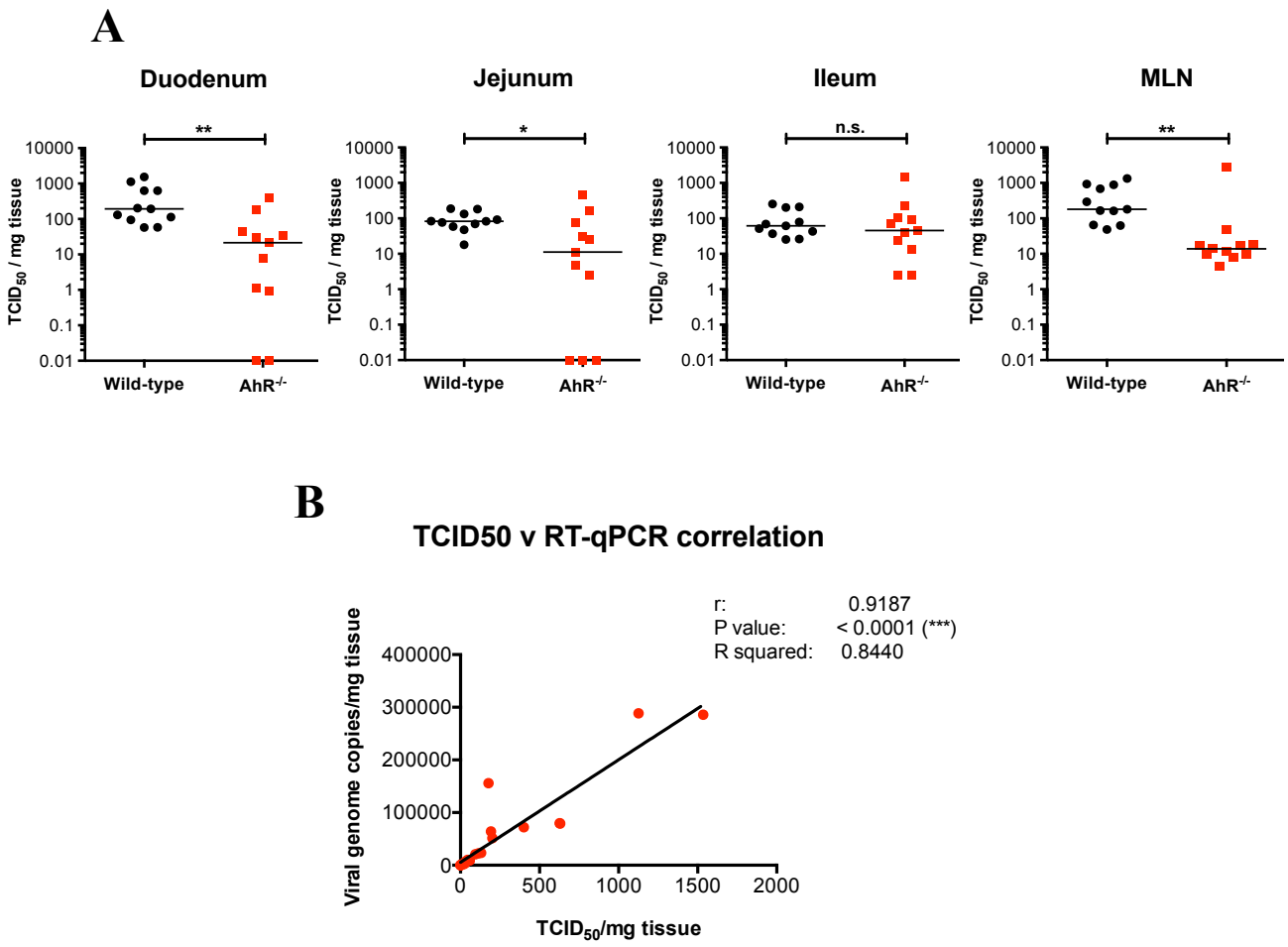

Supplementary Figure 5.1 MNV-O7 viral titres measured by $TCID_{50}$ assay and correlation with those measured by RT-qPCR assay.

Wild type (C57BL/6) and *Ahr*$^{-/-}$ mice were infected orally with MNV-O7 (5 x 10^6 $TCID_{50}$). (**A**) 40 hrs P.I. the mice were sacrificed and gut sections (duodenum, jejunum, and ileum) were collected. Infectious viral titres were measured by a limiting dilution 50 % Tissue Culture Infectious Dose ($TCID_{50}$) assay as detailed in **Section 2.5**. The titres were normalised to the weight of the tissue sections (in mg). Each point represents an individual mouse. The line in each dataset represents the median viral titre. The data shown were pooled from two independent biological repeats. (**B**) The correlation between MNV-O7 viral titres measured by $TCID_{50}$ (plotted in the x-axis) and RT-qPCR (plotted in the y-axis). Statistical significance was calculated by Mann-Whitney test (**A**) and regression analysis (**B**). (n.s.; non-significant, *; P<0.05, **; P<0.01).

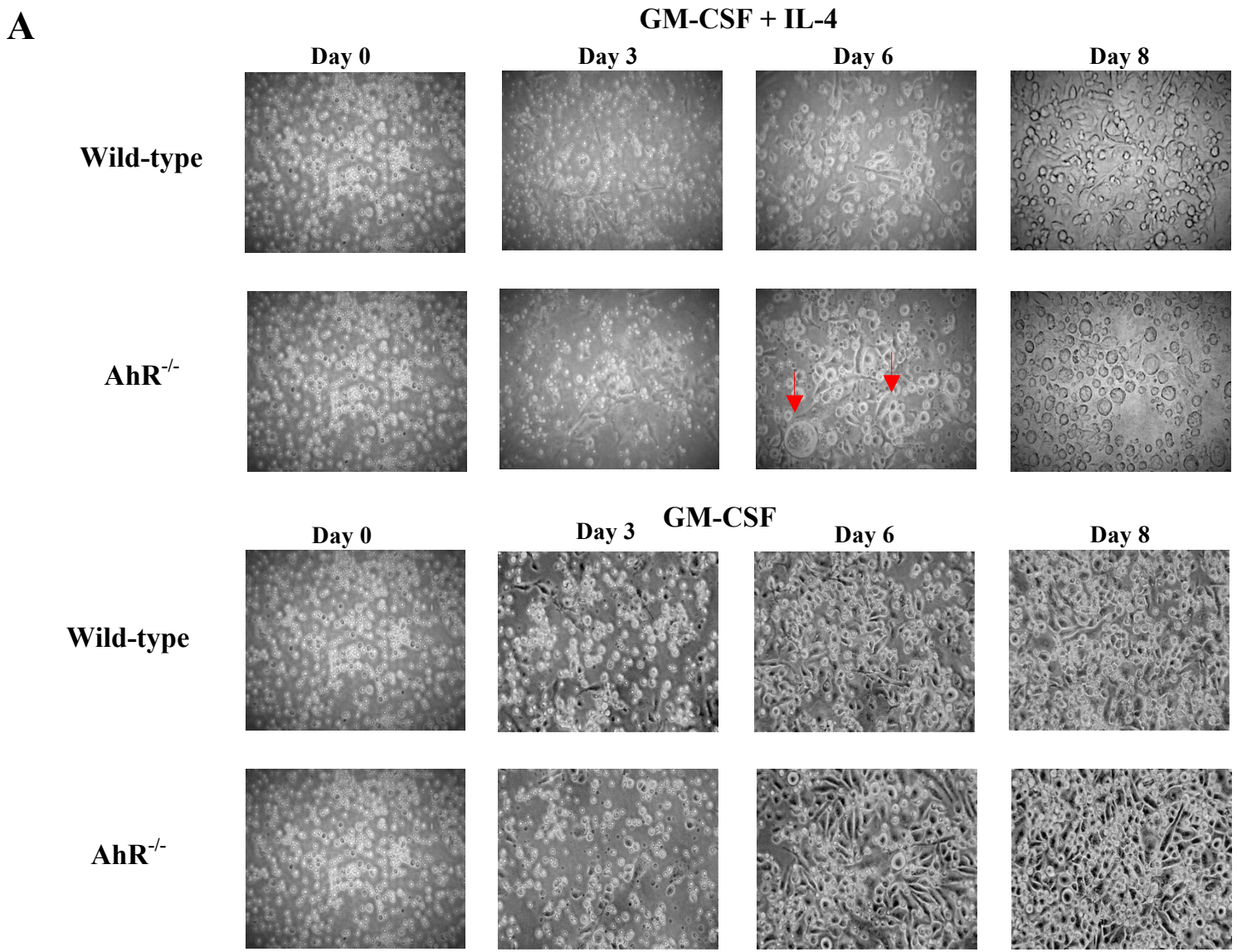

Supplementary Figure 5.2 continued overleaf

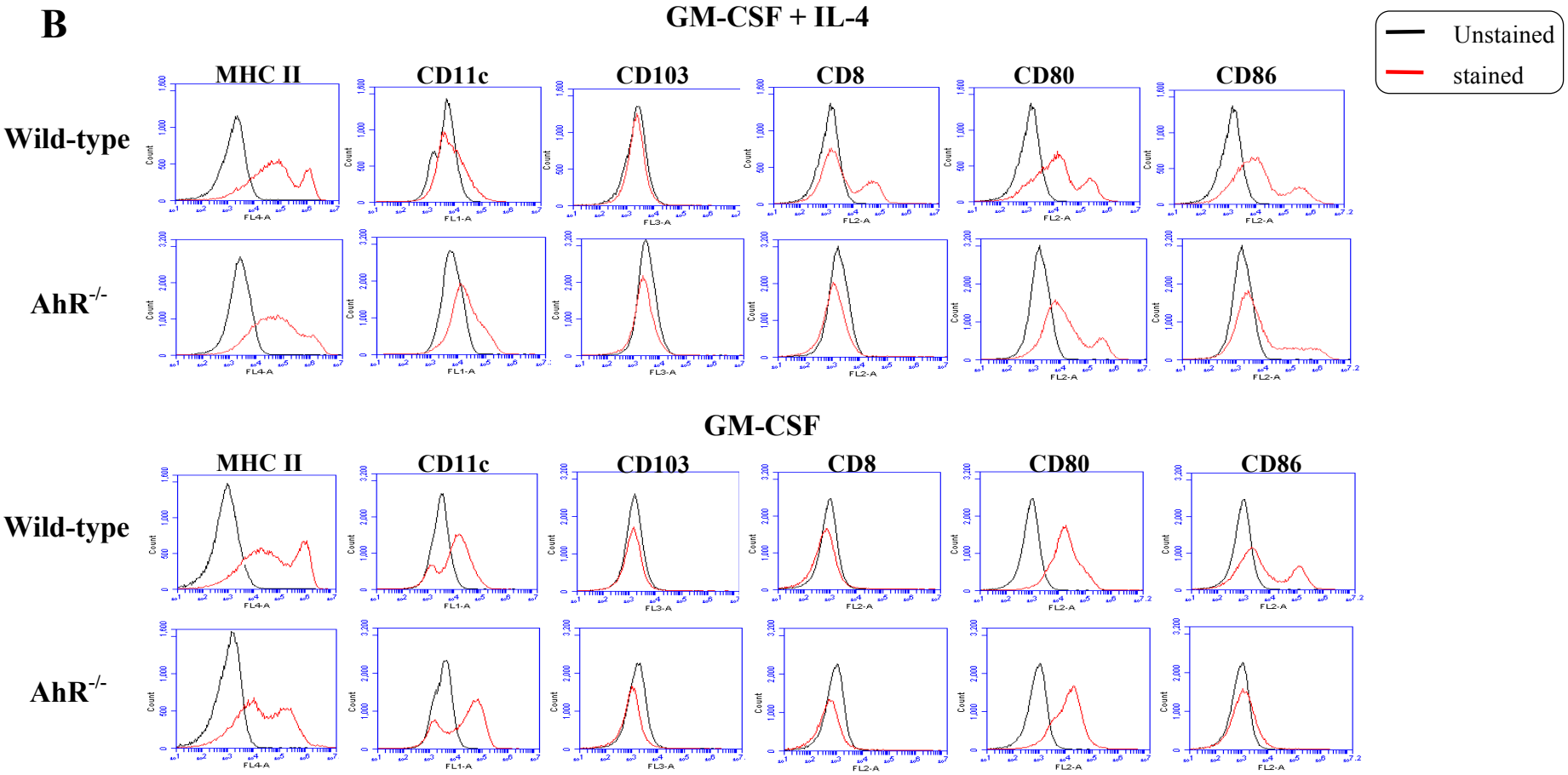

Supplementary Figure 5.2 Microscopic and Flow Cytometric Comparison of BMMC differentiated by GM-CSF + IL-4 Vs GM-CSF alone. BM cells extracted from the long bones of wild-type and *Ahr*$^{-/-}$ mice were differentiated for 8 days in medium containing either a combination of GM-CSF and IL-4 or GM-CSF alone. The BMMC were examined by microscopy with images taken on day 0, day 3, day 6 and day 8 post-addition of the differentiation medium (**A**). The phase contrast images shown were taken at 20x magnification. The red arrows point to the vacuolization. On day 8 of differentiation, the cells were also analysed by flow cytometry for the expression of the surface markers MHC class II, CD11c, CD103, CD8α, CD80 and CD86 (**B**).

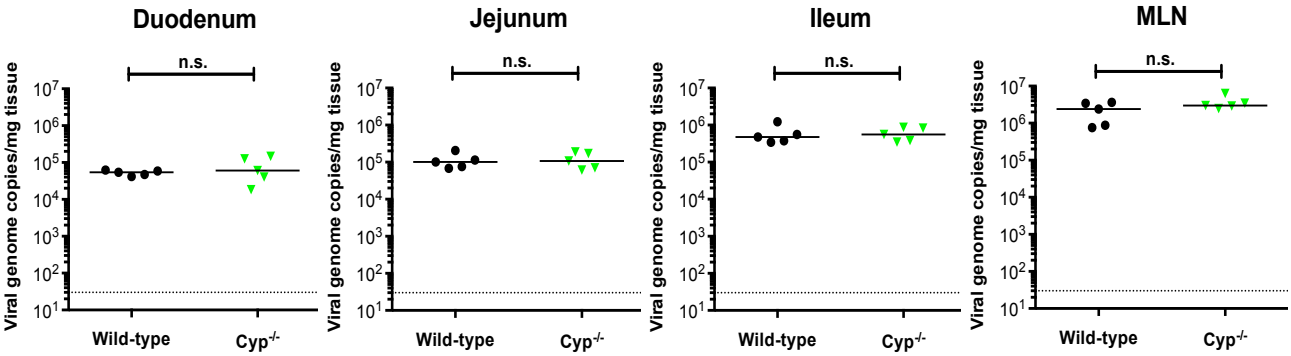

Supplementary Figure 5.3 MNV-O7 infection of Wild-Type and *Cyp*$^{-/-}$ mice.

Wild-type (C57BL/6) and *Cyp*$^{-/-}$ mice were infected orally with MNV-O7 (5 x 10^6 $TCID_{50}$). 40 hrs after infection, the mice were sacrificed and gut sections (duodenum, jejunum, and ileum) were collected. RNA was extracted from the tissues and viral titres (viral RNA copy numbers) were measured by RT-qPCR. The titres were normalised to the weight of the tissue sections. The dotted line indicates the limit of detection (30 viral genome copies per mg tissues). Each point represents an individual mouse. The line in each dataset represents the median viral titre. Statistical significance was calculated by Mann-Whitney test. (n.s.; non-significant)

Acknowledgement

I would like to express my sincere gratitude to my supervisors; Prof. Jonathan Heeney, Dr. Marc Veldhoen and Dr. Barbara Blaclaws for all their invaluable intellectual input into this project and during writing of the thesis, as well as for being supportive and understanding. This work would not have been possible without the great help of Dr. James Chattle, who spent many hours training me with the lab techniques and designed and optimized many of the techniques used in this report. I would also like to thank Mr. Paul Tonks for his help with many of the animal experiments. I also wish to thank the staff in the Pathology animal unit, especially Ms. Lisa Wright and Mr. Danial Gates, for providing me with great technical support. Special thank you to Marisa Stebegg, Ulrika Frising (The Babraham Institute, Cambridge) and Dr Matthias Zilbauer, Ms Komal Nayak (Addenbrooke's Hospital, Cambridge) for the great productive collaborative work. Members of Professor Heeney's laboratory, especially Arden DV, Samuel Stubbs, James Lester, Chinedu Ugwu, Mukarram Hossain, David Seilly, Ian Mickleburgh and Constanza Toro Valdivieso have been a great source of support, both in and out of work. I am very grateful to the Islamic Development Bank and the Cambridge International Trust for making this great opportunity possible for me.

My wife, Muna Ibrahim, and my daughters, Ala and Aya thank you very much for your patience, support and encouragement.

REFERENCES

1. Mestecky J, Lamm ME, StroberW, Bienenstock J, McGhee JR, M. L. . *Mucosal Immunology. 3rd ed.* (London: Elsevier Academic Press, 2005).

2. Turner, J. R. Intestinal mucosal barrier function in health and disease. *Nat. Rev. Immunol.* **9,** 799–809 (2009).

3. Ley, R. E., Peterson, D. A. & Gordon, J. I. Ecological and evolutionary forces shaping microbial diversity in the human intestine. *Cell* **124,** 837–48 (2006).

4. Neish, A. S. Microbes in gastrointestinal health and disease. *Gastroenterology* **136,** 65–80 (2009).

5. Eckmann, L. & Kagnoff, M. F. Intestinal mucosal responses to microbial infection. *Springer Semin. Immunopathol.* **27,** 181–96 (2005).

6. Cho, H. & Kelsall, B. L. The role of type I interferons in intestinal infection, homeostasis, and inflammation. *Immunol. Rev.* **260,** 145–67 (2014).

7. Powell, N., Walker, M. M. & Talley, N. J. The mucosal immune system: master regulator of bidirectional gut–brain communications. *Nat. Rev. Gastroenterol. Hepatol.* **14,** 143–159 (2017).

8. Russo, R. *et al.* Gut-brain axis: Role of lipids in the regulation of inflammation, pain and CNS diseases. *Curr. Med. Chem.* **24,** 1–1 (2017).

9. Gribble, F. M. & Reimann, F. Signalling in the gut endocrine axis. *Physiol. Behav.* (2017). doi:10.1016/j.physbeh.2017.02.039

10. Brown, J. M. & Hazen, S. L. The Gut Microbial Endocrine Organ: Bacterially Derived Signals Driving Cardiometabolic Diseases. *Annu. Rev. Med.* **66,** 343–359 (2015).

11. Mowat, A. M. & Agace, W. W. Regional specialization within the intestinal immune system. *Nat. Rev. Immunol.* **14,** 667–685 (2014).

12. Schumann, M., Siegmund, B., Schulzke, J. D. & Fromm, M. Celiac Disease: Role of the Epithelial Barrier. *C. Cell. Mol. Gastroenterol. Hepatol.* **3,** 150–162 (2017).

13. Vavricka, S. R. & Rogler, G. Intestinal Absorption and Vitamin Levels: Is a New Focus Needed? *Dig. Dis.* **30,** 73–80 (2012).

14. Carter, P. B. & Collins, F. M. The route of enteric infection in normal mice. *J. Exp. Med.* **139,** 1189–203 (1974).

15. Tilney, N. L. Patterns of lymphatic drainage in the adult laboratory rat. *J. Anat.* **109,** 369–83 (1971).

16. Cornes, J. S. Number, size, and distribution of Peyer's patches in the human small intestine: Part I The development of Peyer's patches. *Gut* **6,** 225–9 (1965).

17. Camerini, V., Panwala, C. & Kronenberg, M. Regional specialization of the mucosal immune system. Intraepithelial lymphocytes of the large intestine have a different phenotype and function than those of the small intestine. *J. Immunol.* **151,** 1765–76 (1993).

18. Denning, T. L. *et al.* Functional specializations of intestinal dendritic cell and macrophage subsets that control Th17 and regulatory T cell responses are dependent on the T cell/APC ratio, source of mouse strain, and regional localization. *J. Immunol.* **187,** 733–47 (2011).

19. Lin, M., Du, L., Brandtzaeg, P. & Pan-Hammarström, Q. IgA subclass switch recombination in human mucosal and systemic immune compartments. *Mucosal Immunol.* **7,** 511–20 (2014).

20. Rescigno, M. The intestinal epithelial barrier in the control of homeostasis and immunity. *Trends Immunol.* **32,** 256–64 (2011).

21. Karam, S. M. Lineage commitment and maturation of epithelial cells in the gut. *Front. Biosci.* **4,** D286-98 (1999).

22. Johansson, M. E. V *et al.* The inner of the two Muc2 mucin-dependent mucus layers in colon is devoid of bacteria. *Proc. Natl. Acad. Sci. U. S. A.* **105,** 15064–9 (2008).

23. Hansson, G. C. Role of mucus layers in gut infection and inflammation. *Curr. Opin. Microbiol.* **15,** 57–62 (2012).

24. Clevers, H. C. & Bevins, C. L. Paneth cells: maestros of the small intestinal crypts. *Annu. Rev. Physiol.* **75,** 289–311 (2013).

25. VanDussen, K. L. *et al.* Genetic variants synthesize to produce paneth cell phenotypes that define subtypes of Crohn's disease. *Gastroenterology* **146,** 200–9 (2014).

26. Adolph, T. E. *et al.* Paneth cells as a site of origin for intestinal inflammation. *Nature* **503,** 272–6 (2013).

27. Mankertz, J. & Schulzke, J.-D. Altered permeability in inflammatory bowel disease: pathophysiology and clinical implications. *Curr. Opin. Gastroenterol.* **23,** 379–83 (2007).

28. Brenchley, J. M. *et al.* Microbial translocation is a cause of systemic immune activation in chronic HIV infection. *Nat. Med.* **12,** 1365–71 (2006).

29. Sandler, N. G. *et al.* Host Response to Translocated Microbial Products Predicts Outcomes of Patients With HBV or HCV Infection. *Gastroenterology* **141,** 1220–1230.e3 (2011).

30. Kagnoff, M. F. The intestinal epithelium is an integral component of a communications network. *J. Clin. Invest.* **124,** 2841–3 (2014).

31. Bjerknes, M. & Cheng, H. in *Methods in enzymology* **419,** 337–383 (2006).

32. Takeda, N. *et al.* Interconversion between intestinal stem cell populations in distinct niches. *Science* **334,** 1420–4 (2011).

33. Barker, N. *et al.* Identification of stem cells in small intestine and colon by marker gene Lgr5. *Nature* **449,** 1003–7 (2007).

34. van der Flier, L. G. & Clevers, H. Stem Cells, Self-Renewal, and Differentiation in the Intestinal Epithelium. *Annu. Rev. Physiol.* **71,** 241–260 (2009).

35. Sato, T. *et al.* Single Lgr5 stem cells build crypt–villus structures in vitro without a mesenchymal niche. *Nature* **459,** 262–265 (2009).

36. Haramis, A.-P. G. *et al.* De novo crypt formation and juvenile polyposis on BMP inhibition in mouse intestine. *Science* **303,** 1684–6 (2004).

37. Sato, T. & Clevers, H. Primary mouse small intestinal epithelial cell cultures. *Methods Mol. Biol.* **945,** 319–28 (2013).

38. Sato, T. & Clevers, H. Growing self-organizing mini-guts from a single intestinal stem cell: mechanism and applications. *Science* **340,** 1190–4 (2013).

39. Kurashima, Y. & Kiyono, H. Mucosal Ecological Network of Epithelium and Immune Cells for Gut Homeostasis and Tissue Healing. 119–147 (2016). doi:10.1146/annurev-immunol-051116-052424

40. Bäckhed, F., Ley, R. E., Sonnenburg, J. L., Peterson, D. A. & Gordon, J. I. Host-bacterial mutualism in the human intestine. *Science* **307,** 1915–20 (2005).

41. Moens, E. & Veldhoen, M. Epithelial barrier biology: Good fences make good neighbours. *Immunology* **135,** 1–8 (2012).

42. Ley, R. E. *et al.* Evolution of mammals and their gut microbes. *Science* **320,** 1647–51 (2008).

43. Qin, J. *et al.* A human gut microbial gene catalogue established by metagenomic sequencing. *Nature* **464,** 59–65 (2010).

44. Dethlefsen, L., McFall-Ngai, M. & Relman, D. A. An ecological and evolutionary perspective on human-microbe mutualism and disease. *Nature* **449,** 811–8 (2007).

45. Lozupone, C. A., Stombaugh, J. I., Gordon, J. I., Jansson, J. K. & Knight, R. Diversity, stability and resilience of the human gut microbiota. *Nature* **489,** 220–230 (2012).

46. Columpsi, P. *et al.* Beyond the gut bacterial microbiota: The gut virome. *J. Med. Virol.* **88,** 1467–1472 (2016).

47. Sonnenburg, J. L. & Bäckhed, F. Diet–microbiota interactions as moderators of human metabolism. *Nature* **535,** 56–64 (2016).

48. Modi, S. R., Collins, J. J. & Relman, D. A. Antibiotics and the gut microbiota. *J. Clin. Invest.* **124,** 4212–4218 (2014).

49. Ahmed, S. *et al.* Mucosa-associated bacterial diversity in relation to human terminal ileum and colonic biopsy samples. *Appl. Environ. Microbiol.* **73,** 7435–42 (2007).

50. Hu, S. *et al.* Regional differences in colonic mucosa-associated microbiota determine the physiological expression of host heat shock proteins. *Am. J. Physiol. Gastrointest. Liver Physiol.* **299,** G1266-75 (2010).

51. Bongers, G. *et al.* Interplay of host microbiota, genetic perturbations, and inflammation promotes local development of intestinal neoplasms in mice. *J. Exp. Med.* **211,** 457–72 (2014).

52. Blumberg, R. & Powrie, F. Microbiota, disease, and back to health: a metastable journey. *Sci. Transl. Med.* **4,** 137rv7 (2012).

53. Cho, I. & Blaser, M. J. The human microbiome: at the interface of health and disease. *Nat. Rev. Genet.* **13,** 260 (2012).

54. Hooper, L. V & Gordon, J. I. Commensal host-bacterial relationships in the gut. *Science* **292,** 1115–8 (2001).

55. Round, J. L. & Mazmanian, S. K. The gut microbiota shapes intestinal immune responses during health and disease. *Nat. Rev. Immunol.* **9,** 313–323 (2009).

56. Talham, G. L., Jiang, H. Q., Bos, N. A. & Cebra, J. J. Segmented filamentous bacteria are potent stimuli of a physiologically normal state of the murine gut mucosal immune system. *Infect. Immun.* **67,** 1992–2000 (1999).

57. Ivanov, I. I. *et al.* Induction of intestinal Th17 cells by segmented filamentous bacteria. *Cell* **139,** 485–98 (2009).

58. Atarashi, K. *et al.* Treg induction by a rationally selected mixture of Clostridia strains from the human microbiota. *Nature* **500,** 232–6 (2013).

59. Furusawa, Y. *et al.* Commensal microbe-derived butyrate induces the differentiation of colonic regulatory T cells. *Nature* **504,** 446–50 (2013).

60. Kernbauer, E., Ding, Y. & Cadwell, K. An enteric virus can replace the beneficial function of commensal bacteria. *Nature* **516,** 94–8 (2014).

61. Virgin, H. W. The virome in mammalian physiology and disease. *Cell* **157,** 142–50 (2014).

62. Cadwell, K. *et al.* Virus-plus-susceptibility gene interaction determines Crohn's disease gene Atg16L1 phenotypes in intestine. *Cell* **141,** 1135–45 (2010).

63. Randall, T. D. & Mebius, R. E. The development and function of mucosal lymphoid tissues: a balancing act with micro-organisms. *Mucosal Immunol.* **7,** 455–66 (2014).

64. Mabbott, N. A., Donaldson, D. S., Ohno, H., Williams, I. R. & Mahajan, A. Microfold (M) cells: important immunosurveillance posts in the intestinal epithelium. *Mucosal Immunol.* **6,** 666–77 (2013).

65. Masahata, K. *et al.* Generation of colonic IgA-secreting cells in the caecal patch. *Nat. Commun.* **5,** (2014).

66. McDole, J. R. *et al.* Goblet cells deliver luminal antigen to CD103+ dendritic cells in the small intestine. *Nature* **483,** 345–9 (2012).

67. Chieppa, M., Rescigno, M., Huang, A. Y. C. & Germain, R. N. Dynamic imaging of dendritic cell extension into the small bowel lumen in response to epithelial cell TLR engagement. *J. Exp. Med.* **203,** 2841–52 (2006).

68. Bekiaris, V., Persson, E. K. & Agace, W. W. Intestinal dendritic cells in the regulation of mucosal immunity. *Immunol. Rev.* **260,** 86–101 (2014).

69. Bilsborough, J. & Viney, J. L. Gastrointestinal dendritic cells play a role in immunity, tolerance, and disease. *Gastroenterology* **127,** 300–9 (2004).

70. Rescigno, M. Dendritic cell-epithelial cell crosstalk in the gut. *Immunol. Rev.* **260,** 118–128 (2014).

71. Coombes, J. L. *et al.* A functionally specialized population of mucosal CD103+ DCs induces Foxp3+ regulatory T cells via a TGF-beta and retinoic acid-dependent mechanism. *J. Exp. Med.* **204,** 1757–64 (2007).

72. Wershil, B. K. & Furuta, G. T. 4. Gastrointestinal mucosal immunity. *J. Allergy Clin. Immunol.* **121,** S380–3; quiz S415 (2008).

73. Salmi, M. & Jalkanen, S. Molecules controlling lymphocyte migration to the gut. *Gut* **45,** 148–53 (1999).

74. Brandtzaeg, P. The gut as communicator between environment and host: immunological consequences. *Eur. J. Pharmacol.* **668 Suppl,** S16-32 (2011).

75. Brucklacher-Waldert, V., Carr, E. J., Linterman, M. A. & Veldhoen, M. Cellular Plasticity of CD4+ T Cells in the Intestine. *Front. Immunol.* **5,** 488 (2014).

76. Schulz, O. *et al.* Intestinal CD103+, but not CX3CR1+, antigen sampling cells migrate in lymph and serve classical dendritic cell functions. *J. Exp. Med.* **206,** 3101–14 (2009).

77. Kayama, H. *et al.* Intestinal CX3C chemokine receptor 1(high) (CX3CR1(high)) myeloid cells prevent T-cell-dependent colitis. *Proc. Natl. Acad. Sci. U. S. A.* **109,** 5010–5 (2012).

78. Cherrier, M., Ohnmacht, C., Cording, S. & Eberl, G. Development and function of intestinal innate lymphoid cells. *Curr. Opin. Immunol.* **24,** 277–83 (2012).

79. Spits, H. *et al.* Innate lymphoid cells--a proposal for uniform nomenclature. *Nat. Rev. Immunol.* **13,** 145–9 (2013).

80. Walker, J. A., Barlow, J. L. & McKenzie, A. N. J. Innate lymphoid cells--how did we miss them? *Nat. Rev. Immunol.* **13,** 75–87 (2013).

81. Johansen, F.-E. & Kaetzel, C. S. Regulation of the polymeric immunoglobulin receptor and IgA transport: new advances in environmental factors that stimulate pIgR expression and its role in mucosal immunity. *Mucosal Immunol.* **4,** 598–602 (2011).

82. Shulzhenko, N. *et al.* Crosstalk between B lymphocytes, microbiota and the intestinal epithelium governs immunity versus metabolism in the gut. *Nat. Med.* **17,** 1585–93 (2011).

83. Peterson, L. W. & Artis, D. Intestinal epithelial cells: regulators of barrier function and immune homeostasis. *Nat. Rev. Immunol.* **14,** 141–153 (2014).

84. Zeuthen, L. H., Fink, L. N. & Frokiaer, H. Epithelial cells prime the immune response to an array of gut-derived commensals towards a tolerogenic phenotype through distinct actions of thymic stromal lymphopoietin and transforming growth factor-beta. *Immunology* **123,** 197–208 (2008).

85. Artis, D. Epithelial-cell recognition of commensal bacteria and maintenance of immune homeostasis in the gut. *Nat. Rev. Immunol.* **8,** 411–20 (2008).

86. Chen, Y., Chou, K., Fuchs, E., Havran, W. L. & Boismenu, R. Protection of the intestinal mucosa by intraepithelial gamma delta T cells. *Proc. Natl. Acad. Sci. U. S. A.* **99,** 14338–43 (2002).

87. Okazawa, A. *et al.* Human intestinal epithelial cell-derived interleukin (IL)-18, along with IL-2, IL-7 and IL-15, is a potent synergistic factor for the proliferation of intraepithelial lymphocytes. *Clin. Exp. Immunol.* **136,** 269–76 (2004).

88. He, B. *et al.* Intestinal bacteria trigger T cell-independent immunoglobulin A(2) class switching by inducing epithelial-cell secretion of the cytokine APRIL. *Immunity* **26,** 812–26 (2007).

89. Matzinger, P. The Danger Model: A Renewed Sense of Self. *Science (80-.).* **296,** 301–305 (2002).

90. Fitch, P. M., Henderson, P. & Schwarze, J. Respiratory and gastrointestinal epithelial modulation of the immune response during viral infection. *Innate Immun.* **18,** 179–189 (2012).

91. Black, R. E. *et al.* Global, regional, and national causes of child mortality in 2008: a systematic analysis. *Lancet* **375,** 1969–87 (2010).

92. Enserink, R. *et al.* High detection rates of enteropathogens in asymptomatic children attending day care. *PLoS One* **9,** e89496 (2014).

93. Phillips, G., Tam, C. C., Rodrigues, L. C. & Lopman, B. Prevalence and characteristics of asymptomatic norovirus infection in the community in England. *Epidemiol. Infect.* **138,** 1454–8 (2010).

94. Liévin-Le Moal, V. & Servin, A. L. The front line of enteric host defense against unwelcome intrusion of harmful microorganisms: mucins, antimicrobial peptides, and microbiota. *Clin. Microbiol. Rev.* **19,** 315–37 (2006).

95. Snoeck, V., Goddeeris, B. & Cox, E. The role of enterocytes in the intestinal barrier function and antigen uptake. *Microbes Infect.* **7,** 997–1004 (2005).

96. Chen, C. C., Baylor, M. & Bass, D. M. Murine intestinal mucins inhibit rotavirus infection. *Gastroenterology* **105,** 84–92 (1993).

97. Blutt, S. E. & Conner, M. E. The Gastrointestinal Frontier: IgA and Viruses. *Front. Immunol.* **4,** 402 (2013).

98. Guaní-Guerra, E., Santos-Mendoza, T., Lugo-Reyes, S. O. & Terán, L. M. Antimicrobial peptides: general overview and clinical implications in human health and disease. *Clin. Immunol.* **135,** 1–11 (2010).

99. Swiecki, M. & Colonna, M. Type I interferons: diversity of sources, production pathways and effects on immune responses. *Curr. Opin. Virol.* **1,** 463–75 (2011).

100. Siegal, F. P. *et al.* The nature of the principal type 1 interferon-producing cells in human blood. *Science* **284,** 1835–7 (1999).

101. Takeuchi, O. & Akira, S. Pattern recognition receptors and inflammation. *Cell* **140,** 805–20 (2010).

102. Jensen, S. & Thomsen, A. R. Sensing of RNA viruses: a review of innate immune receptors involved in recognizing RNA virus invasion. *J. Virol.* **86,** 2900–10 (2012).

103. Wilkins, C. & Gale, M. Recognition of viruses by cytoplasmic sensors. *Curr. Opin. Immunol.* **22,** 41–7 (2010).

104. Sabbah, A. *et al.* Activation of innate immune antiviral responses by Nod2. *Nat. Immunol.* **10,** 1073–80 (2009).

105. Xu, J., Yang, Y., Wang, C. & Jiang, B. Rotavirus and coxsackievirus infection activated different profiles of toll-like receptors and chemokines in intestinal epithelial cells. *Inflamm. Res.* **58,** 585–92 (2009).

106. Honda, K. *et al.* IRF-7 is the master regulator of type-I interferon-dependent immune responses. *Nature* **434,** 772–7 (2005).

107. Osterlund, P. I., Pietilä, T. E., Veckman, V., Kotenko, S. V & Julkunen, I. IFN regulatory factor family members differentially regulate the expression of type III IFN (IFN-lambda) genes. *J. Immunol.* **179,** 3434–42 (2007).

108. Hertzog, P. J. & Williams, B. R. G. Fine tuning type I interferon responses. *Cytokine Growth Factor Rev.* **24,** 217–25 (2013).

109. Young, H. A. & Bream, J. H. IFN-gamma: recent advances in understanding regulation of expression, biological functions, and clinical applications. *Curr. Top. Microbiol. Immunol.* **316,** 97–117 (2007).

110. Kotenko, S. V. IFN-λs. *Curr. Opin. Immunol.* **23,** 583–90 (2011).

111. Hermant, P. & Michiels, T. Interferon-λ in the context of viral infections: production, response and therapeutic implications. *J. Innate Immun.* **6,** 563–74 (2014).

112. Pott, J. *et al.* IFN-lambda determines the intestinal epithelial antiviral host defense. *Proc. Natl. Acad. Sci. U. S. A.* **108,** 7944–9 (2011).

113. Schneider, W. M., Chevillotte, M. D. & Rice, C. M. Interferon-stimulated genes: a complex web of host defenses. *Annu. Rev. Immunol.* **32,** 513–45 (2014).

114. Malireddi, R. K. S. & Kanneganti, T.-D. Role of type I interferons in inflammasome activation, cell death, and disease during microbial infection. *Front. Cell. Infect. Microbiol.* **3,** 77 (2013).

115. Green, D. R., Ferguson, T., Zitvogel, L. & Kroemer, G. Immunogenic and tolerogenic cell death. *Nat. Rev. Immunol.* **9,** 353–63 (2009).

116. Fleeton, M. N. *et al.* Peyer's patch dendritic cells process viral antigen from apoptotic epithelial cells in the intestine of reovirus-infected mice. *J. Exp. Med.* **200,** 235–45 (2004).

117. Longhi, M. P. *et al.* Dendritic cells require a systemic type I interferon response to mature and induce CD4+ Th1 immunity with poly IC as adjuvant. *J. Exp. Med.* **206,** 1589–1602 (2009).

118. Pothlichet, J., Chignard, M. & Si-Tahar, M. Cutting edge: innate immune response triggered by influenza A virus is negatively regulated by SOCS1 and SOCS3 through a RIG-I/IFNAR1-dependent pathway. *J. Immunol.* **180,** 2034–8 (2008).

119. Swiecki, M. *et al.* Type I interferon negatively controls plasmacytoid dendritic cell numbers in vivo. *J. Exp. Med.* **208,** 2367–74 (2011).

120. Fitzgerald, D. C. *et al.* Independent and interdependent immunoregulatory effects of IL-27, IFN-β, and IL-10 in the suppression of human Th17 cells and murine experimental autoimmune encephalomyelitis. *J. Immunol.* **190,** 3225–34 (2013).

121. Dalod, M. *et al.* Interferon alpha/beta and interleukin 12 responses to viral infections: pathways regulating dendritic cell cytokine expression in vivo. *J. Exp. Med.* **195,** 517–28 (2002).

122. Hernández, P. P. *et al.* Interferon-λ and interleukin 22 act synergistically for the induction of interferon-stimulated genes and control of rotavirus infection. *Nat. Immunol.* **16,** 698–707 (2015).

123. Lienenklaus, S. *et al.* Novel reporter mouse reveals constitutive and inflammatory expression of IFN-beta in vivo. *J. Immunol.* **183,** 3229–36 (2009).

124. Reyes, A. *et al.* Viruses in the faecal microbiota of monozygotic twins and their mothers. *Nature* **466,** 334–8 (2010).

125. Minot, S. *et al.* The human gut virome: inter-individual variation and dynamic response to diet. *Genome Res.* **21,** 1616–25 (2011).

126. Tschurtschenthaler, M. *et al.* Type I interferon signalling in the intestinal epithelium affects Paneth cells, microbial ecology and epithelial regeneration. *Gut* **63,** 1921–31 (2014).

127. Basic, M. *et al.* Norovirus triggered microbiota-driven mucosal inflammation in interleukin 10-deficient mice. *Inflamm. Bowel Dis.* **20,** 431–43 (2014).

128. Hayday, A., Theodoridis, E., Ramsburg, E. & Shires, J. Intraepithelial lymphocytes: exploring the Third Way in immunology. *Nat. Immunol.* **2,** 997–1003 (2001).

129. Cheroutre, H., Lambolez, F. & Mucida, D. The light and dark sides of intestinal intraepithelial lymphocytes. *Nat. Rev. Immunol.* **11,** 445–56 (2011).

130. Abreu, M. T. Toll-like receptor signalling in the intestinal epithelium: how bacterial recognition shapes intestinal function. *Nat. Rev. Immunol.* **10,** 131–144 (2010).

131. Cheroutre, H. Starting at the beginning: new perspectives on the biology of mucosal T cells. *Annu. Rev. Immunol.* **22,** 217–46 (2004).

132. Tamura, A. *et al.* Distribution of two types of lymphocytes (intraepithelial and lamina-propria-associated) in the murine small intestine. *Cell Tissue Res.* **313,** 47–53 (2003).

133. Sugahara, S. *et al.* Extrathymic derivation of gut lymphocytes in parabiotic mice. *Immunology* **96,** 57–65 (1999).

134. Cepek, K. L. *et al.* Adhesion between epithelial cells and T lymphocytes mediated by E-cadherin and the alpha E beta 7 integrin. *Nature* **372,** 190–3 (1994).

135. Mosley, R. L., Styre, D. & Klein, J. R. CD4+CD8+ murine intestinal intraepithelial lymphocytes. *Int. Immunol.* **2,** 361–5 (1990).

136. Itohara, S., Nakanishi, N., Kanagawa, O., Kubo, R. & Tonegawa, S. Monoclonal antibodies specific to native murine T-cell receptor gamma delta: analysis of gamma delta T cells during thymic ontogeny and in peripheral lymphoid organs. *Proc. Natl. Acad. Sci. U. S. A.* **86,** 5094–8 (1989).

137. Leishman, A. J. *et al.* Precursors of functional MHC class I- or class II-restricted CD8alphaalpha(+) T cells are positively selected in the thymus by agonist self-peptides. *Immunity* **16,** 355–64 (2002).

138. Jarry, A., Cerf-Bensussan, N., Brousse, N., Selz, F. & Guy-Grand, D. Subsets of CD3+ (T cell receptor alpha/beta or gamma/delta) and CD3- lymphocytes isolated from normal human gut epithelium display phenotypical features different from their counterparts in peripheral blood. *Eur. J. Immunol.* **20,** 1097–103 (1990).

139. Cheroutre, H. & Lambolez, F. Doubting the TCR coreceptor function of CD8alphaalpha. *Immunity* **28,** 149–59 (2008).

140. Guehler, S. R., Finch, R. J., Bluestone, J. A. & Barrett, T. A. Increased threshold for TCR-mediated signaling controls self reactivity of intraepithelial lymphocytes. *J. Immunol.* **160,** 5341–6 (1998).

141. Shires, J., Theodoridis, E. & Hayday, A. C. Biological insights into TCRgammadelta+ and TCRalphabeta+ intraepithelial lymphocytes provided by serial analysis of gene expression (SAGE). *Immunity* **15,** 419–34 (2001).

142. Yamagata, T., Mathis, D. & Benoist, C. Self-reactivity in thymic double-positive cells commits cells to a CD8 alpha alpha lineage with characteristics of innate immune cells. *Nat. Immunol.* **5,** 597–605 (2004).

143. Guy-Grand, D. *et al.* Two gut intraepithelial CD8+ lymphocyte populations with different T cell receptors: a role for the gut epithelium in T cell differentiation. *J. Exp. Med.* **173,** 471–81 (1991).

144. Regnault, A., Cumano, A., Vassalli, P., Guy-Grand, D. & Kourilsky, P. Oligoclonal repertoire of the CD8 alpha alpha and the CD8 alpha beta TCR-alpha/beta murine intestinal intraepithelial T lymphocytes: evidence for the random emergence of T cells. *J. Exp. Med.* **180,** 1345–58 (1994).

145. Latthe, M., Terry, L. & MacDonald, T. T. High frequency of CD8 alpha alpha homodimer-bearing T cells in human fetal intestine. *Eur. J. Immunol.* **24,** 1703–5 (1994).

146. Rocha, B., Vassalli, P. & Guy-Grand, D. Thymic and extrathymic origins of gut intraepithelial lymphocyte populations in mice. *J. Exp. Med.* **180,** 681–6 (1994).

147. Lambolez, F. *et al.* Characterization of T cell differentiation in the murine gut. *J. Exp. Med.* **195,** 437–49 (2002).

148. Masopust, D., Vezys, V., Wherry, E. J., Barber, D. L. & Ahmed, R. Cutting edge: gut microenvironment promotes differentiation of a unique memory CD8 T cell population. *J. Immunol.* **176,** 2079–83 (2006).

149. Masopust, D., Jiang, J., Shen, H. & Lefrançois, L. Direct analysis of the dynamics of the intestinal mucosa CD8 T cell response to systemic virus infection. *J. Immunol.* **166,** 2348–56 (2001).

150. Groh, V., Steinle, A., Bauer, S. & Spies, T. Recognition of stress-induced MHC molecules by intestinal epithelial gammadelta T cells. *Science* **279,** 1737–40 (1998).

151. Manzano, M., Abadía-Molina, A. C., García-Olivares, E., Gil, A. & Rueda, R. Absolute counts and distribution of lymphocyte subsets in small intestine of BALB/c mice change during weaning. *J. Nutr.* **132,** 2757–62 (2002).

152. Hayday, A. C. Gammadelta T cells and the lymphoid stress-surveillance response. *Immunity* **31,** 184–96 (2009).

153. Yang, H., Madison, B., Gumucio, D. L. & Teitelbaum, D. H. Specific overexpression of IL-7 in the intestinal mucosa: the role in intestinal intraepithelial lymphocyte development. *Am. J. Physiol. Gastrointest. Liver Physiol.* **294,** G1421-30 (2008).

154. Yu, Q. *et al.* MyD88-Dependent Signaling for IL-15 Production Plays an Important Role in Maintenance of CD8 TCR and TCR Intestinal Intraepithelial Lymphocytes. *J. Immunol.* **176,** 6180–6185 (2006).

155. Menezes, J. da S. *et al.* Stimulation by food proteins plays a critical role in the maturation of the immune system. *Int. Immunol.* **15,** 447–55 (2003).

156. Bruce, D. & Cantorna, M. T. Intrinsic requirement for the vitamin D receptor in the development of CD8αα-expressing T cells. *J. Immunol.* **186,** 2819–25 (2011).

157. DeVeale, B., Brummel, T. & Seroude, L. Immunity and aging: the enemy within? *Aging Cell* **3,** 195–208 (2004).

158. Gomez, C. R., Boehmer, E. D. & Kovacs, E. J. The aging innate immune system. *Curr. Opin. Immunol.* **17,** 457–62 (2005).

159. Weng, N.-P. Aging of the immune system: how much can the adaptive immune system adapt? *Immunity* **24,** 495–9 (2006).

160. Gardner, I. D. The effect of aging on susceptibility to infection. *Rev. Infect. Dis.* **2,** 801–10

161. Baylis, D., Bartlett, D. B., Patel, H. P. & Roberts, H. C. Understanding how we age: insights into inflammaging. *Longev. Heal.* **2,** 8 (2013).

162. Koga, T. *et al.* Evidence for early aging in the mucosal immune system. *J. Immunol.* **165,** 5352–9 (2000).

163. Man, A. L., Gicheva, N. & Nicoletti, C. The impact of ageing on the intestinal epithelial barrier and immune system. *Cell. Immunol.* **289,** 112–8 (2014).

164. Kato, H. *et al.* Lack of oral tolerance in aging is due to sequential loss of Peyer's patch cell interactions. *Int. Immunol.* **15,** 145–58 (2003).

165. Thoreux, K., Owen, R. L. & Schmucker, D. L. Intestinal lymphocyte number, migration and antibody secretion in young and old rats. *Immunology* **101,** 161–7 (2000).

166. Claesson, M. J. *et al.* Composition, variability, and temporal stability of the intestinal microbiota of the elderly. *Proc. Natl. Acad. Sci.* **108,** 4586–4591 (2011).

167. Kirkwood, T. B. L. Intrinsic ageing of gut epithelial stem cells. *Mech. Ageing Dev.* **125,** 911–5 (2004).

168. Valenkevich, I. N. & Zhukova, N. M. [The structure of the mucous membrane of the human duodenum with aging]. *Arkh. Patol.* **38,** 58–61 (1976).

169. Ouwehand, A. C., Isolauri, E., Kirjavainen, P. V & Salminen, S. J. Adhesion of four Bifidobacterium strains to human intestinal mucus from subjects in different age groups. *FEMS Microbiol. Lett.* **172,** 61–4 (1999).

170. Kobayashi, A. *et al.* The functional maturation of M cells is dramatically reduced in the Peyer's patches of aged mice. *Mucosal Immunol.* **6,** 1027–37 (2013).

171. Moretto, M. M., Lawlor, E. M. & Khan, I. A. Aging mice exhibit a functional defect in mucosal dendritic cell response against an intracellular pathogen. *J. Immunol.* **181,** 7977–84 (2008).

172. Santiago, A. F. *et al.* Aging correlates with reduction in regulatory-type cytokines and T cells in the gut mucosa. *Immunobiology* **216,** 1085–93 (2011).

173. Tran, L. & Greenwood-Van Meerveld, B. Age-associated remodeling of the intestinal epithelial barrier. *J. Gerontol. A. Biol. Sci. Med. Sci.* **68,** 1045–56 (2013).

174. Guigoz, Y., Doré, J. & Schiffrin, E. J. The inflammatory status of old age can be nurtured from the intestinal environment. *Curr. Opin. Clin. Nutr. Metab. Care* **11,** 13–20 (2008).

175. Shin, J. H., High, K. P. & Warren, C. A. Older Is Not Wiser, Immunologically Speaking: Effect of Aging on Host Response to *Clostridium difficile* Infections. *Journals Gerontol. Ser. A Biol. Sci. Med. Sci.* **71,** 916–922 (2016).

176. Beck, M. A., Handy, J. & Levander, O. A. Host nutritional status: the neglected virulence factor. *Trends Microbiol.* **12,** 417–23 (2004).

177. Veldhoen, M. & Brucklacher-Waldert, V. Dietary influences on intestinal immunity. *Nat. Rev. Immunol.* **12,** 696–708 (2012).

178. Beck, M. A. The role of nutrition in viral disease. *J. Nutr. Biochem.* **7,** 683–690 (1996).

179. Hickman, D. *et al.* The effect of malnutrition on norovirus infection. *MBio* **5,** e01032-13 (2014).

180. Devereux, G. The increase in the prevalence of asthma and allergy: food for thought. *Nat. Rev. Immunol.* **6,** 869–74 (2006).

181. Amre, D. K. *et al.* Imbalances in dietary consumption of fatty acids, vegetables, and fruits are associated with risk for Crohn's disease in children. *Am. J. Gastroenterol.* **102,** 2016–25 (2007).

182. Hotamisligil, G. S. Inflammation and metabolic disorders. *Nature* **444,** 860–7 (2006).

183. Fukuda, S. *et al.* Bifidobacteria can protect from enteropathogenic infection through production of acetate. *Nature* **469,** 543–7 (2011).

184. Maslowski, K. M. & Mackay, C. R. Diet, gut microbiota and immune responses. *Nat. Immunol.* **12,** 5–9 (2011).

185. Glass, C. K. & Ogawa, S. Combinatorial roles of nuclear receptors in inflammation and immunity. *Nat. Rev. Immunol.* **6,** 44–55 (2006).

186. Mora, J. R., Iwata, M. & von Andrian, U. H. Vitamin effects on the immune system: vitamins A and D take centre stage. *Nat. Rev. Immunol.* **8,** 685–98 (2008).

187. Hahn, M. E., Karchner, S. I., Shapiro, M. A. & Perera, S. A. Molecular evolution of two vertebrate aryl hydrocarbon (dioxin) receptors (AHR1 and AHR2) and the PAS family. *Proc. Natl. Acad. Sci. U. S. A.* **94,** 13743–8 (1997).

188. Stockinger, B., Di Meglio, P., Gialitakis, M. & Duarte, J. H. The aryl hydrocarbon receptor: multitasking in the immune system. *Annu. Rev. Immunol.* **32,** 403–32 (2014).

189. Gu, Y. Z., Hogenesch, J. B. & Bradfield, C. A. The PAS superfamily: sensors of environmental and developmental signals. *Annu. Rev. Pharmacol. Toxicol.* **40,** 519–61 (2000).

190. Mulero-Navarro, S. & Fernandez-Salguero, P. M. New Trends in Aryl Hydrocarbon Receptor Biology. *Front. cell Dev. Biol.* **4,** 45 (2016).

191. Shimba, S. & Watabe, Y. Crosstalk between the AHR signaling pathway and circadian rhythm. *Biochem. Pharmacol.* **77,** 560–565 (2009).

192. Hernández-Ochoa, I., Karman, B. N. & Flaws, J. A. The role of the aryl hydrocarbon receptor in the female reproductive system. *Biochem. Pharmacol.* **77,** 547–559 (2009).

193. Hahn, M. E. Aryl hydrocarbon receptors: diversity and evolution. *Chem. Biol. Interact.* **141,** 131–60 (2002).

194. Ma, Q., Baldwin, K. T., Renzelli, A. J., McDaniel, A. & Dong, L. TCDD-Inducible Poly(ADP-ribose) Polymerase: A Novel Response to 2,3,7,8-Tetrachlorodibenzo-p-dioxin. *Biochem. Biophys. Res. Commun.* **289,** 499–506 (2001).

195. Hu, W., Sorrentino, C., Denison, M. S., Kolaja, K. & Fielden, M. R. Induction of cyp1a1 is a nonspecific biomarker of aryl hydrocarbon receptor activation: results of large scale screening of pharmaceuticals and toxicants in vivo and in vitro. *Mol. Pharmacol.* **71,** 1475–86 (2007).

196. Mitchell, K. A. & Elferink, C. J. Timing is everything: consequences of transient and sustained AhR activity. *Biochem. Pharmacol.* **77,** 947–56 (2009).

197. Barouki, R., Coumoul, X. & Fernandez-Salguero, P. M. The aryl hydrocarbon receptor, more than a xenobiotic-interacting protein. *FEBS Lett.* **581,** 3608–15 (2007).

198. Kimura, A. *et al.* Aryl hydrocarbon receptor in combination with Stat1 regulates LPS-induced inflammatory responses. *J. Exp. Med.* **206,** 2027–35 (2009).

199. Kimura, A., Naka, T., Nohara, K., Fujii-Kuriyama, Y. & Kishimoto, T. Aryl hydrocarbon receptor regulates Stat1 activation and participates in the development of Th17 cells. *Proc. Natl. Acad. Sci. U. S. A.* **105,** 9721–6 (2008).

200. Veldhoen, M. *et al.* The aryl hydrocarbon receptor links TH17-cell-mediated autoimmunity to environmental toxins. *Nature* **453,** 106–109 (2008).

201. Quintana, F. J. *et al.* Control of T(reg) and T(H)17 cell differentiation by the aryl hydrocarbon receptor. *Nature* **453,** 65–71 (2008).

202. Gagliani, N. *et al.* Th17 cells transdifferentiate into regulatory T cells during resolution of inflammation. *Nature* **523,** 221–225 (2015).

203. Li, Y. *et al.* Exogenous stimuli maintain intraepithelial lymphocytes via aryl hydrocarbon receptor activation. *Cell* **147,** 629–40 (2011).

204. Qiu, J. *et al.* The aryl hydrocarbon receptor regulates gut immunity through modulation of innate lymphoid cells. *Immunity* **36,** 92–104 (2012).

205. Monteleone, I. *et al.* Aryl hydrocarbon receptor-induced signals up-regulate IL-22 production and inhibit inflammation in the gastrointestinal tract. *Gastroenterology* **141,** 237–48, 248.e1 (2011).

206. Lee, J. S. *et al.* AHR drives the development of gut ILC22 cells and postnatal lymphoid tissues via pathways dependent on and independent of Notch. *Nat. Immunol.* **13,** 144–51 (2012).

207. Qiu, J. *et al.* Group 3 innate lymphoid cells inhibit T-cell-mediated intestinal inflammation through aryl hydrocarbon receptor signaling and regulation of microflora. *Immunity* **39,** 386–99 (2013).

208. Fernandez-Salguero, P. *et al.* Immune system impairment and hepatic fibrosis in mice lacking the dioxin-binding Ah receptor. *Science* **268,** 722–6 (1995).

209. Fernandez-Salguero, P. M., Ward, J. M., Sundberg, J. P. & Gonzalez, F. J. Lesions of aryl-hydrocarbon receptor-deficient mice. *Vet. Pathol.* **34,** 605–14 (1997).

210. Stockinger, B., Hirota, K., Duarte, J. & Veldhoen, M. External influences on the immune system via activation of the aryl hydrocarbon receptor. *Semin. Immunol.* **23,** 99–105 (2011).

211. Esser, C. The immune phenotype of AhR null mouse mutants: Not a simple mirror of xenobiotic receptor over-activation. *Biochem. Pharmacol.* **77,** 597–607 (2009).

212. Frericks, M., Meissner, M. & Esser, C. Microarray analysis of the AHR system: tissue-specific flexibility in signal and target genes. *Toxicol. Appl. Pharmacol.* **220,** 320–32 (2007).

213. Kiss, E. A. *et al.* Natural aryl hydrocarbon receptor ligands control organogenesis of intestinal lymphoid follicles. *Science* **334,** 1561–5 (2011).

214. Di Meglio, P. *et al.* Activation of the aryl hydrocarbon receptor dampens the severity of inflammatory skin conditions. *Immunity* **40,** 989–1001 (2014).

215. Denison, M. S. & Nagy, S. R. Activation of the aryl hydrocarbon receptor by structurally diverse exogenous and endogenous chemicals. *Annu. Rev. Pharmacol. Toxicol.* **43,** 309–34 (2003).

216. Moura-Alves, P. *et al.* AhR sensing of bacterial pigments regulates antibacterial defence. *Nature* **22,** 22–24 (2014).

217. Wincent, E. *et al.* Inhibition of cytochrome P4501-dependent clearance of the endogenous agonist FICZ as a mechanism for activation of the aryl hydrocarbon receptor. *Proc. Natl. Acad. Sci. U. S. A.* **109,** 4479–84 (2012).

218. Rannug, A. *et al.* Certain photooxidized derivatives of tryptophan bind with very high affinity to the Ah receptor and are likely to be endogenous signal substances. *J. Biol. Chem.* **262,** 15422–7 (1987).

219. Esser, C., Rannug, A. & Stockinger, B. The aryl hydrocarbon receptor in immunity. *Trends Immunol.* **30,** 447–454 (2009).

220. Duarte, J. H., Di Meglio, P., Hirota, K., Ahlfors, H. & Stockinger, B. Differential influences of the aryl hydrocarbon receptor on Th17 mediated responses in vitro and in vivo. *PLoS One* **8,** e79819 (2013).

221. Prokipcak, R. D. & Okey, A. B. Downregulation of the Ah receptor in mouse hepatoma cells treated in culture with 2,3,7,8-tetrachlorodibenzo-p-dioxin. *Can. J. Physiol. Pharmacol.* **69,** 1204–10 (1991).

222. Ito, S., Chen, C., Satoh, J., Yim, S. & Gonzalez, F. J. Dietary phytochemicals regulate whole-body CYP1A1 expression through an arylhydrocarbon receptor nuclear translocator-dependent system in gut. *J. Clin. Invest.* **117,** 1940–50 (2007).

223. Shertzer, H. G. & Senft, A. P. The micronutrient indole-3-carbinol: implications for disease and chemoprevention. *Drug Metabol. Drug Interact.* **17,** 159–88 (2000).

224. Glass, R. I., Parashar, U. D. & Estes, M. K. Norovirus gastroenteritis. *N. Engl. J. Med.* **361,** 1776–85 (2009).

225. Kapikian, A. Z. *et al.* Visualization by immune electron microscopy of a 27-nm particle associated with acute infectious nonbacterial gastroenteritis. *J. Virol.* **10,** 1075–81 (1972).

226. Dolin, R. *et al.* Biological properties of Norwalk agent of acute infectious nonbacterial gastroenteritis. *Proc. Soc. Exp. Biol. Med.* **140,** 578–83 (1972).

227. Mesquita, J. R., Barclay, L., Nascimento, M. S. J. & Vinjé, J. Novel norovirus in dogs with diarrhea. *Emerg. Infect. Dis.* **16,** 980–2 (2010).

228. Wolf, S. *et al.* Molecular detection of norovirus in sheep and pigs in New Zealand farms. *Vet. Microbiol.* **133,** 184–9 (2009).

229. Martella, V. *et al.* Detection and Molecular Characterization of a Canine Norovirus. *Emerg. Infect. Dis.* **14,** 1306–1308 (2008).

230. WOODE, G. N. & BRIDGER, J. C. Isolation of Small Viruses Resembling Astroviruses and Caliciviruses from Acute Enteritis Of Calves. *J. Med. Microbiol.* **11,** 441–452 (1978).

231. Karst, S. M., Wobus, C. E., Lay, M., Davidson, J. & Virgin, H. W. STAT1-dependent innate immunity to a Norwalk-like virus. *Science* **299,** 1575–8 (2003).

232. Green, K. Y. *Caliciviridae: The noroviruses*. *Fields Virology* (2013). doi:10.1207/s15327035ex0402

233. Sosnovtsev, S. V. *et al.* Cleavage Map and Proteolytic Processing of the Murine Norovirus Nonstructural Polyprotein in Infected Cells. *J. Virol.* **80,** 7816–7831 (2006).

234. McFadden, N. *et al.* Norovirus regulation of the innate immune response and apoptosis occurs via the product of the alternative open reading frame 4. *PLoS Pathog.* **7,** e1002413 (2011).

235. Thorne, L. G. & Goodfellow, I. G. Norovirus gene expression and replication. *J. Gen. Virol.* **95,** 278–291 (2014).

236. Zheng, D.-P. *et al.* Norovirus classification and proposed strain nomenclature. *Virology* **346,** 312–323 (2006).

237. Nilsson, J., Rydell, G. E., Le Pendu, J. & Larson, G. Norwalk virus-like particles bind specifically to A, H and difucosylated Lewis but not to B histo-blood group active glycosphingolipids. *Glycoconj. J.* **26,** 1171–1180 (2009).

238. Lindesmith, L. *et al.* Human susceptibility and resistance to Norwalk virus infection. *Nat. Med.* **9,** 548–53 (2003).

239. Hutson, A. M. M., Atmar, R. L. L., Graham, D. Y. Y. & Estes, M. K. K. Norwalk virus infection and disease is associated with ABO histo-blood group type. *J. Infect. Dis.* **185,** 1335–7 (2002).

240. Ramani, S. *et al.* Mucosal and Cellular Immune Responses to Norwalk Virus. *J. Infect. Dis.* **212,** 397–405 (2015).

241. Lindesmith, L. C. *et al.* Broad Blockade Antibody Responses in Human Volunteers after Immunization with a Multivalent Norovirus VLP Candidate Vaccine: Immunological Analyses from a Phase I Clinical Trial. *PLOS Med.* **12,** e1001807 (2015).

242. Newman, K. L. *et al.* Norovirus in symptomatic and asymptomatic individuals: cytokines and viral shedding. *Clin. Exp. Immunol.* **184,** 347–357 (2016).

243. Atmar, R. L. & Estes, M. K. The epidemiologic and clinical importance of norovirus infection. *Gastroenterol. Clin. North Am.* **35,** 275–90, viii (2006).

244. Rockx, B. *et al.* Natural History of Human *Calicivirus* Infection: A Prospective Cohort Study. *Clin. Infect. Dis.* **35,** 246–253 (2002).

245. TEUNIS, P. F. M. *et al.* Shedding of norovirus in symptomatic and asymptomatic infections. *Epidemiol. Infect.* **143,** 1710–1717 (2015).

246. Woodward, J., Gkrania-Klotsas, E. & Kumararatne, D. Chronic norovirus infection and common variable immunodeficiency. *Clin. Exp. Immunol.* (2016). doi:10.1111/cei.12884

247. Echenique, I. A. *et al.* Prolonged norovirus infection after pancreas transplantation: a case report and review of chronic norovirus. *Transpl. Infect. Dis.* **18,** 98–104 (2016).

248. Gustavsson, L., Nordén, R., Westin, J., Lindh, M. & Andersson, L.-M. Slow clearance of norovirus following infection with emerging variants of genotype GII.4 strains. *J. Clin. Microbiol.* JCM.00061-17 (2017). doi:10.1128/JCM.00061-17

249. Koo, H. L. *et al.* Noroviruses: The Most Common Pediatric Viral Enteric Pathogen at a Large University Hospital After Introduction of Rotavirus Vaccination. *J. Pediatric Infect. Dis. Soc.* **2,** 57–60 (2013).

250. Payne, D. C. *et al.* Norovirus and medically attended gastroenteritis in U.S. children. *N. Engl. J. Med.* **368,** 1121–30 (2013).

251. Ahmed, S. M. *et al.* Global prevalence of norovirus in cases of gastroenteritis: a systematic review and meta-analysis. *Lancet. Infect. Dis.* **14,** 725–30 (2014).

252. Ramani, S., Atmar, R. L. & Estes, M. K. Epidemiology of human noroviruses and updates on vaccine development. *Curr. Opin. Gastroenterol.* **30,** 25–33 (2014).

253. Patel, M. M. *et al.* Systematic Literature Review of Role of Noroviruses in Sporadic Gastroenteritis. *Emerg. Infect. Dis.* **14,** 1224–1231 (2008).

254. Patel, M. M., Hall, A. J., Vinjé, J. & Parashar, U. D. Noroviruses: A comprehensive review. *J. Clin. Virol.* **44,** 1–8 (2009).

255. Bartsch, S. M., Lopman, B. A., Ozawa, S., Hall, A. J. & Lee, B. Y. Global Economic Burden of Norovirus Gastroenteritis. *PLoS One* **11,** e0151219 (2016).

256. Debbink, K., Lindesmith, L. C. & Baric, R. S. The state of norovirus vaccines. *Clin. Infect. Dis.* **58,** 1746–52 (2014).

257. Taube, S. *et al.* A mouse model for human norovirus. *MBio* **4,** (2013).

258. Ettayebi, K. *et al.* Replication of human noroviruses in stem cell – derived human enteroids - SUPP. *Science (80-.).* **5211,** (2016).

259. Wobus, C. E., Cunha, J. B., Elftman, M. D. & Kolawole, A. O. Animal Models of Norovirus Infection. *Viral Gastroenteritis* 397–422 (2016). doi:10.1016/B978-0-12-802241-2.00019-5

260. Wobus, C. E., Thackray, L. B. & Virgin, H. W. Murine Norovirus: a Model System To Study Norovirus Biology and Pathogenesis. *J. Virol.* **80,** 5104–5112 (2006).

261. Baldridge, M. T., Turula, H. & Wobus, C. E. Norovirus Regulation by Host and Microbe. *Trends Mol. Med.* **22,** 1047–1059 (2016).

262. McInnes, E. F. *et al.* Prevalence of viral, bacterial and parasitological diseases in rats and mice used in research environments in Australasia over a 5-y period. *Lab Anim. (NY).* **40,** 341–50 (2011).

263. Kim, J. R. *et al.* Prevalence of murine norovirus infection in Korean laboratory animal facilities. *J. Vet. Med. Sci.* **73,** 687–91 (2011).

264. Hsu, C. C., Wobus, C. E., Steffen, E. K., Riley, L. K. & Livingston, R. S. Development of a Microsphere-Based Serologic Multiplexed Fluorescent Immunoassay and a Reverse Transcriptase PCR Assay To Detect Murine Norovirus 1 Infection in Mice. *Clin. Vaccine Immunol.* **12,** 1145–1151 (2005).

265. Mumphrey, S. M. *et al.* Murine norovirus 1 infection is associated with histopathological changes in immunocompetent hosts, but clinical disease is prevented by STAT1-dependent interferon responses. *J. Virol.* **81,** 3251–63 (2007).

266. Thackray, L. B. *et al.* Murine Noroviruses Comprising a Single Genogroup Exhibit Biological Diversity despite Limited Sequence Divergence. *J. Virol.* **81,** 10460–10473 (2007).

267. Jones, M. K. *et al.* Enteric bacteria promote human and mouse norovirus infection of B cells. *Science (80-.).* **346,** 755–759 (2014).

268. Gonzalez-Hernandez, M. B. *et al.* Murine Norovirus Transcytosis across an In Vitro Polarized Murine Intestinal Epithelial Monolayer Is Mediated by M-Like Cells. *J. Virol.* **87,** 12685–12693 (2013).

269. Elftman, M. D. *et al.* Multiple effects of dendritic cell depletion on murine norovirus infection. *J. Gen. Virol.* **94,** 1761–1768 (2013).

270. Karst, S. M. & Wobus, C. E. A Working Model of How Noroviruses Infect the Intestine. *PLOS Pathog.* **11,** e1004626 (2015).

271. Wobus, C. E. *et al.* Replication of Norovirus in cell culture reveals a tropism for dendritic cells and macrophages. *PLoS Biol.* **2,** e432 (2004).

272. Ward, J. M. *et al.* Pathology of Immunodeficient Mice With Naturally Occurring Murine Norovirus Infection. *Toxicol. Pathol.* **34,** 708–715 (2006).

273. Kahan, S. M. *et al.* Comparative murine norovirus studies reveal a lack of correlation between intestinal virus titers and enteric pathology. *Virology* **421,** 202–10 (2011).

274. Karandikar, U. C. *et al.* Detection of human norovirus in intestinal biopsies from immunocompromised transplant patients. *J. Gen. Virol.* **97,** 2291–300 (2016).

275. Taube, S. *et al.* Ganglioside-Linked Terminal Sialic Acid Moieties on Murine Macrophages Function as Attachment Receptors for Murine Noroviruses. *J. Virol.* **83,** 4092–4101 (2009).

276. Orchard, R. C. *et al.* Discovery of a proteinaceous cellular receptor for a norovirus. *Science (80-.).* **1220,** 1–5 (2016).

277. Haga, K. *et al.* Functional receptor molecules CD300lf and CD300ld within the CD300 family enable murine noroviruses to infect cells. *Proc. Natl. Acad. Sci.* **113,** E6248–E6255 (2016).

278. Thackray, L. B. *et al.* Murine noroviruses comprising a single genogroup exhibit biological diversity despite limited sequence divergence. *J. Virol.* **81,** 10460–73 (2007).

279. Barron, E. L. *et al.* Diversity of murine norovirus strains isolated from asymptomatic mice of different genetic backgrounds within a single U.S. research institute. *PLoS One* **6,** e21435 (2011).

280. Shortland, A. *et al.* Pathology caused by persistent murine norovirus infection. *J. Gen. Virol.* **95,** 413–422 (2014).

281. Taube, S. *et al.* Murine noroviruses bind glycolipid and glycoprotein attachment receptors in a strain-dependent manner. *J. Virol.* **86,** 5584–93 (2012).

282. Bailey, D., Thackray, L. B. & Goodfellow, I. G. A single amino acid substitution in the murine norovirus capsid protein is sufficient for attenuation in vivo. *J. Virol.* **82,** 7725–8 (2008).

283. Arias, A., Bailey, D., Chaudhry, Y. & Goodfellow, I. Development of a reverse-genetics system for murine norovirus 3: long-term persistence occurs in the caecum and colon. *J. Gen. Virol.* **93,** 1432–41 (2012).

284. Nice, T. J., Strong, D. W., McCune, B. T., Pohl, C. S. & Virgin, H. W. A Single-Amino-Acid Change in Murine Norovirus NS1/2 Is Sufficient for Colonic Tropism and Persistence. *doi.org* 327–334 (2013). doi:10.1128/jvi.01864-12

285. McCartney, S. A. *et al.* MDA-5 recognition of a murine norovirus. *PLoS Pathog.* **4,** e1000108 (2008).

286. Lazear, H. M. *et al.* IRF-3, IRF-5, and IRF-7 coordinately regulate the type I IFN response in myeloid dendritic cells downstream of MAVS signaling. *PLoS Pathog.* **9,** e1003118 (2013).

287. Thackray, L. B. *et al.* Critical Role for Interferon Regulatory Factor 3 (IRF-3) and IRF-7 in Type I Interferon-Mediated Control of Murine Norovirus Replication. *J. Virol.* **86,** 13515–13523 (2012).

288. Changotra, H. *et al.* Type I and type II interferons inhibit the translation of murine norovirus proteins. *J. Virol.* **83,** 5683–92 (2009).

289. Nice, T. J. *et al.* Interferon λ cures persistent murine norovirus infection in the absence of adaptive immunity. *Science* **347,** 269–273 (2014).

290. Baldridge, M. T. *et al.* Commensal microbes and interferon- l determine persistence of enteric murine norovirus infection. *Science* **347,** 6–9 (2015).

291. Baldridge, M. T. *et al.* Expression of *Ifnlr1* on intestinal epithelial cells is critical to the antiviral effects of IFN-lambda against norovirus and reovirus. *J. Virol.* **91,** JVI.02079-16 (2017).

292. Thorne, L. & Goodfellow, I. Reply to Kempf et al. *J. Infect. Dis.* **215,** 487–488 (2017).

293. Siddiq, D. M., Koo, H. L., Adachi, J. A. & Viola, G. M. Norovirus gastroenteritis successfully treated with nitazoxanide. *J. Infect.* **63,** 394–397 (2011).

294. Muir, A. J. *et al.* A randomized phase 2b study of peginterferon lambda-1a for the treatment of chronic HCV infection. *J. Hepatol.* **61,** 1238–1246 (2014).

295. Nelson, M. *et al.* Safety and Efficacy of Pegylated Interferon Lambda, Ribavirin, and Daclatasvir in HCV and HIV-Coinfected Patients. *J. Interf. Cytokine Res.* **37,** 103–111 (2017).

296. Chachu, K. A., LoBue, A. D., Strong, D. W., Baric, R. S. & Virgin, H. W. Immune Mechanisms Responsible for Vaccination against and Clearance of Mucosal and Lymphatic Norovirus Infection. *PLoS Pathog.* **4,** e1000236 (2008).

297. Chachu, K. A. *et al.* Antibody Is Critical for the Clearance of Murine Norovirus Infection. *J. Virol.* **82,** 6610–6617 (2008).

298. Zhu, S. *et al.* Identification of immune and viral correlates of norovirus protective immunity through comparative study of intra-cluster norovirus strains. *PLoS Pathog.* **9,** e1003592 (2013).

299. Tomov, V. T. *et al.* Persistent enteric murine norovirus infection is associated with functionally suboptimal virus-specific CD8 T cell responses. *J. Virol.* **87,** 7015–31 (2013).

300. Zhu, S. *et al.* Norovirus antagonism of B-cell antigen presentation results in impaired control of acute infection. *Mucosal Immunol.* **9,** 1–12 (2016).

301. Nice, T. J. *et al.* Type I Interferon Receptor Deficiency in Dendritic Cells Facilitates Systemic Murine Norovirus Persistence Despite Enhanced Adaptive Immunity. *PLoS Pathog.* **12,** 1–19 (2016).

302. Swamy, M. *et al.* Intestinal intraepithelial lymphocyte activation promotes innate antiviral resistance. *Nat. Commun.* **6,** 7090 (2015).

303. Blasi, E., Barluzzi, R., Bocchini, V., Mazzolla, R. & Bistoni, F. Immortalization of murine microglial cells by a v-raf/v-myc carrying retrovirus. *J. Neuroimmunol.* **27,** 229–37 (1990).

304. Bocchini, V. *et al.* An immortalized cell line expresses properties of activated microglial cells. *J. Neurosci. Res.* **31,** 616–21 (1992).

305. Boismenu, R. & Havran, W. L. Modulation of epithelial cell growth by intraepithelial gamma delta T cells. *Science* **266,** 1253–5 (1994).

306. Komano, H. *et al.* Homeostatic regulation of intestinal epithelia by intraepithelial gamma delta T cells. *Proc. Natl. Acad. Sci. U. S. A.* **92,** 6147–51 (1995).

307. Yamamoto, M., Fujihashi, K., Beagley, K. W., McGhee, J. R. & Kiyono, H. Cytokine synthesis by intestinal intraepithelial lymphocytes. Both gamma/delta T cell receptor-positive and alpha/beta T cell receptor-positive T cells in the G1 phase of cell cycle produce IFN-gamma and IL-5. *J. Immunol.* **150,** 106–14 (1993).

308. Fahrer, A. M. *et al.* Attributes of gammadelta intraepithelial lymphocytes as suggested by their transcriptional profile. *Proc. Natl. Acad. Sci. U. S. A.* **98,** 10261–6 (2001).

309. Ismail, A. S. *et al.* Gammadelta intraepithelial lymphocytes are essential mediators of host-microbial homeostasis at the intestinal mucosal surface. *Proc. Natl. Acad. Sci. U. S. A.* **108,** 8743–8 (2011).

310. Findly, R. C., Roberts, S. J. & Hayday, A. C. Dynamic response of murine gut intraepithelial T cells after infection by the coccidian parasite Eimeria. *Eur. J. Immunol.* **23,** 2557–64 (1993).

311. Roberts, S. J. *et al.* T-cell alpha beta + and gamma delta + deficient mice display abnormal but distinct phenotypes toward a natural, widespread infection of the intestinal epithelium. *Proc. Natl. Acad. Sci. U. S. A.* **93,** 11774–9 (1996).

312. Smith, A. L. & Hayday, A. C. An alphabeta T-cell-independent immunoprotective response towards gut coccidia is supported by gammadelta cells. *Immunology* **101,** 325–32 (2000).

313. Clark, K. *et al.* Novel cross-talk within the IKK family controls innate immunity. *Biochem. J.* **434,** 93–104 (2011).

314. Shortland, A. *et al.* Pathology caused by persistent murine norovirus infection. *J. Gen. Virol.* **95,** 413–22 (2014).

315. da Cunha, A. P. & Weiner, H. L. Induction of Immunological Tolerance by Oral Anti-CD3. *Clin. Dev. Immunol.* **2012,** 1–5 (2012).

316. Halota, W. *et al.* Oral anti-CD3 immunotherapy for HCV-nonresponders is safe, promotes regulatory T cells and decreases viral load and liver enzyme levels: results of a phase-2a placebo-controlled trial. *J. Viral Hepat.* **22,** 651–657 (2015).

317. Lodolce, J. P. *et al.* IL-15 Receptor Maintains Lymphoid Homeostasis by Supporting Lymphocyte Homing and Proliferation. *Immunity* **9,** 669–676 (1998).

318. Schluns, K. S. *et al.* Distinct cell types control lymphoid subset development by means of IL-15 and IL-15 receptor alpha expression. *Proc. Natl. Acad. Sci. U. S. A.* **101,** 5616–21 (2004).

319. Philpott, K. L. *et al.* Lymphoid development in mice congenitally lacking T cell receptor alpha beta-expressing cells. *Science* **256,** 1448–52 (1992).

320. Mombaerts, P. *et al.* Spontaneous development of inflammatory bowel disease in T cell receptor mutant mice. *Cell* **75,** 274–82 (1993).

321. Bhan, A. K., Mizoguchi, E., Smith, R. N. & Mizoguchi, A. Spontaneous chronic colitis in TCR alpha-mutant mice; an experimental model of human ulcerative colitis. *Int. Rev. Immunol.* **19,** 123–38 (2000).

322. Nanno, M. *et al.* Exacerbating role of gammadelta T cells in chronic colitis of T-cell receptor alpha mutant mice. *Gastroenterology* **134,** 481–90 (2008).

323. Stankovic, S., Zhan, Y. & Harrison, L. C. Homeostatic proliferation of intestinal intraepithelial lymphocytes precedes their migration to extra-intestinal sites. *Eur. J. Immunol.* **37,** 2226–33 (2007).

324. Schenkel, J. M. *et al.* T cell memory. Resident memory CD8 T cells trigger protective innate and adaptive immune responses. *Science* **346,** 98–101 (2014).

325. do Canto, F. B. *et al.* Enlarged colitogenic T cell population paradoxically supports colitis prevention through the B-lymphocyte-dependent peripheral generation of CD4+Foxp3+ Treg cells. *Sci. Rep.* **6,** 28573 (2016).

326. Agenès, F. & Freitas, A. A. Transfer of small resting B cells into immunodeficient hosts results in the selection of a self-renewing activated B cell population. *J. Exp. Med.* **189,** 319–30 (1999).

327. Roth, R. & Mamula, M. J. Trafficking of adoptively transferred B lymphocytes in B-lymphocyte-deficient mice. *J. Exp. Biol.* **200,** 2057–62 (1997).

328. Karst, S. M. Identification of a novel cellular target and a co-factor for norovirus infection – B cells & commensal bacteria. *Gut Microbes* **6,** 266–271 (2015).

329. Jones, M. K. *et al.* Human norovirus culture in B cells. *Nat. Protoc.* **10,** 1939–1947 (2015).

330. Aujla, S. J. & Kolls, J. K. IL-22: A critical mediator in mucosal host defense. *J. Mol. Med.* **87,** 451–454 (2009).

331. Nikoopour, E., Bellemore, S. M. & Singh, B. IL-22, cell regeneration and autoimmunity. *Cytokine* **74,** 35–42 (2015).

332. Puleston, D. Detection of Mitochondrial Mass, Damage, and Reactive Oxygen Species by Flow Cytometry. *Cold Spring Harb. Protoc.* **2015,** pdb.prot086298 (2015).

333. van der Windt, G. J. W. *et al.* Mitochondrial Respiratory Capacity Is a Critical Regulator of CD8+ T Cell Memory Development. *Immunity* **36,** 68–78 (2012).

334. Buck, M. D. *et al.* Mitochondrial Dynamics Controls T Cell Fate through Metabolic Programming. *Cell* **166,** 63–76 (2016).

335. Stromberg, P. E. *et al.* CD4+ lymphocytes control gut epithelial apoptosis and mediate survival in sepsis. *FASEB J.* **23,** 1817–1825 (2009).

336. Nishiyama, Y. *et al.* Homeostatic Regulation of Intestinal Villous Epithelia by B Lymphocytes. *J. Immunol.* **168,** (2002).

337. Golovkina, T. V., Shlomchik, M., Hannum, L. & Chervonsky, A. Organogenic Role of B Lymphocytes in Mucosal Immunity. *Science (80-.).* **286,** (1999).

338. Kernéis, S., Bogdanova, A., Kraehenbuhl, J.-P. & Pringault, E. Conversion by Peyer's Patch Lymphocytes of Human Enterocytes into M Cells that Transport Bacteria. *Science (80-.).* **277,** (1997).

339. United Nations, Department of Economic and Social Affairs, P. D. (2015). *World population, ageing*. **United Nat,** (2015).

340. United Nations Population Fund (UNFPA), New York, and HelpAge International, L. *Ageing in the twenty-first century : a celebration and a challenge.* (2012).

341. Lloyd-Sherlock, P. Population ageing in developed and developing regions: implications for health policy. *Soc. Sci. Med.* **51,** 887–95 (2000).

342. Beard, J. R. *et al.* The World report on ageing and health: a policy framework for healthy ageing. *The Lancet* **387,** 2145–2154 (2016).

343. Franceschi, C., Garagnani, P., Vitale, G., Capri, M. & Salvioli, S. Inflammaging and 'Garb-aging'. *Trends Endocrinol. Metab.* **28,** 199–212 (2017).

344. Cannizzo, E. S., Clement, C. C., Sahu, R., Follo, C. & Santambrogio, L. Oxidative stress, inflamm-aging and immunosenescence. *J. Proteomics* **74,** 2313–2323 (2011).

345. McElhaney, J. E. *et al.* The unmet need in the elderly: How immunosenescence, CMV infection, co-morbidities and frailty are a challenge for the development of more effective influenza vaccines. *Vaccine* **30,** 2060–2067 (2012).

346. Pawelec, G., Derhovanessian, E. & Larbi, A. Immunosenescence and cancer. *Crit. Rev. Oncol. Hematol.* **75,** 165–172 (2010).

347. Sambhara, S. & McElhaney, J. E. Immunosenescence and Influenza Vaccine Efficacy. 413–429 (2009). doi:10.1007/978-3-540-92165-3_20

348. Lindsay, L., Wolter, J., De Coster, I., Van Damme, P. & Verstraeten, T. A decade of norovirus disease risk among older adults in upper-middle and high income countries: a systematic review. *BMC Infect. Dis.* **15,** 425 (2015).

349. Jones, T. F. When Diarrhea Gets Deadly: A Look at Gastroenteritis Outbreaks in Nursing Homes. *Clin. Infect. Dis.* **51,** 915–916 (2010).

350. Pillai, P. S. *et al.* Mx1 reveals innate pathways to antiviral resistance and lethal influenza disease. *Science (80-.).* **352,** (2016).

351. Zhang, S., Kodys, K., Li, K. & Szabo, G. Human Type 2 Myeloid Dendritic Cells Produce Interferon-λ and Amplify Interferon-α in Response to Hepatitis C Virus Infection. *Gastroenterology* **144,** 414–425.e7 (2013).

352. Sirén, J., Pirhonen, J., Julkunen, I. & Matikainen, S. IFN-alpha regulates TLR-dependent gene expression of IFN-alpha, IFN-beta, IL-28, and IL-29. *J. Immunol.* **174,** 1932–7 (2005).

353. Mordstein, M. *et al.* Lambda interferon renders epithelial cells of the respiratory and gastrointestinal tracts resistant to viral infections. *J. Virol.* **84,** 5670–7 (2010).

354. Jewell, N. A. *et al.* Lambda Interferon Is the Predominant Interferon Induced by Influenza A Virus Infection In Vivo. *J. Virol.* **84,** 11515–11522 (2010).

355. Davidson, S. *et al.* IFNλ is a potent anti-influenza therapeutic without the inflammatory side effects of IFNα treatment. *EMBO Mol. Med.* **8,** 1099–112 (2016).

356. Mahlakõiv, T., Hernandez, P., Gronke, K., Diefenbach, A. & Staeheli, P. Leukocyte-derived IFN-α/β and epithelial IFN-λ constitute a compartmentalized mucosal defense system that restricts enteric virus infections. *PLoS Pathog.* **11,** e1004782 (2015).

357. Angel, J., Franco, M. A., Greenberg, H. B. & Bass, D. Lack of a Role for Type I and Type II Interferons in the Resolution of Rotavirus-Induced Diarrhea and Infection in Mice. *J. Interf. Cytokine Res.* **19,** 655–659 (1999).

358. Forrest, J. C. & Dermody, T. S. Reovirus receptors and pathogenesis. *J. Virol.* **77,** 9109–15 (2003).

359. Lin, J. Da *et al.* Distinct Roles of Type I and Type III Interferons in Intestinal Immunity to Homologous and Heterologous Rotavirus Infections. *PLoS Pathog.* **12,** 1–29 (2016).

360. Koch, S. *et al.* Multiparameter flow cytometric analysis of CD4 and CD8 T cell subsets in young and old people. *Immun. Ageing* **5,** 6 (2008).

361. Moro-García, M. A., Alonso-Arias, R. & López-Larrea, C. When Aging Reaches CD4+ T-Cells: Phenotypic and Functional Changes. *Front. Immunol.* **4,** 107 (2013).

362. Singh, U. P., Venkataraman, C., Singh, R. & Lillard, J. W. CXCR3 axis: role in inflammatory bowel disease and its therapeutic implication. *Endocr. Metab. Immune Disord. Drug Targets* **7,** 111–23 (2007).

363. Groom, J. R. & Luster, A. D. CXCR3 in T cell function. *Exp. Cell Res.* **317,** 620–631 (2011).

364. Yoon, P., Keylock, K. T., Hartman, M. E., Freund, G. G. & Woods, J. A. Macrophage hypo-responsiveness to interferon-gamma in aged mice is associated with impaired signaling through Jak-STAT. *Mech. Ageing Dev.* **125,** 137–43 (2004).

365. Qian, F. *et al.* Impaired interferon signaling in dendritic cells from older donors infected in vitro with West Nile virus. *J. Infect. Dis.* **203,** 1415–24 (2011).

366. Murayama, T., Inoue, M., Nomura, T., Mori, S. & Eizuru, Y. 2,3,7,8-Tetrachlorodibenzo-p-dioxin is a possible activator of human cytomegalovirus replication in a human fibroblast cell line. *Biochem. Biophys. Res. Commun.* **296,** 651–6 (2002).

367. Ohata, H., Tetsuka, T., Hayashi, H., Onozaki, K. & Okamoto, T. 3-methylcholanthrene activates human immunodeficiency virus type 1 replication via aryl hydrocarbon receptor. *Microbiol. Immunol.* **47,** 363–70 (2003).

368. Warren, T. K., Mitchell, K. A. & Lawrence, B. P. Exposure to 2,3,7,8-tetrachlorodibenzo-p-dioxin (TCDD) suppresses the humoral and cell-mediated immune responses to influenza A virus without affecting cytolytic activity in the lung. *Toxicol. Sci.* **56,** 114–23 (2000).

369. Vorderstrasse, B. A., Bohn, A. A. & Lawrence, B. P. Examining the relationship between impaired host resistance and altered immune function in mice treated with TCDD. *Toxicology* **188,** 15–28 (2003).

370. Jin, G.-B., Winans, B., Martin, K. C. & Lawrence, B. P. New insights into the role of the aryl hydrocarbon receptor in the function of $CD11c^+$ cells during respiratory viral infection. *Eur. J. Immunol.* **44,** 1685–98 (2014).

371. Wheeler, J. L. H., Martin, K. C., Resseguie, E. & Lawrence, B. P. Differential consequences of two distinct AhR ligands on innate and adaptive immune responses to influenza A virus. *Toxicol. Sci.* **137,** 324–34 (2014).

372. Xue, L., Pestka, J. J., Li, M., Firestone, G. L. & Bjeldanes, L. F. 3,3'-Diindolylmethane stimulates murine immune function in vitro and in vivo. *J. Nutr. Biochem.* **19,** 336–44 (2008).

373. Kim, S. Cellular and Molecular Mechanisms of 3,3′-Diindolylmethane in Gastrointestinal Cancer. *Int. J. Mol. Sci.* **17,** 1155 (2016).

374. Baba, T. *et al.* Intrinsic function of the aryl hydrocarbon (dioxin) receptor as a key factor in female reproduction. *Mol. Cell. Biol.* **25,** 10040–51 (2005).

375. Zhou, Q., Lavorgna, A., Bowman, M., Hiscott, J. & Harhaj, E. W. Aryl hydrocarbon receptor interacting protein targets IRF7 to suppress antiviral signaling and the induction of type I interferon. *J. Biol. Chem.* **290,** jbc.M114.633065 (2015).

376. Nguyen, N. T. *et al.* Aryl hydrocarbon receptor negatively regulates dendritic cell immunogenicity via a kynurenine-dependent mechanism. *Proc. Natl. Acad. Sci. U. S. A.* **107,** 19961–6 (2010).

377. Vogel, C. F. A., Goth, S. R., Dong, B., Pessah, I. N. & Matsumura, F. Aryl hydrocarbon receptor signaling mediates expression of indoleamine 2,3-dioxygenase. *Biochem. Biophys. Res. Commun.* **375,** 331–5 (2008).

378. Ciorba, M. A. Indoleamine 2,3 dioxygenase in intestinal disease. *Curr. Opin. Gastroenterol.* **29,** 146–152 (2013).

379. Bankoti, J., Rase, B., Simones, T. & Shepherd, D. M. Functional and phenotypic effects of AhR activation in inflammatory dendritic cells. *Toxicol. Appl. Pharmacol.* **246,** 18–28 (2010).

380. Vogel, C. F. A. *et al.* Aryl hydrocarbon receptor signaling regulates NF-κB RelB activation during dendritic-cell differentiation. *Immunol. Cell Biol.* **91,** 568–75 (2013).

381. Hwang, S. *et al.* Nondegradative role of Atg5-Atg12/ Atg16L1 autophagy protein complex in antiviral activity of interferon gamma. *Cell Host Microbe* **11,** 397–409 (2012).

382. Maloney, N. S. *et al.* Essential cell-autonomous role for interferon (IFN) regulatory factor 1 in IFN-γ-mediated inhibition of norovirus replication in macrophages. *J. Virol.* **86,** 12655–64 (2012).

383. Lacey, D. C. *et al.* Defining GM-CSF- and macrophage-CSF-dependent macrophage responses by in vitro models. *J. Immunol.* **188,** 5752–65 (2012).

384. Masurier, C. *et al.* Immunophenotypical and functional heterogeneity of dendritic cells generated from murine bone marrow cultured with different cytokine combinations: implications for anti-tumoral cell therapy. *Immunology* **96,** 569–77 (1999).

385. Helft, J. *et al.* GM-CSF Mouse Bone Marrow Cultures Comprise a Heterogeneous Population of CD11c+MHCII+ Macrophages and Dendritic Cells. *Immunity* **42,** 1197–1211 (2015).

386. den Haan, J. M., Lehar, S. M. & Bevan, M. J. CD8(+) but not CD8(-) dendritic cells cross-prime cytotoxic T cells in vivo. *J. Exp. Med.* **192,** 1685–96 (2000).

387. Menges, M. *et al.* IL-4 supports the generation of a dendritic cell subset from murine bone marrow with altered endocytosis capacity. *J. Leukoc. Biol.* **77,** 535–543 (2004).

388. Sallusto, F. & Lanzavecchia, A. Efficient presentation of soluble antigen by cultured human dendritic cells is maintained by granulocyte/macrophage colony-stimulating factor plus interleukin 4 and downregulated by tumor necrosis factor alpha. *J. Exp. Med.* **179,** 1109–18 (1994).

389. Sato, M. *et al.* Functional heterogeneity among bone marrow-derived dendritic cells conditioned by T(h)1- and T(h)2-biasing cytokines for the generation of allogeneic cytotoxic T lymphocytes. *Int. Immunol.* **12,** 335–42 (2000).

390. Hosoya, T. *et al.* Inducibility of cytochrome P450 1A1 and chemical carcinogenesis by benzo[a]pyrene in AhR repressor-deficient mice. *Biochem. Biophys. Res. Commun.* **365,** 562–567 (2008).

391. Dragin, N. *et al.* Phenotype of the Cyp1a1/1a2/1b1-/- triple-knockout mouse. *Mol. Pharmacol.* **73,** 1844–56 (2008).

392. Ilchmann, A. *et al.* Impact of culture medium on maturation of bone marrow-derived murine dendritic cells via the aryl hydrocarbon receptor. *Mol. Immunol.* **51,** 42–50 (2012).

393. De Clercq, E. Interferon induction by polynucleotides, modified polynucleotides, and polycarboxylates. *Methods Enzymol.* **78,** 227–36 (1981).

394. Pitha, P. M. Interferon induction with insolubilized polynucleotides and their preparation. *Methods Enzymol.* **78,** 236–42 (1981).

395. Au, W. C., Moore, P. A., Lowther, W., Juang, Y. T. & Pitha, P. M. Identification of a member of the interferon regulatory factor family that binds to the interferon-stimulated response element and activates expression of interferon-induced genes. *Proc. Natl. Acad. Sci. U. S. A.* **92,** 11657–61 (1995).

396. Boitano, A. E. *et al.* Aryl hydrocarbon receptor antagonists promote the expansion of human hematopoietic stem cells. *Science* **329,** 1345–8 (2010).

397. Veldhoen, M., Hirota, K., Christensen, J., O'Garra, A. & Stockinger, B. Natural agonists for aryl hydrocarbon receptor in culture medium are essential for optimal differentiation of Th17 T cells. *J. Exp. Med.* **206,** 43–49 (2009).

398. Kim, S.-H. *et al.* Novel Compound 2-Methyl-2H-pyrazole-3-carboxylic Acid (2-methyl-4-o-tolylazo-phenyl)-amide (CH-223191) Prevents 2,3,7,8-TCDD-Induced Toxicity by Antagonizing the Aryl Hydrocarbon Receptor. *Mol. Pharmacol.* **69,** 1871–1878 (2006).

399. Yamada, T. *et al.* Constitutive aryl hydrocarbon receptor signaling constrains type I interferon–mediated antiviral innate defense. *Nat. Immunol.* **17,** 687–694 (2016).

400. Balzola, F. *et al.* Aryl hydrocarbon receptor-induced signals up-regulate IL-22 production and inhibit inflammation in the gastrointestinal tract: Commentary. *Inflamm. Bowel Dis. Monit.* **12,** 73–74 (2011).